Intermolecular hydrophosphination of alkynes and dehydrocoupling studies using iron catalysts

King, Andrew

Award date:
2018

Awarding institution:
University of Bath

Intermolecular hydrophosphination of alkynes and dehydrocoupling studies using iron catalysts

Andrew Kevin King

A thesis submitted for the degree of Doctor of Philosophy

University of Bath

Department of Chemistry

April 2018

Contents -

Acknowledgements

I would like to thank the many people who have helped me over the course of my PhD. It has proved to be the most challenging yet most rewarding experience of my life so far. First and foremost I would like to thank my supervisor Ruth Webster for her support and advice throughout my PhD. I have learnt a lot from Ruth and her knowledge and insight have proved invaluable in conquering the challenges encountered throughout the project.

I would like to thank the members of the Webster group, past and present. Special thanks going to Maialen Espinal for her assistance and guidance in the lab aswell as being the life and soul of the party! I would like to thank Kim Gallagher for her advice on hydrophosphination at the start of my PhD. Nathan Coles for being a good house/lab mate and the interesting chemistry based discussions we've had over the past couple of years. Cei Provis-Evans for some great discussions on chemistry related things. The many MChem and MRes students who have populated the lab over the years most notably Oli Driscoll for being an excellent and highly enthusiastic project student.

I would like to thank Mary Mahon for her invaluable crystallography expertise and for solving the X-ray structures presented in this thesis. John Lowe for help and advice with NMR experiments. Antoine Buchard for conducting DFT calculations on the iron complexes presented within this thesis and Anneke Lubben for assistance with air sensitive mass spectrometry.

I would like to thank Mike Whittlesey and the Whittlesey group for providing me with a workspace at the start of my PhD when the department was pushed for space.

Last but certainly not least I would like to thank my parents for their support throughout my PhD. Your patience and support has been essential in my postgraduate studies and has been invaluable throughout the entirety of my education.

Abstract

Iron β-diketiminate complexes have great potential as catalysts. Previous work into the coordination chemistry of complexes bearing the β-diketiminate ancillary ligand (Chapter 1) attest to the useful properties of these complexes in catalysis. A handful of literature reports on catalytic systems hint that this could be further extended. Hydrophosphination is a growing field that continues to generate a lot of interest from industry and academia alike. The aims of this project are to investigate hydrophosphination reactions with iron β-diketiminate complexes, to achieve high degrees of regioselectivity from these sterically encumbered complexes and to investigate iron catalysed dehydrocoupling reactions. A combination of synthetic and mechanistic methodologies will be employed in order to achieve definitive insight *via* NMR spectroscopic analysis, kinetic studies and solid state crystallography.

Initial work presented herein (Chapter 2) will focus on the synthesis of iron(II) β-diketiminate complexes. Previously reported literature methods will be explored in order to determine an optimum procedure to use these precatalyst complexes. Initial investigations into hydrophosphination activity of these iron species will then be explored with alkenes. Results of these studies led to serendipitous findings and unexpected results in phosphine dehydrocoupling. The scope of this reactivity was then probed and mechanistic considerations taken into account with findings detailed herein. Radical catalysed reactivity observed will be further discussed. Solvent selectivity will then be discussed with a simple yet highly effective solvent change yielding a complete shift in catalytic activity.

Further studies (Chapter 3) highlight the orthogonal reactivity of iron(II) β-diketiminate complexes in hydrophosphination catalysis. Less electronically activated and more atypical substrates have been investigated to determine their activity in hydrophosphination reactions. The synthesis of phosphinoalkenes and phosphinoalkynes for cyclic intramolecular hydrophosphination reactions are detailed along with their catalytic activity. Preliminary mechanistic studies are discussed with radical species again proving crucial to catalytic activity. Selective intermolecular hydrophosphination reactions have been investigated with alkynes. A solvent based switch can be employed wherein the regioselectivity of the reaction is completely altered. Substrate scope, mechanistic considerations and potential future applications are examined in full detail.

Dehydrocoupling catalysis can be extended in scope (Chapter 4) from iron catalysed phosphine homocoupling reactions to heterocoupling reactions. Phosphine-silane dehydrocoupling is found to be highly selective for the formation of silaphosphanes, preliminary mechanistic insight and reaction scope is discussed. Analogous amine-silane dehydrocoupling is explored in full. The substrate scope offers insight into reactivity and potential further applications in sequential and tandem catalysis. In depth mechanistic insight is discussed with kinetic analyses. Iron-amido complexes are observed to react in a metathesis mediated cycle *via* iron hydride species. Finally catalytic alcohol-silane dehydrocoupling is investigated as a synthetic route to protected natural products in organic synthesis.

Unsaturated silazanes are potential targets for further dehydrocoupling reactions. Catalytic reactions with pinacolborane led to highly facile desilylation reactions (Chapter 5). Mechanistic considerations hint that the reactions occur via σ-bond metathesis could through iron hydride species. Desilylation activity is then extended to siloxanes and a model developed with potential applications in the depolymerisation of polysilazanes and polysiloxanes.

Abbreviations and Units

Analytical –

μ_B	Bohr magneton
Da	Daltons
d	doublet
dd	doublet of doublets
DFT	Density functional theory
ESI	Electrospray ionisation
Hz	Hertz
h	hours
IR	Infra-red
J	Joule
KIE	Kinetic isotope effect
k_{obs}	observed rate constant
L	Litres
M	molar concentration
m	multiplet
mol	mole
NMR	Nuclear magnetic resonance
PDI	Polydispersity index
pKa	logarithmic acid dissociation constant
ppm	parts per million
q	quartet
RT	Room temperature
s	singlet
SOMO	Singly occupied molecular orbital
t	triplet
TEM	Transmission Electron Microscopy
UV-vis	Ultra violet- visible

Chemical -

acac	Acetylacetone
AIBN	Azobis(isobutyronitrile)
Ar	Aromatic
Bn	Benzyl
Cp	Cyclopentadienyl
Cy	Cyclohexyl
D	Deuterium
DCM	Dichloromethane
DIBAL-H	Diisobutyl aluminium hydride
Diip	2,6-Diisopropyl phenyl
dippe	1,2-Bis(diisopropylphosphino)ethane
Et	Ethyl
HCl	Hydrochloric acid
HMDS	Hexamethyl disilyl amide
^{i}Pr	Isopropyl
Ln	Lanthanide
MBTE	Methyl butyl tertiary ether
Me	Methyl
nBu	n-Butyl
nPr	n-Propyl
OAc	Acetate
OMe	Methoxy
OTf	Triflate
pin	Pinacol
Ph	Phenyl
py	Pyridyl
salen	N,N-bis(salicyl)ethylenediimine
SO_4	Sulphate
tBu	Tertiary butyl
TEMPO	(2,2,6,6-Tetramethylpiperidin-1-yl)oxyl

THF	Tetrahydrofuran
Tol	Tolyl
To^{M}	Tris(4,4-dimethyl-2-oxazolinyl)phenylborate
Tp	Hydridotris(pyrazolyl)borato
TMS	Trimethylsilyl
Xyl	Xylyl

1-Introduction –

The ubiquitous influence of phosphines in chemical synthesis is striking. The syntheses of these important and inherently useful compounds would ideally be trivial with little waste generated in chemical processes. However, current synthetic processes do not meet these criteria. Hydrophosphination offers an alternative to these cumbersome and somewhat rigorous strategies as it has the potential to be 100% atom economical. Previous work on hydrophosphination has focused on platinum group metals with the earliest work focusing on the use of platinum and palladium complexes in phosphine synthesis.[1] These complexes have many advantages not least of which is their high levels of reactivity in these reactions, but suffer in that they are rare metals that are costly. Thus alternatives are required when resources are eventually depleted. Iron is the most earth abundant transition metal by mass and as such is a much cheaper and more readily available alternative to conventional platinum group metals. Studies on iron systems are less well defined than that of platinum and palladium complexes, though recent work has seen a renaissance in iron in organic synthesis.[2] Iron complexes do not come without their disadvantages. A high sensitivity to aerobic conditions leading to oxidation poses a difficulty in the handling of iron complexes.

1.1 - β-Diketiminate complexes

In order to facilitate high activity and efficiency, iron precatalysts would ideally be electron poor complexes (i.e. less than 18 electron) and as such would be highly reactive. They would also be sterically encumbered to increase reactivity at the metal centre and low coordinate (two or three co-ordinate complexes) in order to coordinate substrates forming key catalytic intermediates. Additionally, complexes would ideally be cheap and easy to synthesise. One well defined class of ligand compounds that adheres to these criteria are the β-diketiminate ligands (Figure 1).

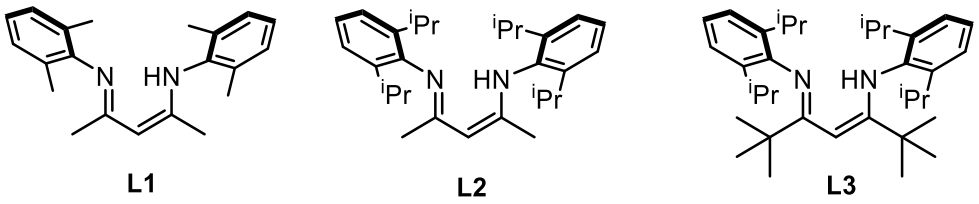

Figure 1: β-diketiminate ligands.

Often referred to as ˝Nacnac" ligands these compounds have been used to form a variety of coordination complexes from across the periodic table.[3-5] Concentrating primarily on iron Nacnac complexes and specifically low coordinate species, the most common of these complexes are three coordinate.[6]

Property wise the general trend with three coordinate iron Nacnac complexes is that they are high spin in the ground state, where S=2 and S= 5/2 for iron(II) and iron(III) complexes respectively. High spin trigonal planar iron complexes are therefore intrinsically paramagnetic which makes their spectroscopic characterisation challenging. To put this in perspective a typical solution magnetic moment for an iron(II) alkyl complex is 5.6 μ_B, somewhat higher than the spin only value for an S=2 complex of 4.9 μ_B.[7] This greatly affects

^{1}H NMR spectra of the complexes. The magnetic susceptibility affects the Lamor frequencies of the nuclei in close proximity. As Figure 2 exemplifies protons along the y-axis are shifted downfield due to this phenomenon and conversely protons in the xz plane are shifted upfield. This typically leads to spectra like that in Figure 2 in which the chemical shift can range from -150 ppm to +150 ppm and therefore vastly shifted from a typical spectrum for a diamagnetic complex in which the nuclei typically lie within the region of 0 to 12 ppm. As ^{1}H NMR is one of the most information rich forms of spectroscopy it still provides characterisable data for iron(II) Nacnac complexes. Conversely for iron(III) Nacnac complexes proton NMR provides very little information as spectra tend to be very broad or effectively non-existent for these complexes.

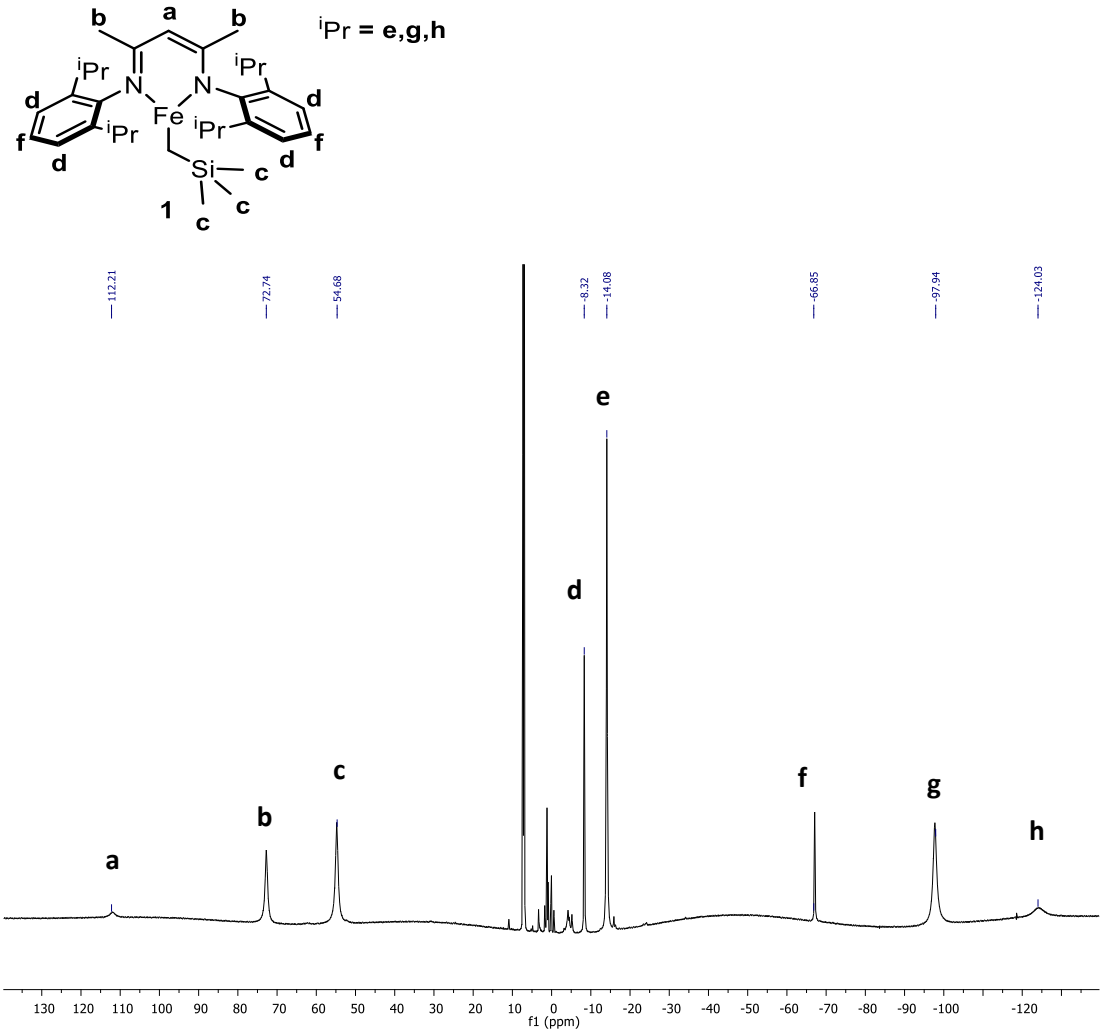

Figure 2: The ^{1}H spectrum of ^{Diip}LFeCH$_2$TMS, (**1**) (500 MHz, C_6D_6, 298 K).

Proton nuclei that are more distant from the paramagnetic iron centre are more easily distinguishable whereas protons and other nuclei bound directly to iron are often absent.[8] Full characterisation *via* NMR can be difficult due to the lack of spin-spin coupling between nuclei with each nuclear environment appearing as a broad singlet. However, use of an internal standard and the relative integration of the peaks makes characterisation of these complexes feasible.

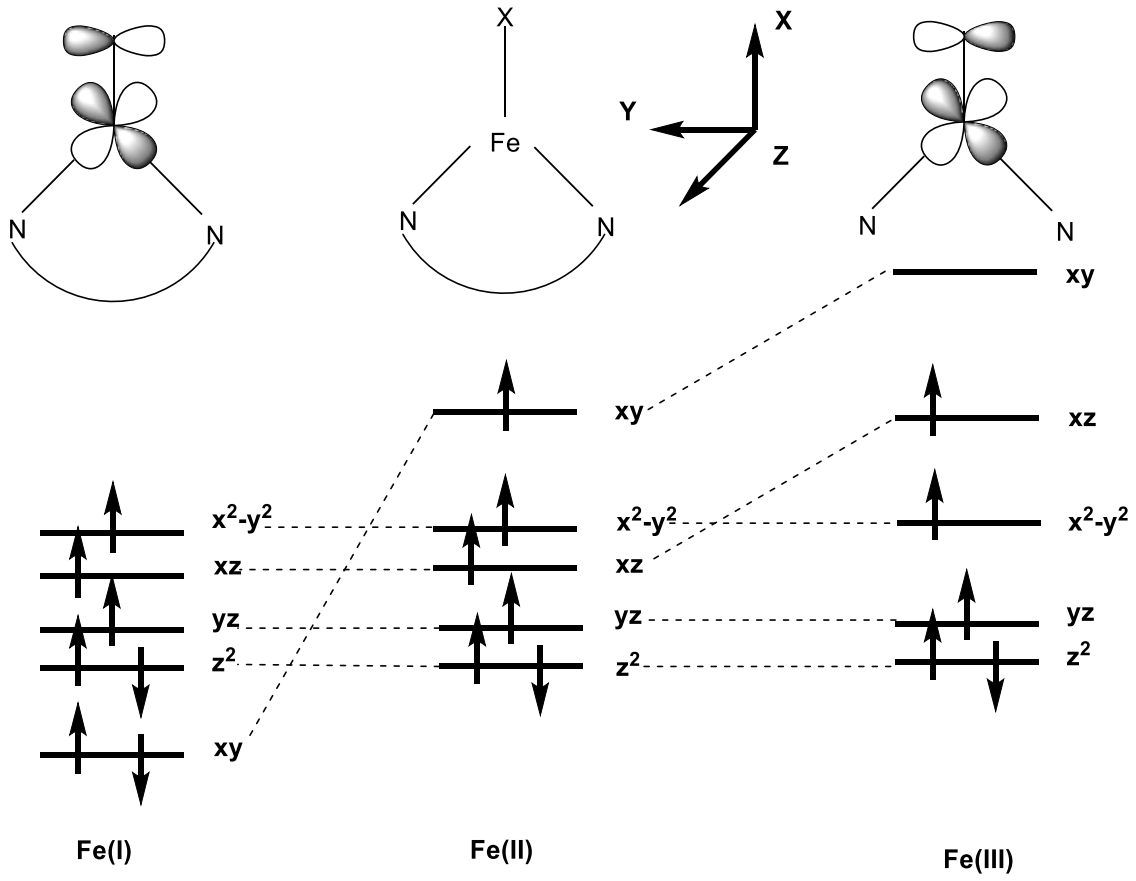

Scheme 1: d-orbital diagrams of three coordinate Nacnac iron complexes.

Scheme 1 shows the relative energies of the d orbitals on iron in the trigonal planar geometry, as the oxidation state of the iron centre is varied the effects of π interactions from the co-ligand coordinated directly to iron can be observed. π interactions have a large effect on high spin iron complexes as orbitals in the plane of the co-ligand X are singly occupied. The higher lying d-orbitals xz, x^2-y^2 and yz can overlap with p-orbitals on the co-ligand leading to favourable interactions making π backbonding with unoccupied orbitals on the co-ligand viable. Iron(I) alkyne complexes have been observed to show significant π-back bonding character.[9] Computational studies *via* DFT calculations have determined that there is a large overlap between the d_{xy} orbital on iron and the alkyne π* orbital significantly lowering the energy of the corresponding molecular orbital. As π - back bonding is key to the stability of these complexes electron density at aryl alkynes has a significant effect. Electron withdrawing groups on the aryl ring such as fluorine will therefore have a large effect on the stability of the complexes, conversely electron donating groups such as methoxy or amino groups will have the opposite effect. The higher oxidation states of iron(II) and (III) exhibit similar π acceptance from co-ligands wherein a lone pair is donated into singly occupied d-orbitals. There is potential then for iron(II) Nacnac alkyne complexes to be further investigated.[10]

Holland's extensive work on the coordination chemistry of three coordinate iron complexes has uncovered various trends between these compounds. Notably in stoichiometric reactions in which the co-ligand on the Nacnac complex undergoes exchange, the reaction is thermodynamically favourable when the co-ligand of the resultant complex is more electronegative than its precursor. To rationalise these observations with respect to molecular orbitals one might expect that π backbonding is playing a significant role. However

this is not in keeping with the observed trend as oxygen containing alkoxides have a higher degree of electronegativity at oxygen than nitrogen containing amido species and yet the amido group is the most strongly π donating.

In order to properly account for this phenomenon Holland devised a study of alkyl complexes with varying degrees of electron withdrawing and donating capabilities (Scheme 2). More strongly electron withdrawing groups lead to more inherently stable complexes with the equilibrium lying further to the right for stronger electron withdrawing groups (**2-4**).

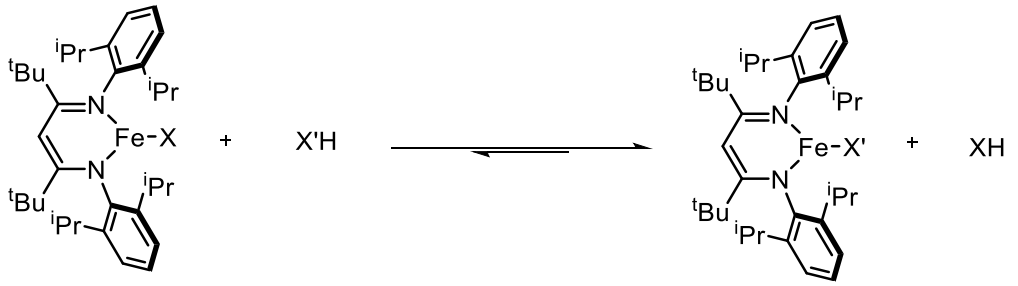

X= CCPh (**2**), NH(*p*-Tol) (**3**), O(*p*-Tol) (**4**)

Observed trend in ligation = C < N < O

Scheme 2: Trends in co-ligand exchange at three coordinate iron.

Holland's previous work then demonstrated the widespread advantages of Nacnac ligands in the co-ordination chemistry of iron complexes. The formation of alkyl, alkenyl and alkynyl complexes and the study of their inherent properties provides a good scope and basis for catalytic functionalisation reactions in which these complexes are potential intermediates (Figure 3). These 12 valence electron species are highly electron deficient complexes. As such they are highly reactive which poses great potential for functionalisation reactions.

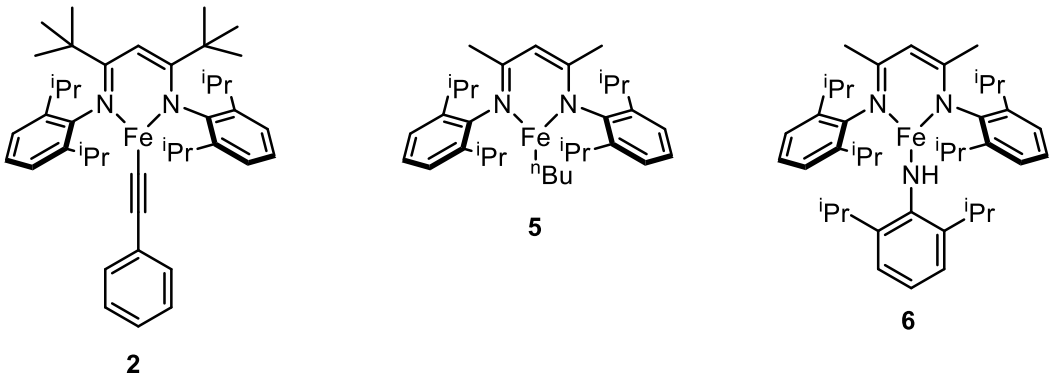

Figure 3: Three co-ordinate iron complexes characterised by Holland and co-workers.

Although the work of Holland and others on the co-ordination chemistry of these complexes has been extensive and detailed in the literature there are very few examples of iron Nacnac complexes being used as precatalysts.[11] However, one early example worthy of note is the work by Gibson and co-workers demonstrating that Nacnac iron alkoxide complexes (**7**) are effective intiators in the polymerisation of lactide (Scheme 3).[12]

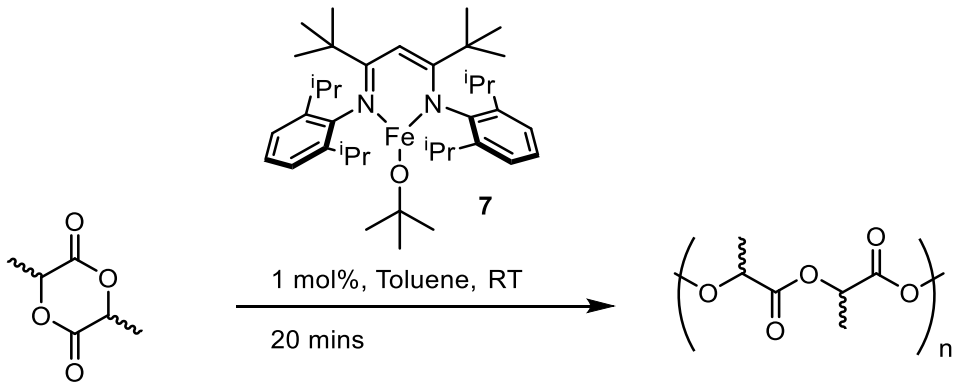

Scheme 3: Gibson's polymerisation of rac-lactide intiated by Nacnac iron tertbutoxide complexes.

The catalysts proved to be relatively efficient. The polymers synthesised in the reactions had generally high molecular weights with typical M_n and M_w values of 37,500 Da and 35,000 Da respectively. As such the polydispersities of the materials were uniform with typical PDI values of 1.12 showing a good degree of control over polymerisation. As Gibson and co-workers had shown that iron Nacnac complexes were effective polymerisation catalysts these complexes were further investigated by Liu and co-workers.[13] Liu evaluated four coordinate iron Nacnac complexes as catalysts in the polymerisation of ethylene. In contrast the iron catalysts were found to be very poor at polymerising ethylene.

Although the work from the Holland group has focused heavily on stoichiometric studies, they have demonstrated that their iron complexes are effective as precatalysts. A rather elegant report demonstrated that iron Nacnac fluoride complexes (**8**) were catalytically active for the hydrodefluorination of fluorocarbons (Scheme 4).[7]

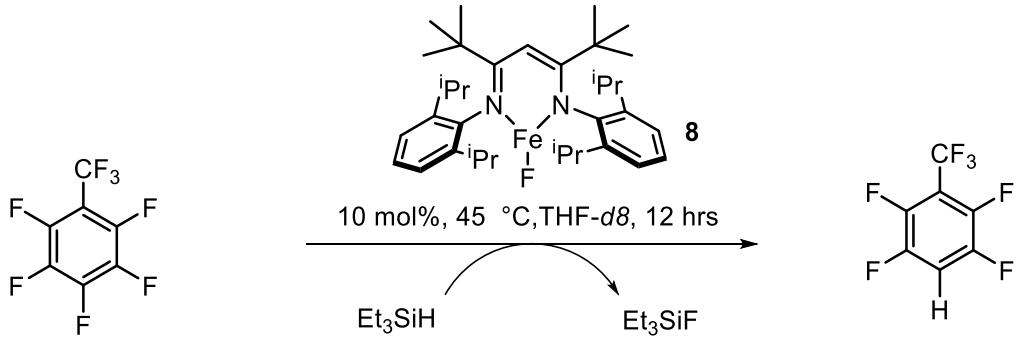

Scheme 4: Holland's Nacnac iron(II) catalysed hydrodefluorination of fluorocarbons.

The reactions require a stoichiometric equivalent of silane as a hydride source facilitating catalytic turnover. The particular silane employed is key to reactivity. Where triethylsilane is effective in facilitating the reaction phenylsilane and triphenylsilane are not effective. This is due to the combined steric and electronic effects of the silanes. Over the course of the reaction iron hydride complexes are generated *in situ* (Scheme 5). Evidence for this is demonstrated by hydride ^{1}H NMR signals and in the isolation of the dimeric resting state [NacnacFe –H]$_2$, (**9**). To date the exact role the silane plays in the reaction is not known. However, experimental observations suggest that an iron-silyl species is not a catalytic intermediate.

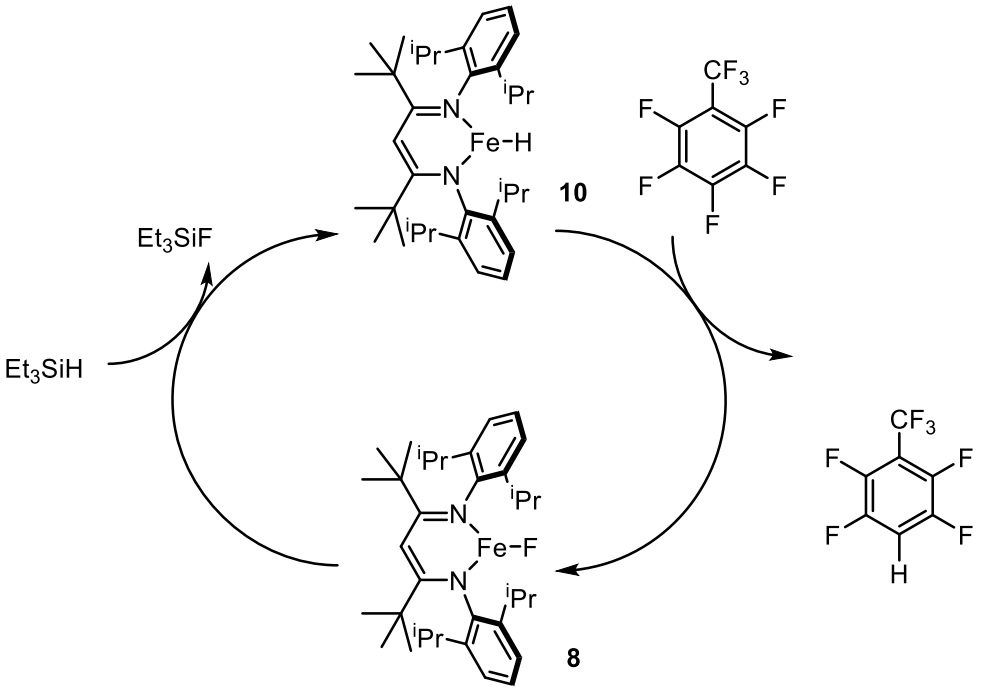

Scheme 5: Holland's proposed catalytic mechanism for the hydrodefluorination of fluorocarbons.

Another example by the Holland group showed that an iron Nacnac complex (**11**) was competent in the catalytic synthesis of carbodiimides (Scheme 6).[14]

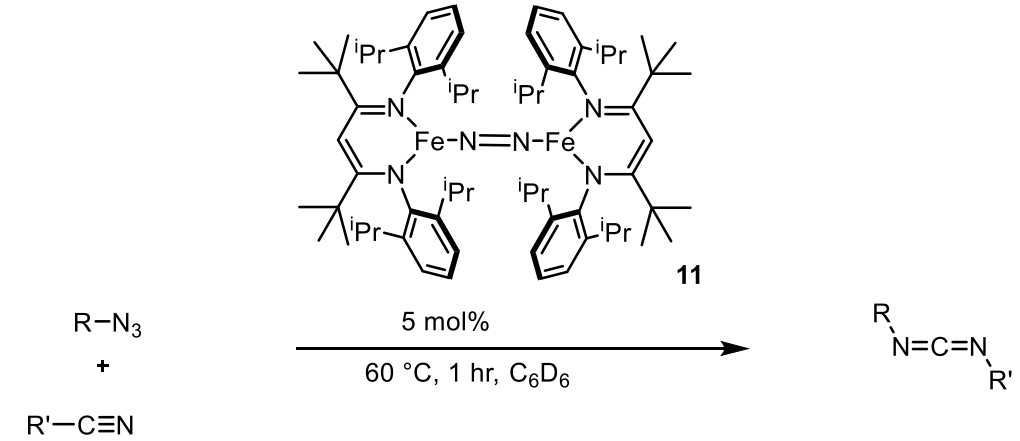

Scheme 6: Iron catalysed formation of carbodiimides.

Reports by Hannedouche and co-workers have demonstrated that iron Nacnac complexes can be used as catalysts in hydrofunctionalisation reactions by using them as catalysts for intramolecular hydroamination.[15]

It is clear that, thus far, very little work has been done studying iron Nacnac complexes in catalysis. Given the desirable properties of these complexes mentioned previously this is somewhat perplexing. Extensive work in catalysis has been carried out using the Nacnac complexes of the alkaline-earth metals, titanium and copper but iron remains largely uninvestigated.[16-18] Work by Hill and co-workers on alkaline-earth metal Nacnac complexes (**12a**, **13a**) has demonstrated their orthogonality in hydrofunctionalisation catalysis (Scheme 7).[19, 20]

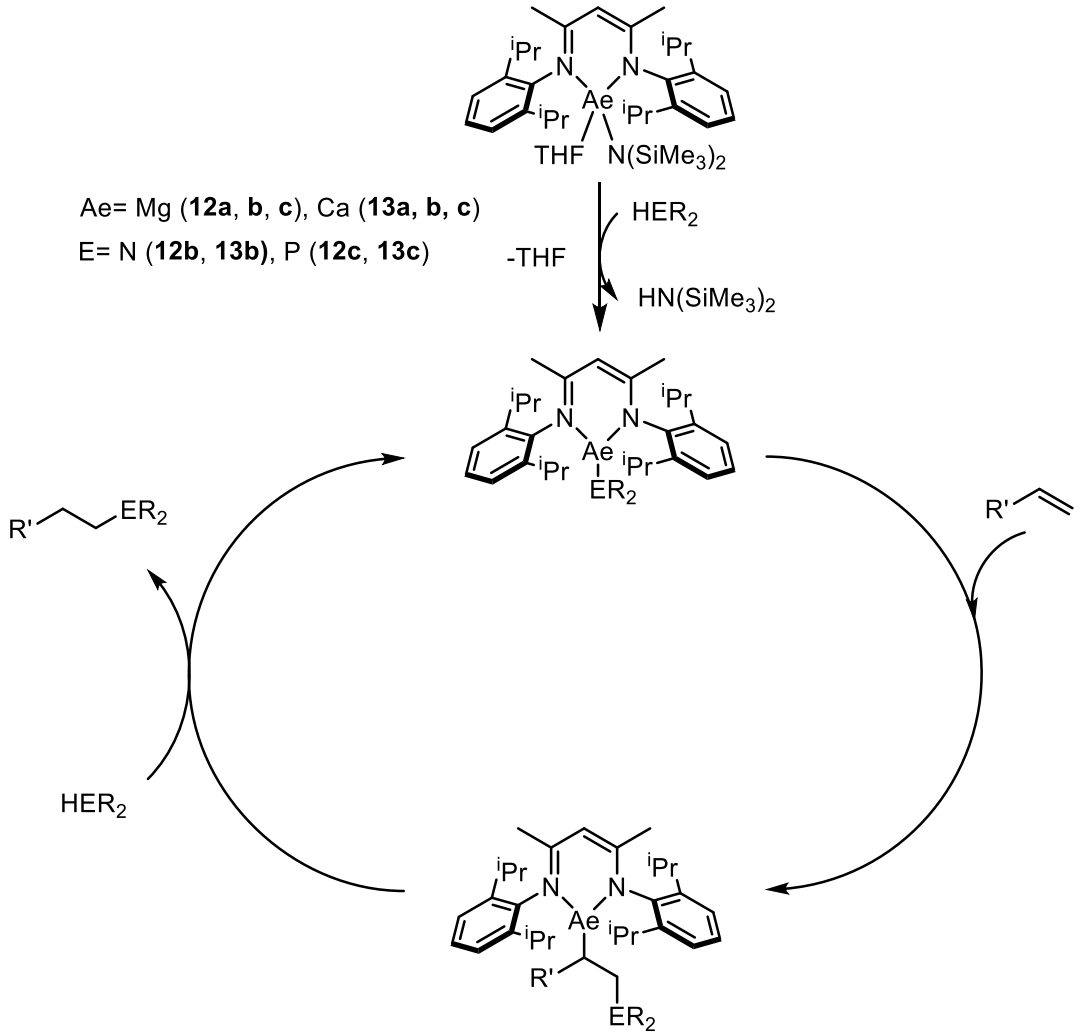

Scheme 7: Calcium and Magnesium Nacnac complexes in hydrofunctionalisation catalysis.

Of particular interest are the syntheses of phosphines in hydrophosphination reactions. Calcium catalysed hydrophosphination of styrenes was achieved under moderate conditions with *anti*-Markovnikov selectivity (Scheme 8).[21] Hill then demonstrated that hydrophosphination reactions are also feasible when introducing carbodiimides as substrates.[22] In this report hydrophosphination activity was again observed with Nacnac calcium complexes. Reactions were observed to progess through the formation of diimido complexes.

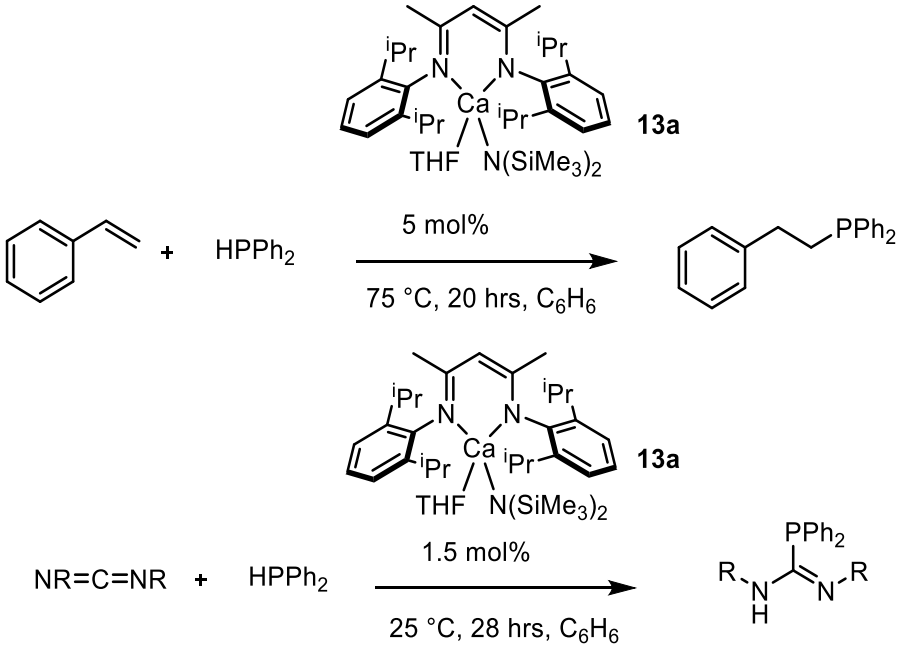

Scheme 8: Alkaline-earth metal catalysed hydrophosphination.

Phosphine synthesis *via* Nacnac complex catalysis has likewise been investigated by Mindiola and co-workers.[23] Cationic titanium complexes were found to be active catalysts in P-C bond forming reactions.

1.2 - Phosphines

Novel phosphine compounds are incredibly important in the optimisation and development of synthetic technologies. Phosphines are used ubiquitously as ligands in coordination chemistry. This is due to their inherently good σ- donating and π- accepting properties in forming metal complexes. Phosphines have been used abundantly in coordination chemistry for over fifty years (**14**-**16**) (Figure 4).[24, 25]

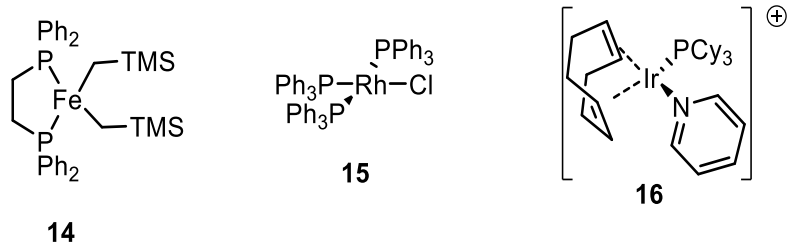

Figure 4: Phosphines as ligands in metal complexes.

In addition to these properties phosphines provide a significant advantage over amines in that the lone pair at phosphorus has a much higher inversion barrier than the lone pair at

nitrogen (Figure 5).[26] This is incredibly advantageous as it allows for stereocontrol at a phosphorus centre generating P- stereogenic centres and by extension chiral phosphines. When considering the barriers associated with asymmetric synthesis, controlled reactions *via* asymmetric catalysts comprised of chiral phosphine ancillary ligands are of continued interest both industrially and academically.[27, 28]

Figure 5: Comparison of the lone pair inversion barrier in phosphines and amines.

1.3 - Hydrophosphination catalysis

Synthesis of these ligands and general phosphine synthesis is particularly challenging. Given the propensity for phosphines (phosphorus(III)) to oxidise to phosphine oxides (phosphorus(V)), handling of compounds is generally done under an inert atmosphere. The oxidising potential of various phosphines has been previously reported on and, as may be expected, there is a large dependence on the substituents at phosphorus and their stereoelectronic properties.[29]

Classical methods for the synthesis of phosphines can be very wasteful often requiring vast excesses of reductants to form the desired products.[30] In a bid towards a more sustainable chemical future, alternative methodologies would then be highly desirable. Hydrophosphination reactions are a distinctive alternative as they have the potential to be 100% atom economical. This is highly desirable as in principle no waste materials are generated as a result of the reactions. Catalytic hydrophosphination reactions are not a new concept : the first reported example of a metal catalysed hydrophosphination reaction was reported in 1990 by Pringle and co-workers (Scheme 9).[31]

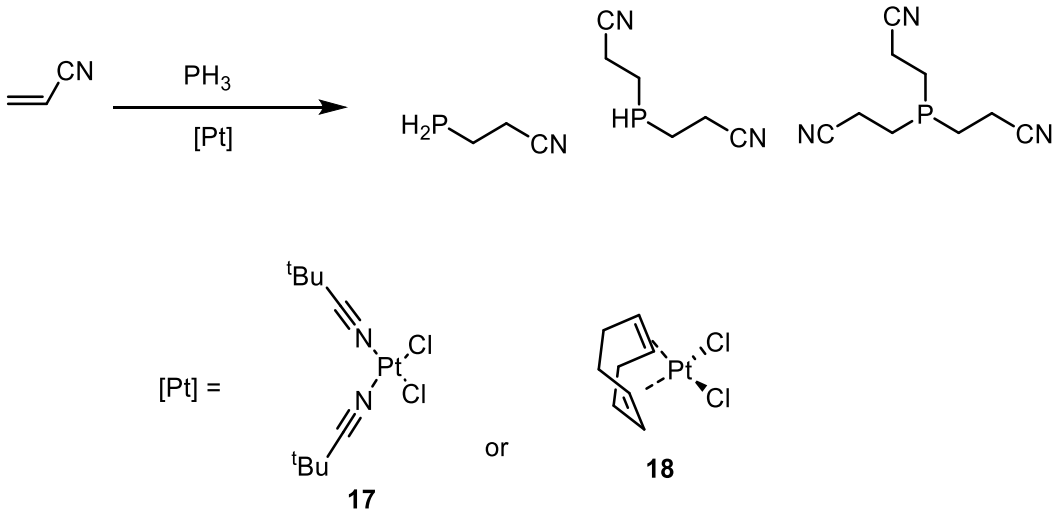

Scheme 9: Pringle's hydrophosphination of acrylonitrile with phosphine (PH_3).

In this platinum catalysed (**17** and **18**) system hydrophosphination of acrylonitrile was achieved with phosphine (PH_3). Three consecutive hydrophosphination reactions occur yielding $P(CH_2CH_2CN)_3$.

Other notable early examples of stoichiometric and catalytic hydrophosphination reactions include work by Glueck and co-workers with platinum and palladium catalysed hydrophosphination reactions (Scheme 10).[32-34]

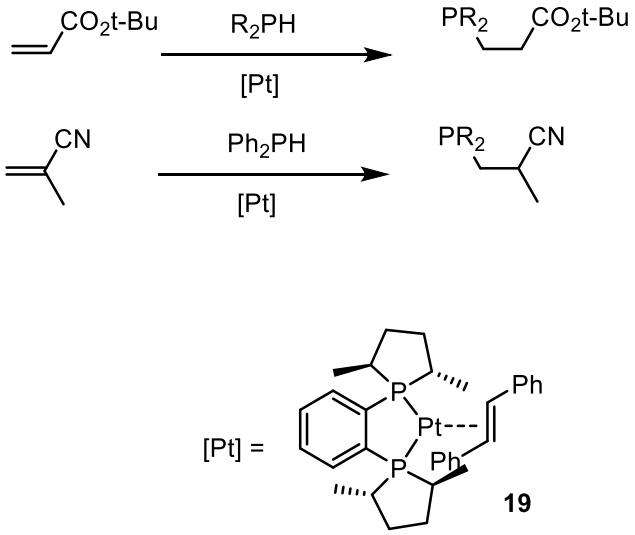

Scheme 10: Glueck platinum catalysed hydrophosphination reactions of unsaturated substrates.

Glueck's systems are of particular interest as with the chosen substrates and the chiral platinum catalyst employed (**19**) asymmetric synthesis is feasible. The potential products yielded are chiral phosphines with C-stereogenic centres.[35] Asymmetric synthesis is particularly challenging and in the platinum catalysed hydrophosphination reactions with enantiomeric excesses of up to 56% were yielded. Work by Melchiorre and co-workers found that organocatalysts (**20**) were more favourable for asymmetric hydrophosphination (Scheme 11).[36] Enantiomeric excesses of up to 99% could be achieved when isolating the products as phosphine-boranes.

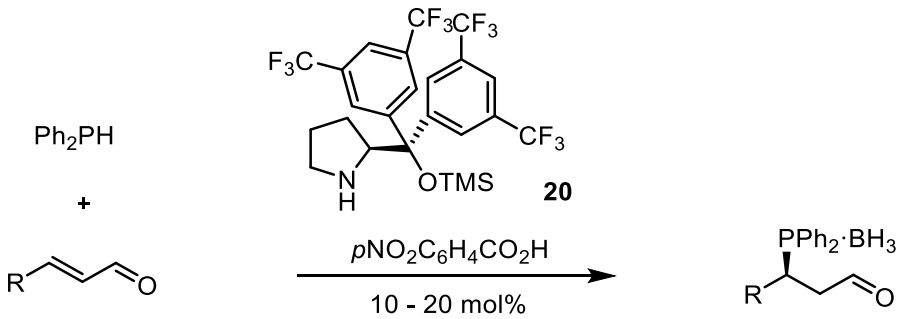

Scheme 11: Organocatalytic asymmetric hydrophosphination by Melchiorre.

In addition to this, work by Togni and co-workers showed that nickel catalysts are excellent at mediating asymmetric hydrophosphination reactions.[37]

Similarly asymmetric hydrophosphorylation reactions have been achieved with chiral iron complexes (Scheme 12).[38] Work by Sekar showed that hydrophosphorylation of aldehydes can be accomplished enantioselectively. Based on this work it can be postulated that enantioselective hydrophosphination reactions catalysed by enantiopure iron complexes could be carried out.

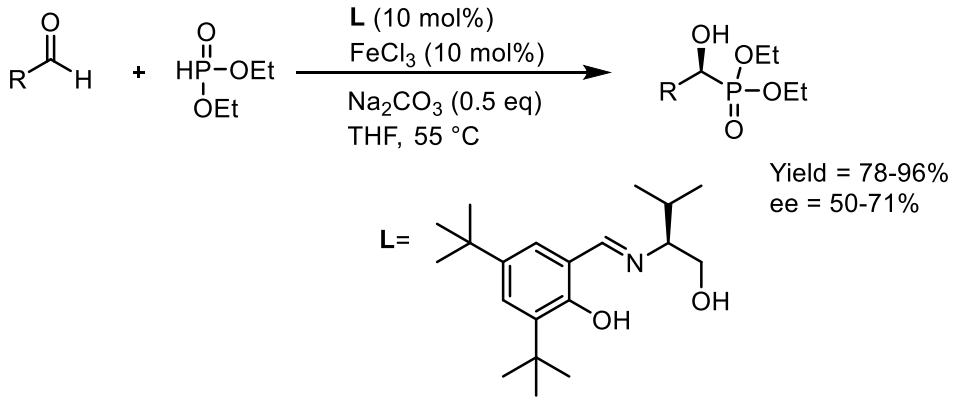

Scheme 12: Iron catalysed asymmetric hydrophosphorylation of aldehydes by Sekar.

These initial examples demonstrate well defined intermolecular hydrophosphination activity but up until 2001 intramolecular hydrophosphination remained completely unexplored. Drawing on previous analogous work on intramolecular hydroamination catalysis, Marks and co-workers demonstrated that lanthanide catalysts $Cp'_2LnCH(TMS)_2$ (Ln = La, Sm and Y; **21**, **22**, **23**) were highly effective at catalysing the hydrophosphination of phosphinoalkenes and phosphinoalkynes (Scheme 13).[39-42] A variety of substrates were screened and trends correlated with respect to catalytic activity. In initial kinetic studies the substrate was observed to be zero order suggesting that the rate limiting step in the reaction is the on-metal cyclisation and concurrent phosphorus-carbon bond formation. In addition to this it was observed that a phosphido species does not form instaneously. When mixing the substrate with the precatalyst a delay in catalyst activation is observed. Further mechanistic studies led to the rationalisation of two plausible substrate dependant mechanistic pathways by which the reaction could proceed. The first plausible pathway is a 1,2-insertion pathway (Scheme 13) and the alternative pathway is a 2,1-insertion pathway. The preferred pathway was observed to be substrate dependent.

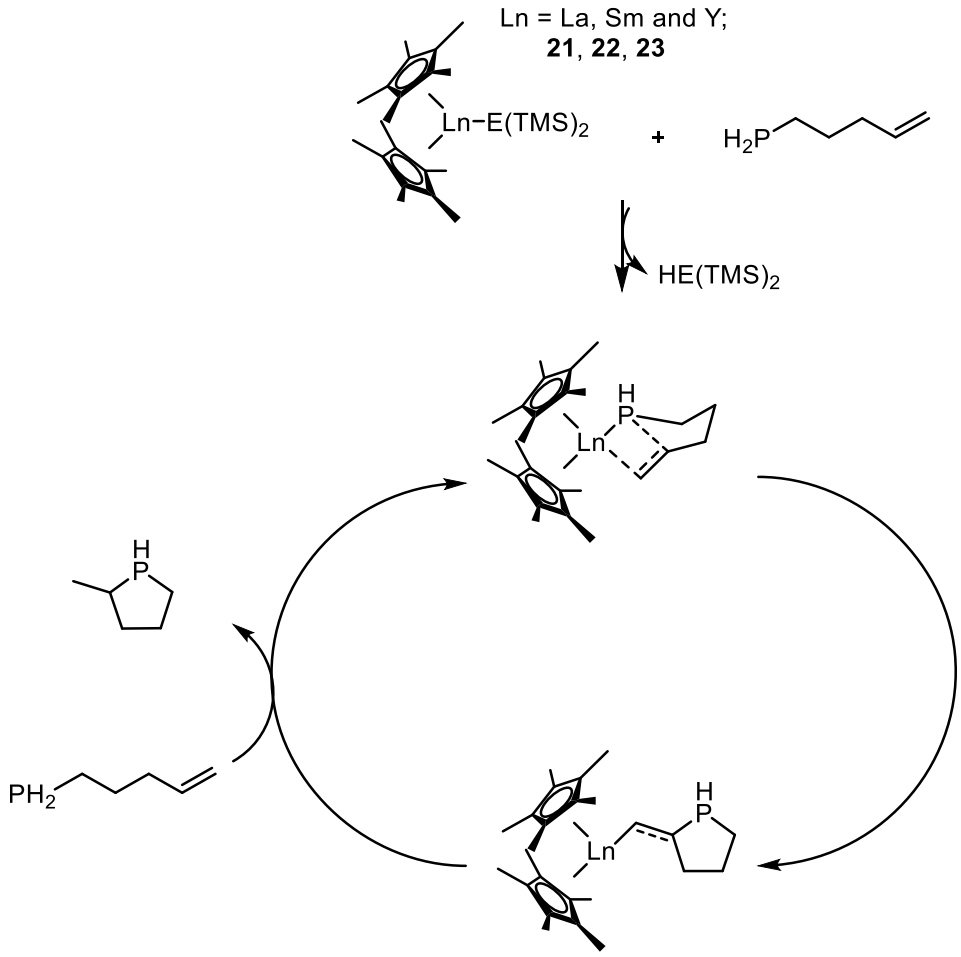

Scheme 13: Marks' proposed catalytic pathway for lanthanide catalysed intramolecular hydrophosphination.

As saturated phosphorus centres can be P-stereogenic and due to the achiral nature of the lanthanide complexes a mixture of diastereomers are formed in the hydrophosphination reactions. It can be inferred then that by changing from an achiral precatalyst to a chiral catalyst diastereoselectivity could be controlled to form single diastereomers. This has previously been reported for analogous transformations with aminoalkenes.[43-45] Marks followed up on this work and demonstrated that diastereoselectivity is achievable with chiral lanthanide catalysts.[46] This was achieved due to the C_1-symmetry of the lanthanide catalysts which whilst susceptible to racemisation rarely reach a diastereomeric equilibrium of 1:1. It is therefore feasible to achieve high diastereoselectivities.

Synthesising substituted cyclopentadienyl ligands and subsequent ligation generates C_1-symmetric complexes of the type $Me_2Si(Cp'')(CpR^*)LnE(TMS)_2$ (R= (+)-neomenthyl, (-)-menthyl; Ln= La, Sm, Y, Lu; E= N, CH; **24a-b**, **25a-b**, **26a-b**, **27a-b**). These complexes then serve as asymmetric precatalysts for intramolecular hydrophosphination (Figure 6).

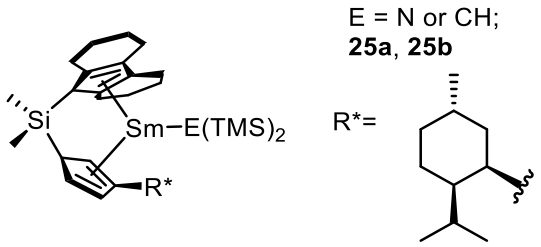

Figure 6: Marks' chiral lanthanide precatalysts.

Utilising an analogous ligand architecture was preferential as the electronic properties of the complex are equivalent making catalyst competency more likely. This strategy proved successful with up to 96% diastereomeric excess achieved.

Base metal catalysed hydrophosphination reactions have been explored to a certain extent and have gained more popularity of late due to the earth abundancy of the metals and their under-scrutinised mechanisms.[47-49] Beletskaya and co-workers reported that the phosphite based nickel catalyst $Ni[P(OEt)_3]_4$, (**28**) was a competent catalyst for styrene hydrophosphination.[50] In Beletskaya's study, during the optimisation of catalytic conditions, it was observed that a side reaction was occurring wherein tetraphenyldiphosphane (Ph_2P-PPh_2) was being formed. In order to suppress this side reaction an equivalent of trimethylamine is added. The optimum catalytic conditions are very forcing: at a temperature of 130 °C in a period of 40 hours an almost quantitative yield is achieved. Beletskaya postulated a potential catalytic cycle but provided very little experimental evidence upon which to prove it (Scheme 14).

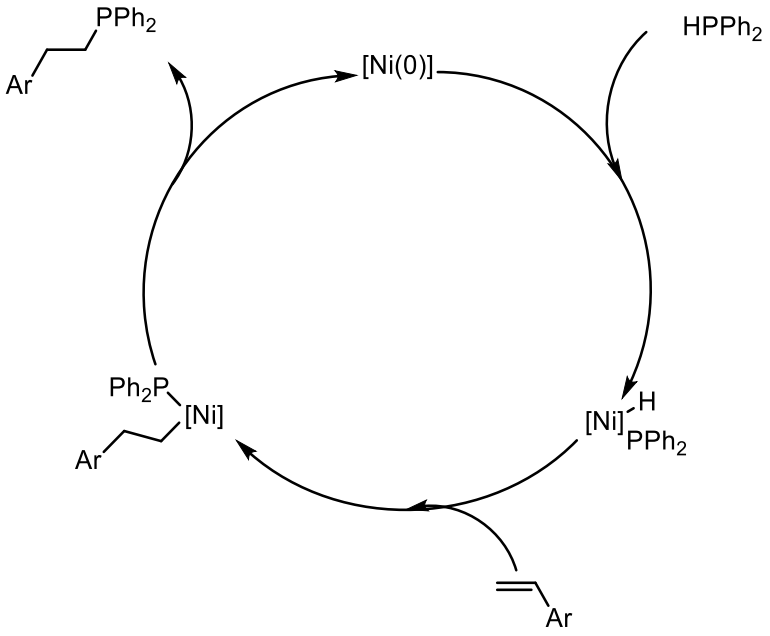

Scheme 14: Beletskaya's proposed catalytic cycle for nickel catalysed hydrophosphination of styrenes.

In addition to the hydrophosphination of styrenes Beletskaya's work has looked at nickel and palladium catalysed hydrophosphination of alkynes.[51] Ligand effects at nickel were observed to have a great impact on the regioselectivity of the hydrophosphination of phenylacetylene. The phosphite nickel catalyst **28** used in the previous study gave considerable selectivity for *anti*-Markovnikov addition with a 1:1 mixture of *E* and *Z* stereoisomers, whereas the simple nickel salt, nickel(II) bromide, gave well defined selectivity for Markovnikov addition (Figure 7).

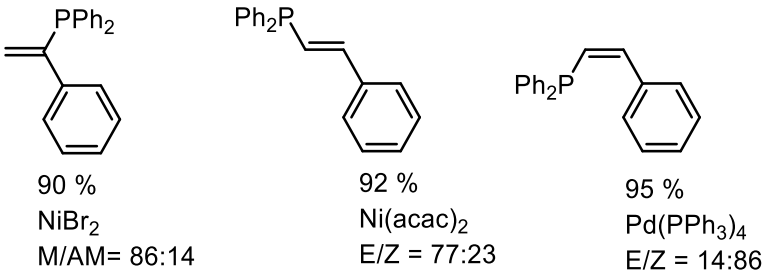

Figure 7: Regioisomers in the hydrophosphination of phenylacetylene and product distribution with different nickel and palladium catalysts in Beletskaya's study.

Diethyl phosphite was discovered to be an effective additive in promoting Markovnikov addition rather than *anti*-Markovnikov addition. When nickel(II) acac is employed as a catalyst in addition to diethyl phosphite a switch in selectivity from *anti*-Markovnikov to Markovnikov addition was observed. Other catalytic systems had been and have since been reported for alkyne hydrophosphination but few give such high selectivity for Markovnikov addition.[52-54]

Iron catalysed hydrophosphination was first reported by Gaumont and co-workers.[55] Gaumont demonstrated that the simple iron salts iron(II) chloride and iron(III) chloride were functional catalysts for the hydrophosphination of styrenes. Catalytic conditions showed some improvements on Beletskaya's nickel system operating at 60 °C in a 12 hour period. However a 30 mol% loading of iron salt is required in order for the reaction to proceed quantitatively. Intriguingly, a change in the oxidation state of the iron salt precatalyst leads to regioselective hydrophosphination reactions. Using iron(II) chloride gave good selectivity for *anti*-Markovnikov addition whereas iron(III) chloride gave the converse result with the formation of the α-adduct *via* Markovnikov addition. Gaumont postulated that the two iron salt precatalysts gave rise to strikingly different mechanisms (Scheme 15).

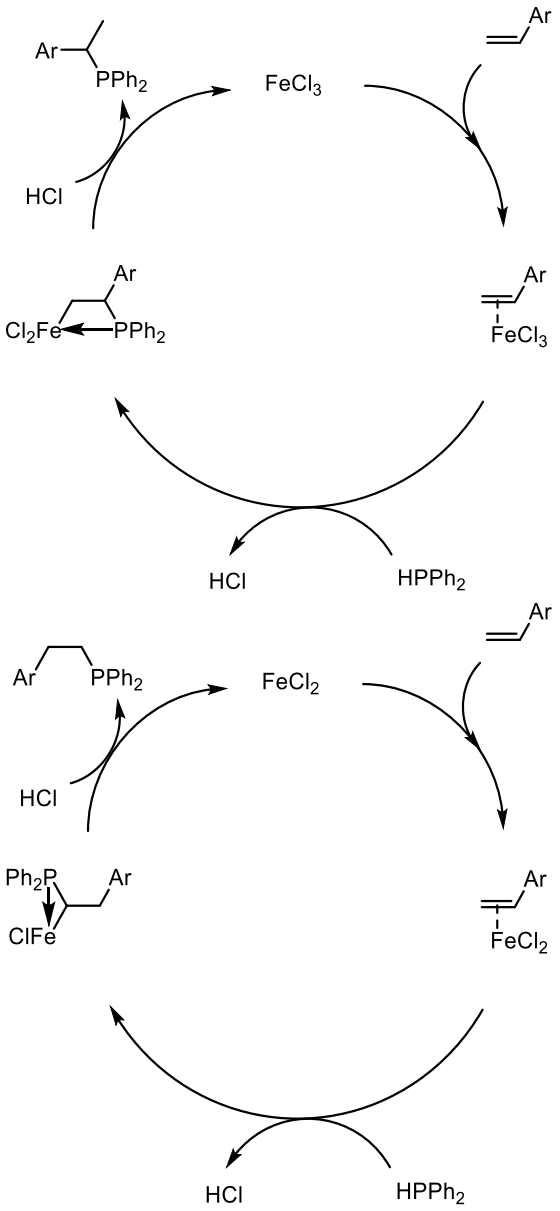

Scheme 15: Gaumont's postulated catalytic cycles for iron(II)/(III) chloride catalysed hydrophosphination of styrenes.

Gaumont's study provided little evidence to support these mechanistic hypotheses, not even testing the pH of the reaction solution for the presence of hydrochloric acid (HCl). Reports in the literature with genuine mechanistic insight into iron-catalysed hydrophosphination remain relatively scarce.

Work in the Webster group has focused on iron catalysed hydrophosphination reactions particularly on the hydrophosphination of styrenes. Investigations into catalysis with the simple air stable iron(III)-μ-oxo(salen), (**29**) complex found it to be a highly potent precatalyst for the hydrophosphination of styrenes (Scheme 16).[56] At a catalyst loading of only 0.5 mol% under ambient conditions near quantitative yields of hydrophosphination products were isolated.

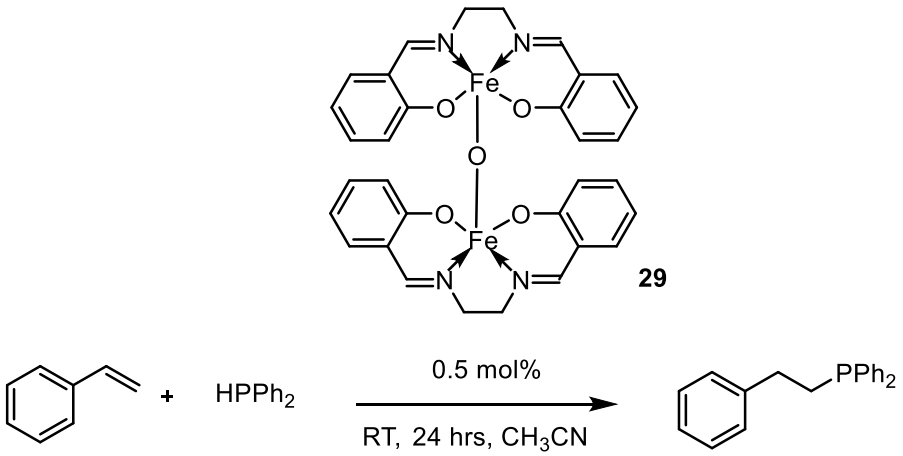

Scheme 16: Webster's iron(III) salen catalysed hydrophosphination of styrene.

Preliminary mechanistic insight was gauged through reaction monitoring and kinetic studies. The mechanism is not radical catalysed as determined by radical trap experiments. Initial rate studies suggested a deviation from a first order relationship in catalyst. An order of 1.6 suggested that the dimeric catalyst has a dual role to play in the mechanism. Break-up of the dimeric iron complex was not suggested as if this were to occur initial rates would demonstrate a half order relationship with respect to **29**.

Further studies extended the scope of hydrophosphination reactions with **29** and investigated a porphyrin ligand architecture.[57] Focusing attention on hydrophosphination reactions with phenylphosphine led to some intriguing results. Double hydrophosphination is achieved with complex **29** used as a precatalyst. Interestingly running the background reaction in the absence of the precatalyst led to very good selectivity for the mono-substituted hydrophosphination product. This thermally induced hydrophosphination was optimised and led to the isolation of secondary phosphines in high yields. Double hydrophosphination required the iron catalyst **29**. Addition of the products from the thermal hydrophosphination reaction to a different alkene demonstrated that the method could be used to synthesise non-symmetric tertiary phosphines (Scheme 17).

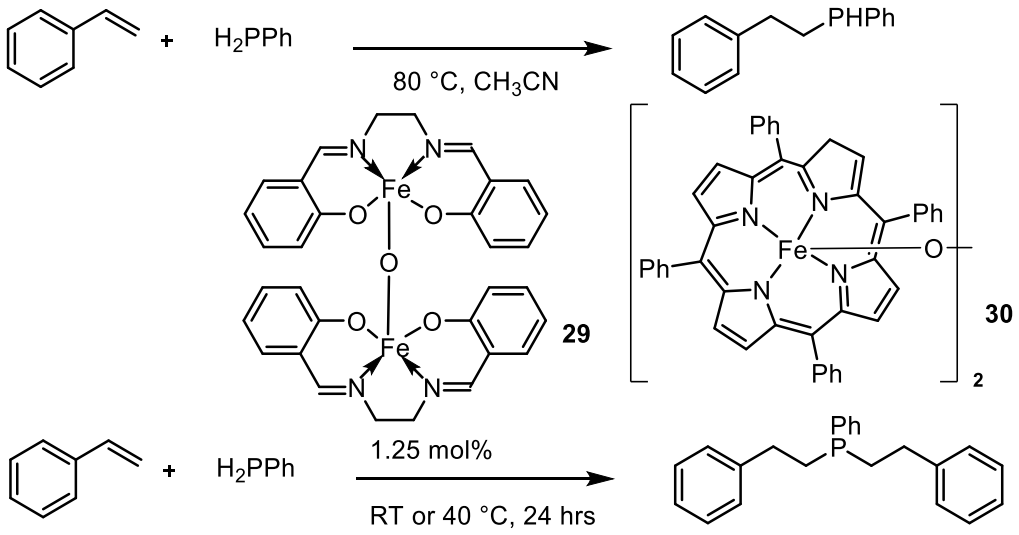

Scheme 17: Webster's catalyst free and iron catalysed hydrophosphination of styrenes with phenylphosphine.

Comparative studies with an iron(III)-μ-oxo(porphyrin), (**30**) complex as a precatalyst showed that it was as potent at catalysing the hydrophosphination of styrenes as **29**. Initial optimisation studies on the hydrophosphination of styrenes showed similar reactivity to that of **29** reported in the previous study. 0.5 mol% of **30** gives almost quantitative conversion at room temperature in 24 hours under solvent free conditions. Upon further scrutinisation of hydrophosphination catalysis with **30** some interesting deviations in reactivity are observable. Hydrophosphination reactions with certain substrates like 2-vinylpyridine are considerably more efficient with **30**. This is attributed higher degree of steric congestion at the central iron atom in the porphyrin ligand architecture.

Recent work by Waterman and co-workers has demonstrated that alkene hydrophosphination can be achieved photocatalytically with the iron complex $[CpFe(CO)_2]_2$, (**31**).[58] Irridiation with visible light and use of neat substrates gave high yields of hydrophosphination products at room temperature.

Iron catalysed hydrophosphination has also seen some focus on alkynes. Studies by Nakazawa and co-workers demonstrated the first catalytic example of the double hydrophosphination of alkynes with the iron precatalyst $CpFe(CO)_2(Me)$, (**32**).[59] Nakazawa's initial study demonstrated that under solvent free conditions in the presence of 5 mol% of this iron catalyst, high yields of 1,2- diphos products could be achieved. It can be noted that reaction conditions are particularly forcing in order to achieve high yields, with the reactants heated at 110 °C for a period of three days. Investigations into the substrate scope of the reaction demonstrate that potential coordinating groups such as amino and pyridyl functionalities do not hinder the catalytic system. There are however some limitations in the scope of the reaction. Alkynes bearing alkyl chains and secondary alkyl phosphines show no catalytic activity. Nakazawa postulated a mechanism for this iron catalysed system based on some preliminary mechanistic investigations (Scheme 18).

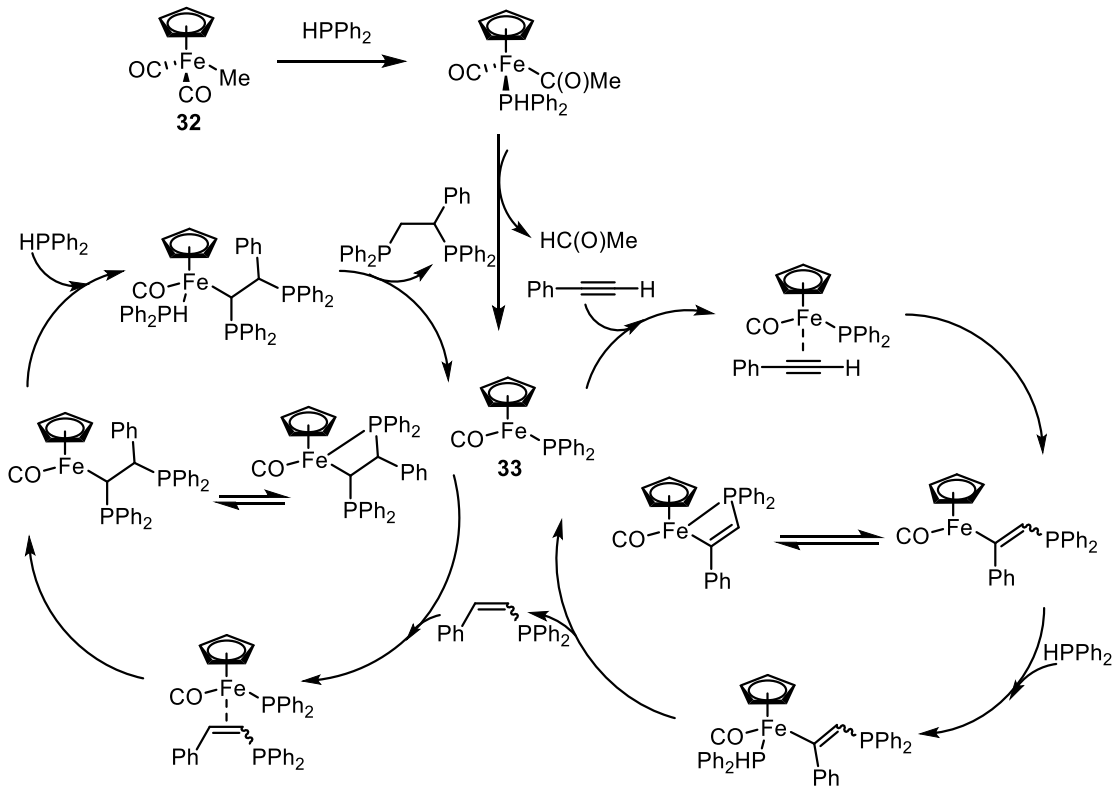

Scheme 18: Nakazawa's proposed catalytic cycle for iron catalysed double hydrophosphination of alkynes.

Radical trap experiments using an equivalent of TEMPO (2,2,6,6-tetramethylpiperidine-1-oxyl) show no loss of yield suggesting that the mechanism is not radical in nature. A possible cationic mechanism is discussed but not anticipated in this system as no hydrophosphination reactivity is observed between the precatalyst and dimethyl acetylenedicarboxylate (DMAD), a highly electrophilic substrate. Reaction monitoring determined that the first hydrophosphination step involves the formation of (*Z*)-vinylphosphine *via anti*-Markovnikov addition. Some of the *E* isomer is observed to form in the reaction, this then presumably is isomerised by the iron catalyst before undergoing a second hydrophosphination step to form the diphosphine product. Nakazawa postulates that the active catalyst is the phosphido species $CpFe(CO)PPh_2$, (**33**) either *via* rearrangement and concerted elimination of formaldehyde from the precatalyst, or *via* an oxidative addition reductive elimination pathway. This is evidenced by the observation of acetaldehyde formation *via* NMR.

Further studies by Nakazawa focused on single hydrophosphination activity and applications with cyclopentadienyl iron complexes.[60] Under almost identical conditions to Nakazawa's previous study, using Cp*Fe(CO)(py)(Me), (**34**) as a precatalyst, high selectivity was achieved for the mono substituted *Z*-isomer *via anti*-Markovnikov addition. The conditions for the reaction are harsh (10 mol% [Fe], 110 °C, 48 hrs). By comparison Beletskaya's previously discussed nickel catalysis operates under more appealing conditions (2 mol% [Ni], 80 °C, 10 hrs). Stoichiometric reactions of the catalyst with diphenylphosphine and phenylacetylene led to the isolation of catalytic intermediates $Cp^*Fe(CO)(PHPh_2)(PPh_2)$, (**35**) and $Cp^*Fe(CO)(E\text{-}PhCHCHPPh_2)$, (**36**). This was confirmed by reintroducing the compounds into hydrophosphination reactions as the precatalyst and observing catalytic turnover. Based upon these observations and previous hydrophosphination studies Nakazawa postulated a mechanism (Scheme 19).

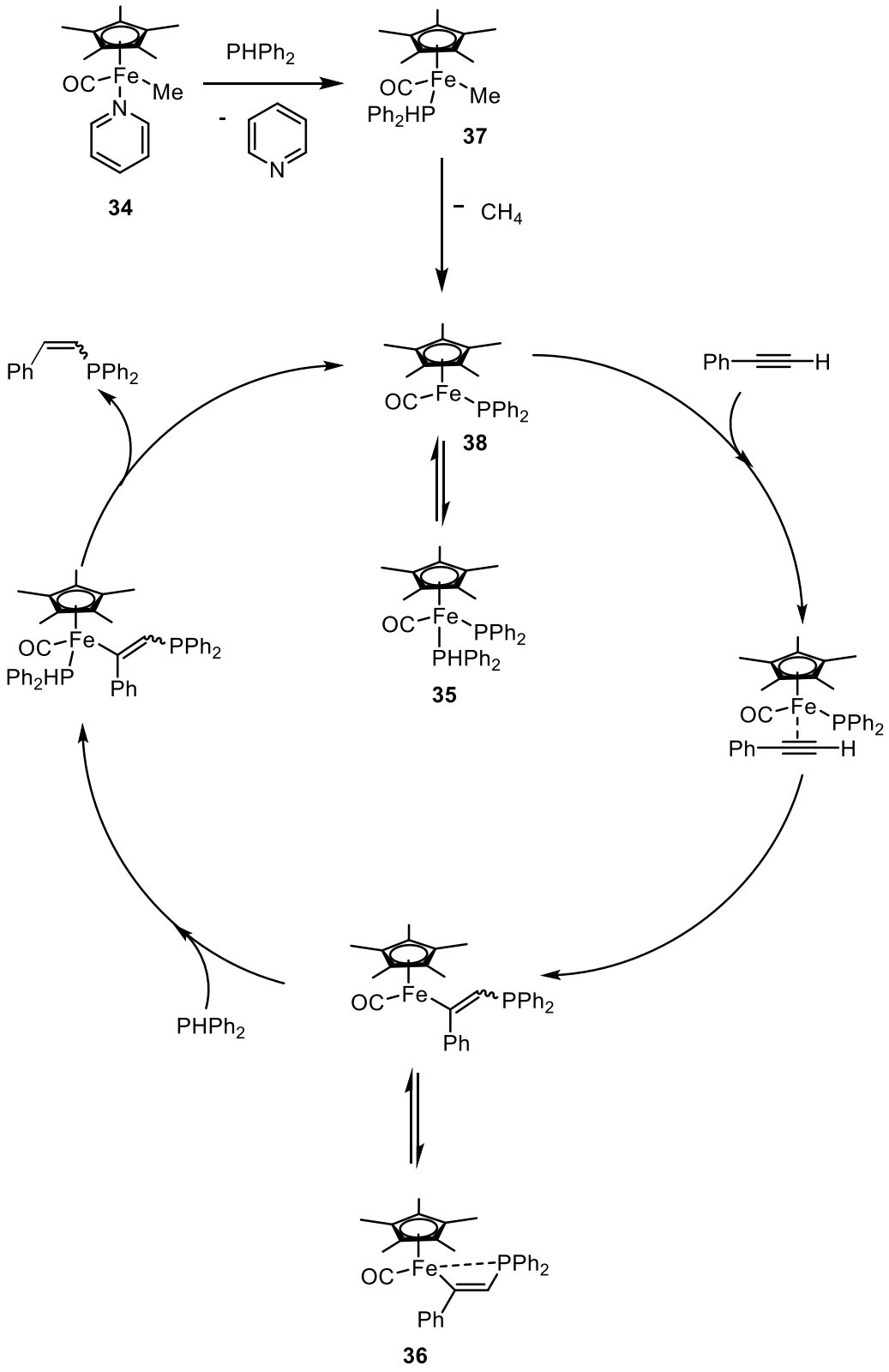

Scheme 19: Nakazawa's proposed catalytic cycle for the iron catalysed hydrophosphination of alkynes.

Conceivably loss of pyridine from the precatalyst Cp*Fe(CO)(py)(Me), (**34**) and concurrent coordination of diphenylphosphine gives the isolated compound Cp*Fe(CO)($PHPh_2$)(Me),

(**37**) which then undergoes a loss of methane *via* reductive elimination to generate the active catalyst Cp*Fe(CO)(PPh_2), (**38**). The active catalytic species is analogous to that of the catalyst in Nakazawa's double hydrophosphination study. Isolation of the phosphido species **35** provides evidence for the existence of **38** as the active species with **35** a resting state for the catalyst. The isolation of the complex **36** may at first seem perplexing as it seems to contradict the preference for the catalyst to form the *Z*-isomer in catalysis. However, some of the *E*-isomer is formed in catalysis and the isolation of this species hints at the isomerisation from *E* to *Z* previously postulated by Nakazawa. Building on the previous study with the complex $CpFe(CO)_2(Me)$, (**32**), and by isolating the *Z*-vinylphosphines, Nakazawa demonstrated that unsymmetrical bisphosphine synthesis was achievable with an iron catalyst.

Reports by Waterman and co-workers demonstrated that irradiation with visible light can give more optimal catalytic conditions towards the double hydrophosphination of alkynes.[61] As with Waterman's previous work **31** was employed as a photocatalyst and reactions gave almost quantative yields of bisphosphines at room temperature.

Work by Kays and co-workers has shown that iron catalysts (**39**) are highly effective for the hydrophosphination of isocyanates (Scheme 20).[62] Iron terphenyl complexes were used as catalysts to great effect. Intriguingly further reactivity is observed when the solvent is altered. Reactions in THF lead exclusively to hydrophosphination whilst reactions in benzene also gave a second product resulting from the insertion of two equivalents of isocyanate into a P-H bond. Altering the ratios of phosphine and isocyanate gives the di-insertion species as the major product. As with Beletskaya's study on nickel catalysed hydrophosphination a small quantity of tetraphenyldiphosphane is observed as a side product.

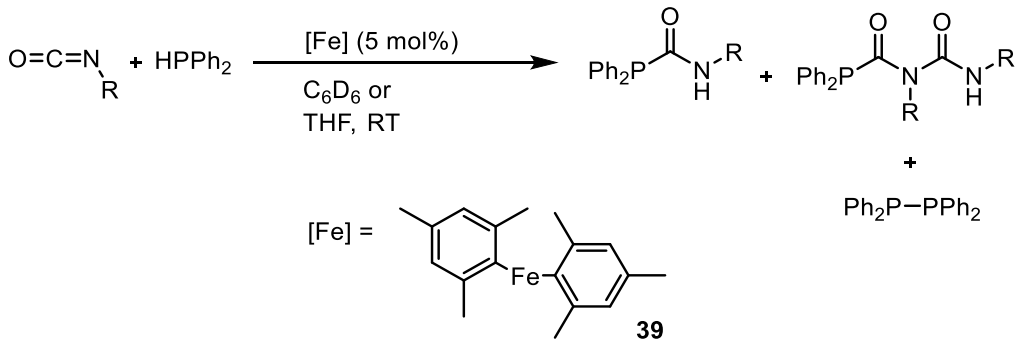

Scheme 20: Iron catalysed hydrophosphination of isocyanates by Kays.

Solvent-free organic synthesis has the potential to prevent waste and increase environmental protection through sustainability. Work by Alonso and co-workers determined that under solvent free conditions in the absence of a catalyst hydrophosphination reactions were feasible by heating the mixture of substrates at 70 °C.[63] Despite the lack of a catalyst these hydrophosphination reactions were found to be entirely regioselective for *anti*-Markovnikov addition. Remarkably, under the same conditions in the presence of a solvent such as DCM, synthetic yields were observed to be negligible. Extending the substrate scope Alonso was able to demonstrate that these solvent and catalyst-free conditions worked for a variety of activated alkene substrates. Intriguingly the most activated substrates such as ethyl acrylate were found to react quantitatively at room temperature.

Preliminary mechanistic studies into the nature of these catalyst-free hydrophosphination reactions *via* radical trapping experiments with TEMPO and cumene showed no inhibition of hydrophosphination activity. The hydrophosphination reactivity in this system is therefore not mediated by the presence of phosphine radicals. Further work by Alonso and co-workers delved deeper into the mechanistic origins of alkene hydrophosphination.[64] Deuterium labelling experiments and kinetic studies were undertaken to eliminate the less favourable reaction pathways (Scheme 21).

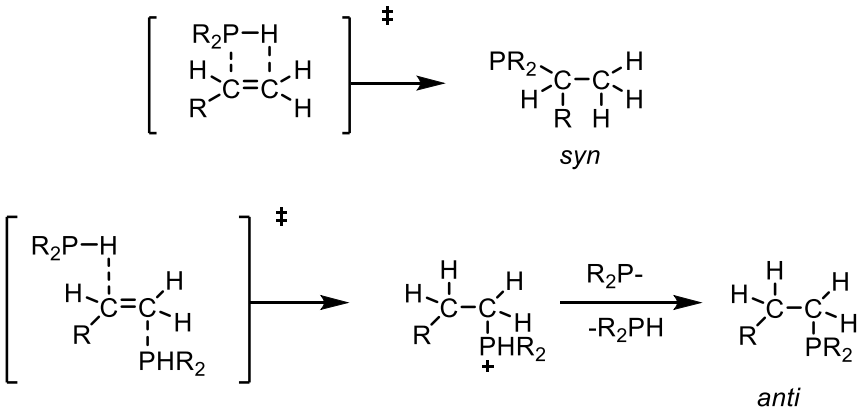

Scheme 21: Alonso's mechanistic proposal for the hydrophosphination of alkenes, which could proceed *via* a *syn* (top) or *anti* (bottom) pathway.

Taking into consideration these investigations the kinetic studies show a near second order relationship with respect to phosphine. This suggests that two equivalents of diphenylphosphine are involved in the rate determining step. Deuterium labelling studies suggest that the proton and phosphine in the product are from two separate precursor phosphine molecules. Some H/D scrambling is observed between deutero-cyclohexylacetylene and diphenylphosphine (80% D incorporation in product). This suggests that the *anti*- addition mechanism is the functional mechanistic pathway in the reaction.

It can therefore be remarked upon that hydrofunctionalisation reactions, and in particular hydrophosphination reactions, are of great interest due to the potential ability to form a great range of products, including enantiopure species, in a completely atom economical manner under mild reaction conditions. Arguably, catalysis is key to achieving optimal reaction conditions and hydrophosphination has been studied with a range of transition metal catalysts including some catalytic reports with iron. Alternative highly economical routes to catalytic bond formation in organic and main group compounds are also of great interest.

As remarked upon in Beletskaya's and Kays' hydrophosphination studies tetraphenyldiphosphane is observed as a side product. Tetraphenyldiphosphane is likely formed as a result of competitive phosphine dehydrocoupling.

1.4 - Dehydrocoupling catalysis

Catalytic reactions involving the coupling of main group compounds and the prior or successive evolution of hydrogen have grown increasingly relevant.[65-67] These reactions were first referred to as dehydrocoupling reactions as early as 1984 by Sneddon and co-workers.[68, 69] These reactions are of considerable interest from a synthetic, materials based and hydrogen storage perspective. From a synthetic perspective the formation of E-E and E-E' in a highly selective manner is appealing. Syntheses of E-E and E-E' bonds *via* dehydrocoupling are relatively atom economical with hydrogen gas the only by-product generated in the reaction (Scheme 22).

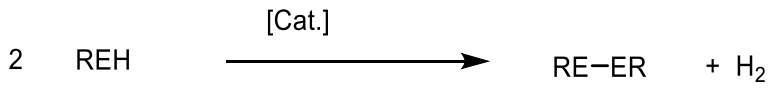

Scheme 22: A typical catalytic dehydrocoupling reaction.

Homocoupling type reactions have been explored with a plethora of main group compounds. Notably Brookhart and co-workers demonstrated that the rhodium complex [Cp*Rh{CH_2=CH(TMS)}$_2$], (**40**) is highly effective as a precatalyst for phosphine dehydrocoupling.[70] Brookhart demonstrated potent activity for P-P bond forming catalysis with this complex. Brookhart's proposed catalytic cycle is of interest. In it a Rh(V) species is postulated to play a role (Scheme 23). This seems somewhat unlikely and more plausibly it may be that the active species is in fact Rh(III) with the reaction proceeding *via* a more complex pathway.

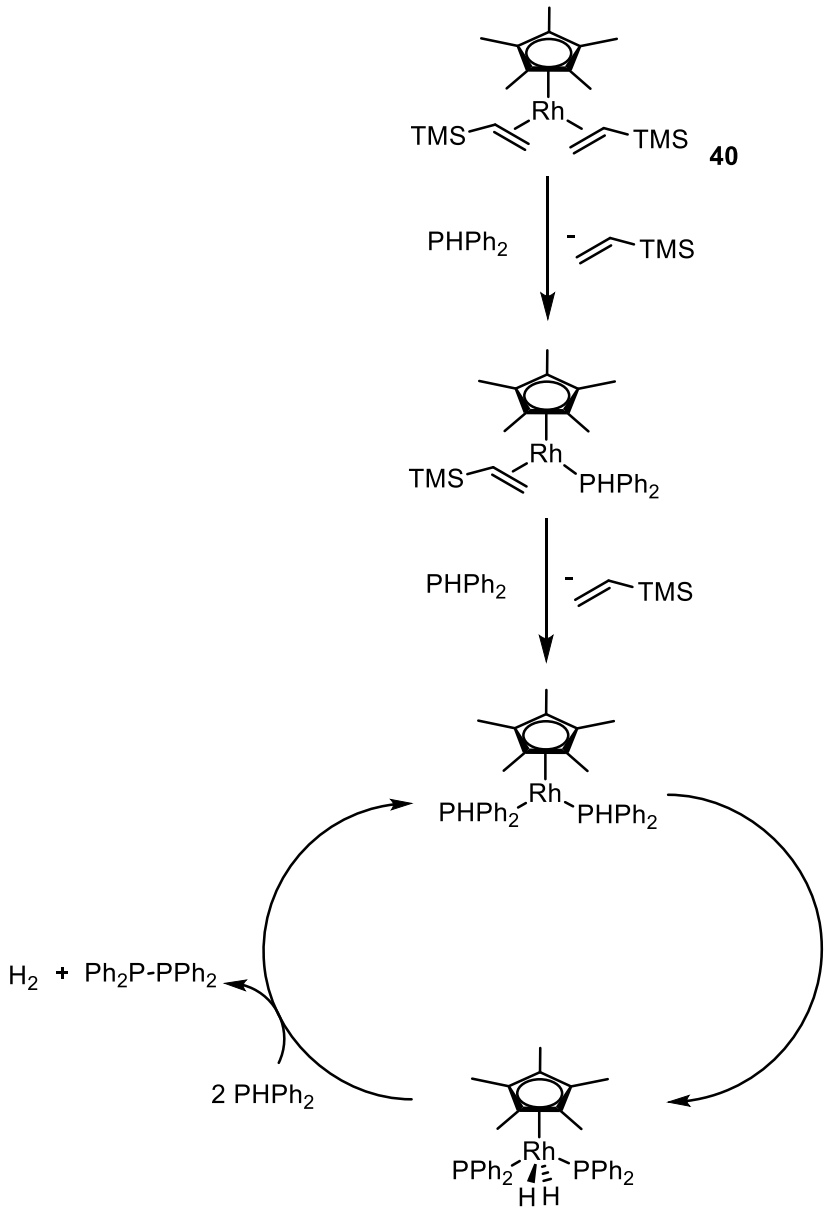

Scheme 23: Brookhart's proposed catalytic cycle for phosphine dehydrocoupling.

Leading on from this, work by Stephan and co-workers showed that catalytic phosphine dehydrocoupling was achievable with primary phosphines.[71] Reactions catalysed by titanium and zirconium complexes ([CpTi-(NP*t*Bu$_3$)(CH$_2$)$_4$] and [Cp*Zr-(NP*t*Bu$_3$)(CH$_2$)$_4$], (**41** and **42**) yielded P-P bonded cyclic phosphines. Catalysis in Stephan's study repeatedly required very stringent conditions with heating of up to 120 °C for a period of 10 days necessary with certain substrates.

Recent advances in dehydrocoupling chemistry have demonstrated that transition metals are not required in order to attain high synthetic yields.[72-74] Gessner and co-workers demonstrated that lithium carbene complexes (**43**) were highly competent at promoting phosphine dehydrocoupling (Scheme 24). Gessner's study includes an in-depth investigation into substituted secondary phosphines as well as some scope for primary phosphines.[74]

Reactions were facile with high yields achieved at low temperatures (-20 °C) in a matter of minutes. In depth mechanistic studies *via* experimental analysis and complementary DFT studies revealed that in addition to acting as a hydrogen acceptor the carbene acts as a chloride donor, the true nature of the reaction is then deduced to be a dehydrochlorination reaction.[75] Gessner's system is stoichiometric requiring the carbene to accept protons in order to progress the reaction.

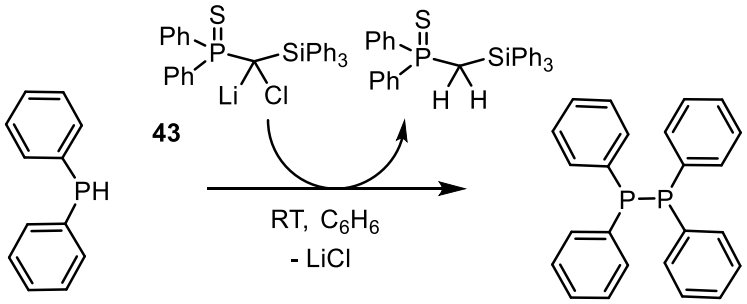

Scheme 24: Gessner's carbene mediated phosphine dehydrocoupling.

Stephan and co-workers have recently reported a metal free phosphine dehydrocoupling system.[76] Initial stoichiometric reactions between diphenylphosphine and $[Ph_3C][B(C_6F_5)_4]$, (**44**) afforded $[Ph_2(H)PPPh_2][B(C_6F_5)_4]$, (**45**); with the formation of a phosphorus-phosphorus bond suggesting potential catalytic activity. Stephan then demonstrated that by using $B(p\text{-}HC_6F_4)_3$, (**46**) as a catalyst phosphine dehydrocoupling was achievable (Scheme 25). The mechanism is postulated to proceed *via* the *in situ* formation of a frustrated Lewis pair $[Ph_2(H)PPPh_2][HB(p\text{-}HC_6F_4)_3]$, (**47**), analogous to the aforementioned compound, isolated through stoichiometric reactions.

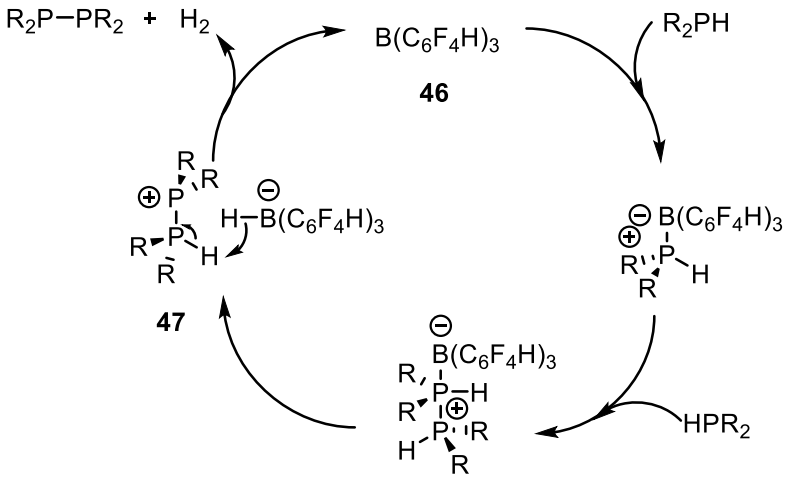

Scheme 25: Stephan's proposed borane catalysed phosphine dehydrocoupling mechanism.

The conditions required to achieve catalytic turnover are particularly forcing at a temperature of 130 °C in a time period of 120 hours. It can be noted then that while this is an early example of catalytic phosphine dehydrocoupling with a non-metal there is significant room for catalyst optimisation. Addition of a hydrogen acceptor such as *N*-benzylidene-*tert*-butylamine can greatly improve catalytic conditions. In addition to this it can be noted that Stephan's catalytic system is inherently reversible; by removing hydrogen generated in the reaction from the sealed system, catalytic conversion is increased suggesting a dynamic equilibrium in keeping with Le Chatelier's principle. Stephan has previously reported on this reversibility with transition metal catalysts.[77]

Other recent studies on phosphine dehydrocoupling catalysis have focused otherwise on rhodium catalysts.[78] Work by Tejel and co-workers has demonstrated that the hydridotris(pyrazolyl)borato rhodium complex [Rh(Tp)(C_2H_4)$_2$], (**48**) can be used in P-P bond forming catalysis *via in situ* formation of terminal rhodium phosphide species. Catalytic conditions do not show any real improvement from Brookhart's reported rhodium system and, as with previously reported systems, addition of a hydrogen acceptor (in this case ethylene) improves catalytic turnover. Tejel's system offers some further insight into rhodium catalysed phosphine dehydrocoupling *via* preliminary DFT studies and the isolation of the first reported terminal rhodium phosphide [Rh(Tp)(H)(PMe_3)(PPh_2)], (**49**).

Following on from Brookhart's initial report Tilley and co-workers determined that the rhodium complex [(dippe)Rh(η^3-CH_2Ph)], (**50**) was likewise a competent catalyst for phosphine dehydrocoupling.[79] Tilley managed to extend the substrate scope from Brookhart's initial study accessing dehydrocoupling reactivity with primary phosphines. Tilley's catalyst shows improved catalytic turnover with comparison to Brookhart's. Presumably this is due to the phosphine ligand imparting good σ-donating and π-accepting properties onto the complex that are facilitating this superior activity. In addition to homonuclear coupling Tilley demonstrated that **50** was a competent catalyst for heteronuclear dehydrocoupling in the cross coupling of phosphines and thiols (Scheme 26).

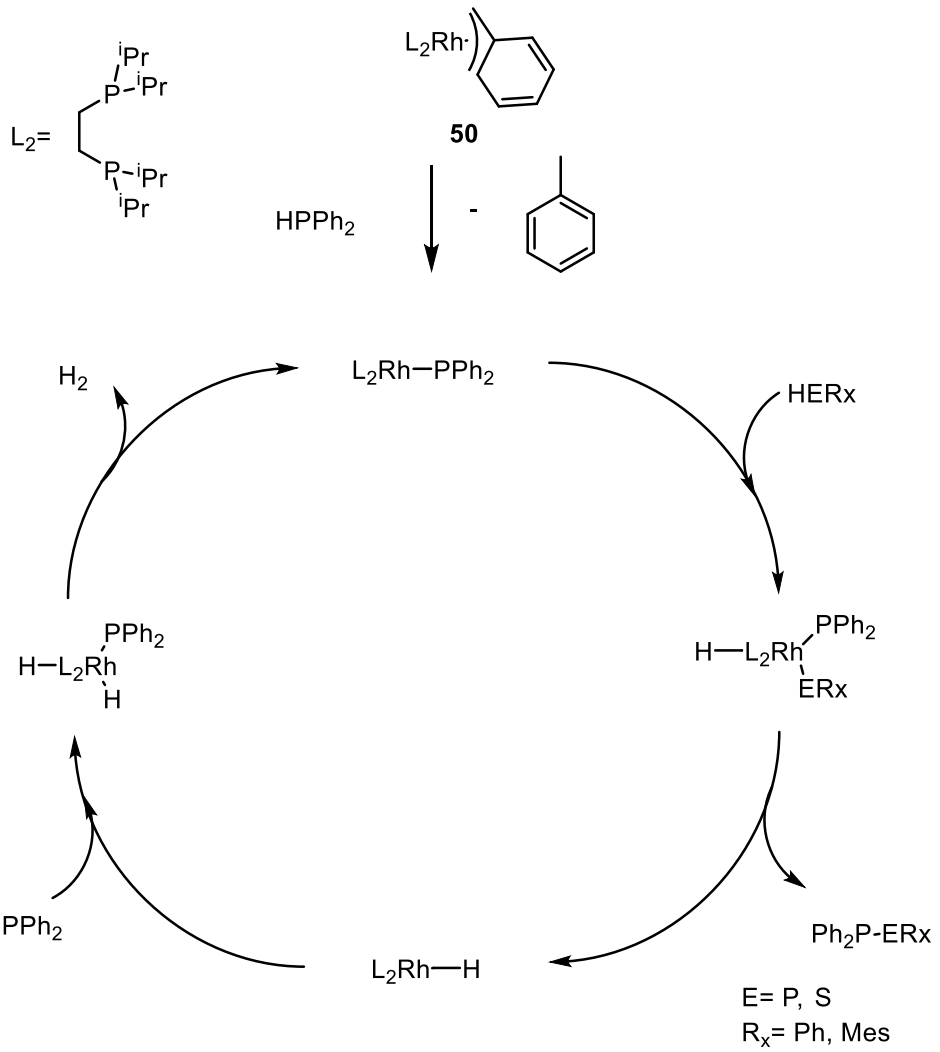

Scheme 26: Tilley's proposed catalytic cycle for homonuclear and heteronuclear dehydrocoupling.

Heteronuclear dehydrocoupling had been previously reported by Harrod and co-workers.[80] In this system the titanium complex $[Cp_2Ti(PMe_3)_2]$, (**51**) was used as a precatalyst to facilitate the cross coupling of phosphines and silanes. The titanium precatalyst promoted high catalytic activity at ambient temperatures leading to good synthetic yields of silaphosphanes (Scheme 27).

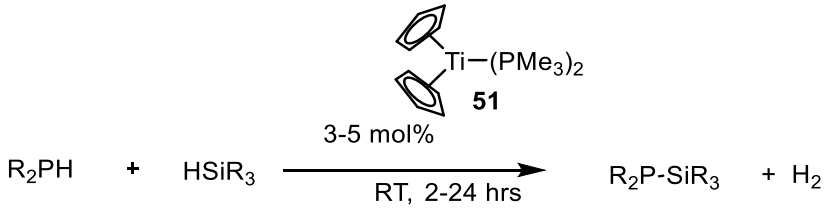

Scheme 27: Titanium catalysed heterodehydrocoupling of phosphines and silanes.

In view of this work Waterman and co-workers reported that the tripodal zirconium complex $N(CH_2CH_2NSiMe_3)_3ZrMe$, (**52**) displayed catalytic activity for hetero-dehydrocoupling of

phosphines and silanes (Scheme 28).[81] Waterman's system demonstrates that primary phosphines can be coupled to silanes which was a limitation of the previously reported study by Harrod. Waterman's system shows relatively modest catalytic activity by comparison to Harrod's wherein catalytic activity occurs at 80 °C with multiple examples of substrates requiring five to seven days to reach appreciable yields. Waterman further extended the scope of heterodehydrocoupling by demonstrating that the zirconium precatalyst was also competent at coupling phosphines to the heavier group 14 congeners: the germanes. As with silanes these coupling reactions required vigorous heating over a period of days and in certain cases led to complex mixtures of products.

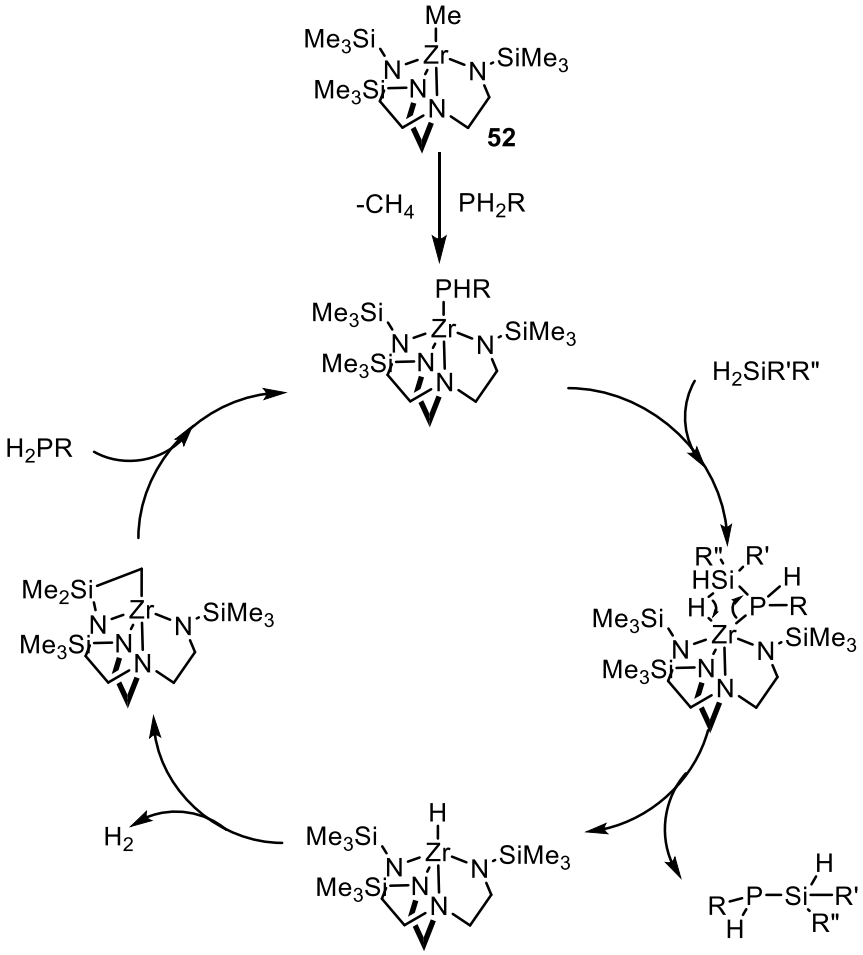

Scheme 28: Waterman's proposed catalytic cycle for phosphine silane dehydrocoupling.

Other than Harrod's and Waterman's reports very little has been described in the literature on catalytic phosphorus silicon bond formation. In stark contrast heterodehydrocoupling reactions between amines and silanes have gathered considerable interest.[82-84]

Reports of amine silane dehydrocoupling date back as early as the 1950s and focused on the synthesis of silazane materials.[85] Work by Harrod and co-workers demonstrated that copper catalysts were competent at coupling amines and silanes.[86, 87] Cross coupling reactions between benzylamine and phenylmethylsilane were achieved with copper(I) chloride employed as the precatalyst. Reactions occurred under forcing conditions, with temperatures as high as 145 °C and catalyst loadings of approximately 7 mol% required to

drive the reaction. Experimental mechanistic insight was incredibly limited. However, Harrod postulated that the reaction occured *via* σ-bond metathesis with a copper hydride acting as an intermediate.

Further studies by Harrod demonstrated that dimethyltitanocene was effective at catalysing the coupling of tertiary silanes with ammonia.[88]

Alkaline earth metals have been used to great effect in amine silane dehydrocoupling reactions. Sadow and co-workers have focused their attention on magnesium complexes as catalysts for amine silane dehydrocoupling.[89] The tridentate ligand tris(4,4-dimethyl-2-oxazolinyl)phenylborate (To^M) complexed to magnesium yielded To^MMgMe, (**53**), which was used as a precatalyst in the study. The magnesium complex was found to be highly potent at catalysing the dehydrocoupling of amines and silanes with room temperature reactions giving quantitative yields of silazanes. A modest substrate scope was explored with primary and secondary silanes reacting readily with primary amines. Tertiary silanes showed no reactivity. It is plausible that this lack of reactivity is due to steric constraints. Very little mechanistic work had been done previously on catalytic amine silane dehydrocoupling. Sadow investigated the mechanism in detail through *in situ* kinetic studies (Scheme 29).

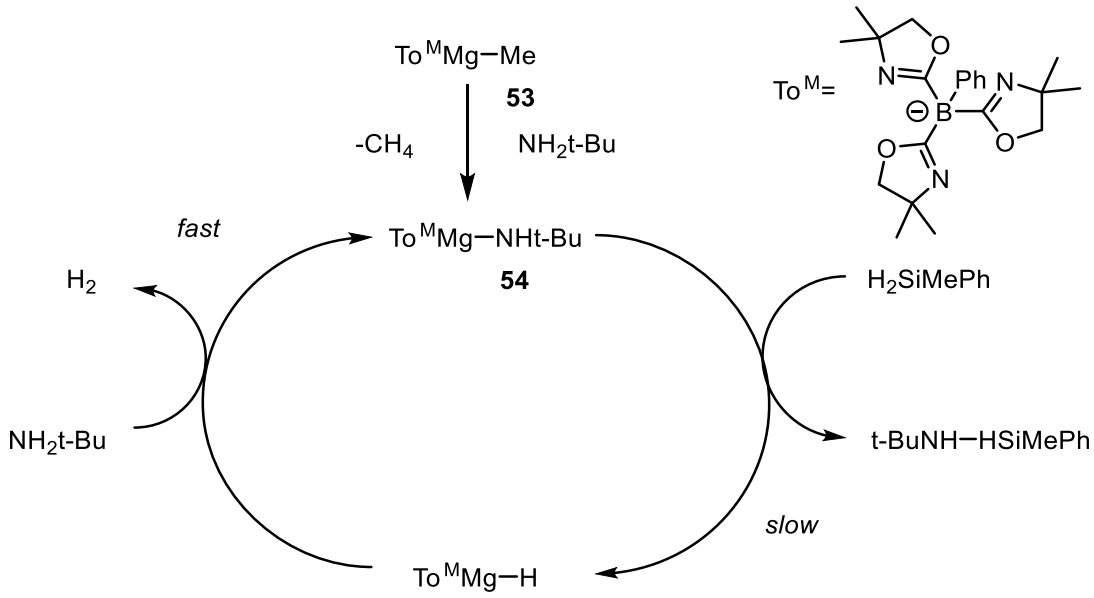

Scheme 29: Sadow's catalytic cycle for magnesium mediated amine silane dehydrocoupling

Analysis *via* proton NMR spectroscopy revealed that magnesium amide species of the type To^MMgNHR, (**54**) formed readily *via* protonolysis. These amide species can be isolated and themselves used in amine silane dehydrocoupling catalysis. This proves that magnesium amides are active in the catalytic cycle. Kinetic studies determined that the reaction was first order with respect to the magnesium catalyst, silane and zero order with respect to amine. From this it can be determined that the amine is not involved in the rate determining step of the reaction. It is therefore likely that the initial σ-bond metathesis step and sequential formation of a hydride species is the rate determining step.

Hill and co-workers demonstrated that simple group 2 amides are effective at catalysing amine silane dehydrocoupling.[90] Comparative studies of magnesium, calcium and strontium amides ($Mg(N(Si(Me)_3)_2$, $Ca(N(Si(Me)_3)_2$ and $Sr(N(Si(Me)_3)_2$; **55**, **56**, and **57**) as precatalysts uncovered some interesting trends. All three were competent as catalysts for amine silane

dehydrocoupling. Where **55** was highly effective at dehydrocoupling primary and secondary silanes with both primary and secondary amines little to no reactivity was observed with tertiary silanes. By contrast **56** shows improved reactivity towards tertiary silanes and **57** proved to be highly effective at catalysing reactions with these bulkier silanes. This is due to sterics as the ionic radii increase in the order Sr>Ca>Mg in group 2 mirrors the reactivity towards more sterically encumbered substrates. The mechanisms of the three group 2 amides were investigated *via in situ* kinetic studies (Scheme 30).

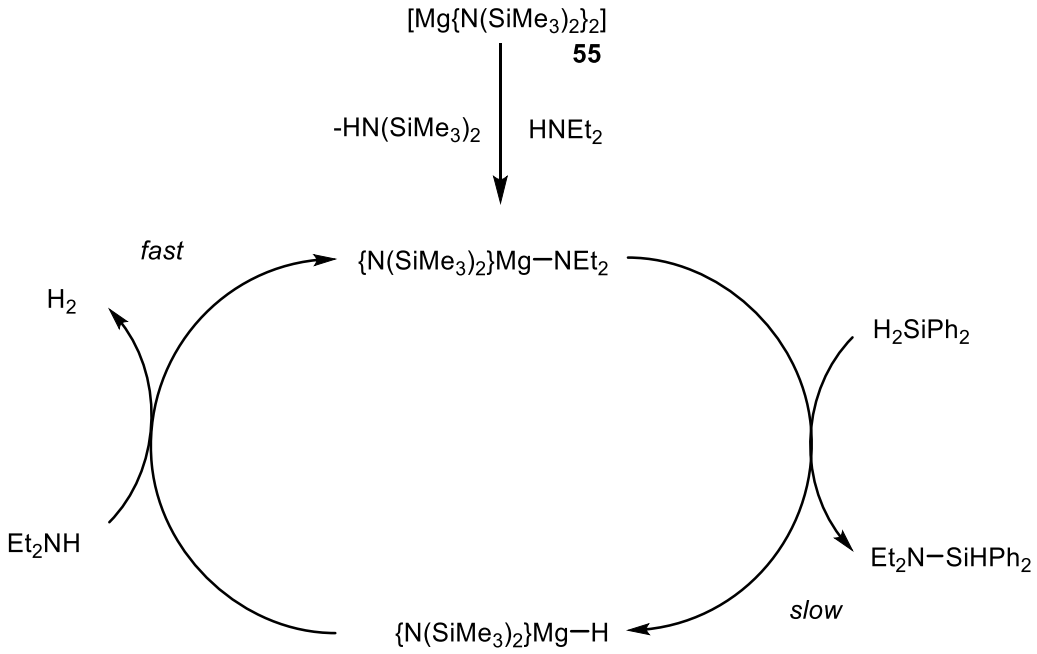

Scheme 30: Hill's catalytic cycle for magnesium mediated amine silane dehydrocoupling

Hill's kinetic studies for magnesium and calcium mediated dehydrocoupling are in agreement with Sadow's wherein there is a first order relationship with respect to catalyst and silane and a zero order relationship with respect to amine. This supports the rate determining step being the first σ-bond metathesis step forming the silazane. This indicates that the presence of an ancillary ligand has no overall effect on the mechanistic pathway. Kinetic studies determined that the mechanism for strontium is more complex than magnesium and calcium. A second order relationship with respect to catalyst was observed and a first order relationship with respect to both silane and amine. Hill postulated that the observation of a second order relationship could be due to a dimeric active catalytic site while first order relationships in silane and amine suggest both are involved in the rate determining step. In measuring the turnover frequencies with each group 2 amide, calcium was observed to have the largest turnover frequency giving the trend Ca>Sr>Mg. This observation is rationalised on the basis of an inherently more complex catalytic mechanism with respect to strontium.

Other work focusing on group 2 mediated amine silane dehydrocoupling has investigated the heavier congener barium complexes. Sarazin and co-workers used the simple barium amide $[Ba(N(SiMe_3)_2)_2{\cdot}(THF)_x]$, (**58**) as a precatalyst.[91] With its larger atomic radius barium

was found to be an excellent precatalyst for the dehydrocoupling of bulkier substrates such as tertiary silanes and secondary amines. Comparative studies with magnesium, calcium and strontium determined barium to have the highest turnover frequency. The overall trend shows an increase in TOF directly correlated to the increase in atomic radii progressing down group 2 in the order Mg<Ca<Sr<Ba. This is opposite to Hill's study where calcium amides were observed to have a higher turnover frequency than their strontium congeners. With barium determined to be the best group 2 metal in coupling secondary amines to tertiary silanes further optimisation studies were undertaken. Use of an iminoanilido ligand to form complexes of type [{N^N}Ba{N-$(SiMe_3)_2$}·$(THF)_x$], (**59**), and subsequent use as a precatalyst was found to be less efficient with respect to catalytic turnover and, as such, ancillary ligands are not a pre-requisite in this system.

Investigations into the substrate scope with barium precatalysts determined that barium amide and barium alkyl complexes had a high degree of efficacy with a wide variety of substrates. These included primary, secondary and tertiary silanes with both primary and secondary amines. Mechanistic studies *via* kinetic analyses were conducted. For convenience of monitoring the less effective precatalyst **59** was used (Scheme 31).

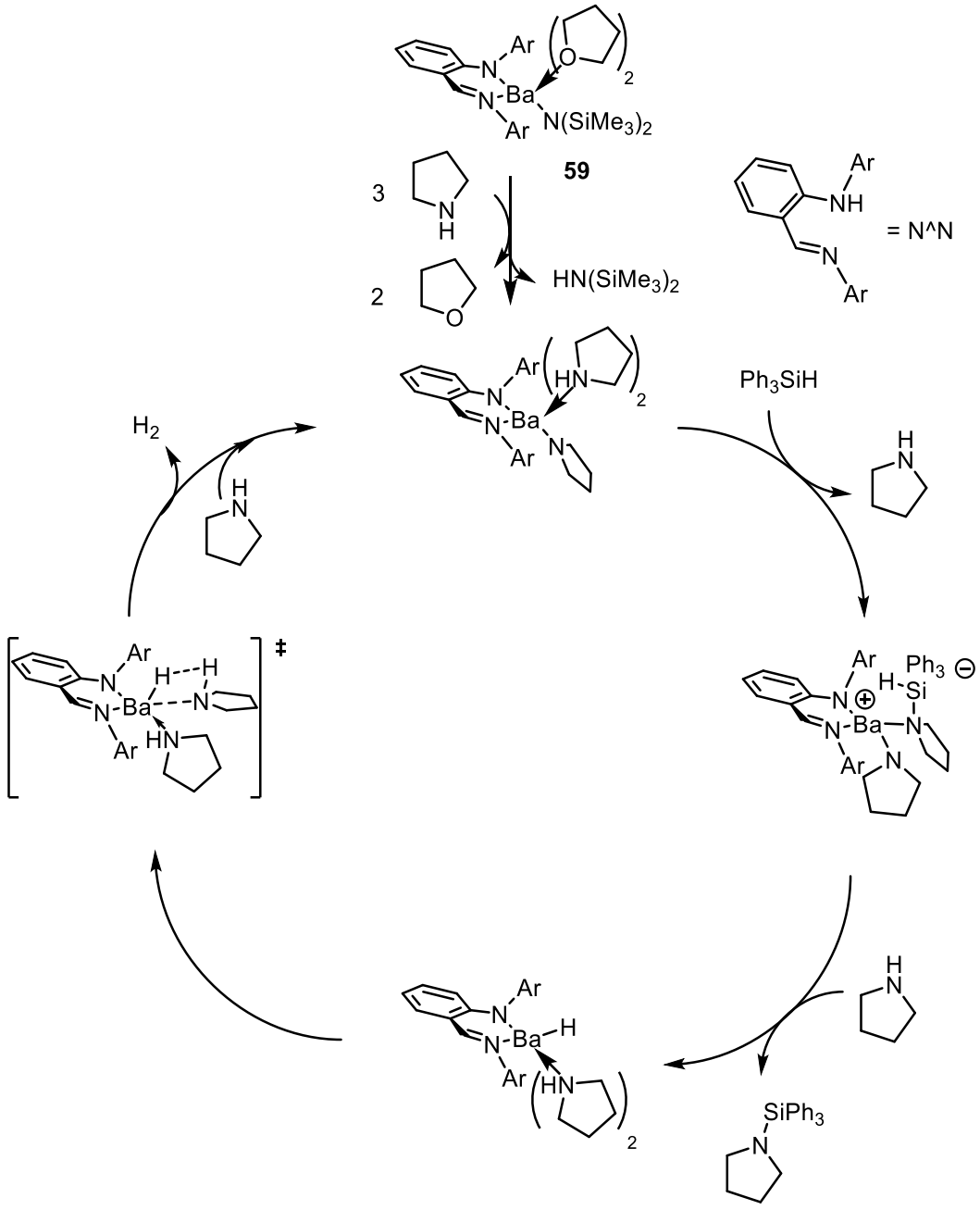

Scheme 31: Sarazin's proposed mechanism for amine silane dehydrocoupling mediated by a barium precatalyst.

The reaction was determined to be first order with respect to the precatalyst, silane and zero order with respect to amine. This is consistent with both Sadow and Hill's studies on magnesium and calcium catalysed amine silane dehydrocoupling respectively. This suggests that, as with those previous studies on group 2 catalysts, a σ-bond metathesis step involving an equivalent of silane is the rate determining step of the reaction. Sarazin postulated two plausible mechanistic pathways based on these kinetic analyses. In addition to these experimental mechanistic investigations computational studies *via* DFT were used to determine the more plausible mechanistic pathway by which the reaction proceeds. The prevailing mechanistic pathway was determined to occur in stepwise manner *via* nucleophilic attack of a barium amido species on triphenylsilane and subsequent hydrogen

transfer. Other studies have demonstrated that non-metals can catalyse the cross coupling of amines and silanes.[92]

Amine- and phosphine-borane dehydrocoupling is an extensive field and as a result iron catalysts have been described to be highly effective catalysts for the formation of P-B and N-B bonds.[93, 94] Despite their propensity towards heterodehydrocoupling reactions similar investigations into P-Si and N-Si bonds remain as of yet unexplored with base metals.

It can be remarked upon that dehydrocoupling catalysis is an incredibly promising field in synthetic main group and materials chemistry. Detailed mechanistic insight is feasible with earth abundant catalysts and high catalytic turnover frequencies can be achieved.

1.5- Aims of this thesis

This thesis will focus on the synthesis of iron(II) β-diketiminates and their use as precatalysts. As discussed this has previously been achieved by Holland and co-workers as well as Hannedouche and Gibson.[7, 13-15] The synthesised iron(II) β-diketiminate will be used in hydrophosphination reactions with alkenes. Previous reports with group 2 metal β-diketiminate complexes have shown excellent hydrophosphination reactivity towards alkenes.[21, 22] Synthetic scope and reactivity will be probed. From these results and further experiments *via* kinetic analysis the aim will be to determine a catalytic mechanism. This will be inherently difficult given the paramagnetic nature of these iron(II) complexes. Stoichiometric reactions between precatalyst and substrates will be attempted to isolate catalytic intermediates and characterise these species. Leading on from this work hydrophosphination reactions with other substrates such as alkynes and phosphinoalkenes will be attempted.[39-42] A further aim of this thesis will be to investigate other catalytic reactions with iron(II) β-diketiminates.[65-67]

Work in Chapter 2 focuses on iron(II) β-diketiminates as catalysts in phosphine dehydrocoupling reactions. Preliminary mechanistic insight is gauged through radical clock experiments and DFT studies. Solvent selection is found to play a large role in reaction selectivity with hydrophosphination reactivity reported in DCM.

Chapter 3 focuses on alkyne hydrophosphination reactions catalysed by iron(II) β-diketiminates. Regioselectivity is found to be dependant on choice of solvent and mechanistic insight is discussed. Cyclisation reactions with phosphinoalkenes and phosphinoalkynes catalysed by iron(II) β-diketiminates are discussed. Synthesis of asymmetric iron catalysts is reported.

Chapter 4 discusses heterodehydrocoupling reactions with iron(II) β-diketiminates further extending the chemistry discussed in Chapter 2. Phosphine-silane coupling reactions are investigated with good selectivity towards phosphorus-silicon bond formation reported. Further experiments discuss amine-silane coupling reactions. Mechansitic insight for amine-silane coupling is then gauged through *in situ* kinetic analyses. Lastly alcohol-silane coupling reactions are reported.

Chapter 5 investigates desilylation reactions with iron(II) β-diketiminates following work reported in Chapter 4 on amine-silane and alcohol-silane coupling reactions.

2- Dehydrocoupling of phosphines and hydrophosphination of alkenes

2.1- Dehydrocoupling of phosphines - synthesis

As discussed previously, iron(II) β-diketiminate complexes have, by and large, been scarcely investigated in catalysis. Complexes that are analogous to Hannedouche's four coordinate hydroamination precatalyst have been devised as potential precatalysts in hydrophosphination reactions.[15]

Initially work focused on the synthesis of β-diketiminate ligands, or Nacnac ligands, as they are more commonly referred to. These were achieved in good yields following methods reported in the literature *via* generation of the chloride salt followed by a basic workup (Scheme 32).[95, 96]

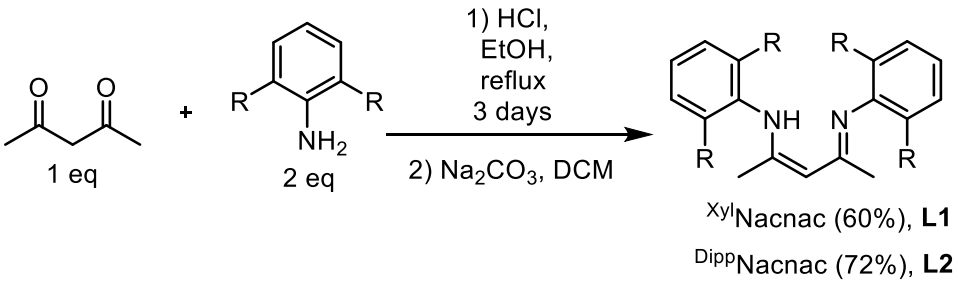

Scheme 32: Synthesis of Nacnac ligands (R= Me or ^{i}Pr).

Following the successful synthesis of the ligands the next step was to synthesise low coordinate iron complexes. Initial experiments followed Hannedouche's two step methodology for the synthesis of $LFeCH_2TMS$ type complexes (where L=^{Dipp}Nacnac or ^{Xyl}Nacnac, **L1** or **L2**) (Scheme 33). While the first step to generate the precursor heterobimetallic complexes $[LFeCl_2Li(THF)_2]$ was repeated successfully, the subsequent step to synthesise the $LFeCH_2TMS$ complexes could not be replicated.

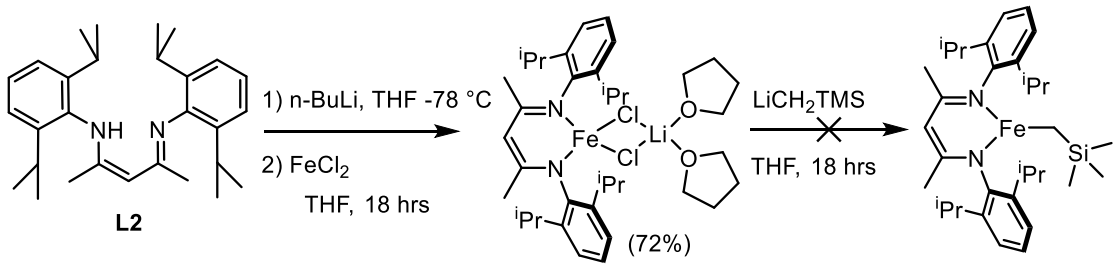

Scheme 33: Hannedouche's method for the synthesis of $LFeCH_2TMS$.

One plausible explanation as to why this route did not work could be that the iron intermediate species $[LFeCl_2Li(THF)_2]$ is relatively unstable and highly sensitive. As a compound it is therefore difficult to work with in further chemical procedures. Previous reports would seem to agree with this hypothesis.[97]

An alternative synthesis was then sought from the literature. The procedure reported by Hessen and co-workers as a one pot synthesis was found to be more readily reproduceble (Scheme 34).[7]

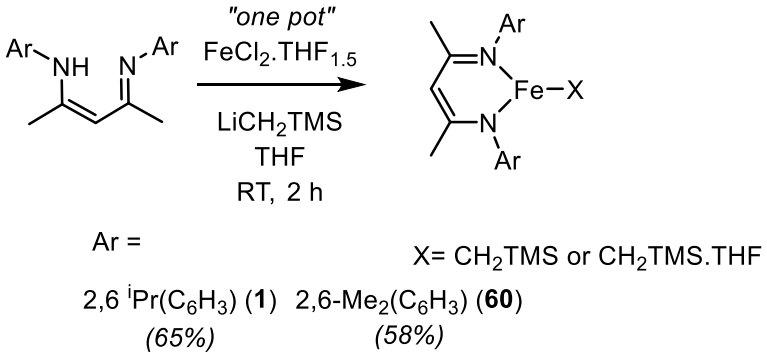

Scheme 34: One pot synthesis of the iron complexes $LFeCH_2TMS$ (where L=^{Xyl}Nacnac (**L1**) or ^{Dipp}Nacnac (**L2**)).

The $LFeCH_2TMS$ complexes were synthesised in good yields and, surprisingly, were an improvement on those reported in Hessen's protocol (65% versus 27% for **1**). Crystals were grown of both complexes; interestingly $^{Dipp}LFeCH_2TMS$ (**1**) (Figure 8) crystallised as the expected three-coordinate structure (Figure 9) reported by Hessen whereas the novel complex $^{Xyl}LFeCH_2TMS$ (**60**) (Figure 9) crystallised with THF as a ligand and is therefore a four coordinate structure analogous to Hannedouche's precatalyst (Figure 9). This can be attributed to the increased steric hindrance due to bulkier isopropyl groups on the aromatic rings and the overall increased steric bulk associated with the ^{Dipp}Nacnac ligand. The steric constraints of the bulkier ancillary ligand facilitate the isolation of the three coordinate "THF free" complex.[4] The Fe-N-C angle in $^{Dipp}NacnacFeCH_2TMS$ (**1**) is 114.1(2) ° whereas the Fe(1)-N(1)-C(6) angle at $^{Xyl}NacnacFeCH_2TMS.THF$ (**60**) is 116.2(11) °. By contrast the N(1)-Fe(1)-N(2) angle in $^{Dipp}NacnacFeCH_2TMS$ (**1**) is larger at 93.84(14) ° whereas in $^{Xyl}NacnacFeCH_2TMS.THF$ (**60**) it is 92.42(6) °. The Fe(1)-N(1) (1.994(3) Å and 2.015(14) Å respectively) and N(1)-C(6) bond lengths (1.446(5) Å and 1.439(2) Å) in both complexes are almost identical, as expected given the similarities in the structures of the complexes. The Fe(1)-C(30) and Fe(1)-C(22) bond lengths (2.026(4) Å and 2.0613(18) Å) likewise do not show significant disparity. Selected bond lengths and angles are listed below (Tables 1-4).

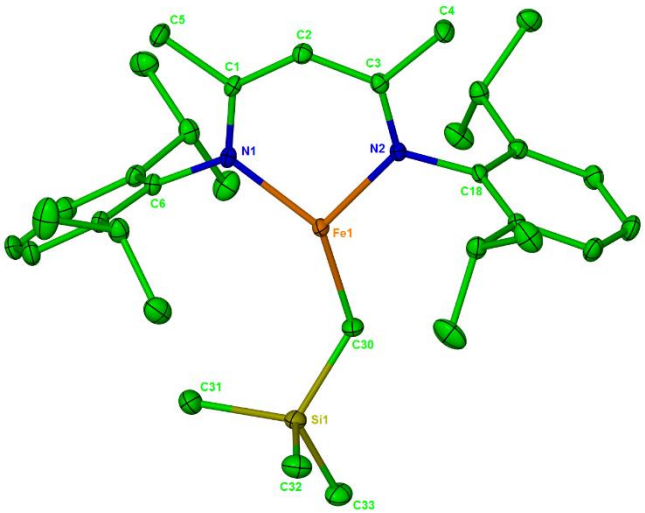

Figure 8: Crystal structure of complex **1**. Ellipsoids displayed at 50% probability.

Table 1: Selected bond lengths for complex **1**

Atoms	Bond length (Å)
Fe(1)-N(1)	1.994(3)
Fe(1)-C(30)	2.026(4)
Fe(1)-N(2)	2.002(3)
Si(1)-C(30)	1.844(4)
N(1)-C(6)	1.446(5)
N(2)-C(18)	1.440(5)
N(2)-C(3)	1.315(5)

Table 2: Selected bond angles for complex **1**

Atoms	Bond angle (°)
N(1)-Fe(1)-N(2)	93.84(14)
N(2)-Fe(1)-C(30)	123.58(16)
C(30)-Si(1)-C(31)	110.7(2)
N(1)-Fe(1)-C(30)	141.85(16)
C(1)-N(1)-Fe(1)	124.0(3)
C(3)-N(2)-C(18)	120.7(3)
C(6)-N(1)-Fe(1)	116.6(3)

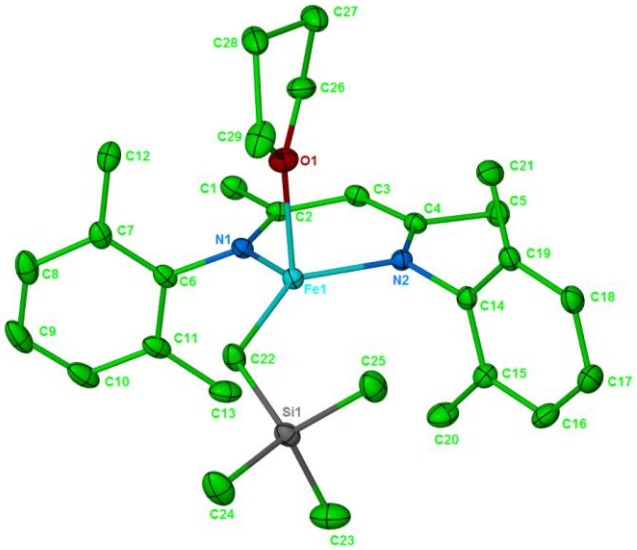

Figure 9: Crystal structure of **60.** Ellipsoids displayed at 50% probability.

Table 3: Selected bond lengths for complex **60**

Atoms	Bond length (Å)
Fe(1)-N(2)	2.0155(14)
Fe(1)-C(22)	2.0613(18)
Fe(1)-N(1)	2.0215(14)
Fe(1)-O(1)	2.2101(13)
N(1)-C(2)	1.334(2)
N(1)-C(6)	1.439(2)
Si(1)-C(22)	1.8378(19)

Table 4: Selected bond angles for complex **60**

Atoms	Bond angle (°)
N(2)-Fe(1)-N(1)	92.42(6)
N(1)-Fe(1)-C(22)	119.32(7)
N(1)-Fe(1)-O(1)	97.19(5)
C(22)-Si(1)-C(23)	112.00(11)
C(23)-Si(1)-C(25)	108.91(13)
N(2)-Fe(1)-C(22)	139.11(7)
N(2)-Fe(1)-O(1)	95.08(6)

In initial test reactions the iron complexes were investigated for catalytic activity in the presence of diphenyl phosphine and range of alkenes with benzene used as a solvent. It was anticipated that these complexes might show some catalytic activity towards intermolecular hydrophosphination. However, no intermolecular hydrophosphination was observed under these conditions. Surprisingly what was observed was catalytic production of tetraphenyldiphosphane as evidenced *via* proton and $^{31}P\{^{1}H\}$ NMR; the key peak in the $^{31}P\{^{1}H\}$ NMR spectrum is a singlet at - 13.8 ppm, whereas if hydrophosphination of an activated alkene such as styrene had taken place one would expect to observe a singlet at -15.0 ppm.[98] This observed reactivity is an example of a dehydrocoupling reaction (Scheme 35).[65] As discussed previously this sort of reactivity towards phosphines, at the time of discovery was and remains, unknown for iron complexes. Given the novelty of this result, the reaction conditions were optimised for the catalytic dehydrocoupling of diphenyl phosphine, the results of which are detailed below (Table 5).

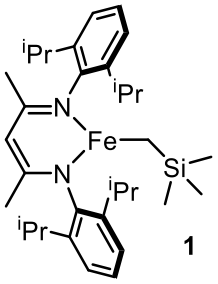

1

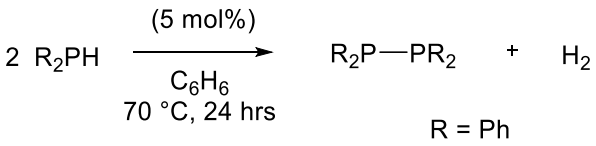

Scheme 35: Iron catalysed dehydrocoupling of phosphines.

Table 5: Optimisation table for the dehydrocoupling of diphenyl phosphine.

Entry	***[Fe]***	*Loading (mol%)*	*Conditions*	***P_2Ph_4 (%)***[a]
1	***60***	*100*	*RT, 30 min*	*100*
2	***60***	*5*	*50 °C, 24 h*	*22*
3	***60***	*5*	*70 °C, 24 h*	*71*
4	***1***	*100*	*RT, 30 min*	*100*
5	***1***	*5*	*50 °C, 24 h*	*48*
6	***1***	*5*	*70 °C, 18 h*	*68*
7	***1***	*5*	*70 °C, 24 h*	*100*
8[b],[c]	***1***	*5*	*50 °C, 24 h*	*100*
9	***$FeCl_2.THF_{1.5}$***	*5*	*70 °C, 24 h*	*Trace*
10[d]	***1***	*5*	*70 °C, 24 h*	*100*
11[e]	***1***	*5*	*RT, 24 h*	*15*
12[f]	***1***	*5*	*70 °C, 24 h*	*78*
13[d]	***1***	*5*	*50 °C, 24 h*	*46*
14[d]	***1***	*5*	*70 °C, 18 h*	*66*

Conditions: $HPPh_2$ (0.5 mmol), C_6H_6 (0.35 mL). [a] Based on loss of loss of P–H signal from ^1H NMR spectra, using 1,3,5-trimethoxybenzene as an analytical standard. [b] 1 mmol 1-hexene added. [c] By $^{31}P\{^1H\}$ NMR spectroscopy. [d] Solvent free [e] Solvent free and degassed after 6 hr intervals. [f] Addition of mercury (4 drops).

Stoichiometric reactions with **1** and **60** both give full conversion to tetraphenyldiphosphane at room temperature (Entries 1 and 4). At a catalyst loading of 5 mol%, **1** was determined to be a better catalyst than **60** for phosphine dehydrocoupling (Entries 2-3 and 5-7). Full conversion is achieved with 5 mol% **1** at 70 °C in 24 hours. These conditions were taken as the optimal reaction conditions. Presumably, as previously reported by Brookhart, the presence of an alkene helps to drive forward the reaction (Entry 8).[70] Conceivably an on-metal process leads to transfer hydrogenation of the unsaturated alkene. Further evidence for this will be discussed in Chapter 4. Replacing **1** with $FeCl_2.THF_{1.5}$ (Entry 9) led to only trace quantities of tetraphenyldiphosphane.

Dehydrocoupling reactions in the absence of solvent (Entries 10 and 13-14) gave the same spectroscopic conversions as in the presence of benzene. This shows that solvent-free reactions are possible, adding to the atom economy. Attempts to lower the temperature, catalyst loading and reaction time proved unsuccessful. By applying a vacuum to the sample (Entry 11) it would be expected that hydrogen would be removed from the system which, following Le Chatelier's principle, should push the equilibrium to the right hand side. However when this was attempted at regular intervals no increase in conversion from the previously stated optimised conditions was observed.

Having established that the reaction works well in benzene, the reaction was attempted in other solvents to determine whether this would lead to improved reactivity. When the reaction was attempted in acetonitrile, toluene or THF, decreased conversion was observed under the same reaction conditions. By stark contrast in DCM with styrene present no dehydrocoupling was observed. Instead hydrophosphination occurred to give the *anti*-Markovnikov addition product.

With optimised dehydrocoupling conditions in hand, a range of secondary phosphines were then synthesised following a literature procedure reported by Busacca and co-workers (Scheme 36).[30] In Busacca's two step methodology diethyl phosphite is added to two equivalents of Grignard reagent. This forms a secondary phosphine oxide. The next step involves reducing the phosphine oxide and requires multiple equivalents of reductant in order to enable high synthetic yields. If a heteroatom functional group is present on the aromatic rings then more DIBAL-H is required as aluminium coordinates to these functional groups. Therefore an even greater excess of reductant is required in order to synthesise these phosphines. This method is well cited and is useful in that it can be done at room temperature. Alternative methodologies using silanes have been reported but these often require forcing conditions with long reaction times (18 h) and heating to high temperatures (110 °C).[99]

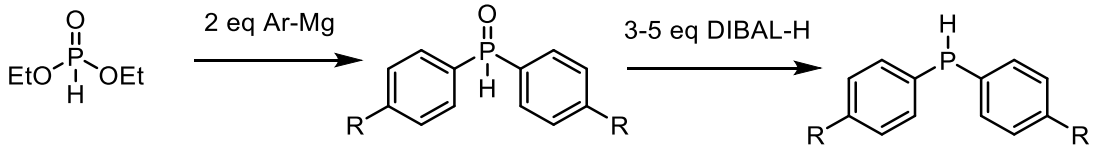

Scheme 36: Busacca's synthesis of secondary phosphines.

While the initial Grignard reactions to synthesise the secondary phosphine oxides could be repeated with relative ease, the subsequent step to reduce the oxide to the secondary phosphine was far from trivial. Problems were encountered due to poor solubility of certain phosphine oxide substrates (*para*-NMe_2, *para*- and *ortho*-OMe). Separations were difficult often with gelation occurring. This was determined to be due to co-crystallisation of the phosphine with its precursor phosphine oxide as verified *via* NMR. However, despite these challenges, high yields of substituted secondary phosphines were achieved.

The optimised catalytic conditions (70 °C, 24 h, C_6H_6) were then used to test the phosphines in dehydrocoupling reactions, the results of which are detailed below (Table 6).

Table 6: Substrate scope for the iron catalysed dehydrocoupling of secondary phosphines.

Entry	*R_2PH*	*Product*	*Spec. Yield (%)[a]* *[Isolated Yield (%)]*
1	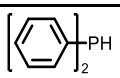	***P_2Ph_4***	*100 [85]*
2	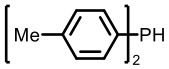	***$P_2(p\text{-}tolyl)_4$***	*95 [76]*
3[b]	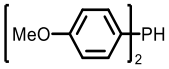	***$P_2(p\text{-}OMeC_6H_4)_4$***	*33 [-]*
4[b]	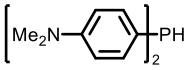	***$P_2(p\text{-}NMe_2C_6H_4)_4$***	*100 [60]*
5	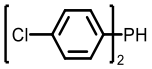	***$P_2(p\text{-}ClC_6H_4)_4$***	*90 [82]*
6	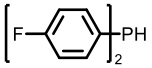	***$P_2(p\text{-}FC_6H_4)_4$***	*100 [90]*
7	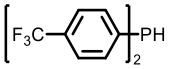	***$P_2(p\text{-}CF_3C_6H_4)_4$***	*72 [57]*
8	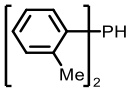	***$P_2(o\text{-}MeC_6H_4)_4$***	*36 [-]*
9[b]	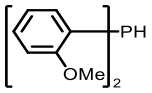	***$P_2(o\text{-}OMeC_6H_4)_4$***	*10 [-]*
10[c]	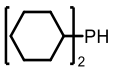	***$P_2(C_y)_4$***	*28 [-]*

*Conditions: 5 mol% **1**, HPR_2 (0.5 mmol), C_6H_6 (0.35 mL). [a] Based on loss of loss of P–H signal from ^{1}H NMR spectra, using 1,3,5-trimethoxybenzene as an analytical standard. [b] 100 °C, 24 hrs. [c] 10 mol %, 120 °C, 72 hrs.*

The catalytic system shows high tolerance for a range of different functional groups. Higher reaction temperatures were required in order to facilitate conversion of phosphines that proved to be poorly soluble in benzene (HP(*p*-$NMe_2C_6H_4)_2$, Table 6, Entry 4) and HP(*o*-$MeOC_6H_4)_2$, Table 6, Entry 9) and HP(*p*-$MeOC_6H_4)_2$, Table 6, Entry 3). The less activated and commercially available phosphine dicyclohexyl phosphine (Table 6, Entry 10) was also tested. Similarly, this substrate required higher temperatures and longer reaction times in order to convert it to the dehydrocoupled product. The commercially available primary phosphines phenyl phosphine and cyclohexyl phosphine were then investigated as they have previously been reported to show dehydrocoupling reactivity (Scheme 37). [79, 100]

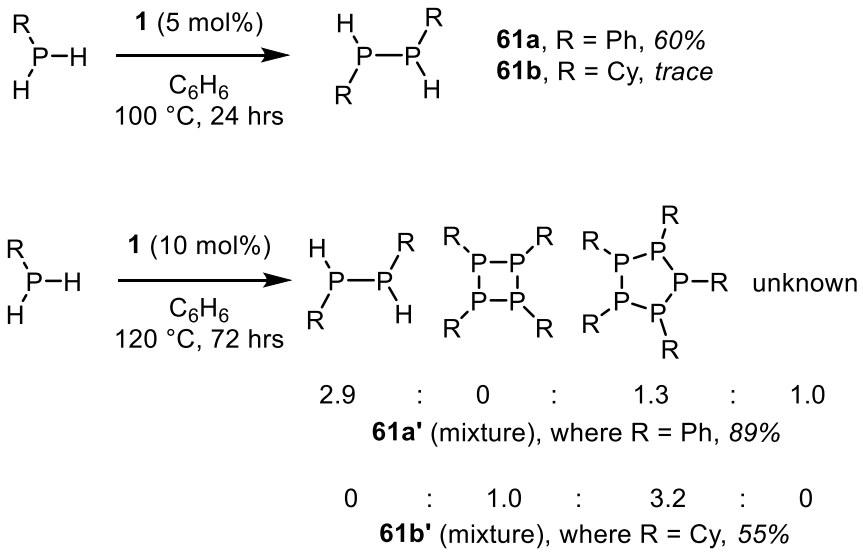

Scheme 37: Dehydrocoupling of primary phosphines.

Again these substrates required higher reaction temperatures and longer reaction times but what is notable is that high conversion can be achieved (Scheme 37). At higher reaction temperatures cyclic four and five membered ring formation occurs presumably with the release of the equivalent number of hydrogen molecules (H_2). Formation of a three membered cyclic phosphine is not observed. Ring strain is likely to be a key factor with respect to this observation as a three membered ring would be too strained disfavouring its formation. Likewise higher rings such as seven-membered rings are not observed on a similar basis. Formation of four and five-membered rings has been previously shown to occur *via* a stepwise mechanism as reported by Wright and co-workers.[101] However preliminary mechanistic experiments on this system led to the discovery that it displays radical character and therefore it can be inferred that a more complex mechanism is at work.

2.2 - Mechanistic considerations

2.2.1 – Radical trap studies

Tests were carried out to determine whether or not the reaction is radical mediated. Diphenylphosphine can produce radicals in the presence of a radical source as has been reported in previous studies.[98] The radical trap TEMPO was added to the reaction mixture at a 20 mol% loading. This led to a significant decrease in chemical yield (from 100 to 20%). This suggests that the reaction mechanism is mediated by radicals. Repeat experiments in the presence of the "radical clock" (iodomethyl)cyclopropane provided further evidence that radicals are present as intermediates in this system (Scheme 38).

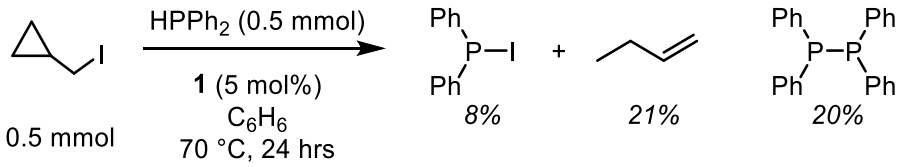

Scheme 38: Radical clock experiment.

A radical clock is a substrate that in the presence of radicals will undergo radical ring opening, radical cyclisation or 1,2-migration in accordance with the rate of the reaction. [102, 103] This can be incredibly useful when determining the kinetics and mechanism of radical mediated reactions. In this case (iodomethyl)cyclopropane is observed to undergo a ring opening reaction forming 1-butene. This occurs by a radical mechanism and implicates radical species in the phosphine dehydrocoupling mechanism. Diphenylphosphine iodide is observed (8% of crude reaction mixture, Figure 11) this suggests that phosphine radicals are formed which in this case terminate by reacting with the radical clock (Scheme 39). This reaction and loss of iodide in turn forms a methyl cyclopropyl radical which undergoes a ring opening reaction. A subsequent termination reaction with diphenylphosphine generates but-1-ene (21% of crude reaction mixture, Scheme 38, Figure 10). This can only occur in the presence of radicals; hence the products observed show that radicals form in reactions with **1**. A sharp decrease (20% of crude reaction mixture) in yield of tetraphenyldiphosphane is observed suggesting its formation is dependent on radicals forming *in situ* which have largely been trapped by the radical clock.

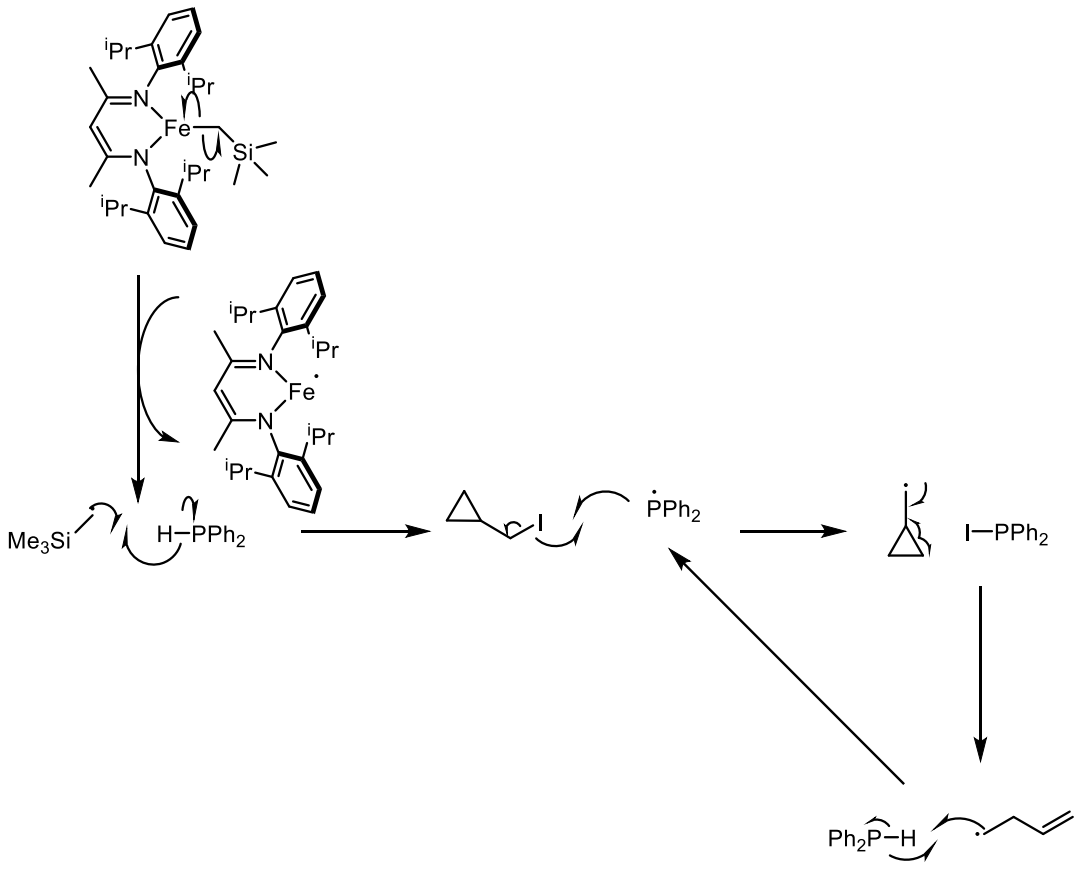

Scheme 39: Radical ring opening cyclisation (origin of experimental products).

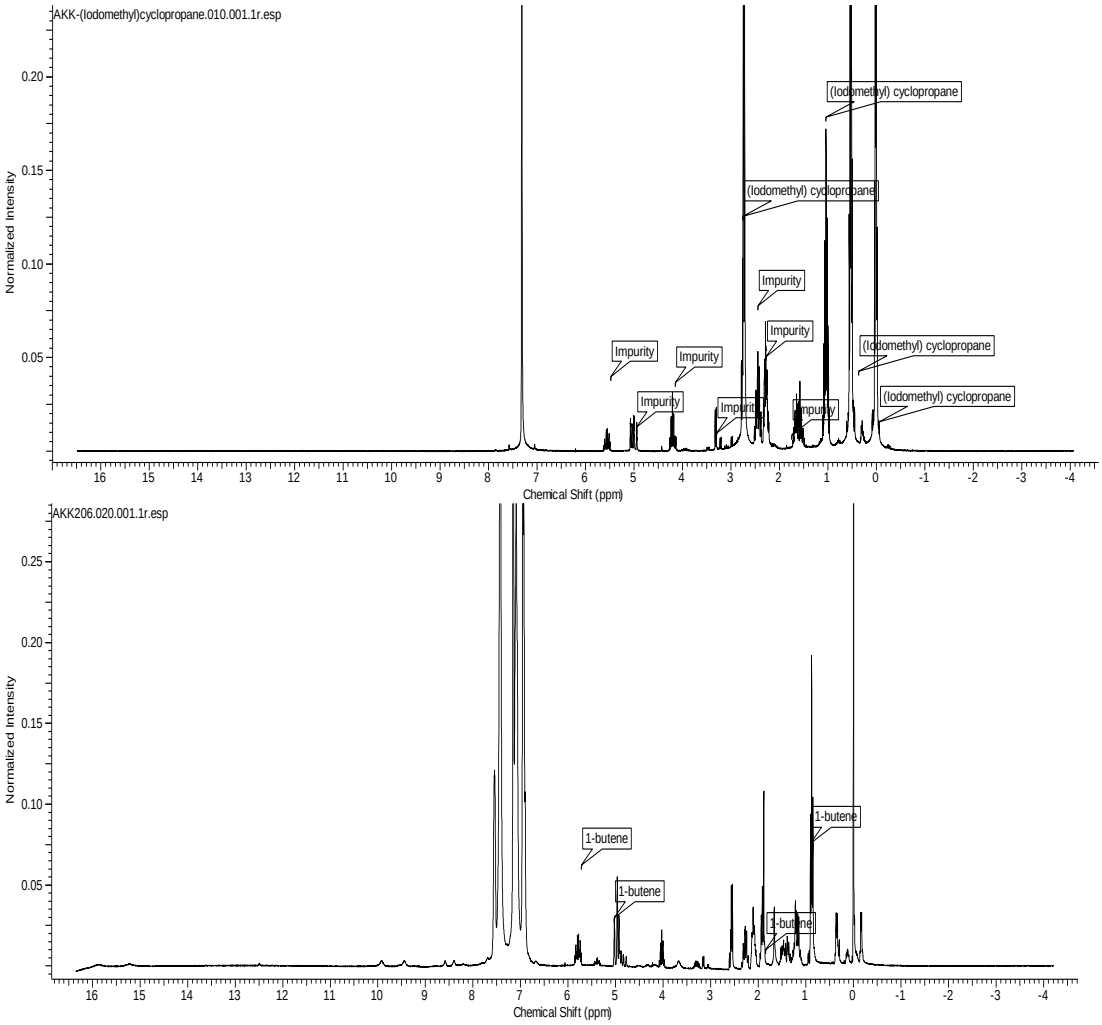

Figure 10: Top: ^{1}H NMR (300 MHz, C_6D_6, 298 K) spectrum of (iodomethyl)cyclopropane prior to addition to reaction mixture. Bottom: ^{1}H NMR (300 MHz, C_6D_6, 298 K) spectrum of reaction mixture with 1 eq. (iodomethyl)cyclopropane added. 1-Butene is observed.

The products of the radical clock experiment provide evidence for the presence of phosphine radicals in the reaction. The ^{1}H NMR spectrum taken after the radical clock experiment shows that 1-butene has been formed from the ring opening of (iodomethyl)cyclopropane with loss of iodine. The ^{31}P NMR spectrum indicates diphenyl phosphine iodide is present which has been formed from a diphenylphosphine radical.

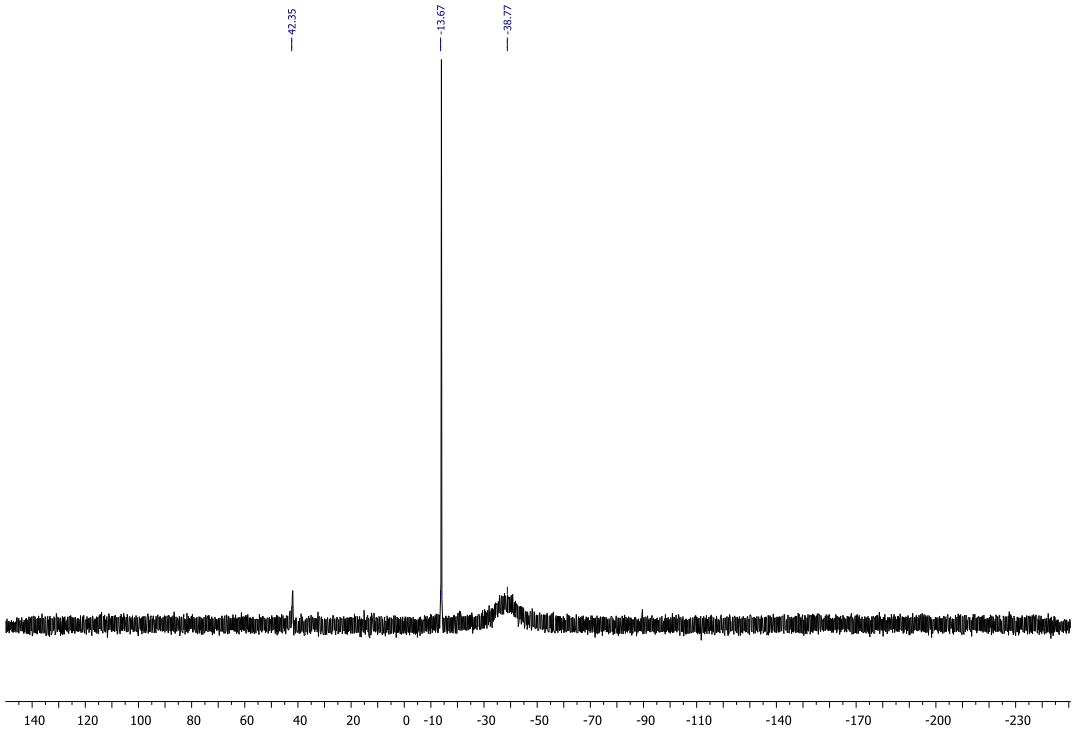

Figure 11: $^{31}P\{^{1}H\}$ NMR (121 MHz, C_6D_6, 298 K) spectrum of the radical clock experiment-evidence for the formation of Ph_2P-I (42.4 ppm).[104]

As with the addition of TEMPO to the reaction mixture, the reactivity was hindered with a depleted spectroscopic conversion of 20%. This observation and the formation of diphenylphosphine iodide suggest that phosphorus centred radicals are forming in the reaction. Stoichiometric reactions of (iodomethyl) cyclopropane with ^{Dipp}LFeCH$_2$TMS (**1**) led to the formation of a new paramagnetic iron species (^{Dipp}LFe-I) and trimethylsilyl pent-1-ene (Scheme 40, Figure 12).

Upon reacting **1** with (iodomethyl) cyclopropane a colour change is observed from yellow to red. The red complex formed is sparingly soluble in benzene; nevertheless ^{1}H NMR confirms the complete consumption of **1** and the formation of a new paramagnetic iron complex. The iron complex formed in the reaction is assigned as ^{Dipp}LFe-I (**62**) as the weak NMR signals (^{1}H NMR (400 MHz, C_6D_6) 18.06 (4H, m-CH), 8.75 (12H, iPr-CH$_3$), 4.34 (12H, iPr-CH$_3$), -19.55 (4H, iPr-CH), -27.90 (2H, p-CH), -62.33 (6H, c-CH$_3$), -88.22 (1H, α-CH)) are comparable with ^{Dipp}LFe-Br·THF (**63**) and iron β-diketiminates are known to be halophilic.[6, 8] An iron radical species formed from **1** ring opens (iodomethyl) cyclopropane forming the iron iodide species. Further evidence for this is provided by the reaction of **1** with another radical clock (chloromethyl) cyclopropane. The paramagnetic iron species formed in this reaction is the previously reported chloro dimer [^{Dipp}LFeCl]$_2$ (**64**).[97] After the halide has been abstracted CH$_2$TMS radicals then react with a ring opened 1-butenyl radical in a radical termination step forming TMS-pent-1-ene. This volatile compound was observed through vacuum distillation of the crude reaction mixture and characterisation of the volatiles. With respect to iron radicals, the role of the β-diketiminate ligand is likely to be non-innocent with resonance effects stabilising radical intermediates.

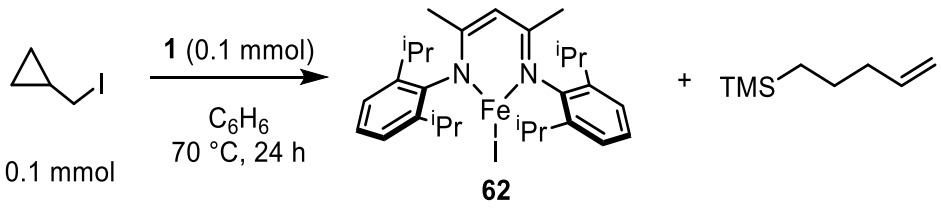

Scheme 40: Stoichiometric reaction of the radical clock with $^{Dipp}LFeCH_2TMS$

This observation suggests that the formation of iron centred radical species is occurring as well as phosphorus centered radicals as proposed (Scheme 39). In a previous study during the synthesis of **1** from the iron(III) chloro complex $^{Diip}LFeCl_2$ (**65**), Hessen and co-workers reported that $TMSCH_2CH_2TMS$ was formed as a by-product.[7] This occurs as a result of CH_2TMS radicals forming during the reaction. This demonstrates that **1** can act as a radical source.

The isolation of reactive intermediates and the identity of the active catalytic species were sought in order to definitively determine the reaction mechanism.

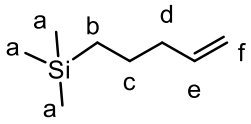

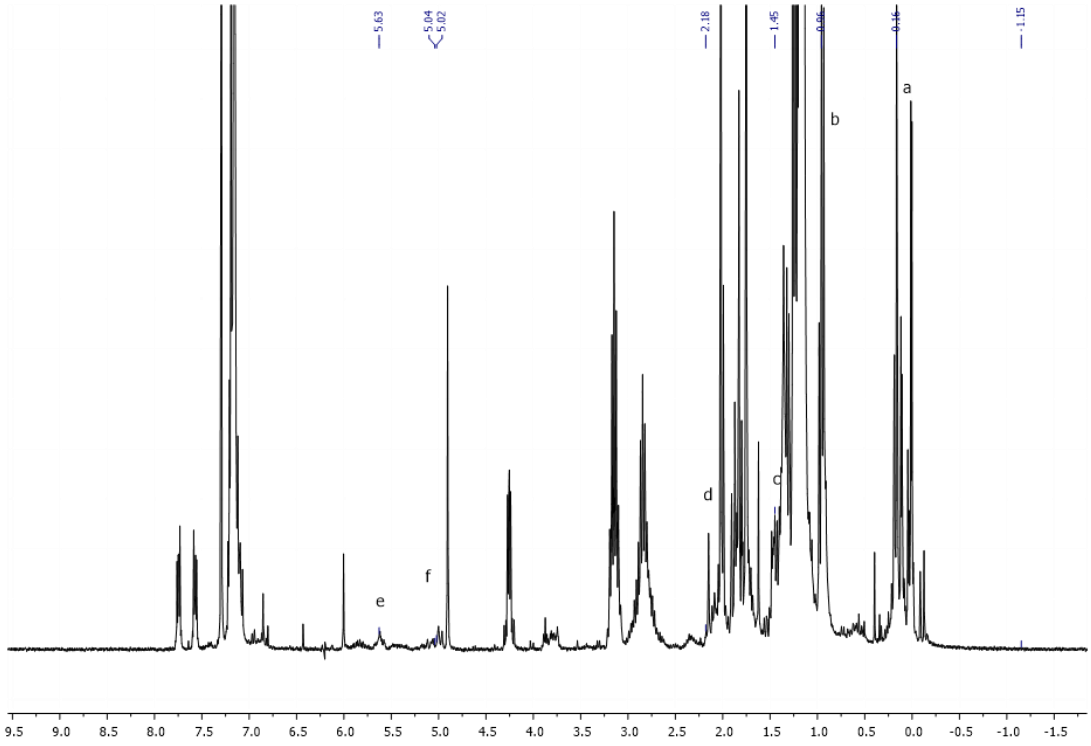

Figure 12: ^1H NMR (300 MHz, C_6D_6, 298 K) spectrum of reaction of **1** with (iodomethyl) cyclopropane. Evidence for the formation of TMS-pent-1-ene.

2.2.2- Synthesis of reactive intermediates

Multiple attempts were made to independently synthesise iron β-diketiminate species with diphenyl phosphide as a ligand. Presumably a reactive intermediate in the catalytic cycle is the phosphido species ^{Dipp}LFe-PPh$_2$ (**66**) (Figure 13). While compounds synthesised could be identified *in situ* as ^{Dipp}LFe-PPh$_2$ *via* ^{1}H NMR spectroscopy (Figure 14) and ESI- Mass spectrometry (Experimental methods, Chapter 8) samples were not sufficiently crystalline to characterise *via* single crystal x-ray diffraction. Presumably this occurs due to decomposition of **66**. Attempts were made to inhibit this decomposition with addition of pyridine to form the pyridine adduct ^{Dipp}LFe-PPh$_2$(py) (**67**). However, this compound was also found to decompose after a few days in solution.

The attempted syntheses (Scheme 41) initially utilised the known complexes **63** and **64** as precursors to the phosphido species (Figure 13) with potassium or lithium diphenylphosphine generated *in situ*.[8, 105, 106] A further attempt was made using a procedure reported by Marks and co-workers with an atmosphere of hydrogen used to promote hydride and subesequentally phosphido formation.[107] These attempts failed to produce crystals of the desired product.

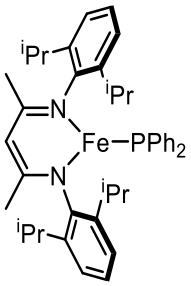

Figure 13: Iron phosphido species **66**.

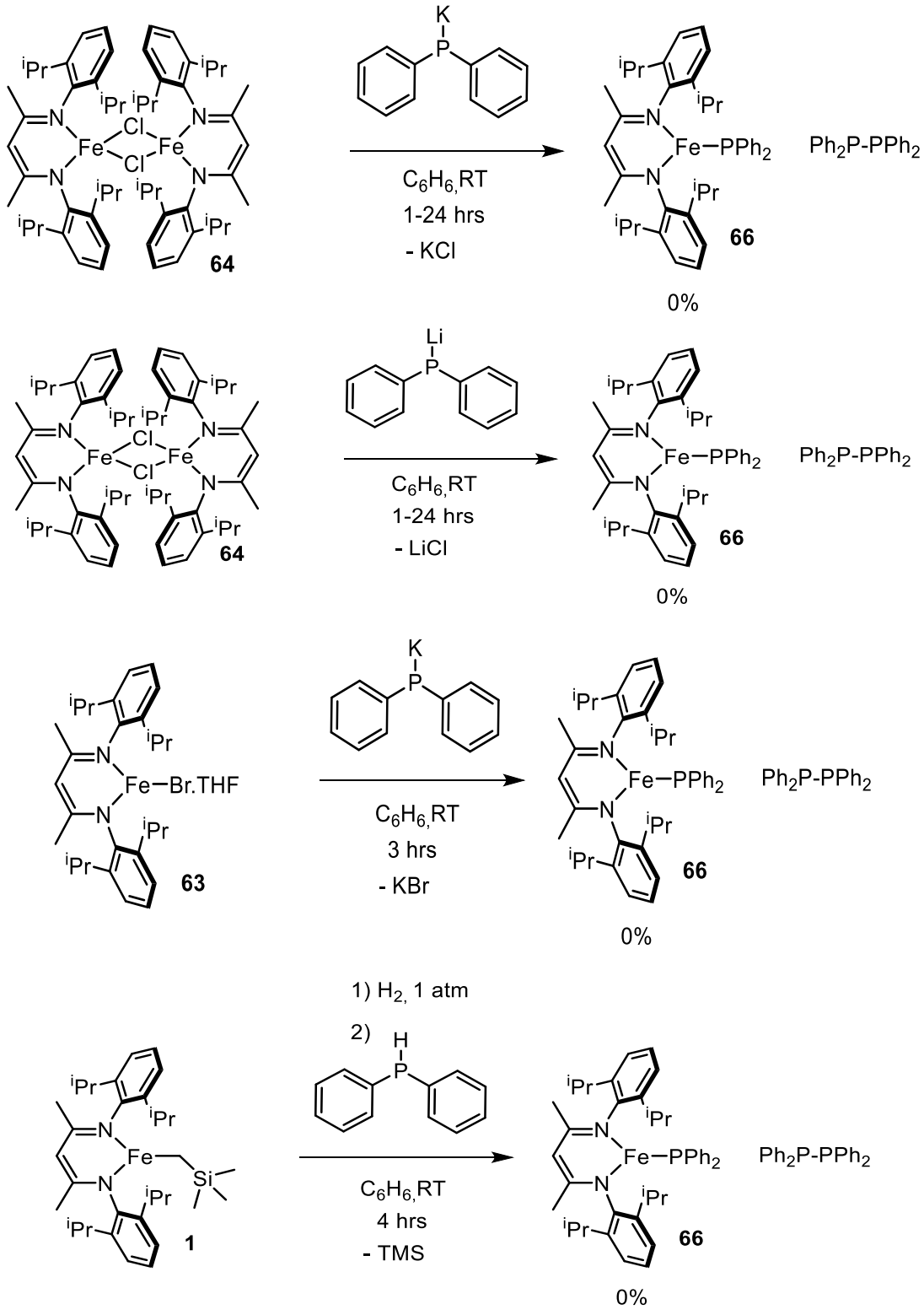

Scheme 41: Attempted syntheses of ^{Dipp}LFe-PPh$_2$ (**66**).

^{1}H NMR spectra of samples taken at the end point of catalysis under the optimised conditions (Figure 8) show that the precatalyst **1** is still present. This suggests that in the initial activation step of the reaction the formation of **66**, a precatalytic equilibrium is operating. This will be further discussed in Chapter 4.

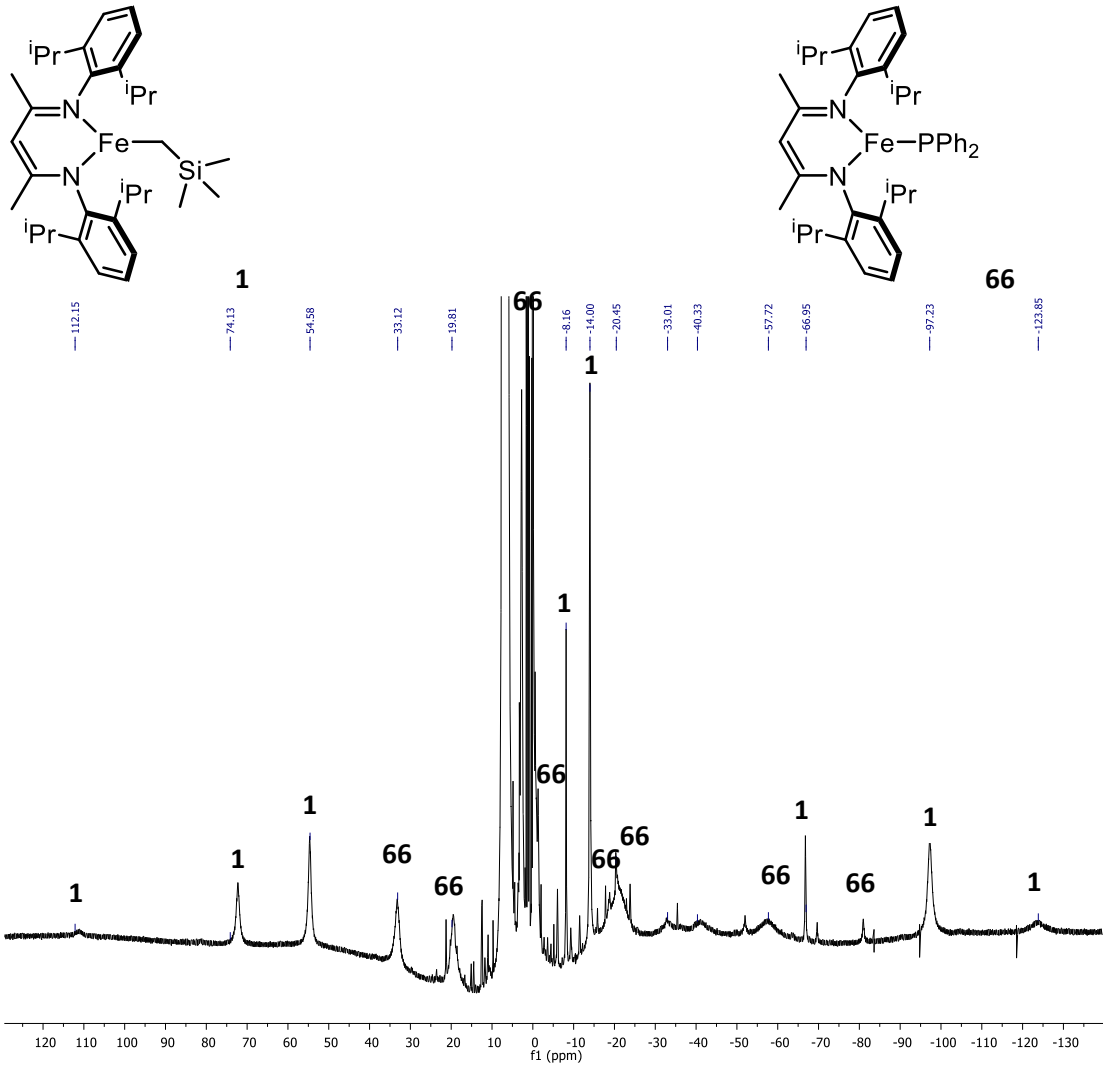

Figure 14: ^{1}H NMR (300 MHz, C_6D_6, 298 K) spectrum of catalytic run with **1** and diphenylphosphine after 24 hrs – (^{Dipp}LFeCH$_2$TMS and ^{Dipp}LFe-PPh$_2$).

1 - ^{1}H NMR: (500.1 MHz, C_6D_6) = 112.35 (s, 1H, a-CH), 74.13 (s, 6H, c-CH_3), 54.58 (s, 9H, Si(CH_3)$_3$), −8.16 (s, 4H, m-H), −14.00 (s , 12H, iPr-CH_3), −66.95 (s, 2H, p-H), −97.23 (s, 12H, iPr-CH_3), −123.85 (s, 4H, iPr-CH)

Signals postulated to be **66 -** ^{1}H NMR: (500.1 MHz, C_6D_6) 33.12 (6H, c-CH_3), 19.81 (4H, o-CH), 3.39 (12H, iPr-CH_3), -1.28 (4H, m-CH),-15.84 (12H, iPr-CH_3), -20.45 (2H, p-CH), -23.83 (2H, p-CH), -57.72 (4H, m-CH), -81.11 (4H, iPr-CH), (α-CH not observed).

Considering the results from these experiments a mechanism is postulated (Scheme 42).

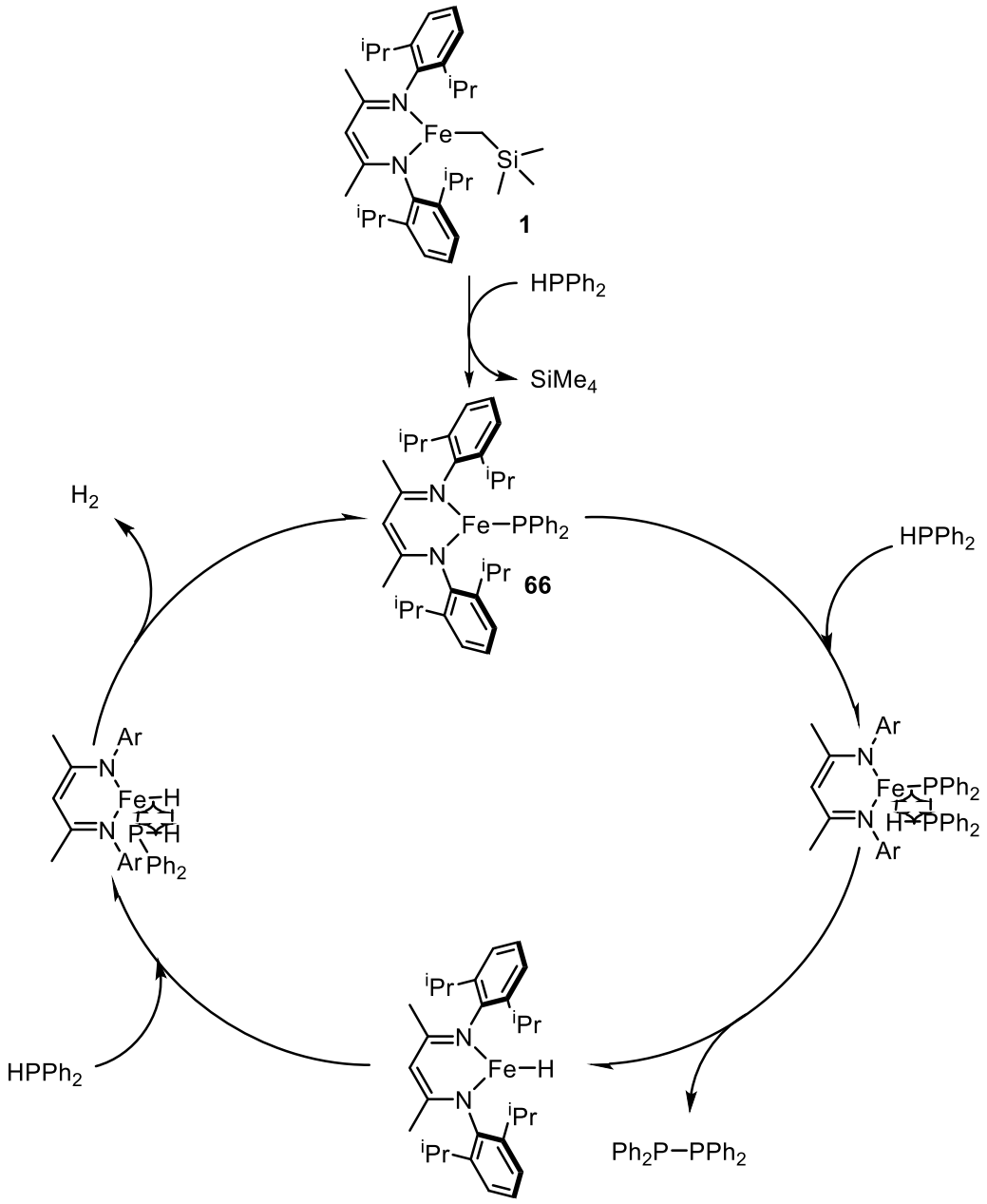

Scheme 42: Plausible DHC mechanism

The initial step in the dehydrocoupling mechanism is the formation of the iron phosphido species ^{Dipp}LFe-PPh$_2$ with loss of tetramethylsilane. This species could then react with diphenylphosphine to give P_2Ph_4 and an iron hydride species. Alternatively the iron phosphido species could undergo homoleptic cleavage forming radicals (Scheme 43). A radical termination step involving two phosphine radicals reacting to form P_2Ph_4 would seem plausible given reports discussed previously.[98]

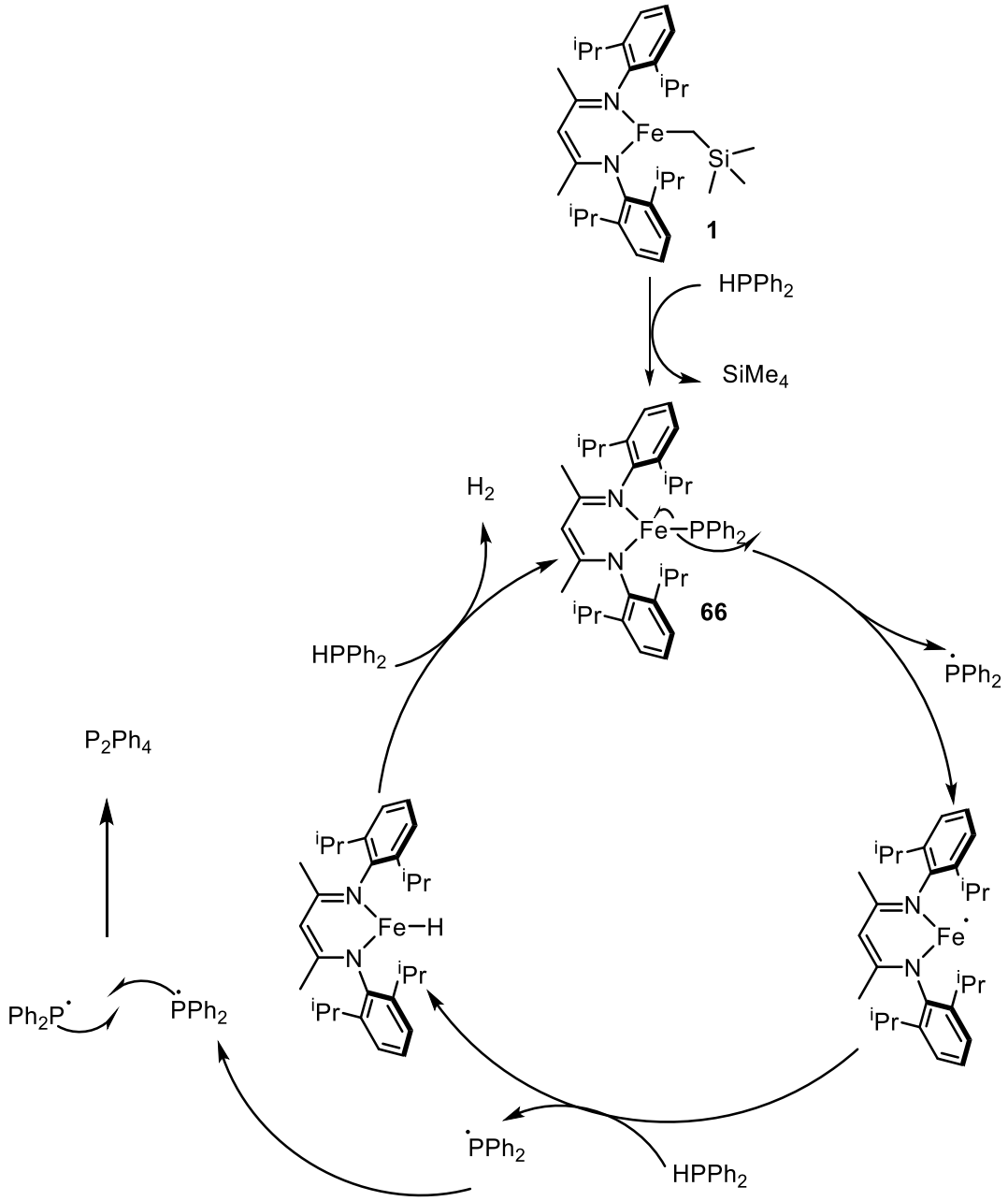

Scheme 43: Alternative DHC mechanism

In an effort to provide further evidence of the existence of the iron phosphido species **66** as a mononuclear species as opposed to a dimer, the synthesis of the analogous iron amido species ^{Diip}LFe-NPh$_2$ (**68**) was devised. This was achieved successfully (Scheme 44) and samples were sufficiently crystalline to characterise *via* single crystal x-ray diffraction (Figure 15).

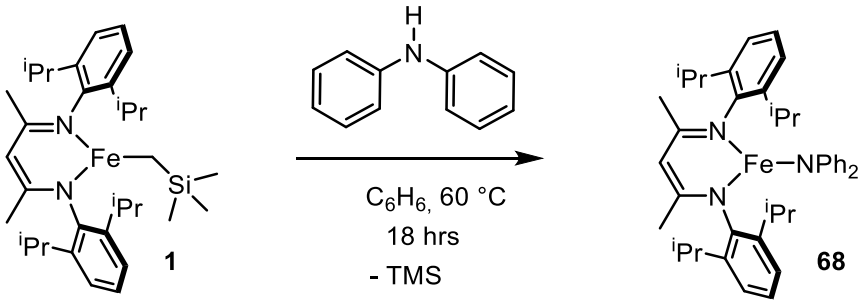

Scheme 44: Synthesis of ^{Diip}LFe-NPh$_2$ (**68**).

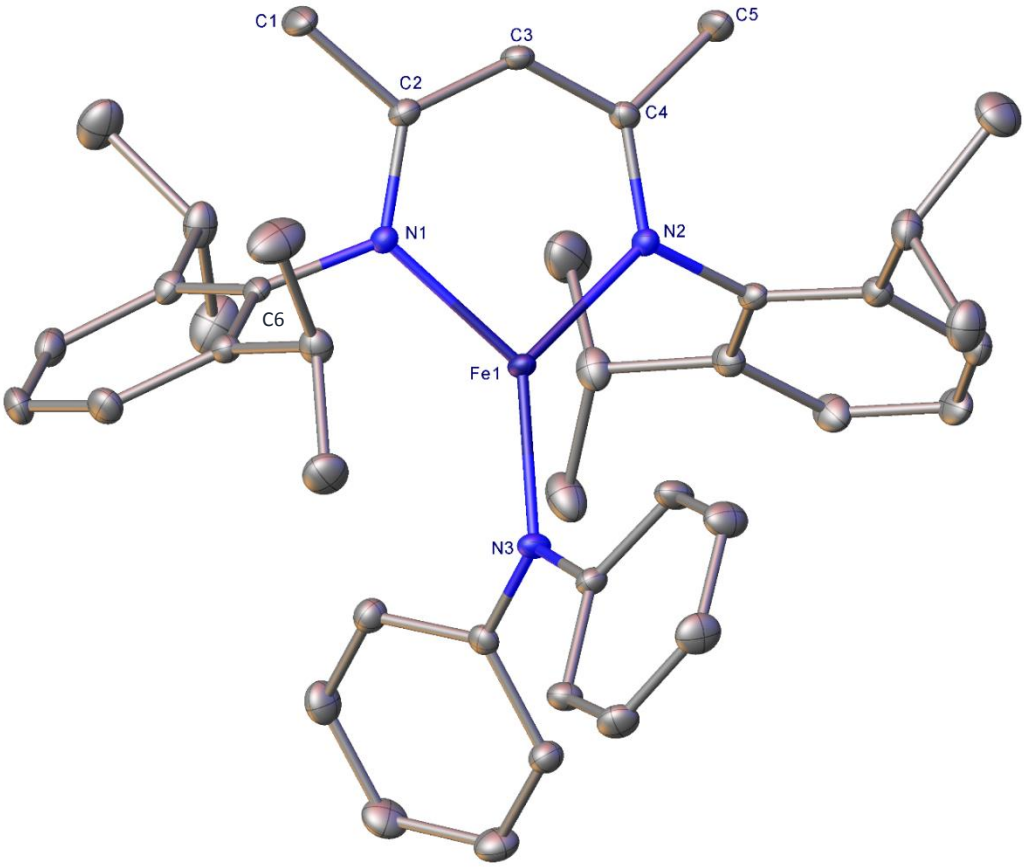

Figure 15: Crystal structure of **68.** Ellipsoids shown at 50% probability.

The major bond lengths and angles for **68** are shown in their respective tables (Tables 7 and 8). The three coordinate iron centre Fe(1) displays a trigonal planar geometry. The Fe(1)-N(3) bond at 1.9381(12) Å and is shorter than the iron-nitrogen bonds of the iron centre to the β-diketiminate ligand Fe(1) –N(1) and Fe(1) –N(2) at 1.9689(11) Å and 1.9845(12) Å respectively. This is presumably due to better π-donation from the amide ligand. The angles N(1) –Fe(1) –N(2) and C(6) –N(1) –Fe(1) (95.67(5)°and 116.74(9)°) are larger than the same angles in complex **2** (93.84(14) ° and 114.1(2) °).

Table 7: Selected bond lengths for complex **68**

Atoms	Bond length (Å)
Fe(1) –N(1)	1.9689(11)
Fe(1) –N(2)	1.9845(12)
Fe(1) –N(3)	1.9381(12)
N(1) –C(2)	1.3400(18)
N(1) –C(6)	1.4406(18)
N(3) –C(30)	1.4042(19)

Table 8: Selected bond angles for complex **68**

Atoms	Bond angle (°)
N(1) –Fe(1) –N(2)	95.67(5)
N(3) –Fe(1) –N(1)	131.27(5)
N(3) –Fe(1) –N(2)	132.91(5)
C(2) –N(1) –Fe(1)	122.61(9)
C(36) –N(3) –C(30)	120.28(12)
C(30) –N(3) –Fe(1)	120.41(9)
C(6) –N(1) –Fe(1)	116.74(9)

The analogous amido structure demonstrates that bulky pnictogens coordinated to the iron β-diketiminate moiety to produce a stable mononuclear species both in the solid state (Figure 15) and in solution (Figure 17).

It was proposed that use of **68** as a precatalyst in phosphine dehydrocoupling could provide further evidence for the *in situ* formation of a monomeric iron phosphido species **66**. The pKa of diphenylphosphine has been previously calculated and was determined to be three orders of magnitude lower than that of diphenylamine (21.7 and 25 respectively). As such diphenylphosphide is expected to readily replace diphenylamide at the active iron site.[108] Experiments were undertaken to profile the reactivity of **1** and **68**. Surprisingly **68** was found to be a very poor catalyst for phosphine dehydrocoupling achieving a 10% spectroscopic yield of tetraphenyldiphosphane in 18 hours. In a stoichiometric competition reaction between diphenylamine and diphenylphosphine with **1** NMR characterisation determined that **68** was forming with diphenylphosphine remaining in solution. The stability of the iron amido complexes due to the electron withdrawing and π donating properties of diphenylamine is postulated as the basis for their preferential formation.[109]

Spectral analysis of the crude reaction mixture of **1** with diphenylphosphine show paramagnetic signals concordant with a high spin iron(II) complex that could be **66** (Figure 16).

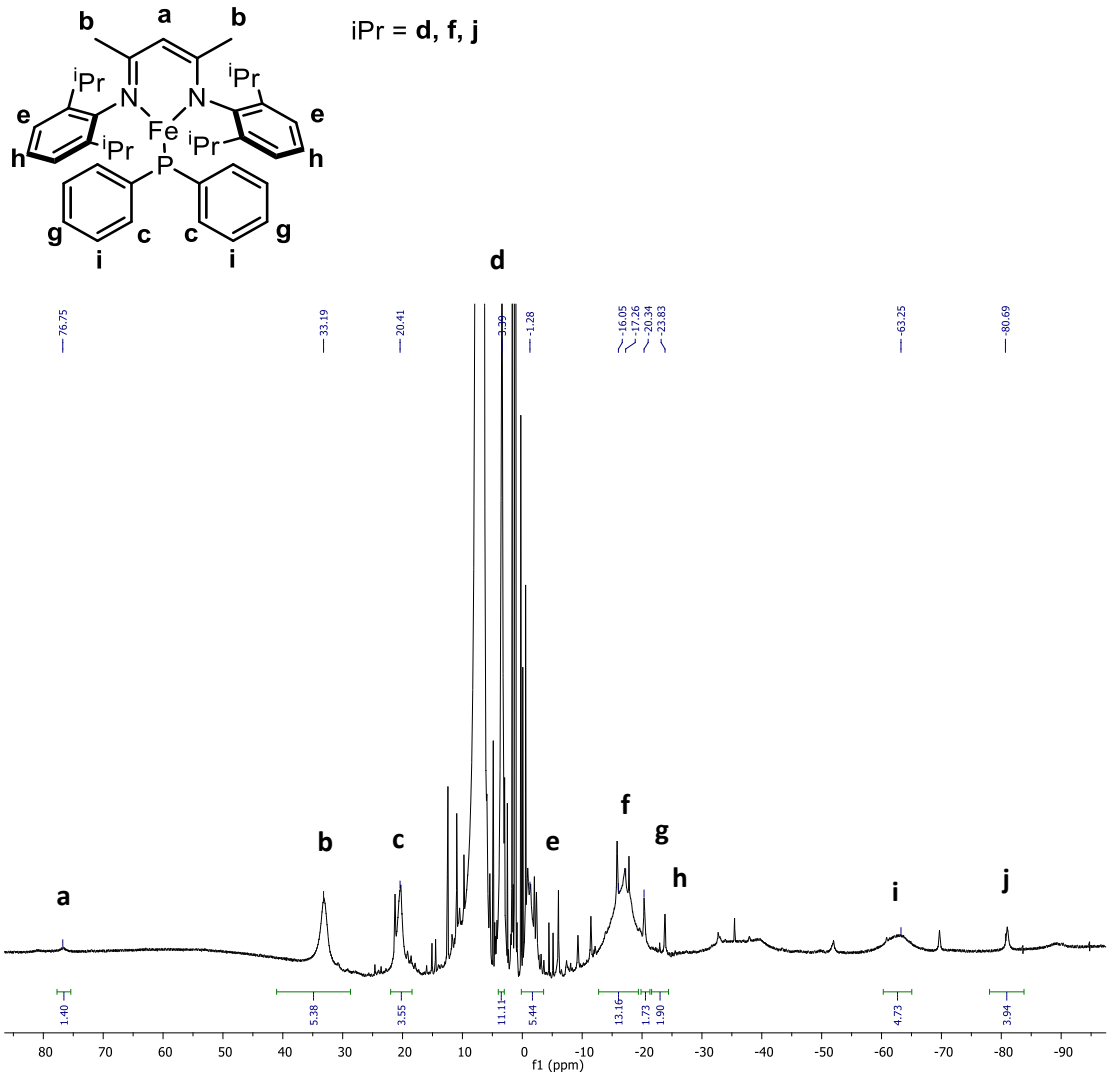

Figure 16: Crude paramagnetic ^{1}H NMR spectrum of ^{Dipp}LFe-PPh$_2$ (**66**).

66 - ^{1}H NMR: (500.1 MHz, C_6D_6) 76.75 (1H, α-CH), 33.19 (6H, c-CH_3), 20.41 (4H, o-CH), 3.39 (12H, iPr-CH_3), -1.28 (4H, m-CH),-17.26 (12H, iPr-CH_3), -20.34 (2H, p-CH), -23.83 (2H, p-CH), -63.25 (4H, m-CH) -80.69 (4H, iPr-CH).

Although not conclusive; assigned signals are comparable to the high spin iron(II) β-diketiminate phosphide reported by Grubba and co-workers.[110] Spectral analysis of **68** via ^{1}H NMR spectroscopy provide further evidence that **66** is a monomeric species (Figure 17).

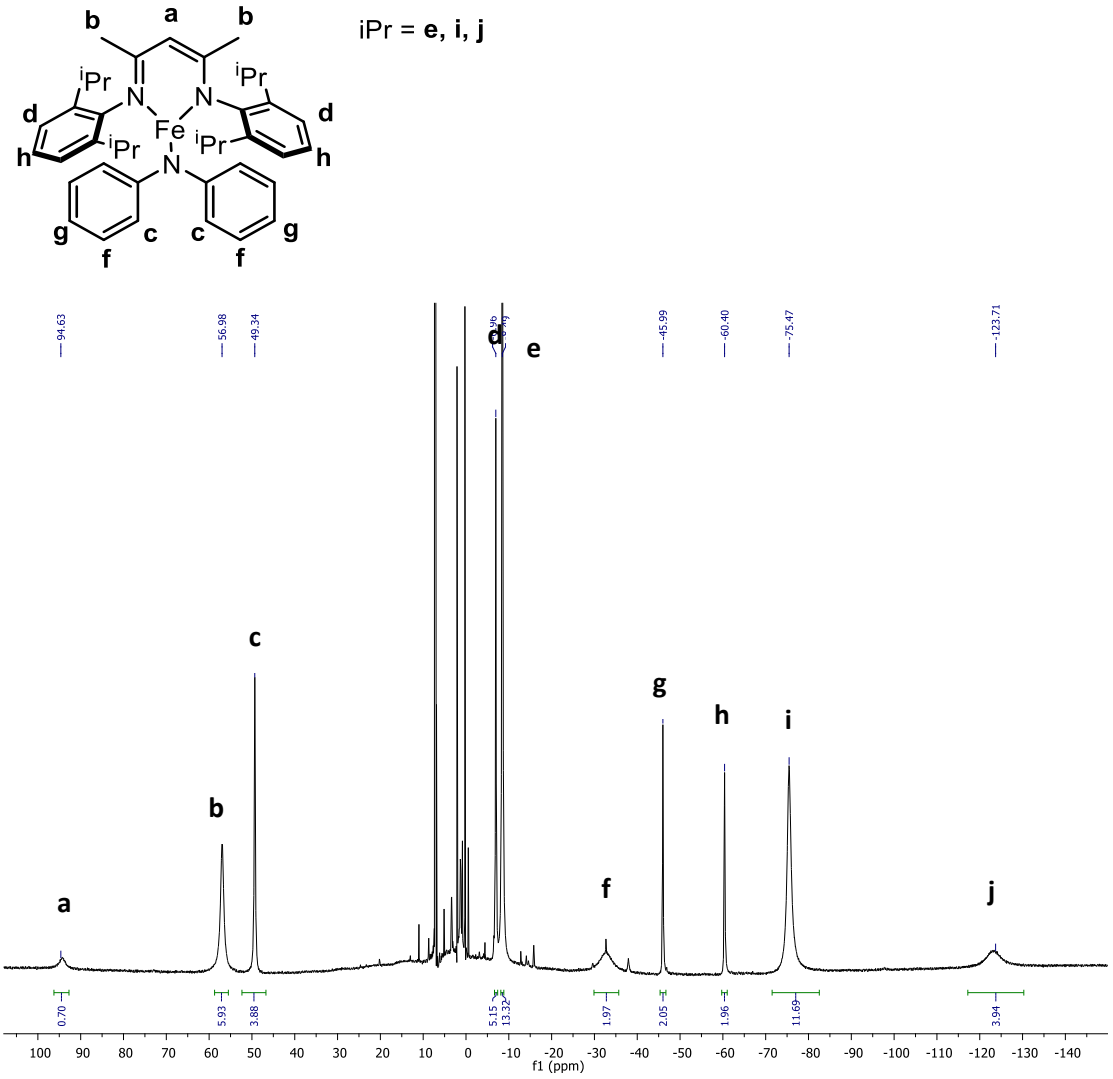

Figure 17: Paramagnetic ^{1}H NMR spectrum of $^{Dipp}LFe\text{-}NPh_2$ (**68**).

68 - ^{1}H NMR (500 MHz, C_6D_6): 94.41 (1H,α-CH), 56.94 (6H, c-CH_3), 49.34 (4H,o-CH), -6.96 (4H,m-CH), -8.49 (12H,iPr-CH_3), -32.83 (4H,m-CH), -45.99 (2H,p-CH), -60.40 (2H,p-CH), -75.47 (12H, iPr-CH_3), -122.99 (4H,iPr-CH).

2.2.3 - Density functional theory calculations

Other methods were devised to provide evidence for the existence of **66** as a monomeric species. Computational studies were used to model the iron phosphido as both a dimer and a monomer. DFT calculations suggest that a dimeric phosphido species of the formula $[^{Dipp}LFe\text{-}PPh_2]_2$ (**69**) would be highly disfavoured from forming. The most favourable phosphido calculated was **66** in a quintet ground state. This high spin complex would give rise to a paramagnetic NMR spectrum as is generally seen for three coordinate iron(II) β-diketiminates. In probing the origin of the radical reactivity discussed previously calculations of the four highest Singly Occupied Molecular Orbitals via two different functionals proposes that they are largely ligand based (Figure 18).[111-117] Ligand non-innocence is suggested and since this is common for β-diketiminates the ancillary ligand likely plays a role in stabilising radical intermediates.[118-120]

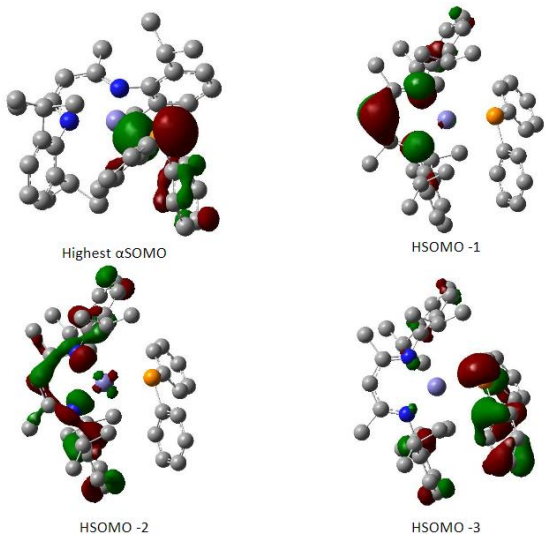

Figure 18: Highest SOMO's calculated for **66** with the M06-2X functional (DFT studies conducted by Dr Antoine Buchard).

2.2.4 - Heterogeneity studies

Experiments were then conducted to determine the origin of phosphine dehydrocoupling activity. Under the initial conditions with diphenylphosphine as a substrate, droplets of mercury were added to the reaction mixture. Some studies suggest that if a large decrease in conversion occurs then that indicates that catalysis is heterogeneous in nature rather than homogeneous.[62, 121] Considering that our precatalyst is an iron complex and on the basis that iron and mercury do not form an amalgam very little insight can be gained from these experiments. A decrease in conversion was observed (~20%) but it seems plausible that this could be due to a favourable interaction of the phosphine with mercury or due to a slower rate of stirring in the presence of mercury.[122, 123] Further experiments with trimethylphosphine (PMe_3) which has been shown to bind preferentially and irreversibly with iron nanoparticles were undertaken to provide clarity.[124] Addition of PMe_3 showed no reduction in spectroscopic yield suggesting that the reactivity is homogeneous in origin.[125]

Work by Liu and Manners has previously described that apparently homogeneous iron catalysed dehydrocoupling systems are in fact heterogeneous.[121, 126] In order to provide further scrutiny of the possibility that the origin of dehydrocoupling catalysis is in fact heterogeneous in nature Transmission Electron Microscopy (TEM) images were recorded. Samples were taken from reactions under optimised conditions and examined for evidence of nano-particulate structures. The results of these studies are detailed below (Figure 19).

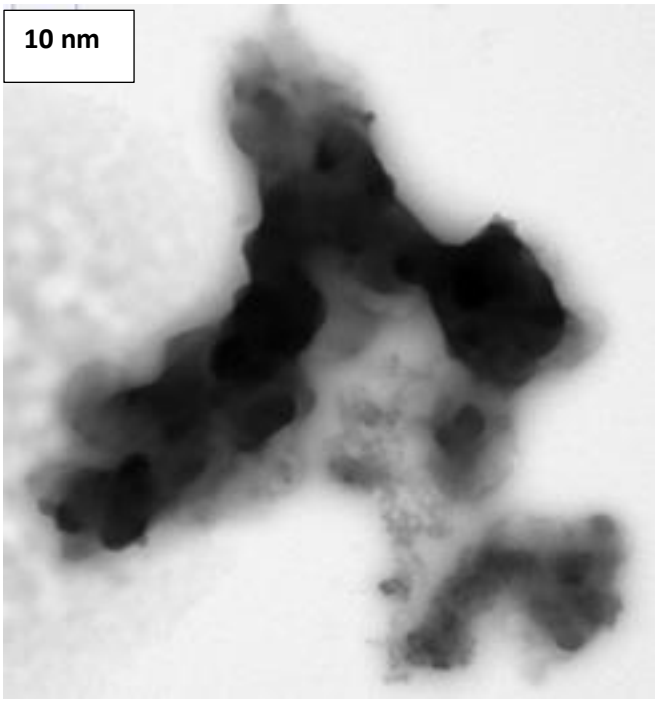

*TEM image of 5 mol % **1** with $HPPh_2$*

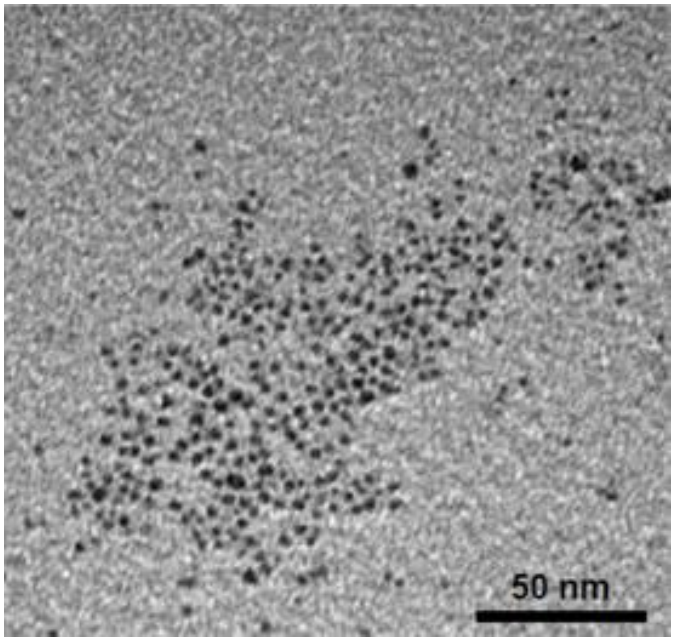

Manners' reported iron nanoparticles

Figure 19: TEM images of catalytic dehydrocoupling reactions compared with that reported by Manners and co-workers.[124]

The structures observed from the reaction mixture are diffuse in appearance with no evidence of repeating nano-particulate structures. The species observed from our dehydrocoupling reaction are dissimilar to the well-defined nanoparticulate material reported by Manners. Multiple samples were taken at 0.5 mmol concentrations but no patterns could be observed that would suggest the presence of nanoparticles. The structures shown appear to be colloidal in nature but are not anticipated to play an active role in reactivity given their sparse distribution. Thus based on these experiments and *in situ* NMR studies, the catalytic reactions have been determined to be homogeneous in nature.

2.3 - Hydrophosphination of styrenes

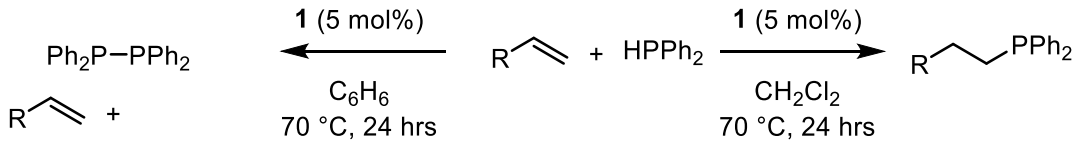

Scheme 45: Effects of solvent on product with **1**.

As stated previously, changing solvent from benzene to DCM led to a change in reactivity and this switch in reaction pathway with only the solvent being altered (Scheme 45) was rather unexpected. Previous studies by Beletskaya and co-workers have demonstrated that phosphine dehydrocoupling and hydrophosphination can be achieved with the same precatalyst.[50] In Beletskaya's study, temperature was key to this, which is clearly not the case in these reactions. The solvent is likely non-innocent and will be further discussed (Chapter 3).

When comparing this with previously discussed reports in the literature for hydrophosphination of alkenes it can be observed that this catalytic system is an improvement on Beletskaya's and Gaumont's system.[50, 55] The conversions are comparative to the solvent free and catalyst free hydrophosphination reactivity reported by Alonso;[63] in DCM at 70 ^{o}C Alonso reported no hydrophosphination reactivity without a catalyst present. Therefore we can determine that the reactivity displayed here is due to the presence of the iron catalyst. This is therefore a rare example of iron catalysed intermolecular hydrophosphination but does not improve on the catalytic activity displayed by **29** previously reported by the Webster group.[56] A selection of alkene substrates were evaluated for hydrophosphination activity (Table 9).

Table 9: Substrate scope for the iron catalysed hydrophosphination of styrenes.

Entry	*Substrate*	*Product*	*Spec. Yield (%)[a]* *[Isolated Yield (%)]*
1	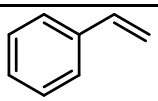	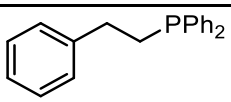	*100 [75]*
2	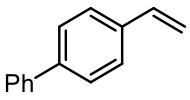	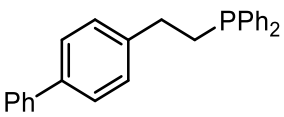	*100 [73]*
3	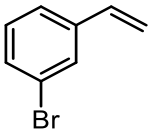	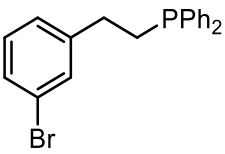	*100 [92]*
4	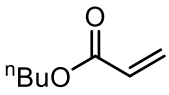	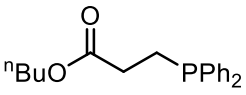	*100 [94]*
5	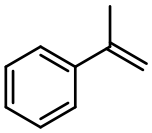	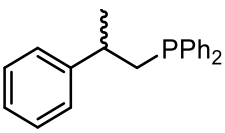	*100 [49]*

*Conditions: 5 mol% **1**, HPR_2 (0.5 mmol), DCM (0.35 mL). [a] Based on loss of loss of P–H signal from ^1H NMR, using 1,3,5-trimethoxybenzene as an analytical standard.*

A moderate substrate scope was investigated and the results were promising. Catalytic hydrophosphination of less activated substrates in this case styrenes (Entries 1-3) was achieved in good yields. N-butyl acrylate (Entry 4) an activated substrate gave good yields as might be expected. The reactivity with α-methyl styrene (Entry 5) is intriguing as previous studies in the Webster group have reported very little activity with this substrate. These results suggest that **1** could be a precatalyst for the hydrophosphination of other substrates and this will be discussed further (Chapter 3).

2.4 - Conclusions from Chapter 2

The results in this chapter detailed the synthesis of iron(II) β-diketiminate complexes *via* the successful replication of literature procedure. These complexes were tested for activity in hydrophosphination catalysis. Initially no catalytic hydrophosphination activity was observed towards alkenes. Instead what was discovered was serendipitous phosphine dehydrocoupling. This reactivity was fully optimised and tested with a range of secondary and primary phosphines. The mechanism was investigated and determined to be radical in nature. Experimental evidence suggests the mechanism proceeds *via* an iron phosphido species. Attempts to isolate this complex proved unsuccessful due to decomposition. Computational studies and isolation of an analogous iron amido complex determined that the iron phosphido species formed in solution is a monomeric complex. DFT studies provide evidence to suggest that the radical character displayed by this phosphido complex is due to ligand non-innocence. Phosphine dehydrocoupling reactions were scrutinised for nanoparticulate structures. No significant evidence could be found and the observed catalysis was determined to be homogeneous. Further reactions in DCM were investigated and under these conditions alkene hydrophosphination was observed. A modest substrate scope has been reported and further mechanistic insight will be discussed (Chapter 3).

3 - Intermolecular hydrophosphination of alkynes and intramolecular hydrophosphination

3.1 - Intermolecular hydrophosphination of alkynes

Having previously discussed the catalytic hydrophosphination activity of **1** towards alkenes (Chapter 2) experimental investigations were undertaken to determine whether this reactivity could be extended to alkynes.

Reactions in the presence of phenylacetylene in benzene gave very good spectroscopic yields for hydrophosphination. Quite surprisingly the major product observed as a result of the reaction was the Markovnikov addition product (Scheme 46).

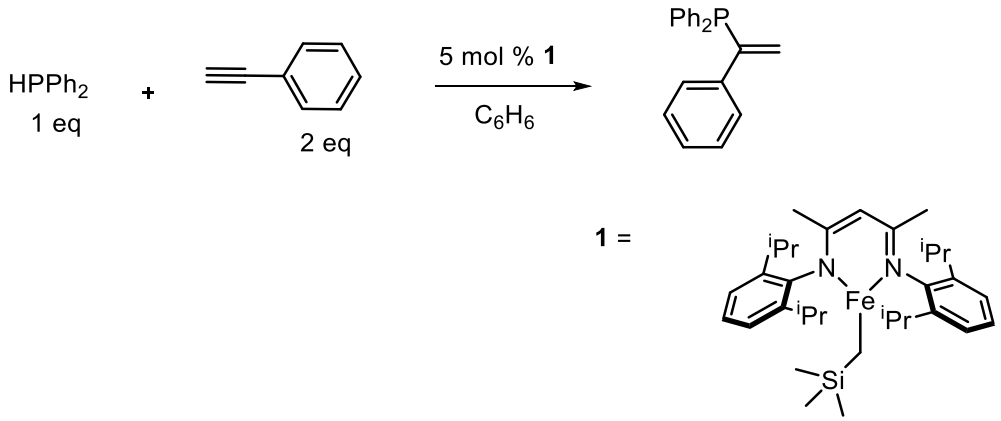

Scheme 46: Hydrophosphination of phenylacetylene to give the Markovnikov addition product.

3.1.1 – Markovnikov addition hydrophosphination

The selectivity for the Markovnikov product is rare with only a handful of catalytic syntheses reported in the literature.[51] These systems often require heating to high temperatures and the use of more expensive palladium catalysts. This intriguing reactivity was fully optimised (Table 10) and is both selective and facile. Interestingly in the absence of solvent and without a catalyst the (*Z*)- isomer of the *anti*-Markovnikov product is the major product observed.[127] The origin of this Markovnikov addition selectivity could potentially be due to the previously discussed phosphine dehydrocoupling occurring *in situ.* Subsequently, hydrophosphination would therefore be expected to occur in a two step process. Some evidence of this has been previously reported in the literature.[127, 128] Remarkably the hydrophosphination of phenylacetylene works well at room temperature with full spectroscopic conversion after 72 h. Upon heating to 50 ^{o}C the reaction goes to completion in 3 h. These conditions were taken as the optimal conditions for the reaction.

Table 10: Optimisation of the reaction conditions of the hydrophosphination of phenylacetylene.

Entry	***[Fe]***	*Loading (mol%)*	*Conditions*	*Spectroscopic yield (%)[a]*	*Selectivity (Markovnikov:Anti-Markovnikov)*
1	***1***	*5*	*RT, 24 h*	*65*	*90:10*
2	***1***	*5*	*RT , 72 h*	*100*	*90:10*
3	***1***	*5*	*50 °C, 24 h*	*100*	*90:10*
4	***1***	*5*	*50°C, 3h*	*100*	*90:10*
5	***1***	*5*	*50 °C, 1h*	*72*	*90:10*
6	***60***	*5*	*50 °C, 24 h*	*90*	*80:20*
7[b]	***1***	*5*	*70 °C, 24 h*	*100*	*0:100*

Conditions: $HPPh_2$ (0.5 mmol), phenylacetylene (1.0 mmol), C_6H_6 (0.35 mL). [a] NMR yield calculated from the consumption of $HPPh_2$ against 1,3,5-trimethoxybenzene as an internal standard. [b] DCM (0.35 mL).

The observed proton coupling constants confirm that the Markovnikov addition product is the major product (Figure 20). The small geminal (^2J) coupling values of the vinyl protons in addition to the $^{31}P\{^1H\}$ chemical shift support this.[127] In contrast, if the *anti*-Markovnikov isomers were present as the major products we would expect larger coupling constants ((*Z*)-isomer $J_{P\text{-}H} \approx 40$ Hz and ≈ 18 Hz, and $J_{H\text{-}H} \approx 3$ Hz). Therefore NMR experiments show that in benzene, intermolecular hydrophosphination of phenylacetylene is selective for Markovnikov addition.

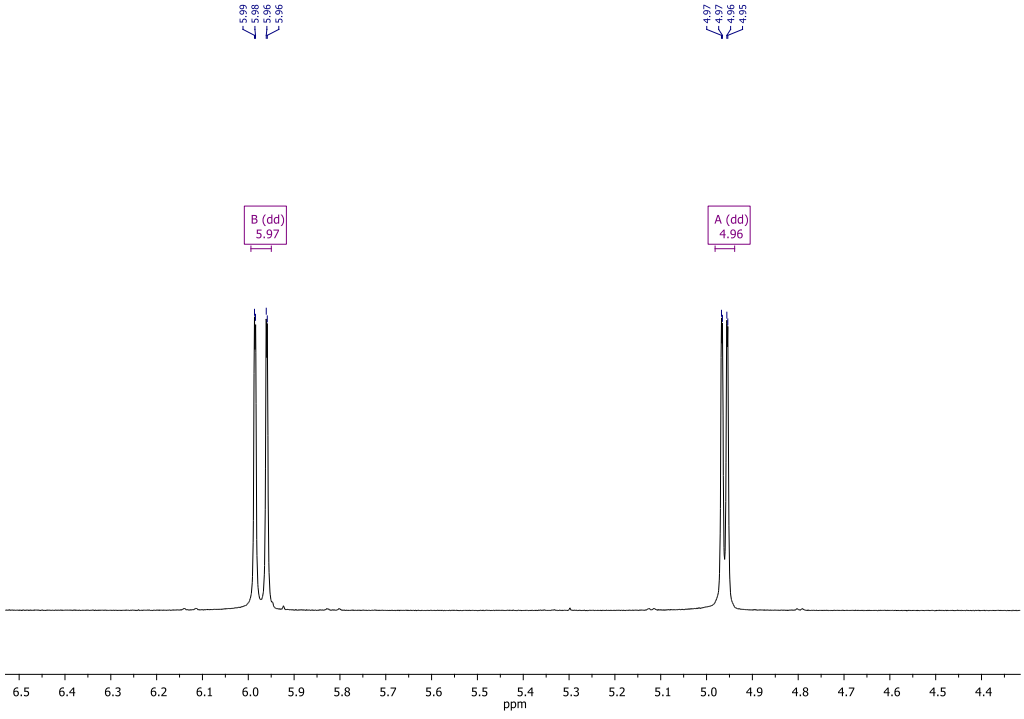

^{1}H NMR (500 MHz, $CDCl_3$, 298 K) δ Ha = 5.97 (dd, $J_{H\text{-}P(Trans)}$ = 12.8 Hz, $J_{H\text{-}H}$ = 1.1 Hz, 1H), Hb = 4.96 (dd, $J_{H\text{-}P(Cis)}$ = 5.8 Hz, $J_{H\text{-}H}$ = 1.1 Hz, 1H).

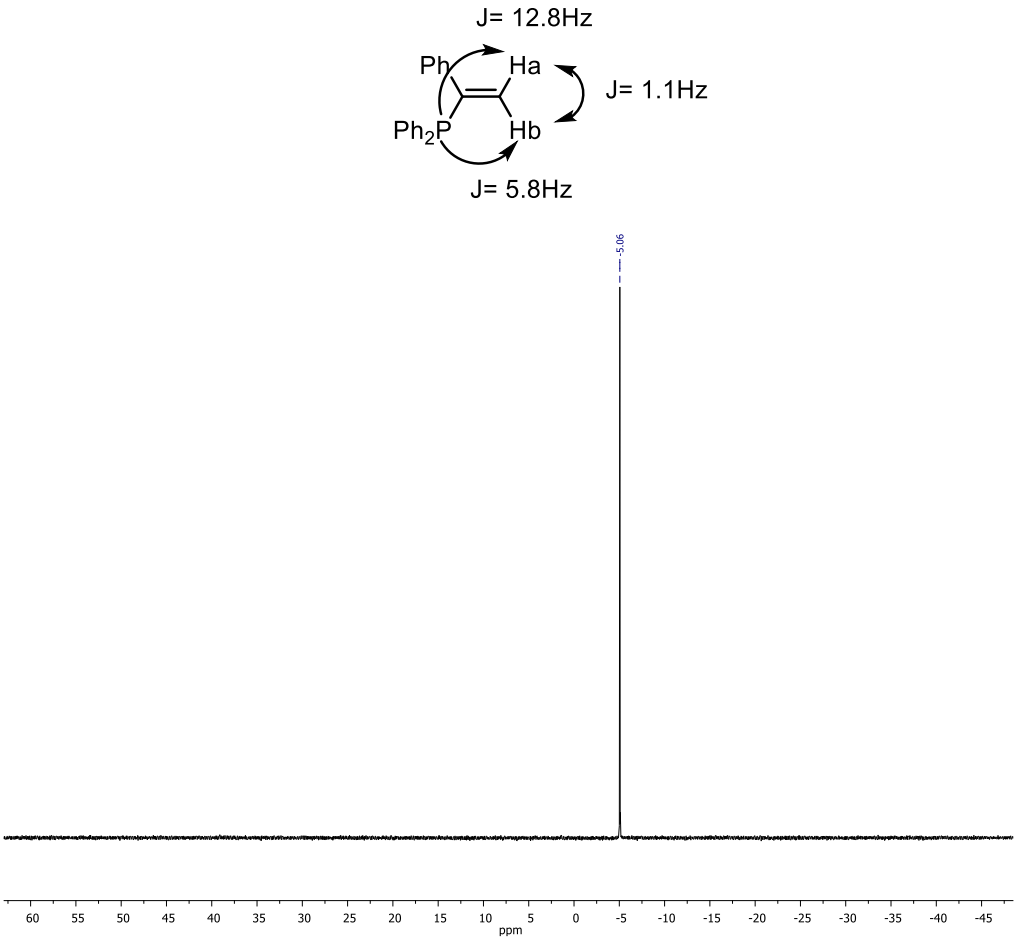

Figure 20: ^{1}H and ^{31}P{^{1}H} NMR (203 MHz, $CDCl_3$, 298 K) spectra of diphenyl(1-phenylethenyl)phosphine (Table 11, Entry 1).

Analysis of the product by ^{1}H NMR shows a doublet of doublets integrating to one H for $J_{H\text{-}P}$ and $J_{H\text{-}H}$ (12.8 Hz and 1.1 Hz) respectively; this is H_a (Figure 20). H_b displays a doublet of doublets integrating to one H for $J_{H\text{-}P}$ and $J_{H\text{-}H}$ (5.8 Hz and 1.1 Hz) respectively. This confirms that the isolated product is diphenyl(1-phenylethenyl)phosphine.

The reaction proceeds very quickly under very mild conditions and with very good regio-selectivity. To test the scope of this reactivity a range of substituted alkynes were used as substrates in hydrophosphination reactions in the presence of the iron precatalyst (Table 11).

Table 11: Substrate scope for the Markovnikov addition hydrophosphination of alkynes.

Entry	*RCCH*	*Spec. Yield (%)[a]* *[Isolated Yield (%)]*	*Selectivity (M:AM)*	*Product*
1	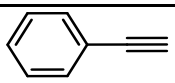	*100 [82]*	*90:10*	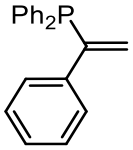
2	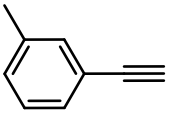	*88 [66]*	*90:10*	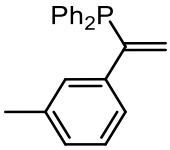
3	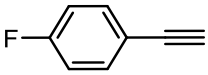	*100 [80]*	*90:10*	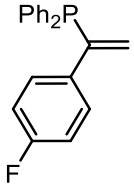
4	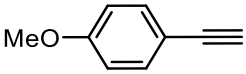	*100 [74]*	*90:10*	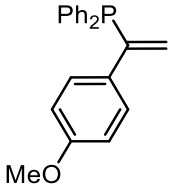
5	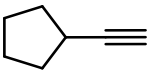	*Trace*	-	
6[c]	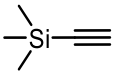	*85 [60]*	*90:10*	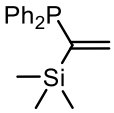
7[c]	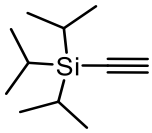	*100 [78]*	*90:10*	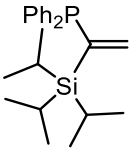
8	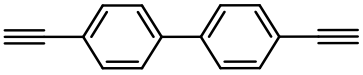	*100 [-]*	*Not determined*	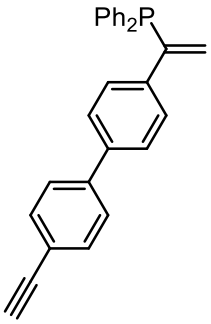

9[b]	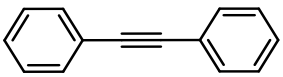	*100 [86]*	*N/A*	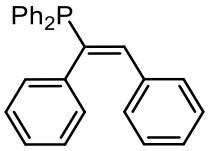
10	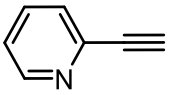	*<20*	*Not determined*	
11	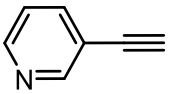	*<20*	*“*	
12	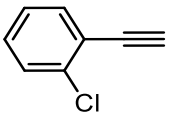	*N. R.*	*“*	
13	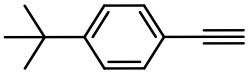	*100 [75]*	*90:10*	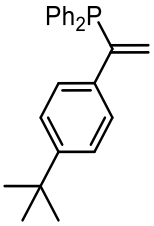
14	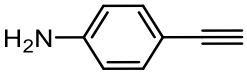	*78 [-]*	*90:10*	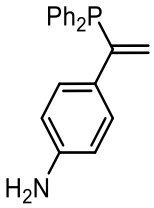
15	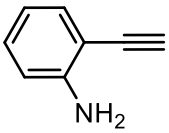	*33*	*Not determined*	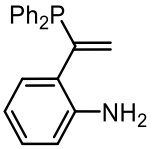
16[d]	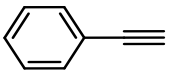	*100 [81]*	*90:10*	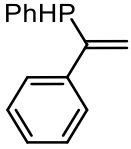

Conditions: *5 mol%* **1**, *$HPPh_2$ (0.5 mmol), alkyne (1.0 mmol), C_6H_6 (0.35 mL), 50 °C, 3 hrs. [a] NMR yield calculated from the consumption of $HPPh_2$ against 1,3,5-trimethoxybenzene as an internal standard. [b] 70 °C, 24 hrs. [c] 90 °C, 24 hrs. [d] Mixture of mono:di alkenyl product (85:15).*

Good spectroscopic and isolated yields were achieved with a range of alkyne substrates showing that reactivity is not limited to phenyl acetylene. Most phenyl derived substrates (Entries 1-4, 8-9, 13-14) work very well. Both strongly electron withdrawing (Entry 3) and strongly electron donating groups (Entry 4) were tolerated in this catalytic system. Likewise good spectroscopic yields were observed with substrates substituted at the *para* and *meta* positions on the aromatic rings whereas significantly lower yields or no reactivity at all was observed with functional groups at the *ortho* position (Entries 12 and 15). This suggests that

steric constraints have a substantial role in reactivity towards different substrates. Alkyl substrates such as cyclopentylacetylene (Entry 5) displayed very little hydrophosphination reactivity. Pleasingly, albeit at increased reaction temperatures, silyl alkynes (Entries 6 and 7) were very reactive giving almost quantative yields. Pyridyl alkynes (Entries 10 and 11) gave very poor yields. This observation is attributed to the ability of pyridyl alkynes to coordinate to the iron centre through the nitrogen atom in the aromatic ring. The competitive coordination of this nitrogen donor atom over the *sp* hybridised carbon atom of the acetylene, hinders catalytic turnover.

Reactions with the primary phosphine phenylphosphine (Entry 16) were distinctly selective. The major product observed was the Markovnikov addition product phenyl(1-phenylethenyl)phosphine. Phenyl(1-phenylethenyl)phosphine is a monomer that can be polymerised to give poly(phenyl(1-phenylethenyl)phosphine).[129] Reactions were attempted under the same optimised reaction conditions whilst varying the phosphine:alkyne ratio (1:2 to 1:1). The major product was the single Markovnikov hydrophosphination product. Some double addition to the phosphine was observed with the formation of a dialkenyl product. In substrates with two alkyne motifs (Entry 8) mono-substitution was observed along with a degree of phosphine dehydrocoupling. Internal alkynes (Entry 9) were found to undergo hydrophosphination albeit at a slightly elevated temperature from the initially optimised conditions.

3.1.2 - *Anti*-Markovnikov addition hydrophosphination

As alluded to previously, reactions with **1** as a catalyst in DCM give the opposite regioselectivity. Under very similar reaction conditions the major product yielded from reactions in DCM is the (*Z*)-*an*ti-Markovnikov product. This surprising switch in reactivity suggests an entirely different mechanism of reactivity in each solvent. The substrate scope of this divergent reaction to form *anti*-Markovnikov addition products was further investigated (Table 12).

Table 12: Substrate scope for *anti*-Markovnikov hydrophosphination of alkynes.

Entry	*RCCH*	*Spec. Yield (%)[a]* *[Isolated Yield (%)]*	*Selectivity (E:Z)*	*Product*
1	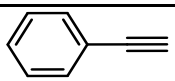	*100 [86]*	*10:90*	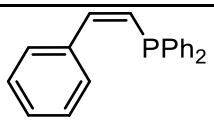
2	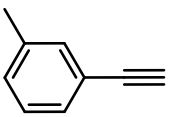	*72 [56]*	*10:90*	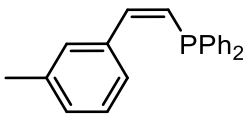

3	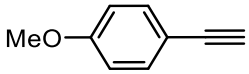	*66*	*10:90*	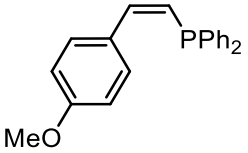
4	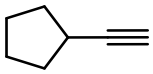	*N.R.*	-	
5[b]	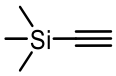	*100 [55]*	*10:90*	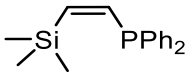
6[b]	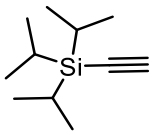	*100 [88]*	*10:90*	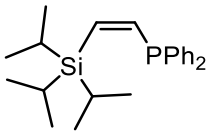
7	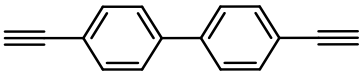	*N.R.*	-	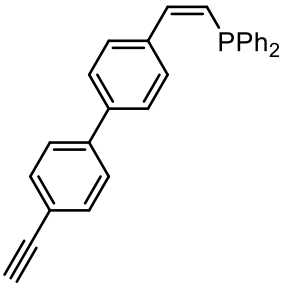
8	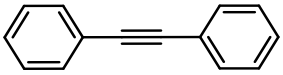	*Trace*	-	
9	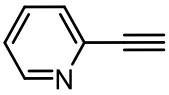	*26*	*Not determined*	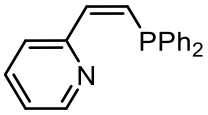
10	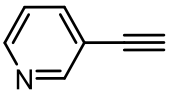	*100 [77]*	*Not determined*	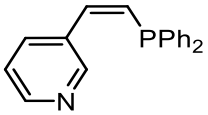
11	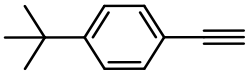	*100 [88]*	*10:90*	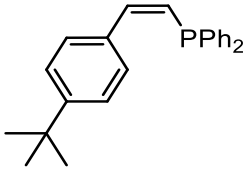

Conditions: *5 mol% **1**, $HPPh_2$ (0.5 mmol), alkyne (1.0 mmol), DCM (0.35 mL), 70 °C, 24 hrs. [a] NMR yield calculated from the consumption of $HPPh_2$ against 1,3,5-trimethoxybenzene as an internal standard [b] 90 °C, 24 hrs.*

Good spectroscopic and isolated yields from a range of alkyne substrates show that the reaction has a high functional group tolerance. Remarkable selectivity for the *Z*-isomer was observed for a wide range of substrates (Entries 1-3, 5-6, 10-11). Phenyl derived substrates (Entries 1-3 and 11) work very well under these conditions. Pyridyl alkynes (Entries 9 and 10) gave very different results depending on where the nitrogen atom is situated in the aromatic ring. This observation is attributed to the difference in stability of intermediates due to the

difference in resonance forms of 2-pyridylacetylene and 3-pyridylacetylene. It also suggests that competitive coordination of nitrogen to iron is not a limiting factor in this system. Silylacetylenes (Entries 5 and 6) were also found to be compatible with this system.

The mechanisms of these two systems with **1** seem to be entirely different. Intrigued by this contrasting chemistry further clarity was sought *via* mechanistic investigations (Scheme 47).

3.2 - Mechanistic considerations

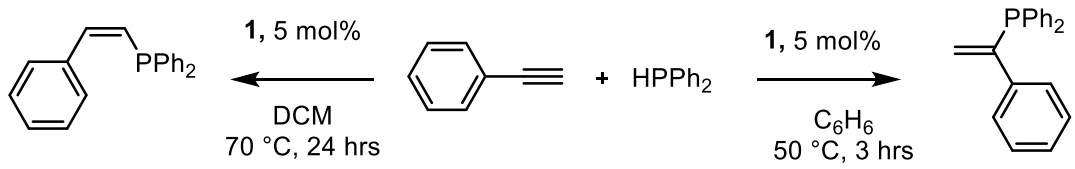

Scheme 47: Regiodivergent hydrophosphination catalysed by **1**.

Having established the synthetic scope of the reaction(s) (Scheme 47, Tables 11 and 12), investigations were undertaken to discriminate the mechanistic origins of the hydrophosphination activity. Initial experiments focused on isolating potential catalytic intermediates or catalytic resting states. As has previously been alluded to (Chapter 2) the iron phosphido complex **66** is unstable and therefore could not be isolated and used in catalytic experiments. As with phosphine dehydrocoupling catalysis, evidence of the formation of this species can be achieved *via in situ* studies.

3.2.1 - Synthesis of potential reactive intermediates

An active species in the catalytic cycle is potentially an entirely novel complex ^{Dipp}LFe(C≡C-Ph) (**70**), which is an analogue of a previously reported iron complex synthesised by Holland and co-workers.[10] Or perhaps the known iron(I) complex ^{Dipp}LFe(HC≡C-Ph) (**71**) (Figure 21).[9] The latter could arise from the dehydrocoupling mechanism previously discussed. This would show that the two mechanisms are inherently linked. Perhaps, rather than one species or the other being involved, both are giving rise to two possible reaction mechanisms leading to the observation of a small degree of *anti*-Markovnikov product when the reaction is undertaken in benzene.

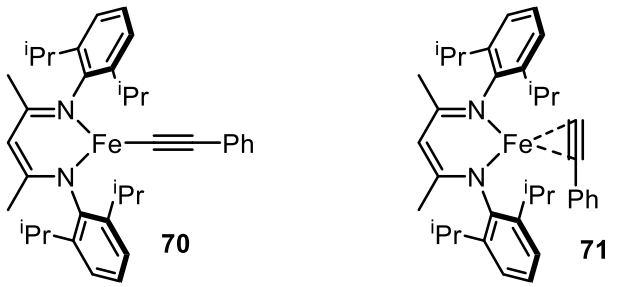

Figure 21: Potential catalytic intermediates **70** and **71**.

In view of this, stoichiometric reactions were undertaken with **1** and phenylacetylene; these reactions yielded a red complex, samples of which were sufficiently crystalline for single crystal x-ray analysis and in the solid state this was determined to be a dimeric iron acetylide complex {[^{Dipp}LFe(C≡C$_6$H$_5$)]$_2$}, **72** (Scheme 48, Figure 22).

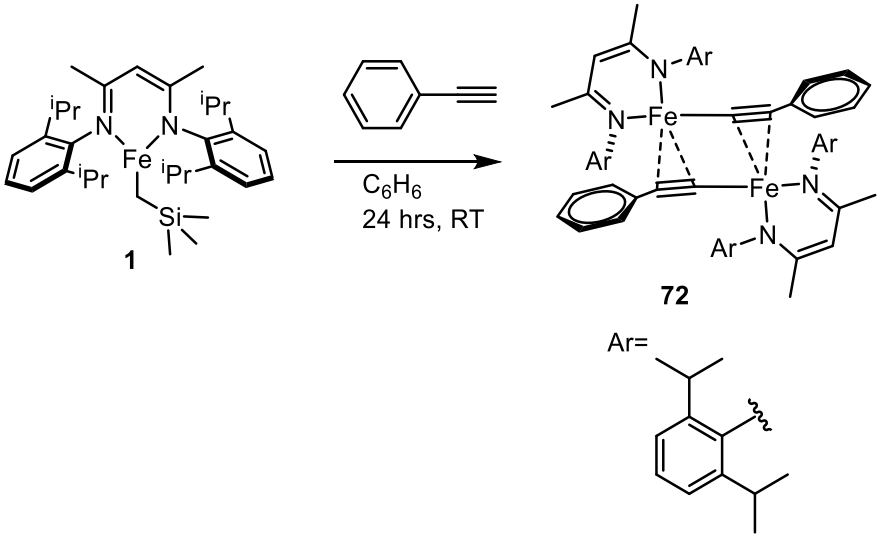

Scheme 48: Synthesis of [^{Dipp}LFe-CC(C$_6$H$_5$)]$_2$ (**72**).

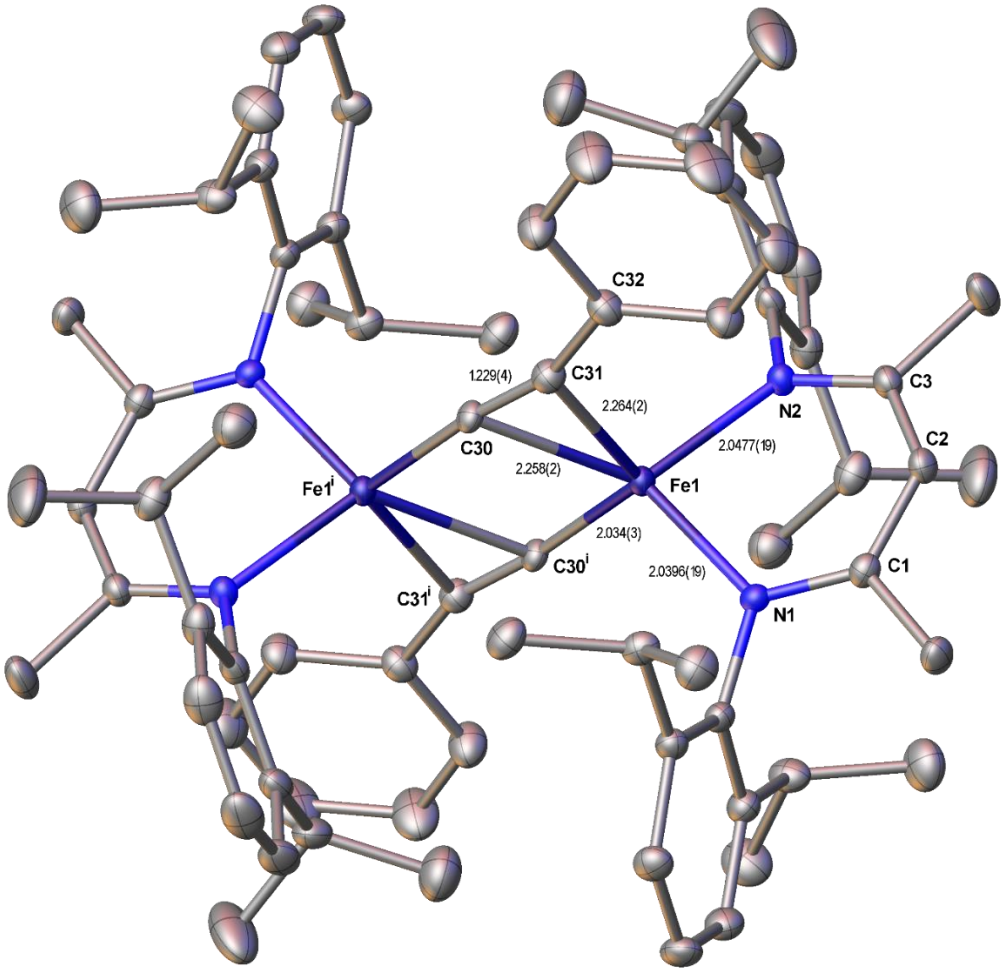

Figure 22: Crystal structure of **72**. Ellipsoids shown at 50% probability.

The major bond lengths and angles for compound **72** are shown in their respective tables (Tables 13 and 14). The iron centres Fe(1) and Fe(1′) are five coordinate in a distorted trigonal bipyramidal geometry. The end-on bound alkyne motifs (C30-C31) have carbon–carbon triple bond lengths of 1.223(3) Å, not too dissimilar to that observed for standard *sp*-hybridised carbon–carbon bonds. We would expect an *sp*-hybridised carbon-carbon to display a standard linear bond angle of 180 °. However, the observed bond angle for C30-C31-C32 is distorted at 159.7(2) °. The distortion in the bond angle occurs due to π-bonding with the iron metal centre.

Table 13: Selected bond lengths for complex **72**.

Atoms	Bond length (Å)
Fe(1) –C(30)	2.2559(18)
Fe(1) –C(31)	2.261(2)
Fe(1) –C(30^1)	2.033(2)
Fe(1) –N(1)	2.0366(17)
Fe(1) –N(2)	2.0450(16)
C(30) –Fe(1^1)	2.033(2)
C(30) –C(31)	1.223(3)
C(31) –C(32)	1.457(3)

Table 14: Selected bond angles for complex **72**.

Atoms	Bond angle (°)
N(1) –Fe(1) –N(2)	90.79(7)
N(1) –Fe(1) –C(30)	124.93(7)
N(1) –Fe(1) –C(31)	108.65(7)
N(2) –Fe(1) –C(30)	127.31(7)
N(2) –Fe(1) –C(31)	106.90(7)
C(30^1) –Fe(1) –N(1)	114.04(7)
C(30^1) –Fe(1) –N(2)	118.18(7)
C(30) –Fe(1) –C(31)	31.42(8)
C(30) –C(31) –C(32)	159.7(2)

The isolation of this stable iron complex enabled further experiments testing its relevance to the hydrophosphination catalytic cycle. Breakup of this dimeric complex could potentially lead to the formation of a monomeric iron acetylide in solution which could be a catalytically relevant species.

3.2.2 - Radical trap experiments

Given the difference in chemistry observed, the mechanism of reaction in benzene is presumably radical in nature. Radical clock and radical trap experiments were once again used as a means to test for potential radical mediated reactivity. The optimised reaction conditions were used for the test reaction. Order of addition was kept the same with phenylacetylene added first. Crucially what was observed in reactions with TEMPO, (iodomethyl)cyclopropane and (chloromethyl)cyclopropane was that no Markovnikov addition product was observed. The Markovnikov addition reactivity previously observed was then completely nullified by the addition of a radical clock/trap. The only observable product was a small spectroscopic yield (10%) of the *Z-anti*-Markovnikov product, presumably formed in a non-radical competitive side reaction. These observations suggest that radicals are key to the observed hydrophosphination reactivity with **1**.

As previously discussed the mechanisms of phosphine dehydrocoupling and alkyne hydrophosphination in benzene could be interlinked. It can be postulated that heating tetraphenyldiphosphane could lead to P-P bond cleavage and the formation of phosphine radicals. As phosphine radicals have been identified in the mechanisms of both phosphine dehydrocoupling and Markovnikov addition hydrophosphination reactions it was presumed that they could be key to the reactivity and selectivity observed with phenylacetylene. Control experiments with tetraphenyldiphosphane as a reactant debunked this theory with only trace amounts of Markovnikov addition product observed. This then suggests that the alkyne hydrophosphination mechanism is more complex than initially anticipated: whilst the reaction is radical mediated, tetraphenyldiphosphane formation does not occur during the reaction.

To test whether or not **1** is simply a radical initiator generating phosphine radicals it was replaced in hydrophosphination reactions with azobis(isobutyronitrile) (AIBN, 20 mol%). Under these conditions the major product observed was the *Z*-isomer *via anti*-Markovnikov addition (98% spectroscopic yield). As no Markovnikov addition is observed under these conditions, this further indicates that **1** has a much larger role in the catalytic cycle than simply generating phosphine radicals.

3.2.3 - Reaction monitoring studies

Kinetic analyses *via* spectroscopic methods can be incredibly diagnostic in the determination of catalytic mechanisms. NMR spectroscopy and in particular proton NMR spectroscopy have drawn heavy focus in kinetic studies due to the wealth of information that can be derived from experimental results.[130, 131] A full kinetic study was attempted for phenylacetylene hydrophosphination with **1** *via in situ* proton NMR spectroscopic monitoring. Preliminary results showed that this would not be a simple study with data often being irreproducible between catalytic runs. Upon changing reaction vessel from a sealed Schlenk with stirring (which was used for all catalytic reactions until this point) to a static J-Young NMR tube, reaction rates and selectivities were significantly hindered.

Rather than conducting a full kinetic study, preliminary mechanistic insight was sought through profiling the reaction. By taking samples of the reaction (containing a standard) at various time periods the progress of the reaction can be followed. Reaction profiles of **1** and **72** were taken for comparison (Figures 23 and 24).

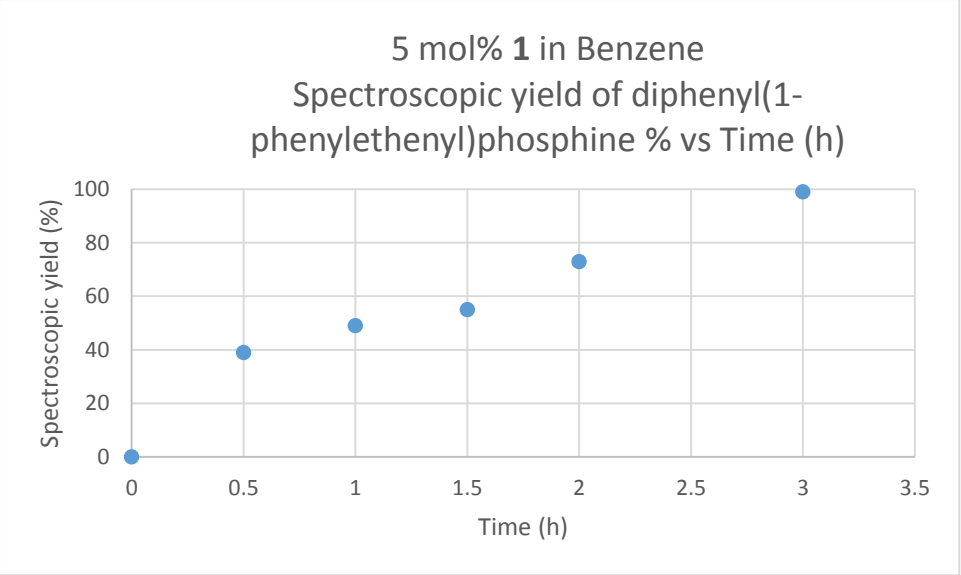

Figure 23: Reaction profile of Markovnikov hydrophosphination of phenylacetylene with **1** as a precatalyst.

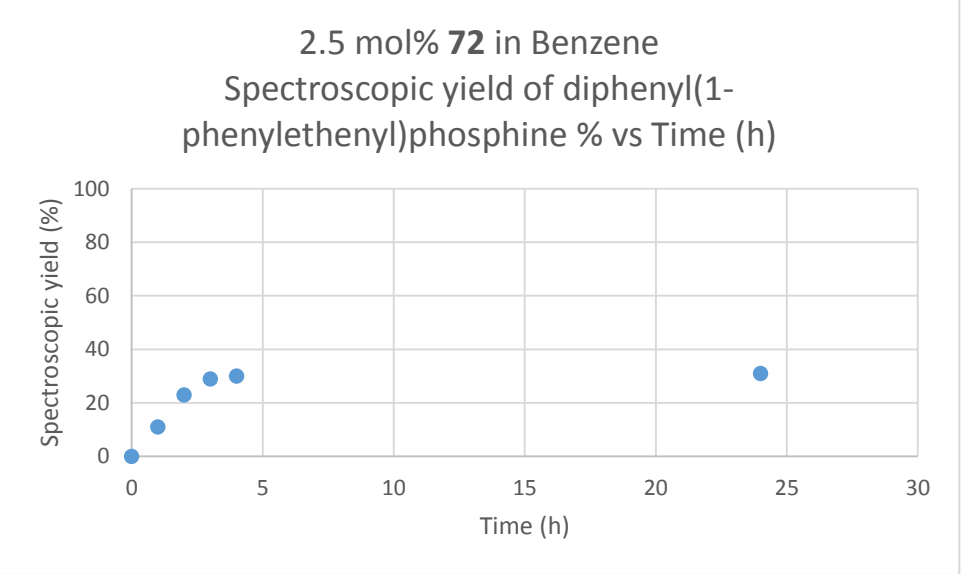

Figure 24: Reaction profile of Markovnikov hydrophosphination of phenylacetylene with **72** as a precatalyst.

It is immediately apparent that the reaction profiles of **1** and **72** are not concordant. Reactions where **1** is used as a precatalyst reach completion in three hours whereas reactions with **72** appear to reach saturation at this point and no further catalytic activity is observed. Based on these observations **72** is not an active species in the Markovnikov-selective catalytic cycle.

Based upon the conclusions drawn from these investigations a mechanism for Markovnikov addition hydrophosphination catalysed by **1** is postulated (Scheme 49).

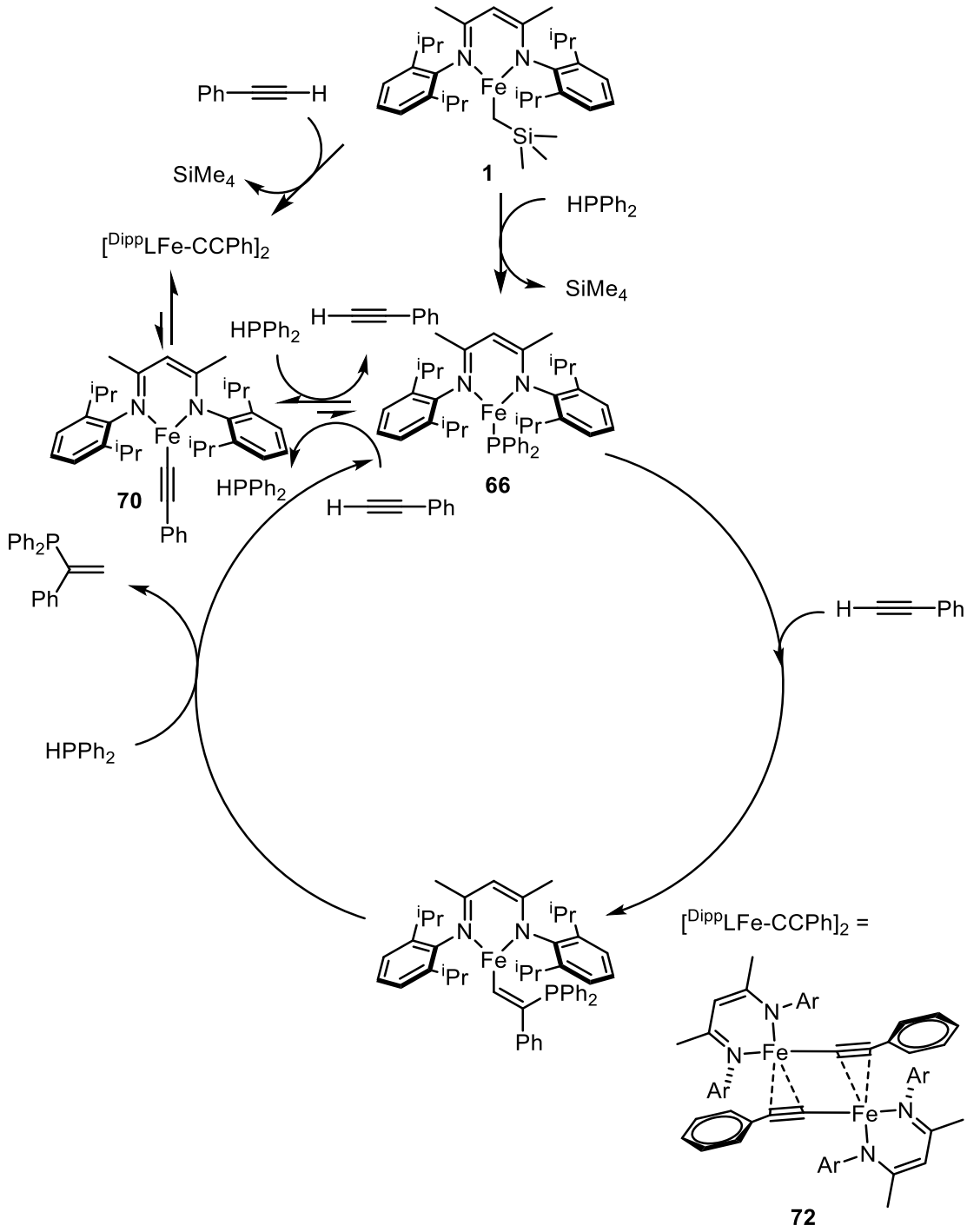

Scheme 49: Postulated catalytic mechanism for Markovnikov hydrophosphination of phenylacetylene.

The proposed mechanism (Scheme 49) is suggested on the basis of the high binding affinity of phenylacetylene to iron as previously reported by Holland and co-workers and on the results of the reaction profiles with **1** and **72**.[10] The iron phosphido species **66** is postulated as the active catalyst reacting with phenyl acetylene in a coordination insertion type mechanism. Subsequent protonlysis with diphenylphosphine completes the catalytic cycle. **72** is postulated to re-enter the catalytic cycle via breakup of the dimer to form **70** which is proposed to be in equilibrium with **66**. Alkynes are reported as having a much larger binding affinity than alkenes, on this basis interaction with the iron centre is expected as an

explanation as to why no hydrophosphination of styrenes is observed under the same conditions.

3.2.4 - Solvent switching.

These intriguing results beg the question as to why the reaction is completely regiodivergent upon a simple switch in solvent. In order to probe this blank reactions were performed with **1** in DCM. What is instantly noticiable is that upon heating the complex in solution a colour change is observed from the usual yellow of **1** to green. Analysis *via* proton NMR reveals a complete loss of signals. These results seem to implicate the solvent as non-innocent in reactivity. Further inspection and trapping experiments with pyridine suggest that **1** is abstracting chloride from DCM leading to an oxidation to the iron(III) complex $^{Dipp}LFeCl_2$ (**65**) (Schemes 50 and 52). **65** has been previously synthesised and is an NMR silent complex due to its inherent paramagnetic properties as a tetrahedral high spin iron(III) complex.[132]

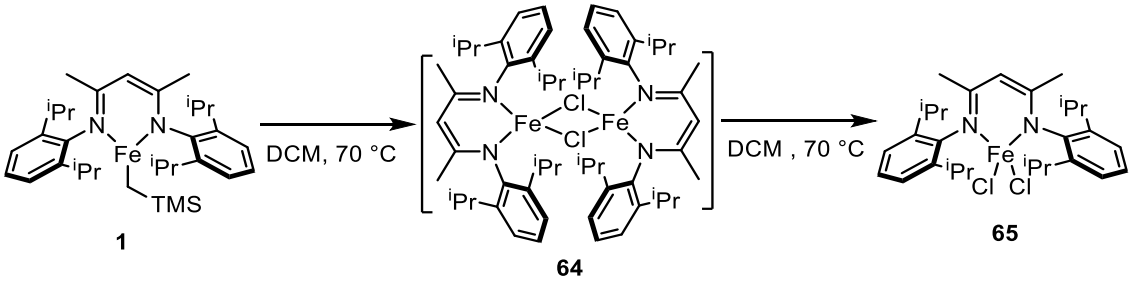

Scheme 50: Blank reaction of iron β-diketiminate (**1**) in dichloromethane.

It is worth noting that work by Hessen and co-workers has demonstrated that **1** can be formed by using **65** as a precursor.[7] Isolation of the green compound formed by reacting **1** with DCM and subsequent addition of two equivalents of (trimethylsilyl)methyl lithium in THF regenerates **1** demonstrating that the reaction is reversible.

Independent synthesis of **65** following literature reports was conducted and the reaction profiles of **1** and **65** were determined (Figures 25 and 26).

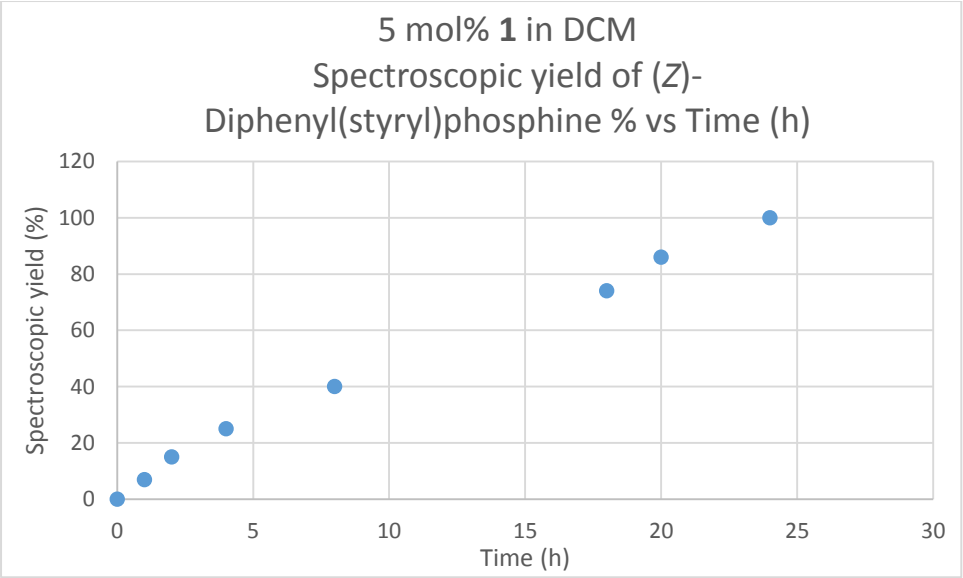

Figure 25: Reaction profile of *anti*-Markovnikov hydrophosphination of phenylacetylene with **1** as a precatalyst.

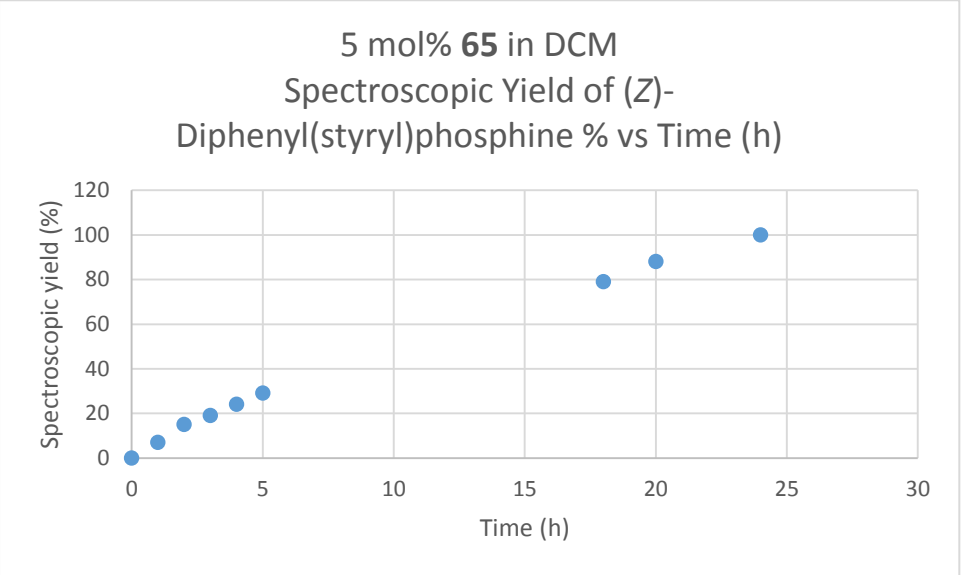

Figure 26: Reaction profile of *anti*-Markovnikov hydrophosphination of phenylacetylene with **66** as a precatalyst.

The reaction profiles with **1** and **65** as precatalysts are essentially identical suggesting that an initial oxidation from iron(II) to iron(III) precedes the hydrophosphination catalytic cycle. The "trapping" of the iron(II) chloride complex **73** (Figure 27) with pyridine (Scheme 51) confirms that oxidation to iron(III) occurs after an initial chloride abstraction step. This suggests that **64** is formed as an intermediate in solution, the dimer is broken up by pyridine as with previously reported iron β- diketiminate dimers.[8] This iron(II) chloro complex then goes on to react with a further equivalent of DCM. In previous studies Holland and co-workers have observed the slow reactivity of **64** with DCM and determined its instability in the solvent.[97] In these prior syntheses explicit detail is not given on the fate of the iron species formed but it seems reasonable to assume it is the NMR silent complex $^{Diip}LFeCl_2$, **65**.

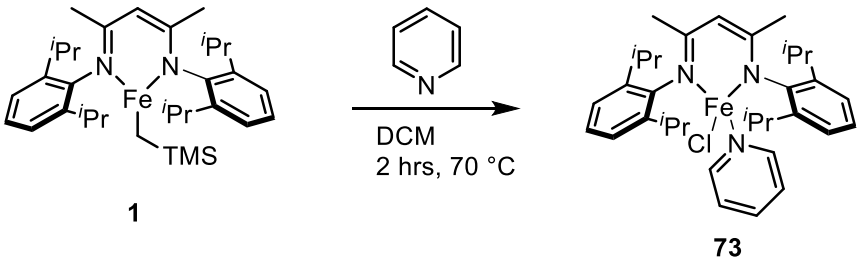

Scheme 51: Blank reaction of iron β-diketiminate (**1**) in DCM with pyridine yields **73**.

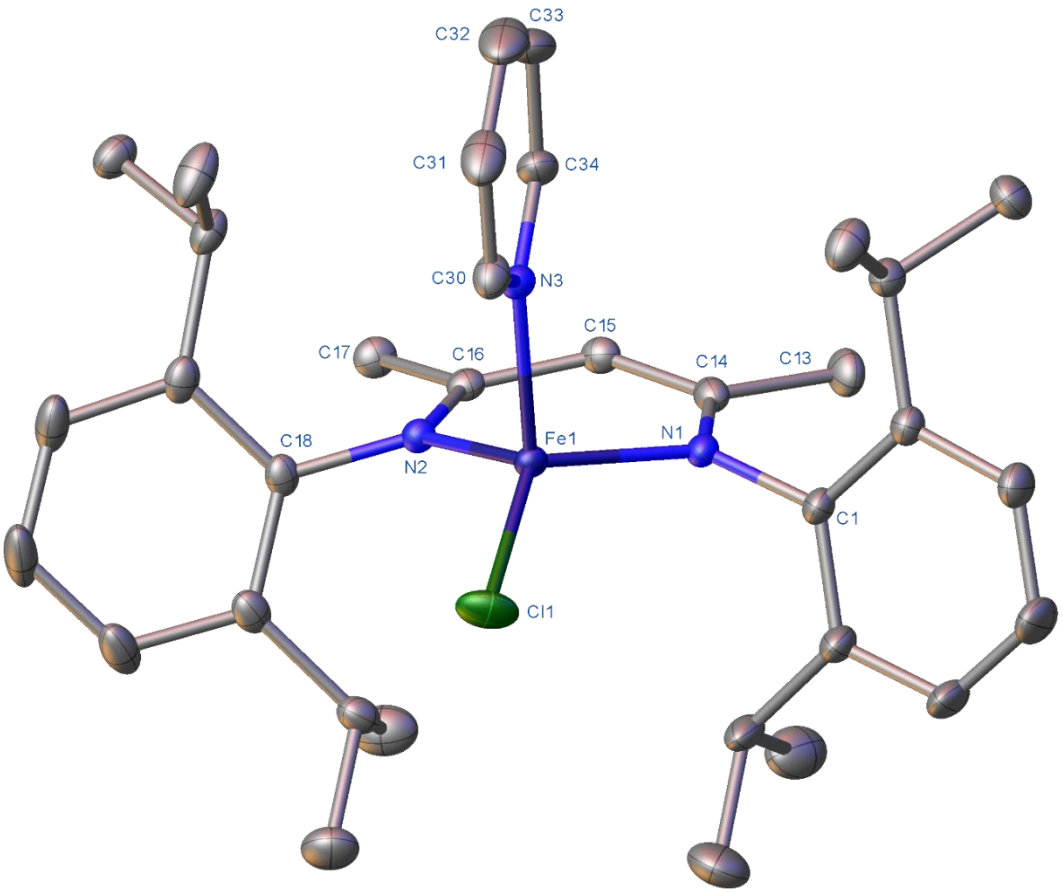

Figure 27: Crystal structure of **73.** Ellipsoids displayed at 50% probability.

The major bond lengths and angles for complex **73** are shown in their respective tables (Tables 15 and 16). The four coordinate iron centre Fe(1) displays a tetrahedral geometry. The iron chlorine bond Fe(1)-Cl(1) at 2.2447(5) Å is shorter than the Fe(1)- Cl(1) bond for the chloro dimer **64** (2.3582(5) Å).[10] The observed N(1)-Fe(1)-N(2) angle of 93.68(6) ° is comparable to the same angle in **1** of 93.84(5) °.

Table 15: Selected bond lengths for complex **73**.

Atoms	Bond length (Å)
Fe(1) –Cl(1)	2.2447(5)
Fe(1) –N(1)	2.0057(14)
Fe(1) –N(2)	2.0126(13)
Fe(1) –N(3)	2.1033(14)
N(1) –C(1)	1.439(2)
N(1) –C(14)	1.331(2)

Table 16: Selected bond angles for complex **73**.

Atoms	Bond angle (°)
N(1) –Fe(1) –N(2)	93.68(6)
N(1) –Fe(1) –Cl(1)	124.83(5)
N(1) –Fe(1) –N(3)	105.15(6)
N(2) –Fe(1) –Cl(1)	124.42(4)
N(2) –Fe(1) –N(3)	105.60(5)
N(3) –Fe(1) –Cl(1)	101.03(4)
C(1) –N(1) –Fe(1)	117.39(12)
C(14) –N(1) –Fe(1)	122.56(11)

Radical clock and radical trap experiments were again used as a means to test for potential radical mediated reactivity in this DCM reaction. In stark contrast to the reaction in benzene under standard conditions with **1**, phenylacetylene and diphenylphosphine in DCM no inhibition of hydrophosphination activity was observed when TEMPO, (iodomethyl)cyclopropane or (chloromethyl)cyclopropane were added. This suggests that the catalytic cycle is not radical mediated.

In catalysing hydrophosphination **65** is postulated to act as a strong Lewis acid. In order to test whether a simple Lewis acid mediated process is taking place, or whether a more discrete iron-mediated reaction is at play, a range of other Lewis acids were tested as catalysts for the hydrophosphination of phenylacetylene (Table 17).

Table 17: Lewis acid catalysed hydrophosphination of phenylacetylene.

Entry	Lewis acid	*Loading (mol %)*	Spec Yield (%)	Product distribution (E:Z:Markovnikov)
1	$FeCl_3$	*5*	56	5:95:0
2	$Fe(acac)_3$	*5*	34	5:95:0
3	$BF_3.Et_2O$	*5*	3	66:33:0
4	$Cu(OTf)_2$	*5*	8	33:33:33
5	$AlCl_3$	*5*	10	20:40:40

Conditions: $HPPh_2$ (0.5 mmol), phenyl acetylene (1.0 mmol), DCM (0.35 mL), 70 °C, 24 hrs.

What is clearly evident from the Lewis acids tested in hydrophosphination catalysis (Table 17) is that the iron salts were the most competent catalysts with iron(III) chloride giving the highest spectroscopic yield. This fits with observed catalytic competence of **65** with the higher spectroscopic yields of the runs with the β-diketiminate complex attributed to steric bulk and greater solubility facilitated by the ancillary ligand. Whilst the other Lewis acids tested proved to be poor hydrophosphination catalysts it is interesting to note that one of the major products with aluminium trichloride (Entry 5) is the Markovnikov addition product. The overall spectroscopic yield and product selectivity are poor but given the relative scarcity

for Markovnikov addition hydrophosphination of alkynes, coupled with the rarity of studies into hydrofunctionalisation with aluminium catalysts, this result implies the potential for further studies.[133]

Based upon these investigations a mechanism is proposed for *anti*-Markovnikov addition hydrophosphination (Scheme 52).

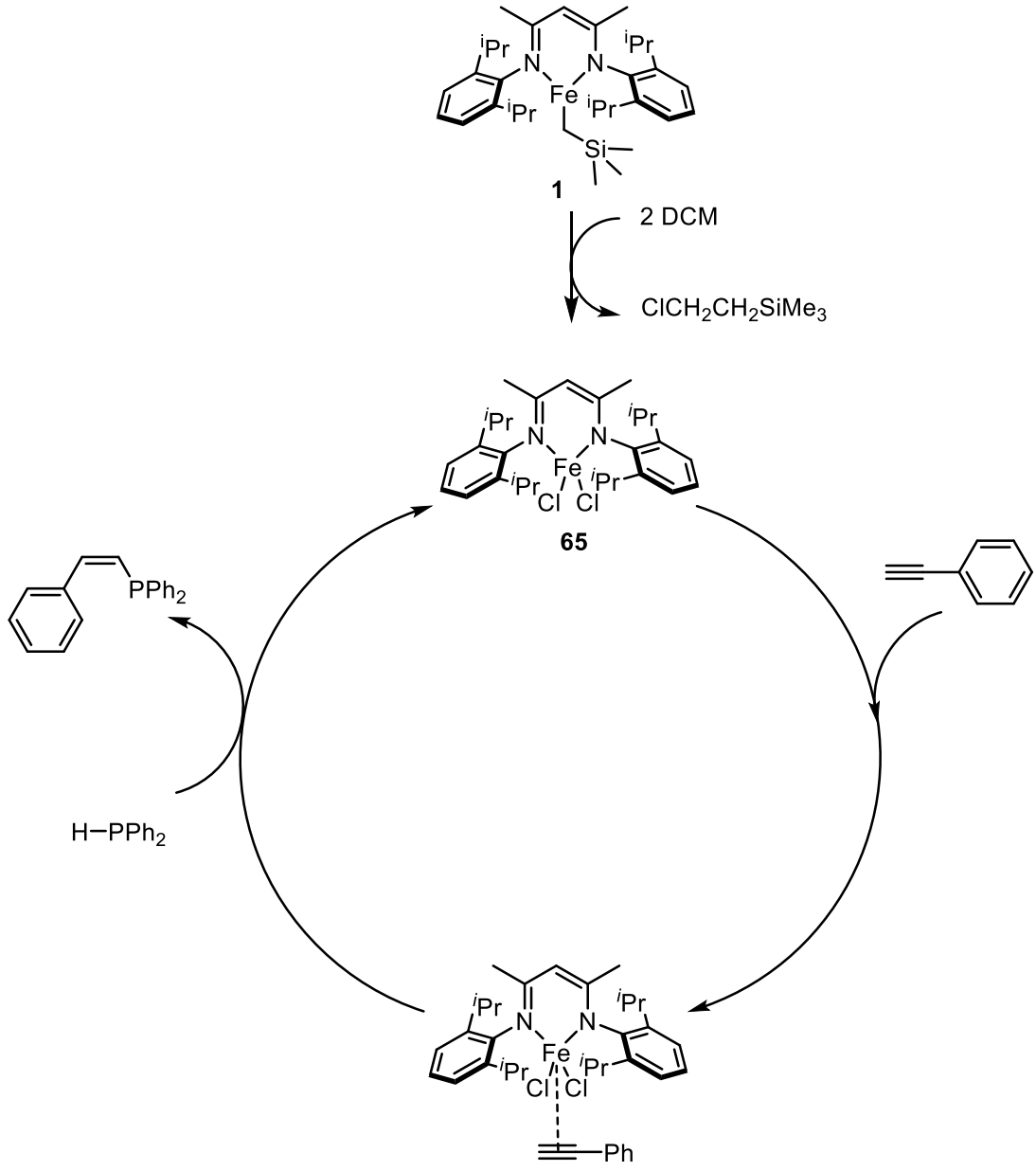

Scheme 52: Proposed catalytic cycle for anti-Markovnikov hydrophosphination.

The proposed catalytic cycle is analogous to the catalytic cycle proposed by Gaumont and co-workers for their iron chloride catalysed alkene hydrophosphination.[55] The selectivity for *anti*-Markovnikov addition over Markovnikov is due to the polarity of the acetylene triple bond, where a nucleophilic phosphine adds to the more electron deficient terminal carbon.

Overall **1** has been determined to be a highly competent precatalyst for intermolecular hydrophosphination reactions. The coordination and insertion of an unsaturated carbon into

an iron-phosphorus bond observed in Markovnikov addition hints that this reactivity could be further explored through intramolecular reactions.

3.3 - Intramolecular hydrophosphination of phosphinoalkenes and phosphinoalkynes

3.3.1 - Phosphinoalkene and phosphinoalkyne synthesis.

Marks' lanthanide-catalysed hydrophosphination of phosphinoalkenes and phosphinoalkynes as discussed previously has yet to be repeated with a transition metal catalyst. Based on the success of intermolecular hydrophosphination of alkenes and alkynes with **1** we proposed that these complexes might show orthogonal intramolecular hydrophosphination reactivity.[41, 42] Reports by Hannedouche and co-workers on intramolecular hydroamination of aminoalkenes catalysed by iron β-diketiminate complexes suggest that analogous reactions with phosphinoalkenes and phosphinoalkynes could prove successful.[15]

Synthesis of the phosphinoalkenes was attempted following Marks' procedures (Schemes 53, 54 and 55). The compounds were synthesised in good yields in accordance with the literature.

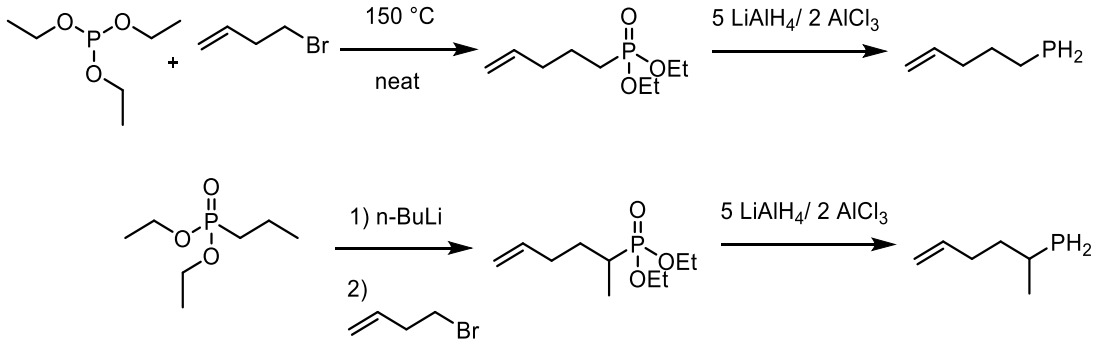

Scheme 53: Synthesis of primary phosphinoalkenes (work carried out by Dr. Maialen Espinal).

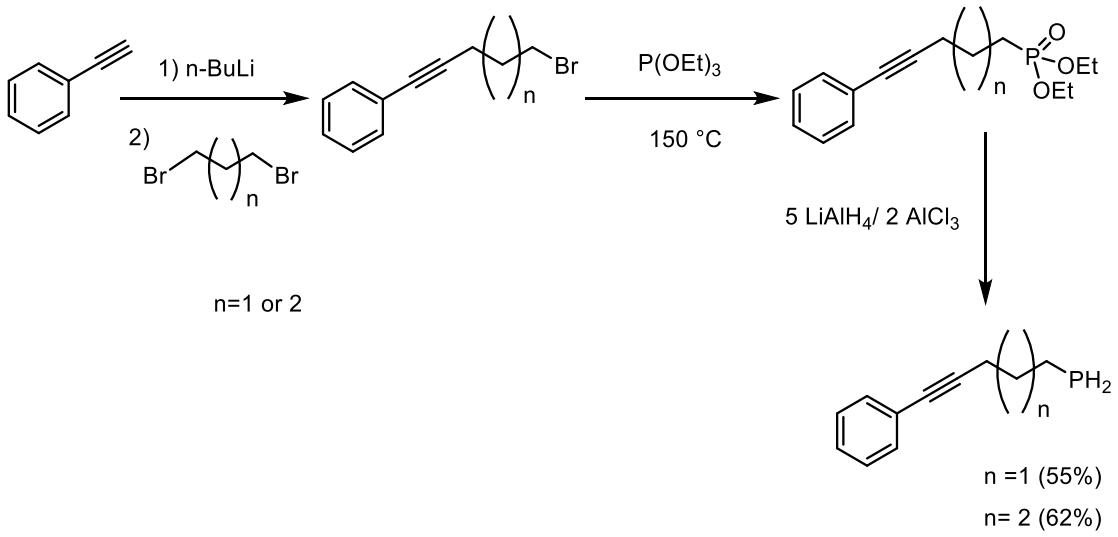

Scheme 54: Synthesis of phosphinoalkynes.

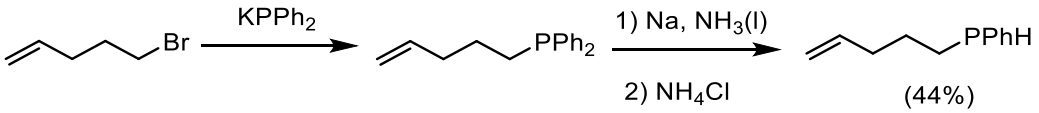

Scheme 55: Synthesis of secondary Phosphinoalkenes.

Synthesis of the linear phosphinoalkenes (Figure 28) substrates pent-4-enylphosphine (Table 19, Entry 1), 1-methylpent-4-enylphosphine (Table 19, Entry 2), hex-5-enylphosphine (Table 19, Entry 3) and 1-methylhex-5-enylphosphine (Table 19, Entry 4) was carried out by Dr. Maialen Espinal.

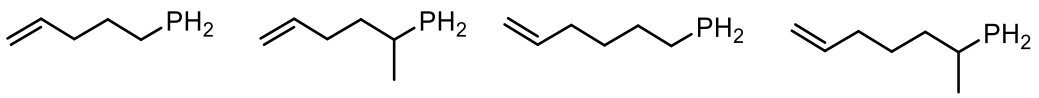

Figure 28: Phosphinoalkene substrates.

3.3.2 - Catalysis

Catalytic synthesis of the cyclic phosphines was then attempted initially at a catalytic loading of 5 mol%, while some intramolecular hydrophosphination products were formed the yield was relatively poor. Increasing the catalytic loading to 10 mol% led to much improved yields. In the absence of a catalyst under the optimised reaction conditions formation of the five-membered cyclic phosphines was not observed. The full optimisation table is detailed below (Table 18).

Table 18: Optimised conditions for the intramolecular hydrophosphination of pent-4-enylphosphine.

Entry	***[Fe]***	*Loading (mol %)*	*Conditions*	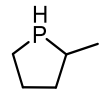 *(%)[a]*
1	***60***	*5*	*70 °C, 48 hrs*	*trace*
2	***60***	*5*	*90 °C, 48 hrs*	*5*
3	***60***	*10*	*90 °C, 24 hrs*	*35*
4[b]	***1***	*10*	*90 °C, 24 hrs*	*100*
5[b]	***1***	*10*	*90 °C, 12 hrs*	*92*
6[b]	***1***	*10*	*90 °C, 18 hrs*	*100*

*Conditions: 10 mol% **1**, pent-4-enylphosphine (0.25 mmol), C_6H_6 (0.35 mL). [a] Based on loss of loss of P–H signal from ^1H NMR spectra, using 1,3,5-trimethoxybenzene as an analytical standard. [b] Carried out by Dr Maialen Espinal*

These optimised conditions were then used for the majority of phosphinoalkenes and phosphinoalkynes. The spectroscopic conversions and isolated yields are detailed (Table 19).

Table 19: Intramolecular hydrophosphination of phosphinoalkenes and phosphinoalkynes.

Entry	*RR'PH*	*Isomer(s)* *(Major : Minor)*	*Spec. Yield (%)[a]* *[Isolated Yield (%)]*
1[b]	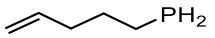	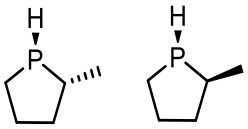 (33) (66)	*100 [86]*
2[b]	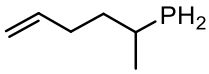	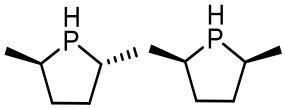 (58) (42)	*90 [72]*
3[b c]	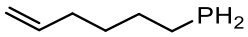	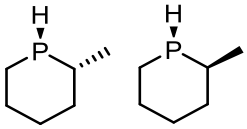 (17) (83)	*69 [33]*
4[b c]	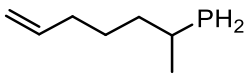	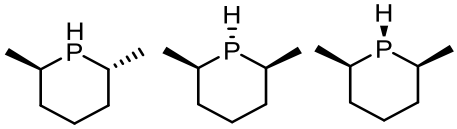 (68) (20) (12)	*74 [20]*
5[bd]	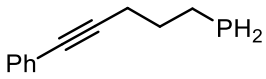	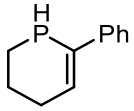	*95 [57]*
6[be]	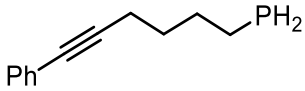	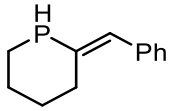	*100 [90]*
7[f]	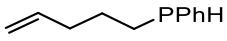	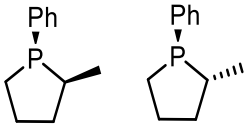 (62) (38)	*100 [44]*

*Conditions: 10 mol% **1**, H_2PR (0.25 mmol), C_6H_6 (0.35 mL), 90 °C, 18 hrs [a] Based on loss of P–H signal from ^1H NMR spectra, using 1,3,5-trimethoxybenzene as an analytical standard , [b] Carried out by Dr. Maialen Espinal, [c] 10 mol% $^{Dipp}LFeCH_2TMS$ (**1**), 90 °C, 36 hrs, [d] 50 °C, 48 hrs, [e] 10 mol% $^{Xyl}LFeCH_2TMS.THF$ (**60**), 90 °C, 17 hrs. [f] 90 °C, 14 hrs.*

The products 2-(1-phenyl-2-ethenyl)phospholane (Entry 5) and 2-(2-phenyl-1-ethenyl)phosphorinane (Entry 6) were found to be thermally unstable, in particular 2-(2-phenyl-1-ethenyl)phosphorinane was found to be so unstable that the reaction temperature could not be raised above 50 °C without full degradation of the products formed during the course of the reaction. Isomers were observed for certain products (Entries 1-4 and 7) due to the formation of stereogenic centres in the products. Light sensitive substrates pent-4-enylphosphine (Entry 1), 1-methylpent-4-enylphosphine (Entry 2), and pent-4-enylphenylphosphine (Entry 7) were all reacted in the dark using tin foil to coat the outside of the Young's tap NMR tube. This was to avoid a competitive side reaction that is light initiated. In the presence of light the phosphinoalkenes undergo *anti*-Markovnikov addition to form six membered rings whereas in the presence of the catalyst under the optimised conditions Markovnikov addition is observed leading to the formation of five membered rings.

3.3.3 - Mechanistic considerations

In probing the mechanism of intramolecular hydrophosphination it is plausible that the reaction proceeds *via* an iron(I) species (Scheme 56). It is anticipated that reactivity proceeds *via* an iron phosphido species. Grubba and co-workers have previously described the dissociation of iron(II) phosphide complexes to form iron(I) species.[110] Thus it was important to probe the reaction with an iron(I) β-diketiminate precatalyst. As with phosphine dehydrocoupling the mechanism of intramolecular hydrophosphination was determined to be radical in nature. As postulated in Chapter 2 iron and phosphorus centred radicals are likely to act as catalytic intermediates. Analogous Fe-P radicals have previously been reported.[134]

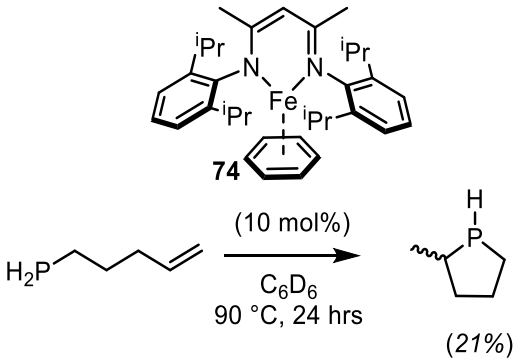

Scheme 56: Iron(I) (**74**) mediated synthesis of 2-methylphospholane.

Given the reaction is undertaken in benzene, synthesis and subsequent utilisation of the iron(I) benzene complex **74** in the hydrophosphination of pent-4-enylphosphine is not comparable with that of **1**, giving a much lower yield under the same reaction conditions. After heating for a further 5 days no further product was formed. This would suggest that the iron(I) complex **74** is not involved as an on-cycle intermediate.

In terms of the mechanism of the reaction it would seem plausible that σ-bond metathesis mechanism analogous to Marks' mechanism is at work (Scheme 57).

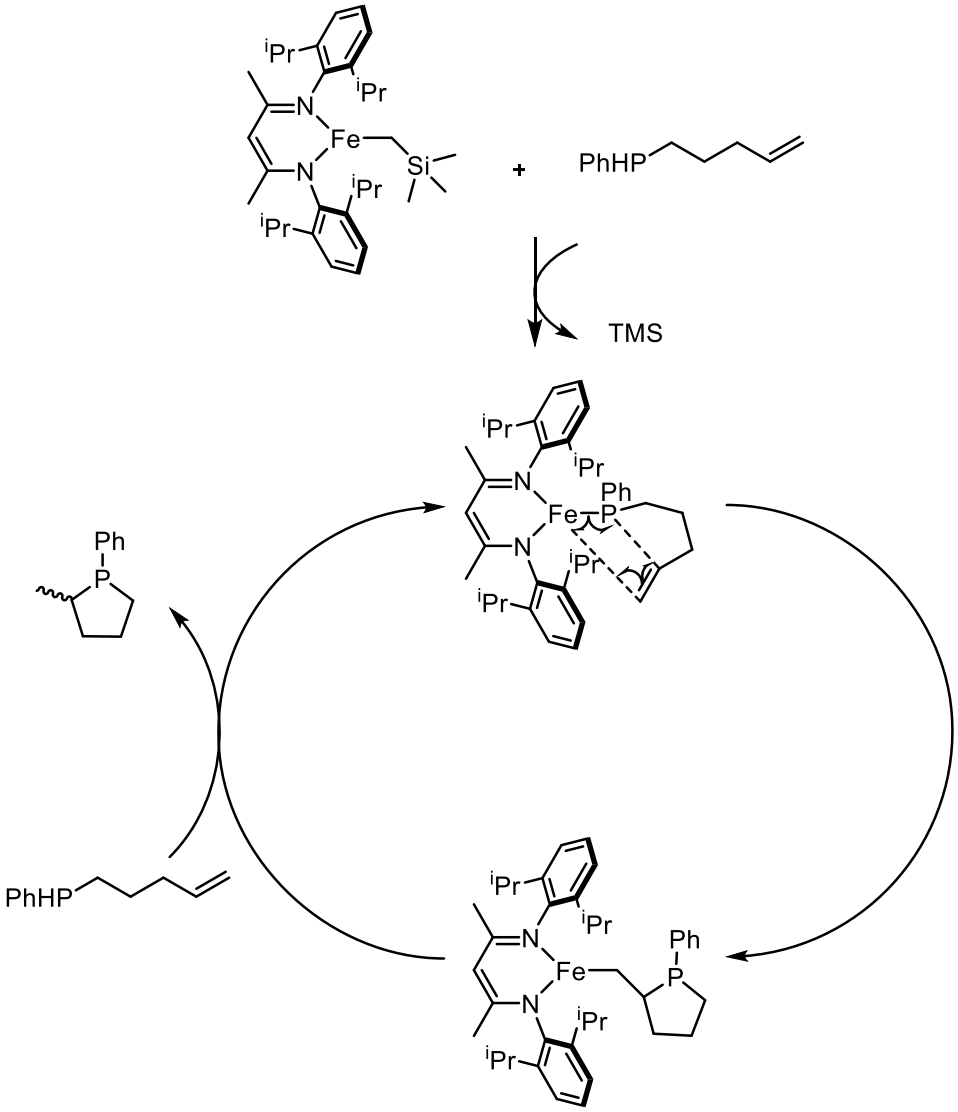

Scheme 57: Plausible mechanism for the iron catalysed intramolecular hydrophosphination of phosphinoalkenes.

3.3.4 - Chiral catalyst synthesis

The cyclic phosphine products 2-methylphospholane, 2,5-dimethylphospholane, 2-methylphosphorinane, 2,6-dimethylphosphorinane and 1-phenyl 2-methyl phospholane (Table 6, Entries 1-4 and 7) all contain stereogenic centres. Therefore with the achiral catalyst **1** a racemic mixture of isomers is formed in the intramolecular hydrophosphination reactions. Marks has shown previously intramolecular hydrophosphination can be achieved enantioselectively by utilising an enantiopure catalyst comprising a chiral ancillary ligand.[46] One such class of chiral β-diketiminate ancillary ligands and their ligated copper complexes have been reported by Schaper and co-workers (Scheme 58).[135, 136]

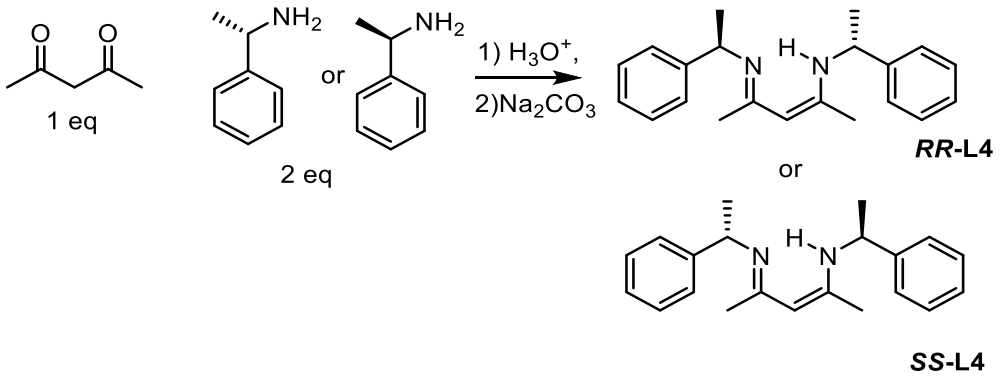

Scheme 58: Synthesis of the chiral β-diketiminate ligands 2-(S-2-phenylethyl) amino-4-(S-4-phenylethyl) iminopent-2-ene (***SS*-L4**) and 2-(R-2-phenylethyl)amino-4-(R-4-phenylethyl)iminopent-2-ene (***RR*-L4**).

Attempts to replicate the synthesis of these ligands proved incredibly testing. Initially, in our hands, the procedure could not be replicated to give a sufficient yield of product. After multiple attempts an alternative methodology was found and the subsequent synthesis attempted.[136] In a method using minimum amount of solvent, one equivalent of amine was added to one equivalent of acetylacetone in order synthesise the *R* or *S* enantiomer of the mono-substituted species 4-[(1-phenylethyl)amino]-3-penten-2-one. After reflux for a period of three hours a second equivalent of the same amine was then added with one equivalent of *para*-toluene sulfonic acid and the resulting mixture was stirred and refluxed with a Dean-Stark apparatus for five days in order to drive the condensation reaction. This methodology proved successful and gram scale yields of chiral β-diketiminates were achieved.

With the chiral β-diketiminate ligands in hand, Hessen's method for the synthesis of iron β-diketiminate complexes was used.[7] As demonstrated previously with **1** and **60**, this proved successful (Scheme 59).

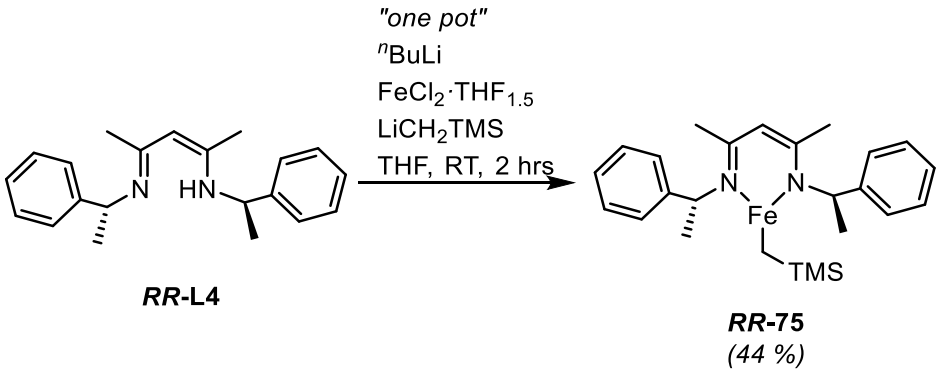

Scheme 59: Synthetic method for preparation of enantiopure iron β-diketiminate species.

With the successful synthesis of enantiopure iron β-diketiminate complexes, attempts were made at enantioselective intramolecular hydrophosphination/cyclisation reactions with pent-4-enylphosphine and hex-5-enylphosphine used as substrates.

This proved to be unsuccessful with very low yields of cyclic phosphine products observed with either **RR-75** or **SS-75** employed as catalysts. A plausible explanation for this is that the alkyl functionalities on the β-diketiminate ligands do not provide the same stereoelectronic resonance stability as the diisopropylphenyl groups on **1**. Ligand non-innocence then likely plays some role in reactivity. This has been previously reported with β-diketiminate ligands.[137]

An alternative chiral ancillary ligand was sought to circumvent this low catalytic activity. Based on reports in the literature of highly enantioselective catalysis with transition metal complexes supported by a *N*,*N*'-chiral bidentate ligand, the synthesis of an iron complex supported by this chiral ancillary ligand was attempted (Figure 29).[138, 139]

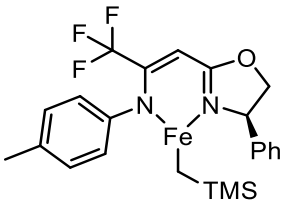

***R*-76**
(33%)

Figure 29: Chiral iron alkyl complexes supported by N, N' ancillary ligands.

This complex was also tested for catalytic efficiency with pent-4-enylphosphine and hex-5-enylphosphine. As with **RR-75** and **SS-75** the chiral iron complex proved to be a poor catalyst for intramolecular hydrophosphination. In light of these results a sufficiently active chiral iron complex was not discovered and iron-catalysed enantioselective hydrophosphination / cyclisation was not achieved in this study. Given that this is the first example of intramolecular hydrophosphination catalysed by a transition metal, the results presented herein are very promising. A full future study on diastereoselective hydrophosphination (and by extension diastereoselective hydroamination) poses a lot of potential but is beyond the scope of this thesis.

3.4 - Conclusions from Chapter 3

The results in this chapter described investigations into hydrophosphination reactions catalysed by **1**. It was determined that when benzene is employed as a solvent hydrophosphination of phenylacetylene occurs *via* Markovnikov addition. This reactivity was reproduced over a broad range of substrates and extended to primary phosphines. A simple switch in solvent to DCM was then described leading to a change in regioselectivity where *anti*-Markovnikov addition is favoured. The *Z*-stereoisomer was observed to be the major product under these conditions. A modest substrate scope has been reported for *anti*-Markovnikov hydrophosphination. Mechanistic insight has been gauged for both reactions providing evidence that supports two very different reaction mechanisms. Markovnikov addition occurs *via* a radical mediated mechanism. In depth kinetic analyses were attempted but failed to produce any discernible mechanistic details. Stoichiometric reactions of **1** with phenylacetylene yield the dimeric acetylide complex **72**. Reaction profiling revealed that **72** is not an on-cycle catalytic intermediate. Background reactions with **1** and DCM revealed that oxidation is occurring to give the iron(III) complex **65**. Reaction profiling confirms that this is a prerequisite to access the *anti*-Markovnikov catalytic cycle. Results detailed suggest the divergent reaction in DCM occurs *via* simple Lewis acid catalysis.

Further investigations determined that **1** is a catalyst for intramolecular hydrophosphination reactions. A good substrate scope is detailed represented by a range of phosphinoalkenes and phosphinoalkynes. Syntheses of asymmetric iron β-diketiminate complexes and their analogues was achieved. However, these complexes were found to display little catalytic activity towards phosphinoalkenes.

4- Heterodehydrocoupling of phosphine-silanes and amine-silanes

4.1 - Phosphine-silane dehydrocoupling - synthesis

Chapter 2 focused on investigations of serendipitous phosphine dehydrocoupling catalysed by **1**. As previously discussed phosphine homodehydrocoupling is facile with the iron β-diketiminate precatalyst. Subsequent investigations were undertaken to determine whether the scope of this reactivity could be extended. Cross-dehydrocoupling reactions between phosphines and silanes have been shown to work efficiently with organometallic complexes.[80, 81] Silaphosphanes are an important class of compounds that can be used as reagents in phosphination reactions.[140-142] Astonishingly, under the same catalytic conditions previously optimised for phosphine coupling, in the presence of a silane, near exclusive selectivity was observed for phosphine-silane dehydrocoupling (Scheme 60).

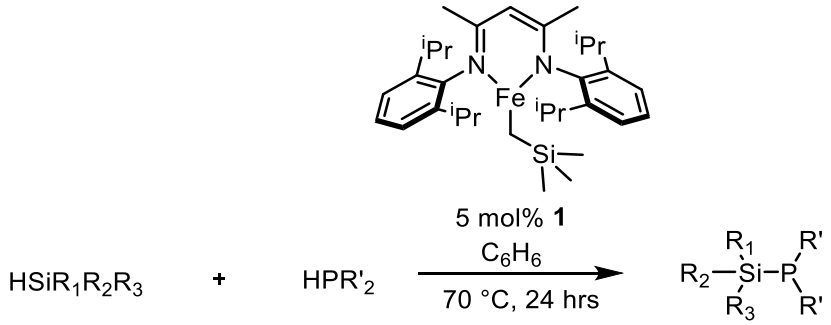

Scheme 60: Phosphine-silane dehydrocoupling catalysed by **1**

Further optimisation of the reaction conditions was attempted (Table 20). However, the reaction conditions previously settled upon for phosphine dehydrocoupling proved to be optimal.

Table 20: Optimisation of phosphine-silane dehydrocoupling

Entry	*Time (hrs)*	*Spec. Yield (%)[a]*	*Temperature (°C)*	*Selectivity (P-Si vs P-P)*
1	*24*	*100*	*90*	*80:20*
2	*24*	*100*	*70*	*85:15*
3	*24*	*88*	*50*	*93:7*
4	*24*	*10*	*RT*	*N.D.*

*Conditions: 5 mol % **1**, $HPPh_2$ (0.5 mmol), H_2SiPh_2 (0.5 mmol), C_6H_6 (0.35 mL). [a] NMR yield calculated from the consumption of $HPPh_2$ against 1,3,5-trimethoxybenzene as an internal standard.*

Having established that phosphine-silane heterocoupling is favoured over phosphine homocoupling, the substrate scope and reactivity were probed (Table 21).

Table 21: Substrate scope for phosphine-silane dehydrocoupling

Entry	*R_1R_2PH* $R_1R_2R_3SiH$	*Spec. Yield (%)[a]*	*Product*	*Selectivity(P-Si: P-P)*
1	Ph_2PH Ph_2SiH_2	*100*	$Ph_2P-SiHPh_2$	*85:15*
2	Cy_2PH Ph_2SiH_2	*100*	$Cy_2P-SiHPh_2$	*99:1*
3	Ph_2PH $MePhSiH_2$	*100*	$Ph_2P-SiHMePh$	*81:19*
4	Cy_2PH $MePhSiH_2$	*100*	$Cy_2P-SiHMePh$	*99:1*
5	Ph_2PH $PhSiH_3$	*100*	Ph_2P-SiH_2Ph	*80:20*
6	Cy_2PH $PhSiH_3$	*100*	Cy_2P-SiH_2Ph	*92:8*
7	Ph_2PH Ph_3SiH	*100*	$Ph_2P-SiPh_3$ Ph_2P-PPh_2	*0:100*
8	Cy_2PH Ph_3SiH	*trace*	$Cy_2P-SiPh_3$ Cy_2P-PCy_2	*0:100*
9	Ph_2PH $MePh_2SiH$	*100*	$Ph_2P-SiMePh_2$ Ph_2P-PPh_2	*0:100*
10	Cy_2PH $MePh_2SiH$	*trace*	$Cy_2P-SiMePh_2$ Cy_2P-PCy_2	*0:100*

*Conditions: 5 mol % **1**, HPR_2 (0.5 mmol), H_2SiR_2 or H_3SiR (0.5 mmol), C_6H_6 (0.35 mL), 70 °C, 24 hrs. [a] NMR yield calculated from the conversion to silaphosphanes with 1,3,5-trimethoxybenzene as an internal standard.*

Whilst high selectivity was observed towards primary and secondary silanes (Entries 1-6) no selectivity towards phosphine-silane coupling was observed with tertiary silanes. This is proposed to be due to the increased steric demands on the catalyst. Rather than promoting phosphine-silane coupling, in these examples (Entries 7-10) only the aforementioned phosphine homocoupling was observed. Reactions with dicyclohexylphosphine (Entries 2, 4 and 6) were surprisingly selective given the harsh conditions required for homocoupling (in

Chapter 2 it was noted that at 120 °C after 72 hours with 10 mol% **1** an 89% yield of P-P was observed). In addition to the substrates in Table 21 primary phosphines were tested but no P-Si bonding was detected. Iron β-diketiminate species with primary phosphine moieties have been previously reported to exist as phosphido-bridged dimers.[143] A reasonable assumption is that these phosphido dimers promote homocoupling over heterocoupling due to the close proximity of phosphorus centres. Analysis of the crude reaction mixture show a modest spectroscopic yield (28%) of diphenyldiphosphane (Scheme 61).

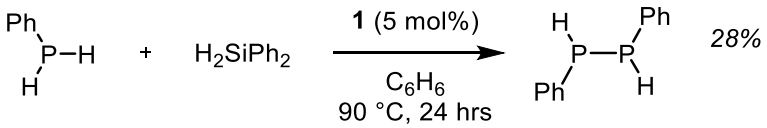

Scheme 61: Reaction with phenylphosphine and diphenylsilane yielding diphenyldiphosphane

Having investigated the substrate scope, further insight was sought to rationalise this high selectivity towards heterocoupling.

4.2 – Phosphine-silane dehydrocoupling mechanistic studies

In order to further scrutinise the mechanistic activity; a full kinetic study was devised. Products in this study (Examples 1-6) have Si-H protons that do not overlap with the aromatic region making an excellent reference point for kinetic analyses *via* proton NMR. This was a significant limitation with mechanistic investigations of catalytic phosphine coupling. Initial optimisation experiments and further experiments developing the substrate scope of the reaction were conducted in sealed screw cap Schlenk tubes. For the purposes of kinetic analyses the reaction vessels were switched to J-Young's NMR tubes.

Upon altering the reaction vessel, quite unexpectedly, no phosphine-silane coupling was observed. Rather than heterocoupling, under these conditions exclusive selectivity was observed for phosphine homocoupling. In order to determine whether this was in fact an anomalous result, repeat reactions were conducted. However, the same results were obtained. Upon unsealing the screw tap a distinguishable "pop" noise is audible due to a build-up in pressure within the tube. This build-up of hydrogen gas in a smaller headspace may have an adverse effect on the selectivity of the reaction.[144, 145]

4.2.1- Radical trap studies

As discussed previously, addition of the radical trap TEMPO would lead to a significant decrease in spectroscopic yield if the dehydrocoupling reaction is radical in origin. In the presence of TEMPO (Scheme 62) phosphine-silane dehydrocoupling activity was completely suppressed.

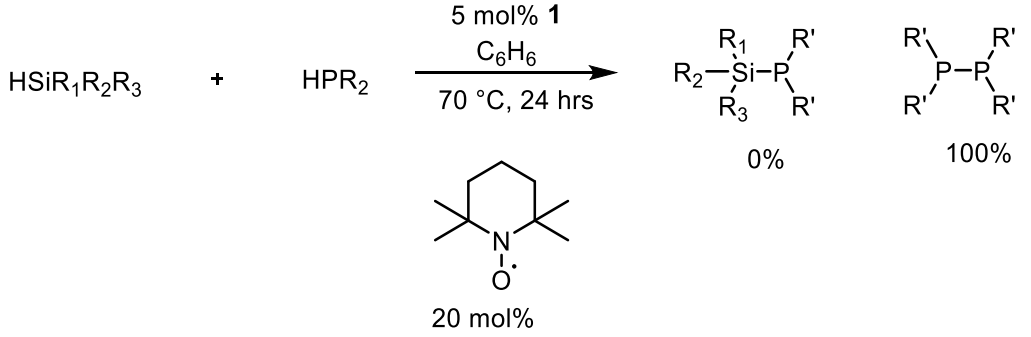

Scheme 62: Phosphine-silane coupling catalytic run in the presence of TEMPO.

Intriguingly the addition of the radical trap led to phosphine homocoupling. Initially this seems to be in contradiction with previous experiments in the presence of TEMPO (see Chapter 2) that led to depleted yields with respect to phosphine dehydrocoupling. Upon further inspection it becomes apparent that the silane has in fact reacted with the TEMPO to form a siloxane. This has been previously reported by Hill and co-workers with magnesium β-diketiminate complexes.[146] This radical coupling to form O-Si bonds then seemingly facilitates an alternative pathway for phosphine dehydrocoupling plausibly *via* the formation of iron centered radicals and iron hydride species (Chapter 2). This appears to be a persistent radical effect wherein persistent TEMPO radicals react with transient silyl radicals mediated by **1**.[147, 148] In order to determine whether or not phosphine-silane coupling is radical catalysed an alternative radical trap was then used. As discussed previously, radical clocks are ideal for determining radical intermediacy in reactions (Scheme 63).[102, 103]

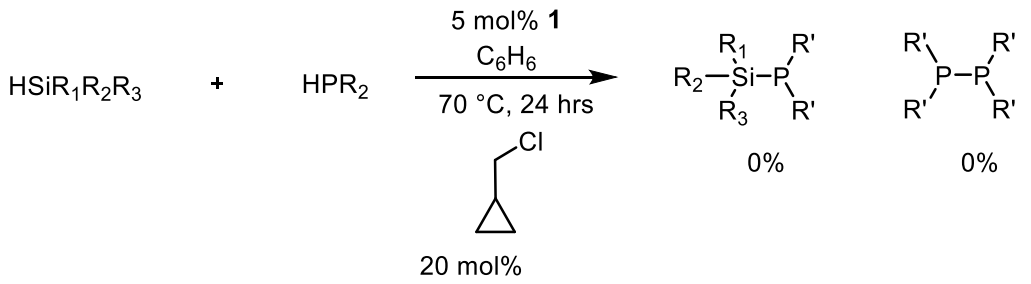

Scheme 63: Catalytic run in the presence of a radical clock ((chloromethyl) cyclopropane)

Given that no dehydrocoupling products were detected in the presence of a radical clock (Scheme 63) phosphine-silane dehydrocoupling with iron β-diketiminates is determined to be a radical mediated process. This is analogous to the reactivity previously described for phosphine homocoupling. The exact nature of the mechanism is somewhat puzzling. However, the emergence of radical species is likely propagated by the formation of the iron phosphido species **66**.[149]

In catalytic reactions, samples were taken at the end point of catalysis. Wide sweep width proton NMR analysis showed that the previously detected signals speculatively assigned as the iron phosphido species ^{Dipp}LFe-PPh_2, **66** were present. This suggests that, as with phosphine homocoupling, the precatalyst **1** reacts with an equivalent of phosphine which then mediates coupling to an equivalent of silane. Interestingly, in samples taken from catalytic phosphine-silane coupling reactions two paramagnetic iron species were present in equimolar quantities. The other species is the unreacted precatalyst **1**. From this observation we can determine that not all of the iron precatalyst reacts to form an on-cycle intermediate. The precatalytic activation step is less facile than might have been expected with the highly labile CH_2TMS ligand. One plausible explanation for this observation is that the binding of a phosphine ligand is more favourable but only modestly. In terms of its chemistry phosphorus is often described as analogous to carbon with phosphines showing similar reactive trends to alkyl species.[150] In terms of Ka the phosphine is clearly more acidic by comparison to tetramethyl silane with a pKa approximately 37 orders of magnitude lower (22.9 to 60).[108] Sterics likely play a role in hindering the formation of **66** from **1**. Coordination of a phosphine ligand to form a four coordinate complex and subsequent protonlysis to the phosphide is expected to occur.[42] With steric hindrance protonlysis to form **66** occurs slowly. By extension it can be remarked upon that the active species in solution is very active as there is less of it in solution at any given time than might have been expected.

4.2.2 - Tetraphenyldiphosphane reactions

Given previous work by Stephan and co-workers on silylation of P-P bonded diphosphanes with rhodium β-diketiminate complexes, one possible rationale for the high selectivity towards phosphine-silane dehydrocoupling is that the reaction is actually a stepwise process.[77] It is plausible that following initial phosphine homocoupling the bisphosphine product then enters a second catalytic cycle yielding silaphosphines. In order to test this hypothesis tetraphenyldiphosphane was reacted with diphenylsilane. At the end point of catalysis only trace quantities of silaphosphine were observed with the bulk of the reaction mixture consisting of unreacted tetraphenyldiphosphane. This suggests that tetraphenyldiphosphane is not a reactive intermediate in this catalytic system.

When comparing the results of Stephan's study with this one it becomes apparent that iron β-diketiminates display the opposite trends to rhodium; where phosphine homocoupling was found to be unfavourable with the rhodium complexes in Stephan's study, **1** is a highly competent catalyst. Stephan reports that the reverse reaction, where hydrogenation and therefore P-P bond cleavage, is favourable, when **1** is used in catalysis P-P bond cleavage is disfavoured and mostly unreacted starting material is observed when tetraphenyldiphosphane is reacted with diphenylsilane. In terms of atomic radii rhodium(I) is very similar in size to high spin iron(II) (0.135 nm to 0.140 nm).[151] Despite this,their β-diketiminate complexes show opposite trends in reactivity suggesting this is as a result of stronger bonding character between rhodium and tetraphenyldiphosphane.[151] Therefore in the case of iron catalysis phosphine-silane bond formation is proposed to be a single cycle reaction without the prior requirement to form diphosphanes as intermediates (Scheme 64).

4.2.3 - Reaction mechanism

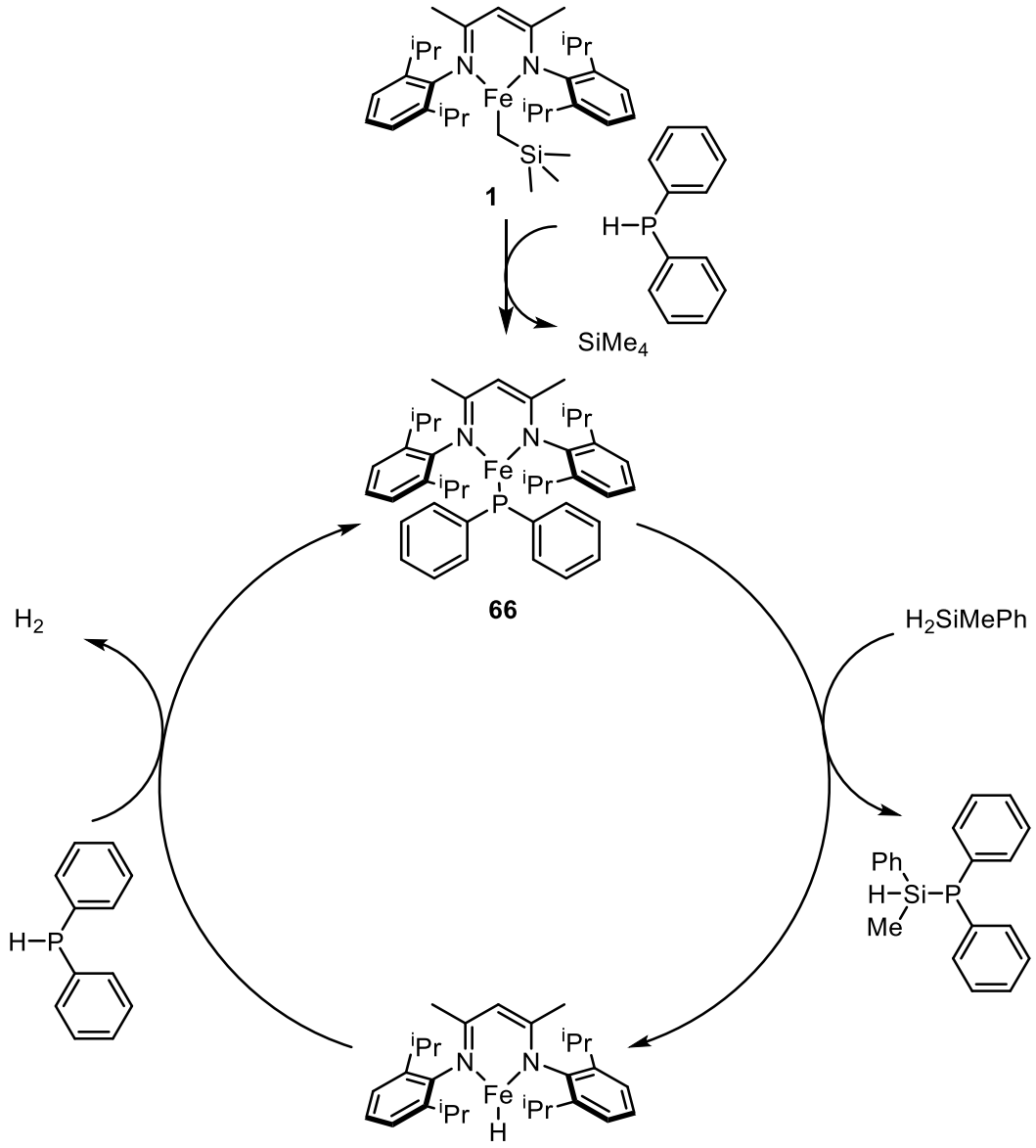

Scheme 64: Postulated catalytic cycle for iron catalysed phosphine-silane dehydrocoupling.

The coordination of an equivalent of phosphine to the iron β-diketiminate and subsequent reaction with a silane *via* σ-bond metathesis, can be postulated to be a feasible pathway (Scheme 64). The basis for this is evidenced by the existence of the previously described complex ^{Dipp}LFe-PPh$_2$ (**66**) and previous studies which suggest that iron-silyl species are unlikely to form as intermediates in catalytic reactions with iron β-diketiminates.[8] Therefore, although we have no explicit evidence for its formation, an iron hydride species is postulated as a reactive intermediate. No kinetic analyses were achieved for this system. However, the lack of observation of hydride species and the observation of **66** suggest that the hydride is too short-lived to be observed. When considering the catalytic cycle this suggests that the reaction of **66** with an equivalent of silane is the rate-determining step but without appreciable kinetic data this is somewhat speculative.

Heterodehydrocoupling reactions of phosphines and silanes catalysed by iron β-diketiminates are facile and show very high selectivity for heterocoupling over previously discussed homocoupling. Dehydrocoupling reactivity is radical in origin and proceeds through the iron phosphido species ^{Dipp}LFe-PPh$_2$, **66**. These positive results suggest that the orthogonality of **1** could be further extended. The ancillary β-diketiminate ligand can greatly influence reactivity but does not come without its limitations, as evidenced by a lack of reactivity with tertiary silanes and secondary phosphines. That being said, the reactivity and selectivity displayed is unprecedented for an iron catalyst.

4.3 - Amine-silane dehydrocoupling - synthesis

Based on successful phosphine-silane dehydrocoupling reactivity and previous work in the Webster group on amine-borane dehydrocoupling, the iron β-diketiminate catalyst was next screened for amine-silane dehydrocoupling reactivity (Scheme 65).[89-91 152] Promisingly high spectroscopic yields were observed for the coupling of methylbenzylamine with diphenylsilane at 70 °C. Further optimisation was carried out as is detailed below (Table 22).

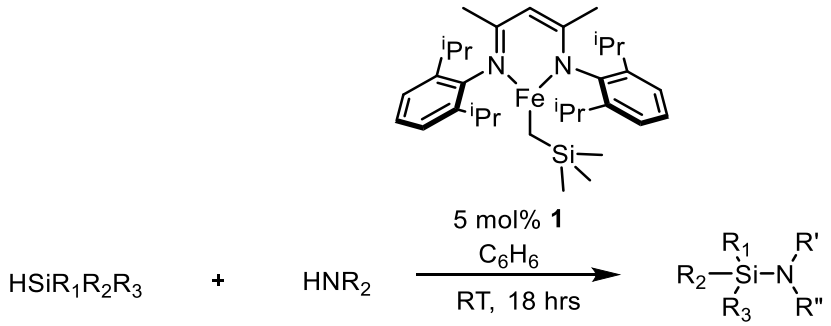

Scheme 65: Iron catalysed amine-silane dehydrocoupling.

Table 22: Optimisation of catalytic amine-silane dehydrocoupling using *N*-methyl benzylamine and diphenylsilane.

Entry	*Time (hrs)*	*Temperature (°C)*	*Spec. Yield (%)[a]*
1	*24*	*70*	*100*
2	*24*	*70*	*100*
3	*24*	*50*	*100*
4	*18*	*RT*	*100*

*Conditions: 5 mol % **1**, (0.5 mmol) HNMeBn, (0.5 mmol) H_2SiPh_2, (0.35 ml) C_6D_6 [a] NMR yield calculated from the conversion to silazane with 1,3,5-trimethoxybenzene as an internal standard.*

Conveniently, the reaction was found to display high catalytic activity at room temperature with full conversion achieved in 18 h. These conditions were taken as optimal catalytic

conditions, a full investigation of the substrate scope was then carried out (Tables 23 and 24). A blank reaction in the absence of the iron catalyst was carried out and no amine-silane coupling activity was observed. It has been previously reported that other dehydrocoupling reactions do not require a catalyst and therefore it was imperative to check this.[153]

4.3.1 -Primary amine - silane dehydrocoupling

Table 23: Substrate scope for primary amine-silane dehydrocoupling.

Entry	*R_1R_2NH* $R_1R_2R_3SiH$	*Spec. Yield (%)[a]*	*Product*	*Selectivity(Mono vs Di)[b]*
1	$BnNH_2$ Ph_2SiH_2	*100*	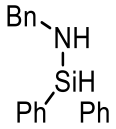	*90:10*
2	$^nBuNH_2$ Ph_2SiH_2	*88*	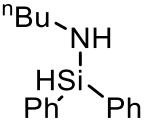	*93:7*
3	$PhNH_2$ Ph_2SiH_2	*100*	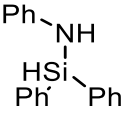	*100:0*
4	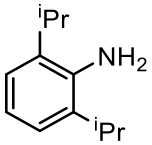 Ph_2SiH_2	*No reaction*	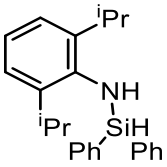	
5	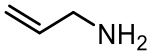 Ph_2SiH_2	*62*	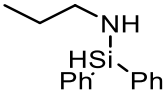	*100:0*
6	$BnNH_2$ $MePhSiH_2$	*100*	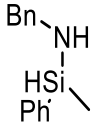	*80:20*
7	$^nBuNH_2$ $MePhSiH_2$	*99*	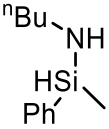	*100:0*

8	$PhNH_2$ $MePhSiH_2$	*100*	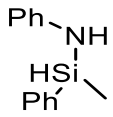	*100:0*
9	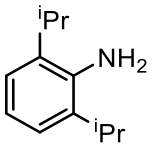 $MePhSiH_2$	*No reaction*	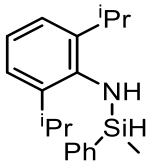	
10	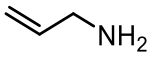 $MePhSiH_2$	*83*	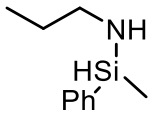	*76:24*
11	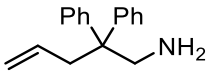 $MePhSiH_2$	*100*	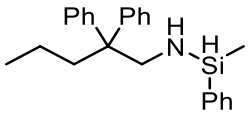	*100:0*
12	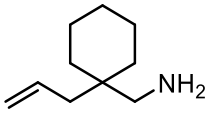 $MePhSiH_2$	*100*	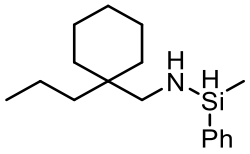	*100:0*
13	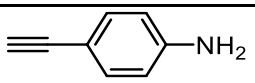 $MePhSiH_2$	*Trace*	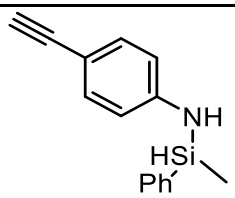	
14	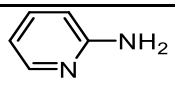 $MePhSiH_2$	*Trace*	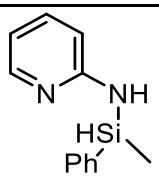	
15	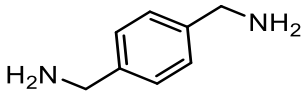 $MePhSiH_2$	*100*	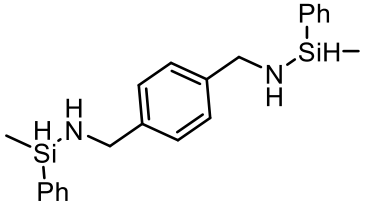	*99:1*
16	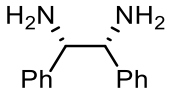 $MePhSiH_2$	*100*	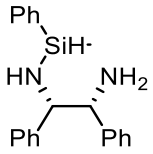	*Not determined*

17	$BnNH_2$ $PhSiH_3$	*100*	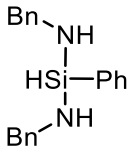	*26:63:7:4*
18	$^{n}BuNH_2$ $PhSiH_3$	*6*	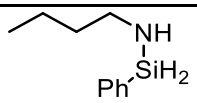	*Not determined*
19	$PhNH_2$ $PhSiH_3$	*100*	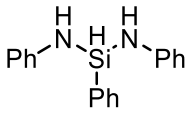	*0:100*
20	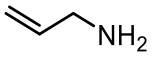 $PhSiH_3$	*53*	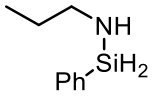	*66:33*
21[c]	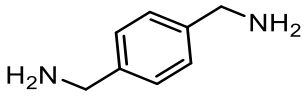 $PhSiH_3$	*100*		*Oligomers*
22[c]	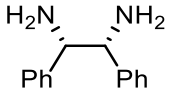 $PhSiH_3$	*100*		*Oligomers*
23	$BnNH_2$ Ph_3SiH	*No reaction*		
24	$PhNH_2$ Ph_3SiH	*No reaction*		
25[d]	$BnNH_2$ $MePhSiH_2$	*100*		*80:20*
26	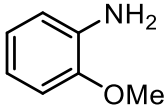 $MePhSiH_2$	*100*	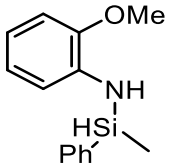	*100:0*
27	$TolNH_2$ $MePhSiH_2$	*100*	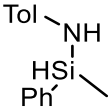	*100:0*
28	$BnNH_2$ Me_2PhSiH	*No reaction*	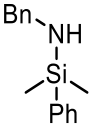	

29	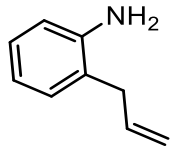 MePhSiH$_2$	*trace*	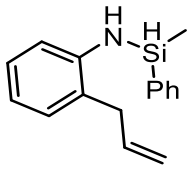	

Conditions: [a] ***1****, 5 mol %, silane (0.5 mmol), amine (0.5 mmol), (0.35 ml) C_6H_6, RT, 18 hrs. 1,3,5-trimethoxybenzene used as an internal standard. [b] Determined via ^{1}H NMR [c] 0.5mmol silane, 0.25 mmol amine, RT, 24 hrs → 0.25 mmol amine, RT, 24 hrs [d] 1 mmol amine, 0.5 mmol silane.*

A broad range of amines were determined to work well in coupling reactions catalysed by the iron β-diketiminate complex **1**. As with previously discussed phosphine-silane coupling reactions the tertiary silanes, triphenylsilane and diphenylmethylsilane, were found to show no reactivity. As previously discussed the steric constraints of the catalyst are unfavourable for reactions with bulkier tertiary silanes. Reactions with primary amines and secondary silanes (Table 23, Entries 1-3, 5-8, 10-12, 15-16, 25-27 and 29) were highly effective with good selectivity shown towards mono-substituted silazane products.

4.3.2 - Secondary amine-silane dehydrocoupling

Table 24: Substrate scope for secondary amine-silane dehydrocoupling.

Entry	*R_1R_2NH* $R_1R_2R_3SiH$	*Spec. Yield (%)[a]*	*Product*	*Selectivity(Mono vs Di)[b]*
1	BnMeNH Ph_2SiH_2	*100*	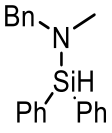	*100:0*
2	Ph_2NH Ph_2SiH_2	*No reaction*	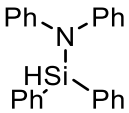	
3	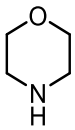 Ph_2SiH_2	*100*	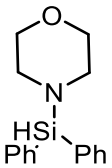	*100:0*
4	BnMeNH MePhSiH$_2$	*100*		*100:0*

5	$^{i}Pr_2NH$ Ph_2SiH_2	*trace*	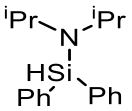	
6	Ph_2NH $MePhSiH_2$	*No reaction*	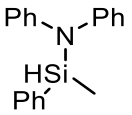	
7	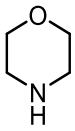 $MePhSiH_2$	*100*	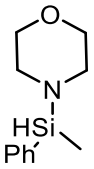	*100:0*
8	$^{i}Pr_2NH$ $MePhSiH_2$	*No reaction*	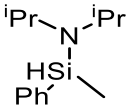	
9	BnMeNH $PhSiH_3$	*100*	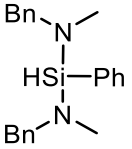	*30:70*
10	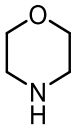 $PhSiH_3$	*100*	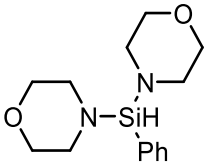	*20:80*
11	BnMeNH Ph_3SiH	*No reaction*		
12	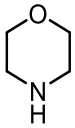 Ph_3SiH	*No reaction*		
13	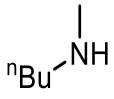 $MePhSiH_2$	*100*	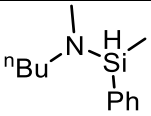	*100:0*

Conditions: [a] ***1****, 5 mol %, silane (0.5 mmol), amine (0.5 mmol), (0.35 ml) C_6H_6, RT, 18 hrs. 1,3,5-trimethoxybenzene used as an internal standard. [b] Determined via ^{1}H NMR.*

Some limitations of dehydrocoupling reactivity with the iron precatalyst can be observed (Table 23, Entries 4-9, 13-14, 18, 23-24, 28-29 and Table 24, Entries 2, 5-6, 8, 11-12). 2,6-Diisopropylaniline is not an effective substrate; the coordinated complex has been previously described in the literature and the low reactivity of this incipient iron species is most likely a

result of steric factors.[10] In stoichiometric reactions between **1** and diisopropylaniline, heating at 90 °C for a period of 36 h was required to generate the amido species **6**. This suggests that catalyst activation is limiting catalytic turnover. Additionally excess diisopropyl aniline leads to the formation of ^{Diip}LFe-(HNDipp)(H_2Dipp) (**77**), this more hindered four-coordinate species presumably reacts less readily with silane and is stabilised by favourable hydrogen bonding interactions.[10] In some examples secondary amines (Table 24, Entries 1, 3-4, 7, 9-10, 13) displayed high reactivity although the substrate scope is more limited than that of primary amines. Diphenylamine (Table 24, Entries 2 and 6) showed no reactivity. The procession of amine-silane coupling through the previously characterised species ^{Dipp}LFe-NPh_2, **68** is most likely hindered as result of steric constraints and low reactivity of the iron amido complex. Reactions with alkenyl amines led to some intriguing observations (Table 24, Entries 5 and 10-12). The substrates react well to form silazanes. However, the products observed are fully saturated. What we can ascertain from this is that transfer hydrogenation has occurred (Figure 30). This has previously been observed in small quantities by Hannedouche and co-workers while investigating intramolecular hydroamination with iron β-diketiminates.[15]

4.3.3 - Transfer hydrogenation

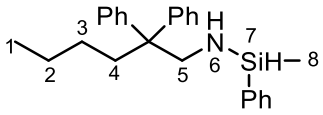

^{1}H NMR (500 MHz, C_6D_6): δ 4.93 (1H, s, SiH, **7**), 3.39 (2H, s, CH_2NH, **5**), 2.07 (2H, s, $Ph_2CCH_2CH_2$, **4**), 1.14 (2H, s, $CH_2CH_2CH_3$, **3**), 0.88 (2H, s, CH_2CH_3, **2**), 0.70 (3H, s, CH_2CH_3, **1**), 0.3 (1H, s, NH, **6**), 0.1 (3H, CH_3, **8**).

^{1}H NMR

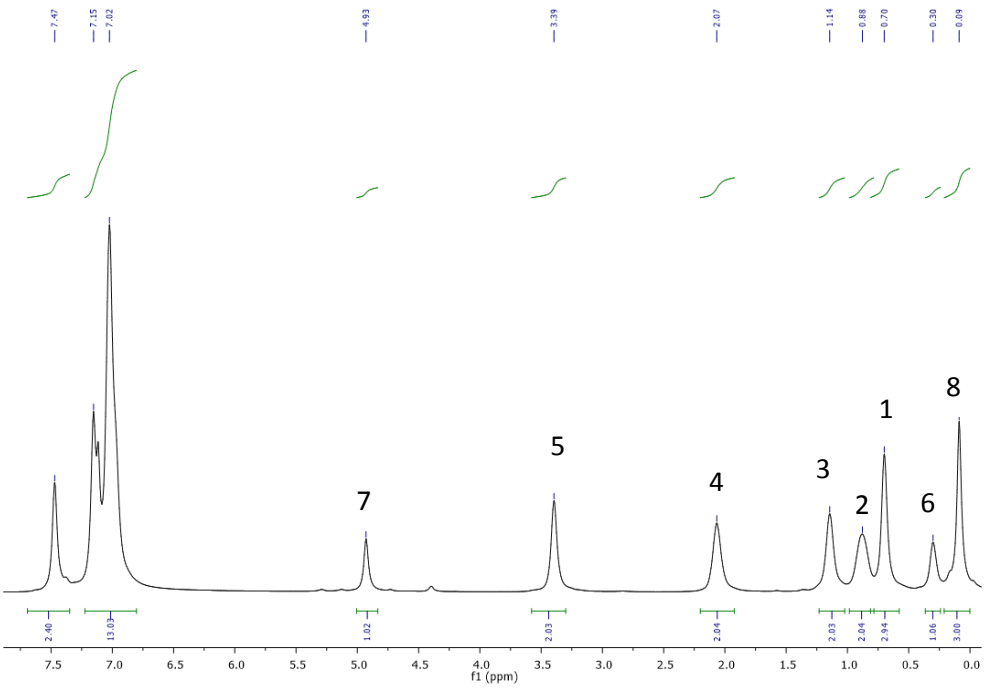

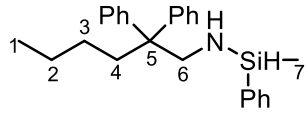

$^{13}C\{^{1}H\}$ NMR (131 MHz, C_6D_6): δ 51.8 ($NHCH_2C(Ph_2)CH_2CH_2CH_2CH_3$, **6**), 49.6 ($NHCH_2C(Ph_2)CH_2CH_2CH_2CH_3$, **5**), 35.9 ($NHCH_2C(Ph_2)CH_2CH_2CH_2CH_3$, **4**), 26.4 ($NHCH_2C(Ph_2)CH_2CH_2CH_2CH_3$, **3**), 23.5 ($NHCH_2C(Ph_2)CH_2CH_2CH_2CH_3$, **2**), 14.1 ($NHCH_2C(Ph_2)CH_2CH_2CH_2CH_3$, **1**), -3.1 (*SiMe*, **7**).

$^{13}C\{^{1}H\}$ NMR

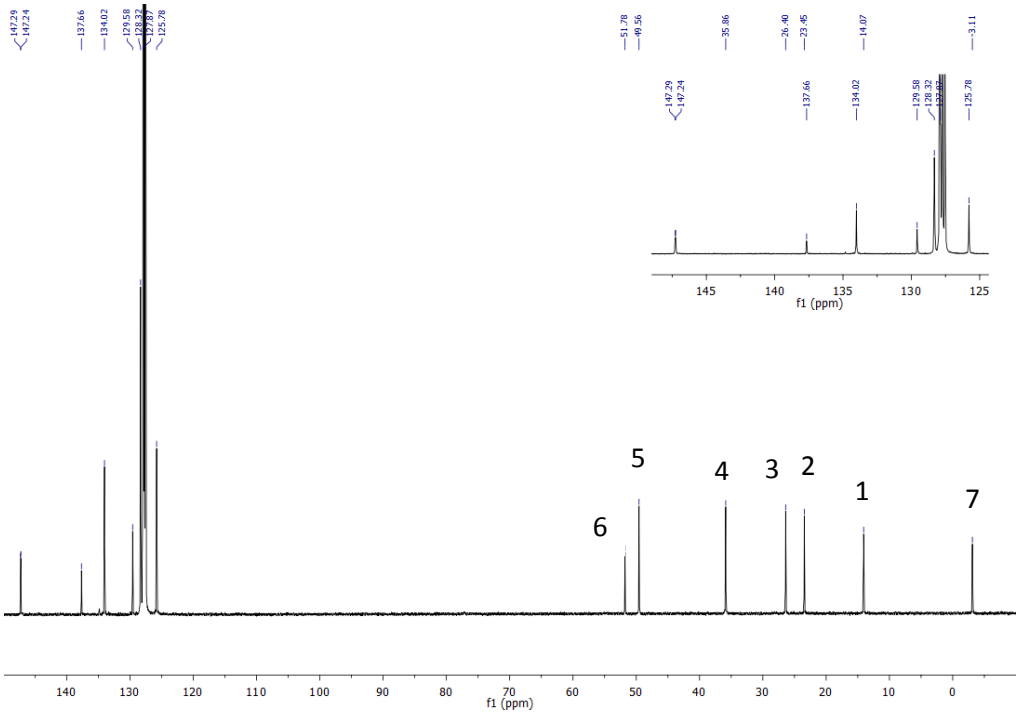

Figure 30: ^{1}H and $^{13}C\{^{1}H\}$ NMR spectra of *N*-(2,2-diphenylhexyl)-1-methyl-1-phenylsilanamine formed *via* transfer hydrogenation (Table 23, Entry 11).

Analysis *via* ^{1}H and $^{13}C\{^{1}H\}$ NMR confirm that the aminoalkene starting material has been hydrogenated confirming that transfer hydrogenation has taken place. This is an intriguing result. A full investigation of transfer hydrogenation catalysed by **1** is of further scientific interest but is beyond the scope of this thesis.

As with previous catalysis with **1** experiments were undertaken to observe the nature of the amine-silane coupling reactive pathways.

4.4- Amine-silane dehydrocoupling - mechanistic studies

As with the other systems catalysed by **1**, radical trap experiments were conducted to determine if intermediates are radical in nature. Addition of the radical trap TEMPO will lead to a significant decrease in spectroscopic yield if the dehydrocoupling reaction is radical in origin. No decrease in spectroscopic yield was observed with TEMPO present suggesting the reaction is not mediated by radicals. Further experiments with (chloromethyl) cyclopropane also proceeded to full conversion unhindered thus confirming that the reaction is not a radical process. It is also important to note that under the reaction conditions oxidation of **1** is not anticipated, and hence it can be hypothesised that this example of amine-silane dehydrocoupling occurs via σ-bond metathesis.

4.4.1 - Kinetic studies

As with mechanistic investigations into phosphine-silane coupling it can be hypothesised that an in depth kinetic study could be undertaken for amine-silane coupling. Initial test reactions with methylbenzylamine and methylphenylsilane in the presence of **1** in a sealed J-Young NMR tube proved promising. By varying the quantities of one of the reaction components whilst keeping all other variables constant, its effect on the overall reaction rate can be determined. No selectivity or catalytic activity issues were observed and as such a full *in situ* kinetic study was carried out with these substrates. In order to conduct this, twelve catalytic runs were carried out with one of the three reaction components (catalyst, amine and silane) varied in molar concentration (Figures 31 - 37).

To allow *in situ* monitoring of the reaction via proton NMR, the catalyst loading was lowered to 3 mol%. At the previously optimised 5 mol%, paramagnetism was found to be a hindrance to reaction monitoring. What became immediately apparent is that **1** is a more active precatalyst for amine-silane dehydrocoupling than it had previously appeared. The reaction reaches completion in just over four hours.

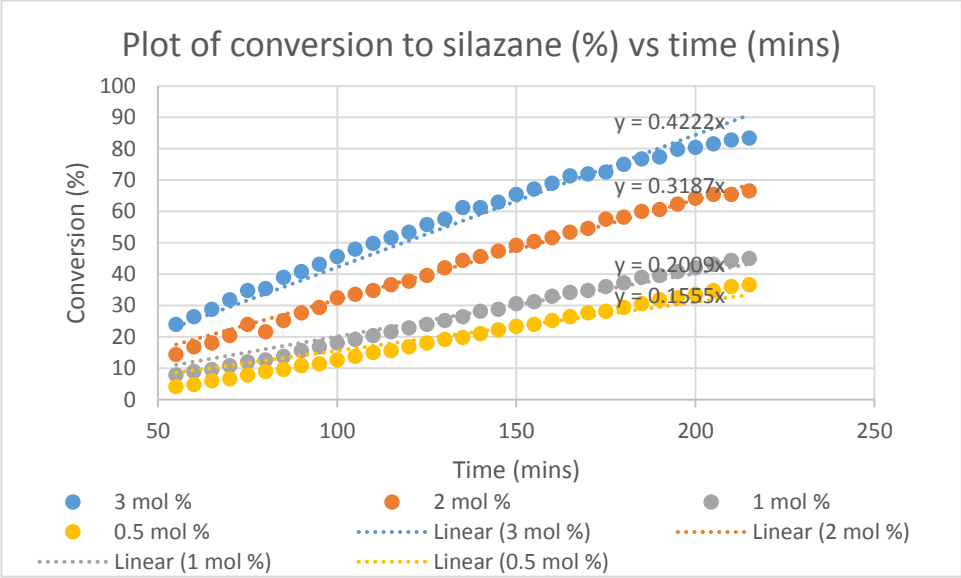

Figure 31: Plot of conversion (%) against time (mins) for amine-silane dehydrocoupling at various precatalyst loadings.

A plot of the rate k_{obs}(mmol dm^{-3} min^{-1}) against precatalyst concentration gives a straight line plot which deviates from the origin (Figure 32).

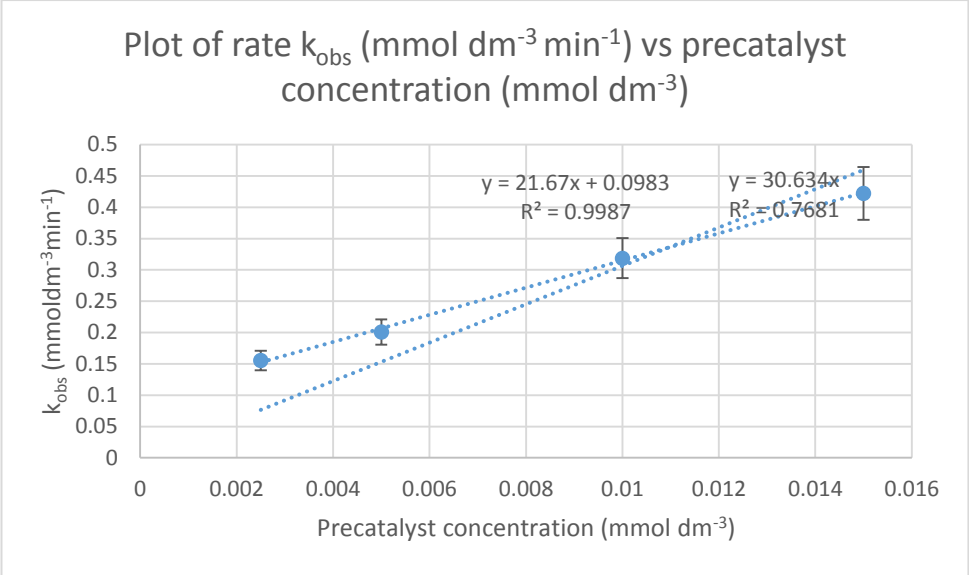

Figure 32: Plot of rate k_{obs} (mmol dm^{-3} min^{-1}) versus precatalyst concentration (mmol dm^{-3}).

A plot of the rate k_{obs}(mmol dm^{-3} min^{-1}) against [precatalyst concentration]$^{1/2}$(µmol dm^{-3}) gives a straight line plot which passes through the origin giving a half order relationship with respect to catalyst (Figure 33).

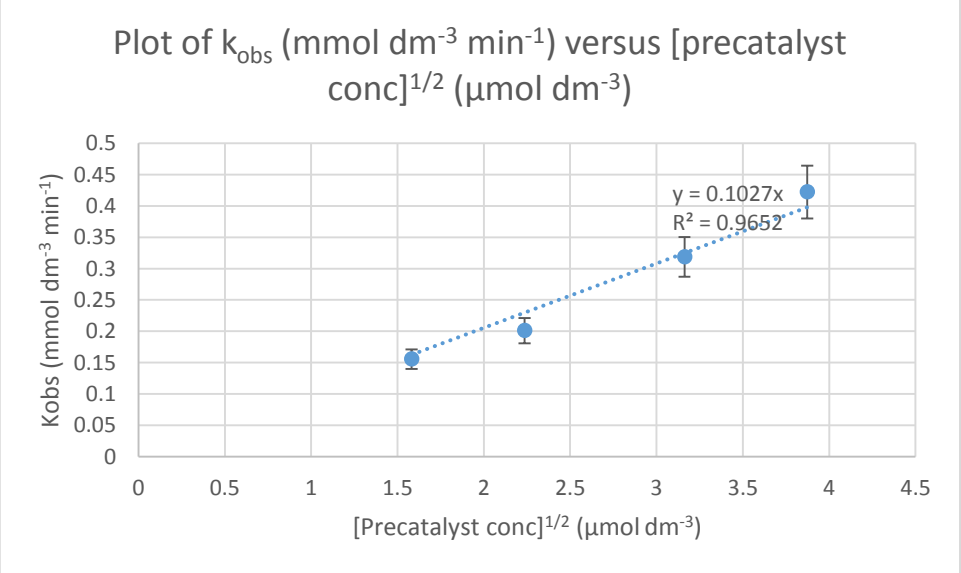

Figure 33: Plot of rate k_{obs} (mmol dm^{-3} min^{-1}) versus [Precatalyst concentration]$^{1/2}$ (µmol dm^{-3}).

After investigating the reaction with varying catalyst loadings silane concentration was varied to observe its effect on the reaction rate (Figure 34).

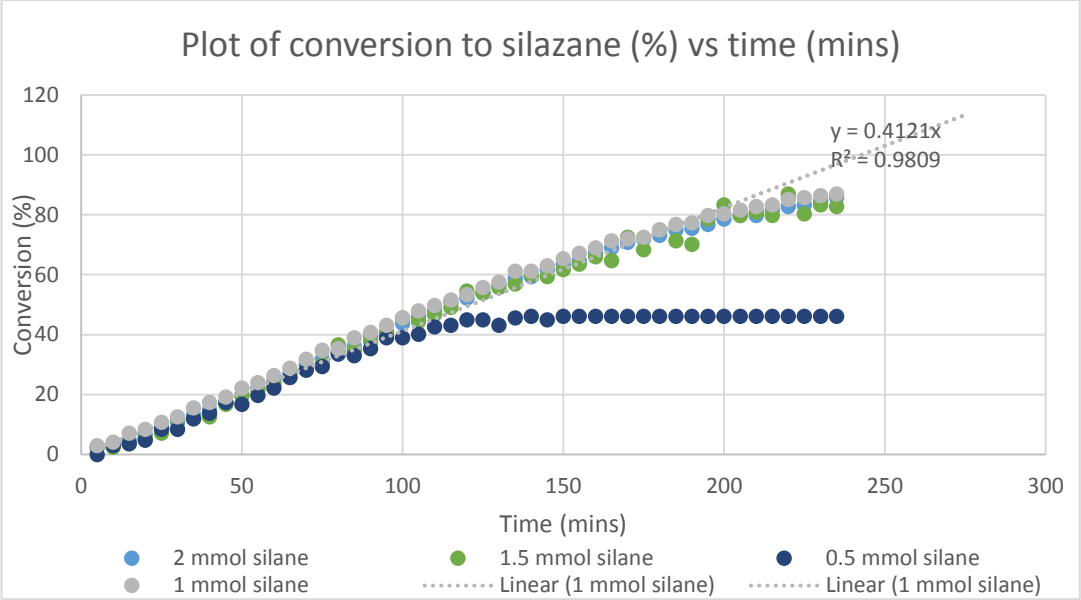

Figure 34: Plot of conversion (%) against time (mins) for amine-silane dehydrocoupling with various equivalents of silane.

When 0.5 mmol of silane is reacted (0.5 equivalents) the reaction reaches 50% conversion as half the amine starting material remains unreacted.

A plot of the observed rate (k_{obs}) against silane concentration (mmol dm^{-3}) shows that varying the concentration of silane has no effect on the rate of reaction. This shows that the reaction is zero order with respect to silane (Figure 35).

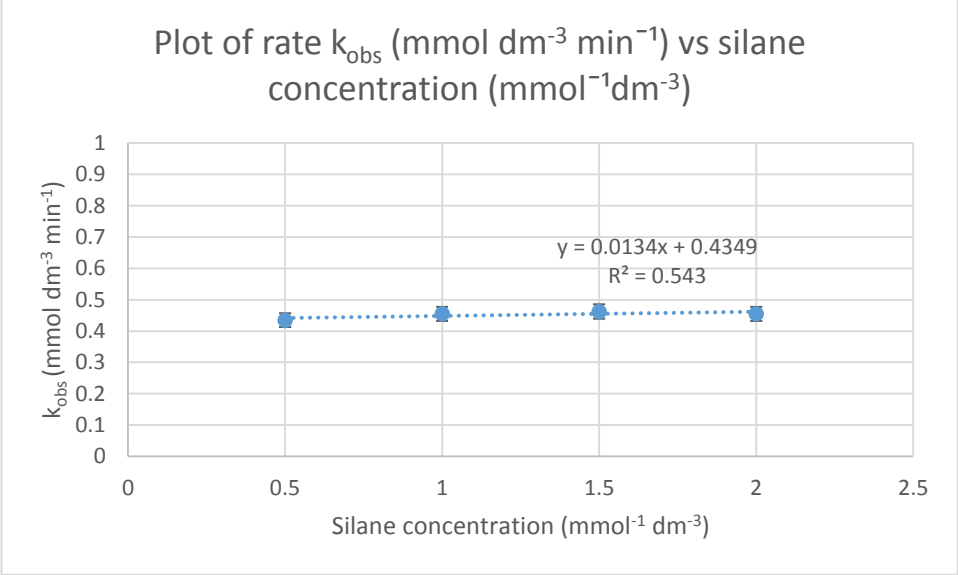

Figure 35: Plot of rate k_{obs} (mmol dm^{-3} min^{-1}) versus silane concentration ($mmol^{-1}$ dm^{-3}).

Once the reaction had been investigated with varying catalyst loadings and silane concentrations the concentration of amine was varied to observe its effect on the reaction rate (Figure 36).

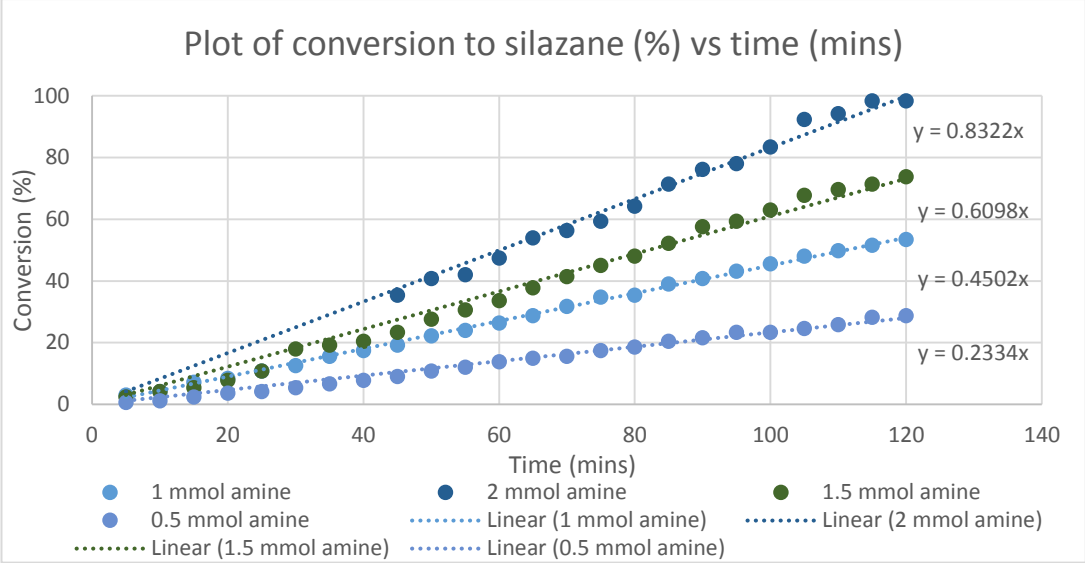

Figure 36: Plot of conversion (%) against time (mins) for amine-silane dehydrocoupling with various equivalents of amine.

A plot of the observed rate (k_{obs}) against amine concentration (mmol dm^{-3}) shows that varying the concentration of amine gives a straight line plot. This shows that the reaction is first order with respect to amine (Figure 37).

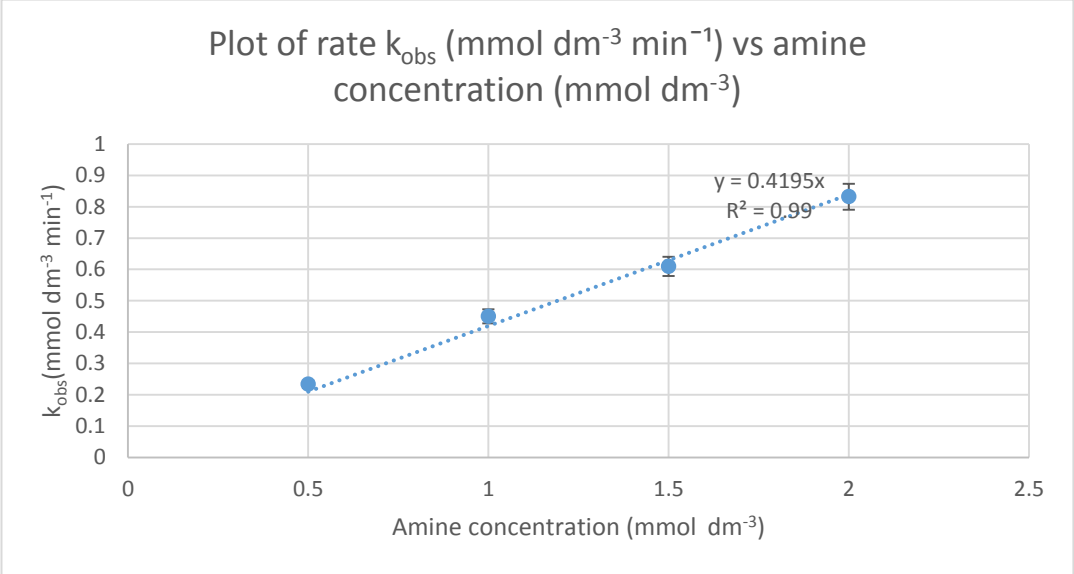

Figure 37: Plot of rate k_{obs} (mmol dm^{-3} min^{-1}) versus amine concentration (mmol dm^{-3}).

In each kinetic run an initial delay period was observed. This suggests an initial catalyst activation step occurs with a slower rate before the active species become more prevalent in solution, leading to catalytic turnover (Scheme 66). By broadening the sweep width to encompass 150 to -150 ppm and monitoring the paramagnetic species via ^{1}H NMR spectroscopy we can shed some light on this activation step. Initially, new very broad peaks are present which do not fit the spectrum associated with **1**. Over time these peaks shift with respect to 0 (i.e. peaks with a positive chemical shift move further downfield and those with

a negative chemical shift move further upfield) until eventually they fit identically with **1**. **1** is the major paramagnetic species at the end point of catalysis. This suggests that the amine coordinates itself to the 12 electron iron centre forming a four-coordinate complex prior to loss of tetramethylsilane and hence the initial induction period which is rate-limiting. Four coordinate iron(II) β- diketiminate complexes have a smaller spectral width in terms of chemical shift than their three coordinate analogues on account of a lesser paramagnetic contribution to chemical shift.[154]

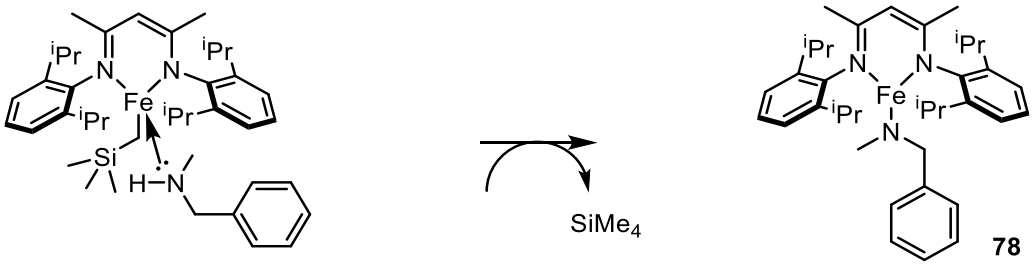

Scheme 66: Catalyst activation step in amine-silane dehydrocoupling.

The iron amido species **78** is a known compound that has been previously characterised.[8] In monitoring catalysis **78** is not observed. This suggests that if it does form it is short lived under the reaction conditions in a J-Young tube.

Overall the kinetic investigations give rise to a rate equation for the cross coupling of amines and silanes based on the order of reactivity in each component (Scheme 67).

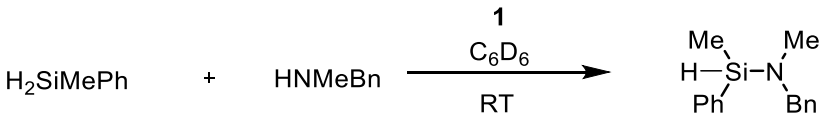

$$r=k[Fe]^{1/2}[Silane]^{0}[Amine]^{1}$$

Scheme 67: Rate equation for iron catalysed amine-silane dehydrocoupling.

The overall rate equation determines that an equivalent of amine is involved in the rate determining step of the reaction.

Based upon these kinetic studies and previous studies within this thesis a mechanism can be postulated for amine-silane dehydrocoupling catalysed by **1** (Scheme 68).

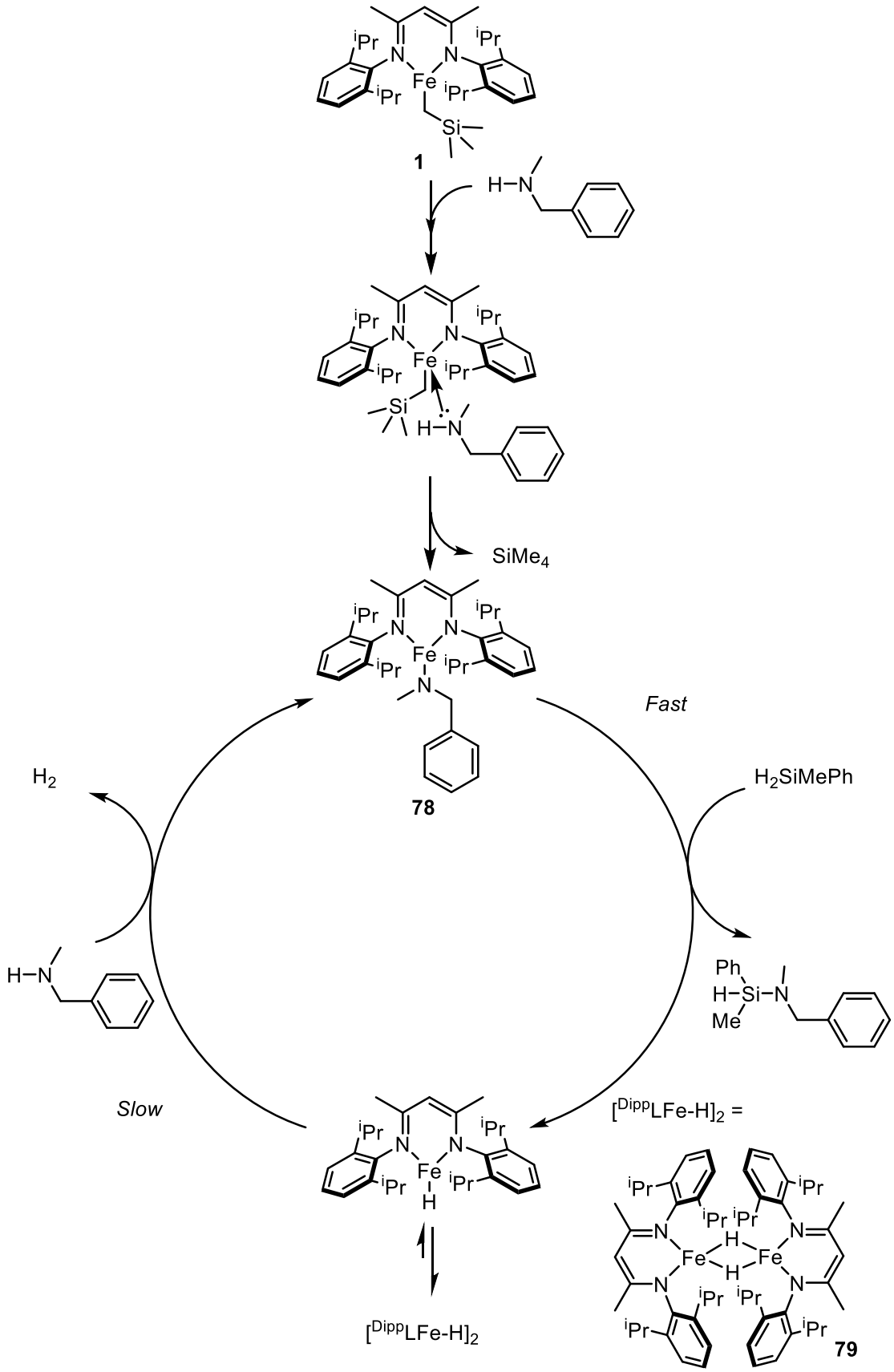

Scheme 68: Catalytic cycle for amine-silane dehydrocoupling.

4.4.2- Catalyst activation and amido kinetics

As the kinetic studies show, the reaction has a half order relationship with respect to the catalyst formed from **1**. This is particularly signifcant when considering the role of the intermediary iron hydride species ^{Dipp}LFe-H. Holland and co-workers have shown previously that in both the solid state and in solution iron hydride species with a diisopropyl β-diketiminate ancillary ligand exist as the dimeric complex [^{Dipp}LFe-H]$_2$, (**79**).[8, 155] This dimeric species is observable *in situ* an hour into the reaction and is deemed to be breaking up as determined by a half order relationship in catalyst. The overall rate of the reaction is dependant on the breakup of the hydride dimer and subsequent reaction with methylbenzylamine. The independent synthesis of the hypothesised active catalyst ^{Dipp}LFe-NMeBn (**78**) has been previously reported by Holland and co-workers (Scheme 69).[10]

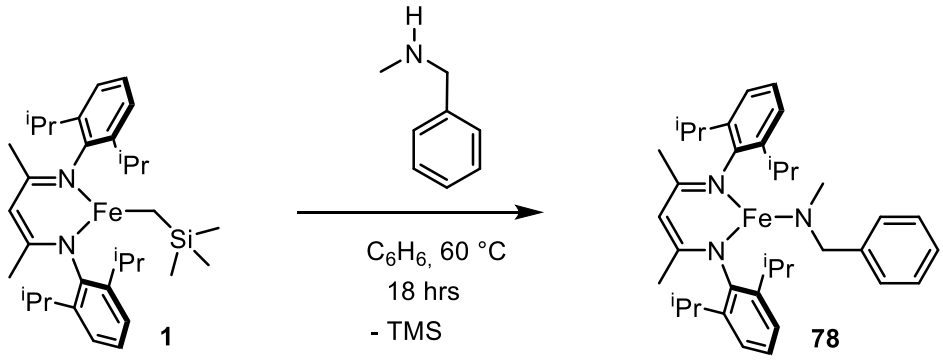

Scheme 69: Synthesis of ^{Dipp}LFe-NMeBn (**78**).

Holland's method was repeated successfully and **78** was then used in place of **1** in a cross-coupling reaction and monitored *in situ*. Subsequent plots of the data determined that the rate of dehydrocoupling was faster when **78** was used as a precatalyst. As discussed, a precatalytic activation step is observed in experiments with **1**, reactions with **78** preclude this and hence the reaction rate is quicker (Figure 38).

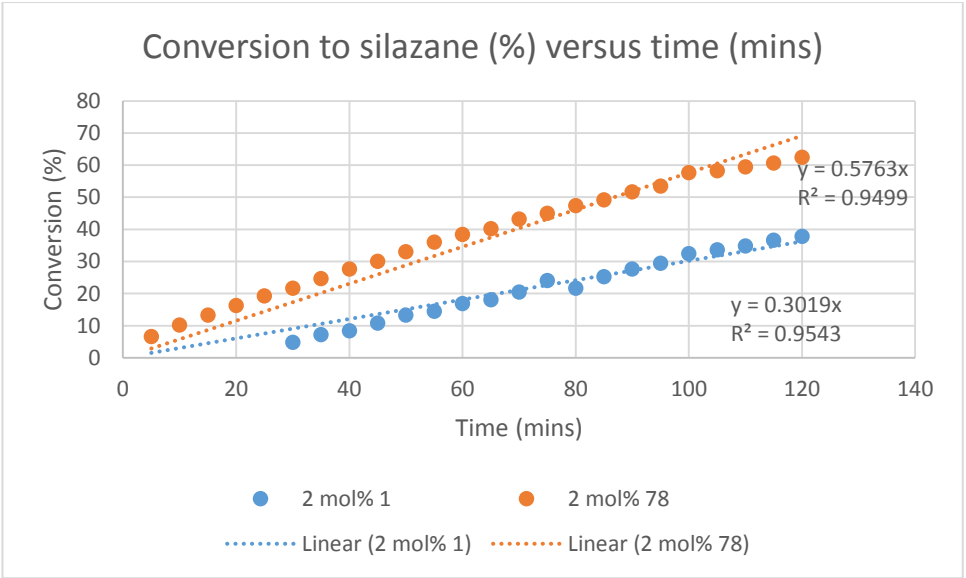

Figure 38: Plot of conversion to silazane (%) versus time (mins) for amine-silane coupling with 2 mol% **1** and 2 mol% **78**.

4.5 - Alcohol-silane dehydrocoupling - synthesis

Given the success of the iron β-diketiminate catalyst **1** in coupling pnictogens with silanes it would seem plausible that these heterocoupling reactions could be extended to include other main group species in synthetic iron-catalysed reactions. Based on previous observations with TEMPO and silanes, coupling to form siloxanes *via* alcohol-silane dehydrocoupling was investigated.[156-158] The established optimal conditions for amine-silane dehydrocoupling were employed in the coupling of benzylalcohol with methylphenylsilane and found to be highly effective. A full substrate scope was then investigated (Tables 25 and 26).

4.5.1 - Alcohol silane dehydrocoupling with secondary silanes

Table 25: Substrate scope for alcohol silane dehydrocoupling with secondary silanes.

Entry	*R_1OH* $R_1R_2R_3SiH$	*Spec. Yield (%)[a]*	*Product*	*Selectivity(Mono vs Di)*
1	BnOH $MePhSiH_2$	*100*	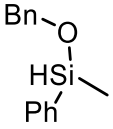	*100:0*
2	PhOH $MePhSiH_2$	*trace*	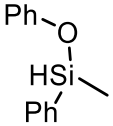	
3	^{t}BuOH $MePhSiH_2$	*100*	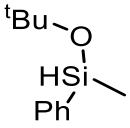	*100:0*
4	^{n}PrOH $MePhSiH_2$	*100*	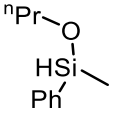	*100:0*
5	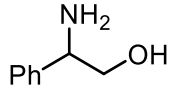 $MePhSiH_2$	*100*	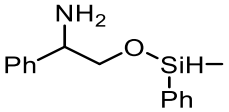	*100:0*

6	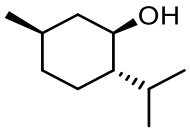 MePhSiH$_2$	*100*	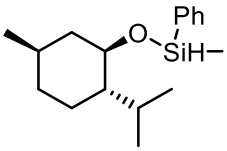	*100:0*
7	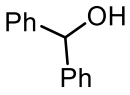 MePhSiH$_2$	*100*	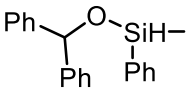	*100:0*
8	MeOH MePhSiH$_2$	*35*	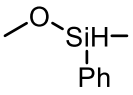	*100:0*
9	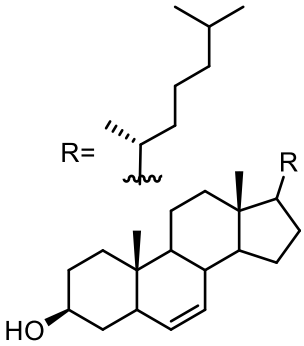 MePhSiH$_2$	*52* *71*[b]	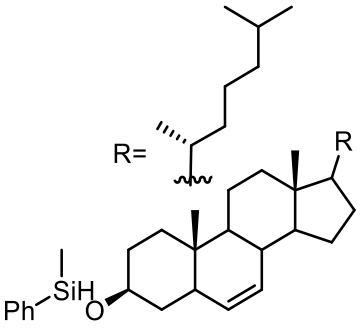	*90:10*
10	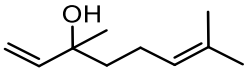 MePhSiH$_2$	*51*	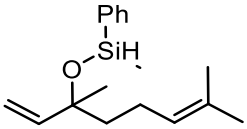	*66:33*
11	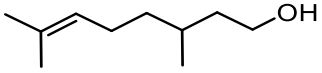 MePhSiH$_2$	*75*	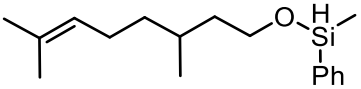	*90:10*
12	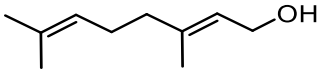 MePhSiH$_2$	*90*	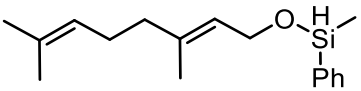	*Intractable mixture*

Conditions: [a] ***1****, 5 mol %, silane (0.5 mmol), alcohol (0.5 mmol), (0.35 ml) C_6H_6, RT, 18 hrs. 1,3,5-trimethoxybenzene used as an internal standard. [b] 50 °C, 24 hrs.*

As evidenced by this study a broad range of alcohols are useful as substrates with iron β-diketiminates. Alcohols such as tert-butanol and iso-propanol (Table 25, Entries 3-4) work well giving quantative spectroscopic yields. Phenols (Table 25, Entry 2) were found to give poorer yields. Catalytic and stoichiometric reactions with phenol showed only trace amounts of siloxane products. The lack of reactivity with respect to phenol is seemingly as a result of the relative stability of the iron alkoxide species ^{Dipp}LFe-OPh formed *in situ.* Natural products (Table 25, Entries 6 and 9-12) give high yields suggesting the utility of this system in protecting group strategies.

4.5.2 - Alcohol-silane dehydrocoupling with primary silanes

Table 26: Substrate scope for alcohol silane dehydrocoupling with primary silanes.

Entry	*R_1OH* $R_1R_2R_3SiH$	*Spec. Yield (%)[a]*	*Product*	*Selectivity(Mono vs Di)*
1	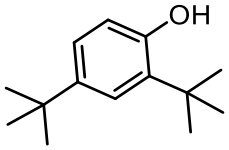 $PhSiH_3$	*80*	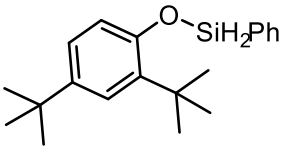	*5:1*
2	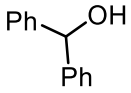 $PhSiH_3$	*100*	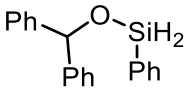	*100:0*
3	BnOH $PhSiH_3$	*100*	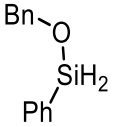	*100:0*
4	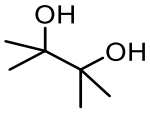 $PhSiH_3$	*100*	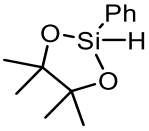	*100:0*
5	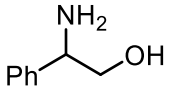 $PhSiH_3$	*100*	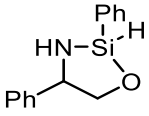	*Intractable mixture*
6	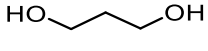 $PhSiH_3$	*100*	oligomeric	

Conditions: [a] ***1****, 5 mol %, silane (0.5 mmol), alcohol (0.5 mmol), (0.35 ml) C_6H_6, RT, 18 hrs. 1,3,5-trimethoxybenzene used as an internal standard. [b] 50 °C, 24 hrs.*

Studies determined that a range of alcohols are useful as substrates in coupling reactions with phenylsilane. Alcohols such as diphenylmethanol and benzylalcohol (Table 26, Entries 2-3) work well giving quantative spectroscopic yields. Phenols (Table 26, Entry 1) were again found to give poorer yields. Substrates with multiple functional groups (Table 26, Entries 4-6) work well but often lead to a mixture of products

4.5.3 - Alcohol-silane-mechanistic investigations

As with the previously described catalytic systems iron silyl species are not anticipated to play a role in catalysis. Thus, with the presence of alcohols, iron alkoxide species (Schemes 70 and 71), which have been previously reported, are expected to be prominent species.[10, 12]

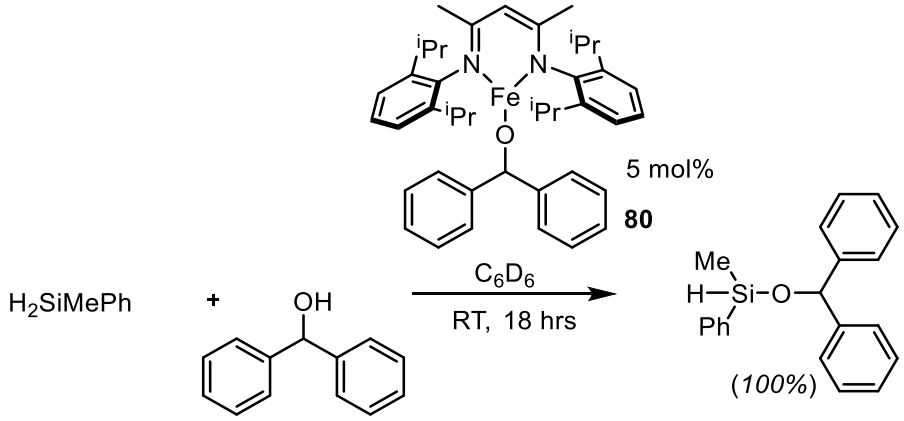

Scheme 70: Iron alkoxide (**80**) catalysed alcohol-silane dehydrocoupling.

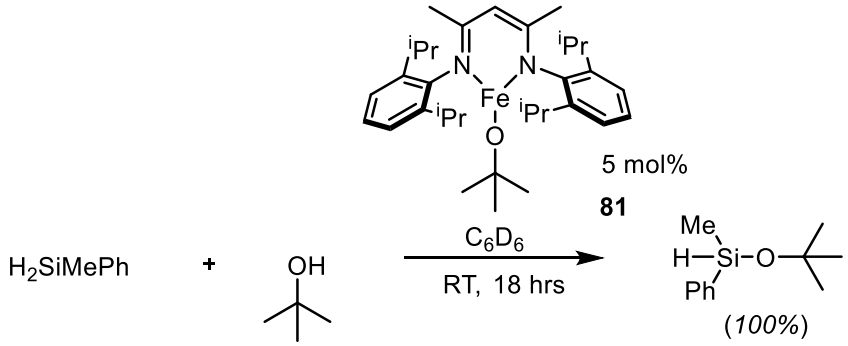

Scheme 71: Iron alkoxide (**81**) catalysed alcohol silane dehydrocoupling.

As with amine-silane dehydrocoupling, an in depth kinetic study was proposed to probe the catalytic cycle of alcohol-silane dehydrocoupling. Addition of alcohol to the catalytic mixture produces a very violent exothermic reaction. In the interest of safety, reactions in a J-Young tube were not attempted thus hindering a full kinetic study. Despite this, it can be assumed that the catalytic cycle is analogous to the one determined for amine-silane dehydrocoupling (Scheme 72).

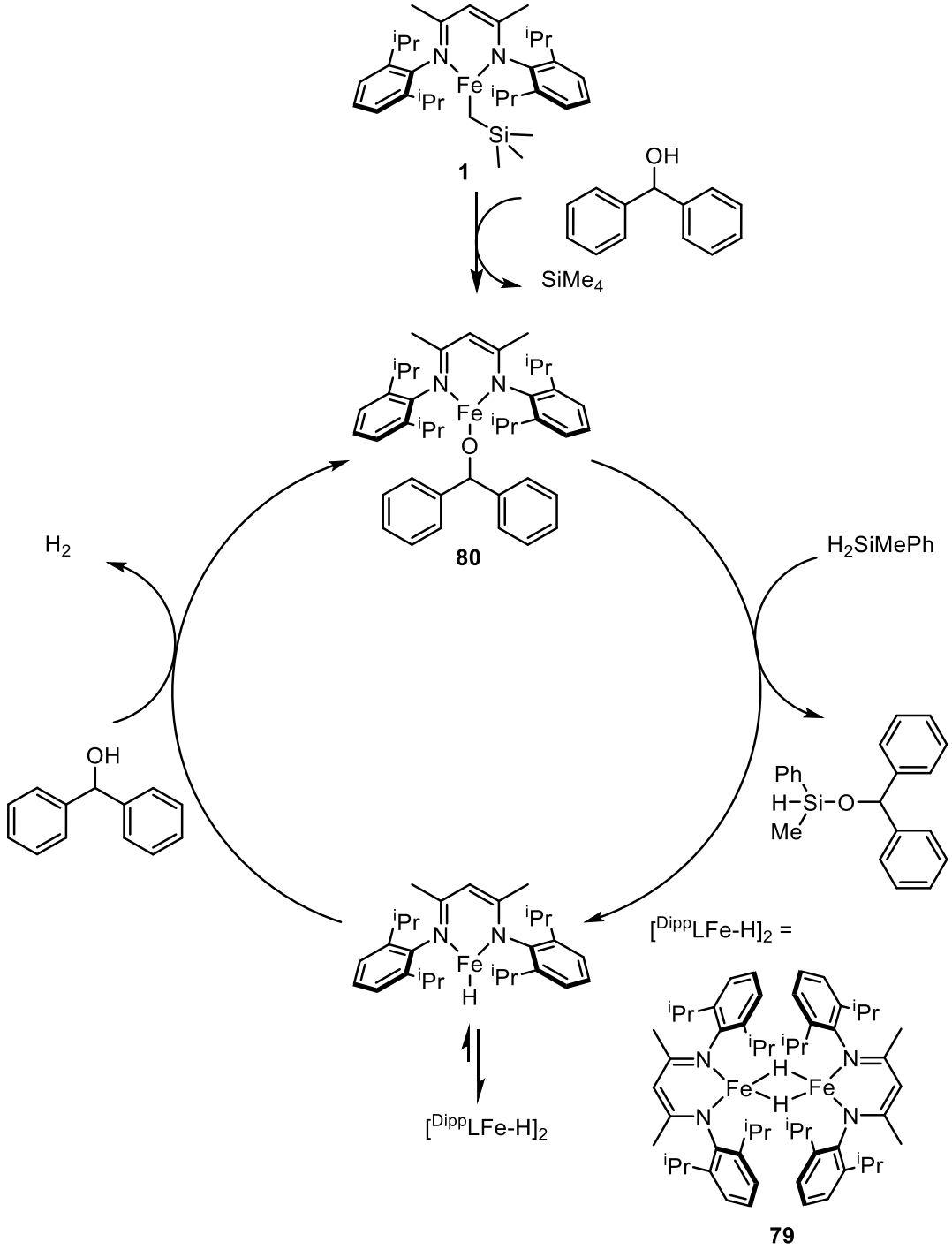

Scheme 72: Postulated catalytic cycle for alcohol silane dehydrocoupling.

No evidence could be found for iron silyl species or iron alkoxide complexes *via* NMR analysis taken at the end of catalysis. The two paramagnetic iron species present at the end of the reaction are **1** and a small quantity of **79**.

4.6 – Conclusions from Chapter 4

In conclusion, further dehydrocoupling studies with the iron β-diketiminate complex **1** showed remarkable selectivity for heterodehydrocoupling in reactions comprising phosphines and silanes. The results show that high spectroscopic yields were achieved with alkyl and aromatic phosphines. Some limitations in this system are reported where tertiary silanes are observed to be unsuitable substrates and primary phosphines favour homocoupling over heterocoupling. Mechanistic experiments determined the catalytic cycle to be radical mediated. Kinetic analyses were attempted on the basis of a "spectroscopic handle" with silaphosphanes. These proved unsuccessful with a change in reaction vessel leading to complete shift in reaction selectivity. These observations are determined to be due to a build up of hydrogen gas. The iron phosphido species **66** was observed to be an intermediate in the catalytic cycle. Reactions with tetraphenyldiphosphane confirmed that it is not a reactive intermediate in phosphine-silane coupling. A reaction mechanism is proposed wherein **66** reacts preferentially with a silane to facilitate heterocoupling. Heterodehydrocoupling studies were extended to explore catalytic reactivity of amines and silanes in the presence of **1**. Reactions were observed to be incredibly facile with catalytic turnover achieved at room temperature. A broad substrate scope has been investigated with a wide range of substrates tolerated in this catalytic system. Limitations in scope again include tertiary silanes as well as bulkier secondary amines. Stereoelectronic properties are also interpreted to play a role in limiting reactivity of iron amido species towards amine-silane coupling. Mechanistic studies provide evidence that the amine-silane coupling mechanism is not radical mediated. A full kinetic study of amine-silane coupling reveals that the reaction is a half order in catalyst, first order in amine and zero order in silane. The active species in the catalytic cycle are iron amido and iron hydride species respectively. Heterodehydrocoupling with **1** has been further extended to alcohol silane coupling. A wide substrate scope has been reported. Results herein provide support for a reaction mechanism for alcohol silane coupling that is analogous to the cycle proposed for amine-silane coupling.

5 - Desilylation

5.1 - Desilylation of silazanes

As discussed previously iron β-diketiminate catalysed dehydrocoupling reactions are often highly selective leading to unsaturated products, which are ideal precursors for further synthetic transformations. With this in mind unsaturated silazane products described in Chapter 4 (Table 23, Entries 2-4, and 7) were postulated to be potential reagents for dehydrocoupling reactions with pinacolborane. While generation of heteroatom-rich molecules was the initial aim of the catalytic study, the generation of borylsilazanes was not observed; instead desilyation occurred (Scheme 73). This is a rather intriguing result with very few reports in the literature of this being achieved catalytically.[159] Desilylation of silazanes in reactions with boranes has also previously been reported under extremely forcing conditions.[160-162]

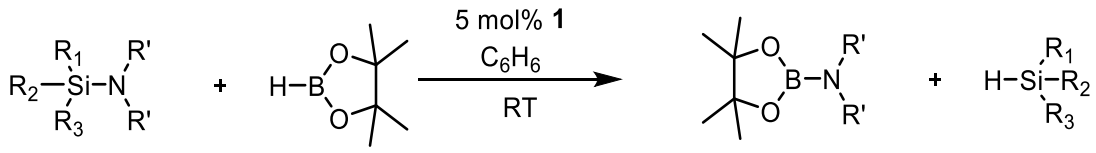

Scheme 73: Iron catalysed desilylation of silazanes

The desilylation reaction was found to work well at ambient temperatures so further optimisation of reaction conditions was not required. As this reaction is very facile a blank reaction was carried out to determine whether the process can operate catalyst-free given the literature precedent.[153, 163] In the blank reaction trimethylsilylaniline was reacted with pinacolborane at room temperature. After a 24 hour period only trace quantities of aminoborane product were observed. This suggests that **1** is required to drive the desilylation reaction. With this determined, a substrate scope of silazanes was fully investigated (Table 27).

5.1.1 - Reaction scope

Table 27**:** Substrate scope for desilyation of silazanes.

Entry	*Substrates*	*Spec. Conversion (%)[a]* *[Isolated Yield (%)]*	*Product*	*Time (hrs)*
1	BnMeN−SiHPhMe HBpin	*88* *100 [67]*	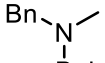	*18* *36*
2	BnHN−SiHPhMe HBpin	*100 [78]*	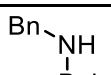	*0.16*
3	PhHN−SiHPhMe HBpin	*50* *100 [88]*	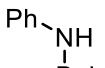	*1* *6*
4	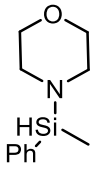 HBpin	*33* *100 [80]*	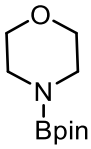	*1* *18*
5	^{n}BuHN−SiHPhMe HBpin	*100 [92]*	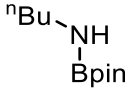	*0.16*
6	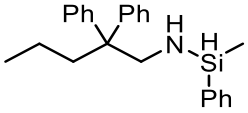 HBpin	*52* *100[b] [82]*	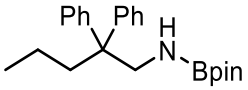	*24* *48*
7[b]	PhHN−SiMe$_3$ HBpin	*trace*	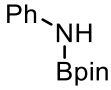	*24*
8	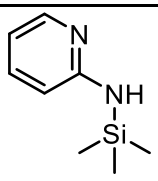 HBpin	*37*	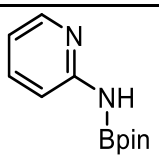	*6*

Conditions: [a] **1**, *(5 mol%), silazane (0.5 mmol), pinacolborane (0.5 mmol), C_6H_6 (0.35 ml), RT, conversion calculated via formation of silane with 1,3,5-trimethoxybenzene used as an internal standard. [b] 50 °C, 24hrs.*

From the substrates investigated some trends are apparent. Silazanes with alkyl and aromatic amino groups (Entries 1-5) are excellent substrates for desilylation. Silazanes with a doubly substituted amino group (Entries 1 and 4) react in a less facile manner than silazanes with a mono substituted amino group (Entries 2, 3 and 5). This suggests that steric hindrance at the iron centre during catalysis leads to slower reactivity (evidenced by direct comparison of Entries 1 and 2). Secondary amine substituted silazanes with alkyl amino groups (Entries 2 and 5) react rapidly with complete spectroscopic conversions reached in a matter of minutes. Secondary amine substituted silazanes with aromatic amino groups (Entry 3) react more slowly reaching full conversion in a matter of hours. This is likely a consequence of stronger nitrogen silicon bonds of mono substituted silazanes with aromatic amino groups due to increased stability through inductive effects from the phenyl aromatic ring.

5.1.2 - *In situ* monitoring

The reaction between 4-(methyl(phenyl)silyl)morpholine and pinacolborane (Entry 4) was monitored *in situ* which led to an intriguing observation (Figure 39).

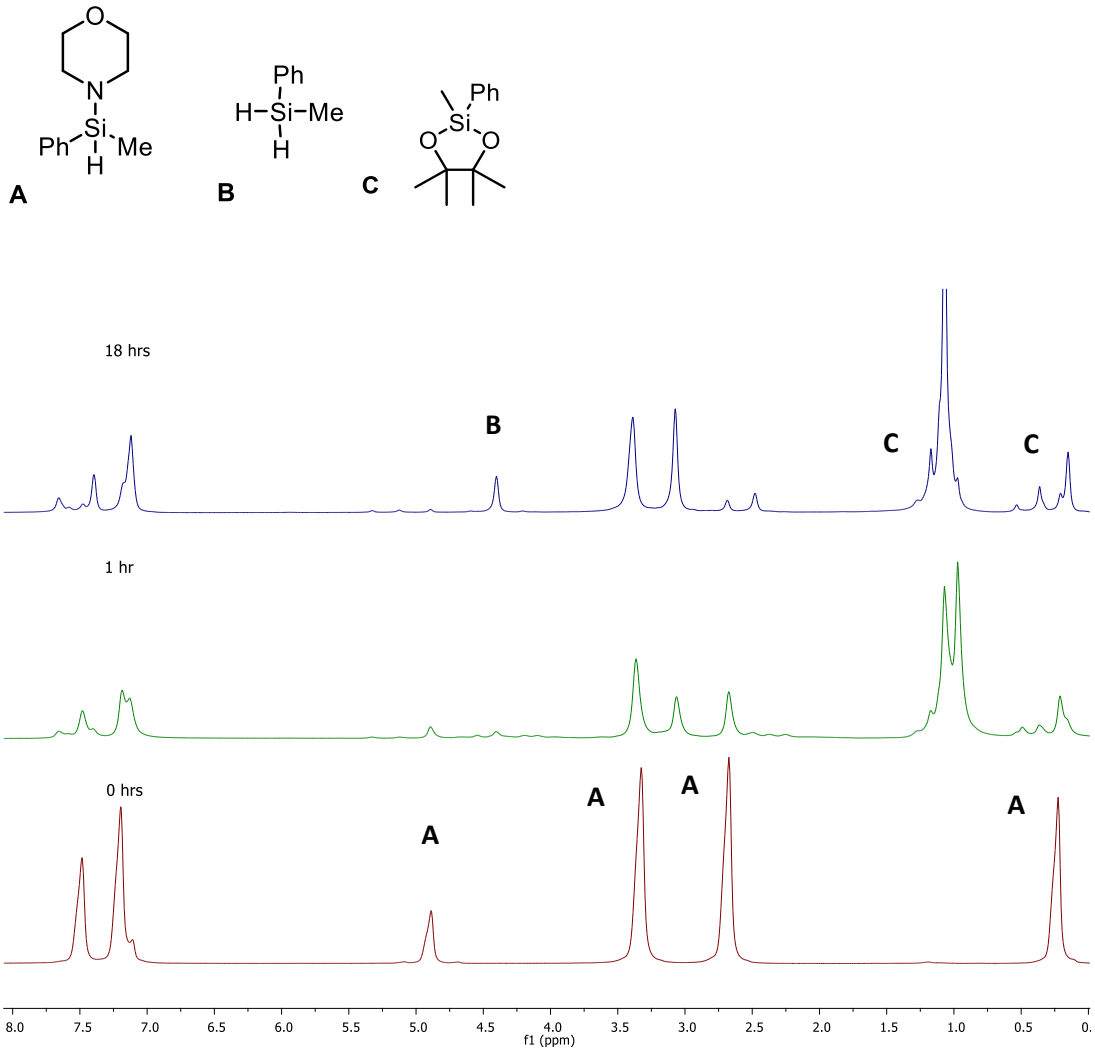

*Desilylation of O(CH₂)₄N-SiHMePh - in situ ^{1}H NMR: Key peaks - 4.89 ppm (*O(CH₂)₄N-Si*H*MePh, **A***), 4.40 ppm (H₂*SiMePh, **B***), 3.33 ppm* (O(C*H₂*)₄N-SiHMePh, **A**), *2.67 ppm (*O(C*H₂*)₄N-SiHMePh, **A***), 1.26 ppm (*PhCH₃Si(OC(C*H₃*)₂)₂, **C***), 0.53 ppm (*PhC*H₃*Sipin, **C***), 0.22 ppm (*O(CH₂)₄N-SiHC*H₃*Ph, **A***).*

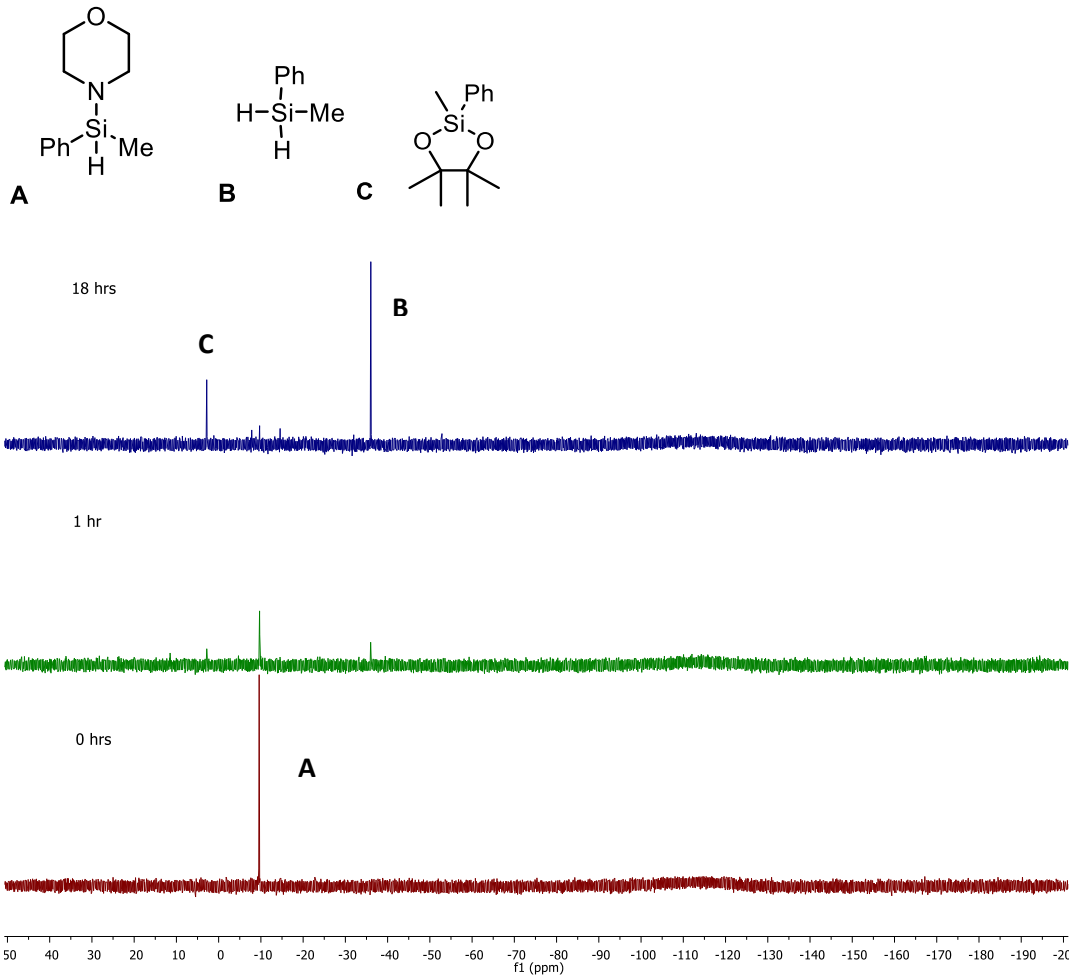

Desilylation of $O(CH_2)_4$N-SiHMePh - in situ $^{29}Si[^1H]$ NMR: - 9.86 ppm ($O(CH_2)_4$N-SiHMePh, **A***), - 36.02 ppm (H_2SiMePh,* **B***), 2.75 ppm (PhMeSipin,* **C***).*

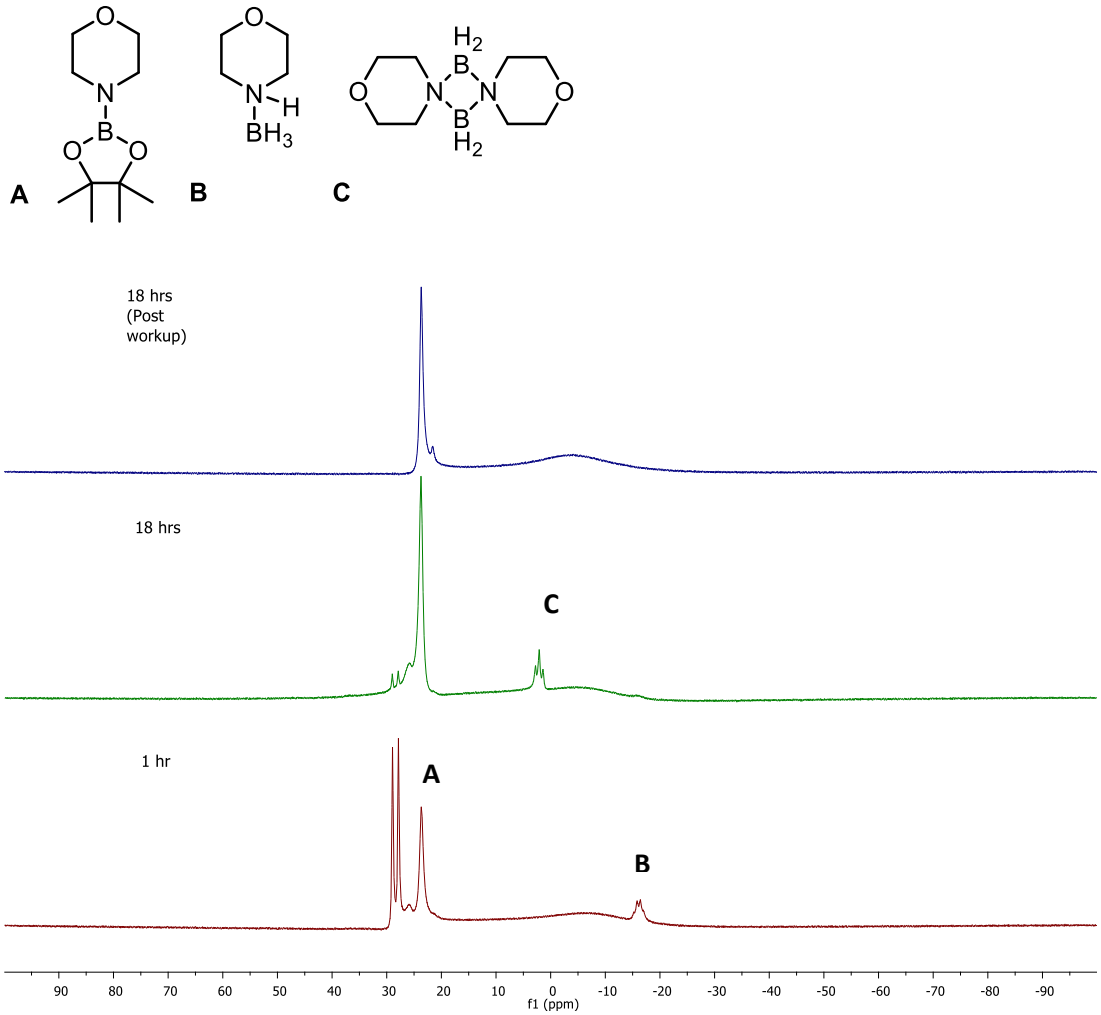

Desilylation of $O(CH_2)_4N$-SiHMePh - ^{11}B NMR : 28.40 ppm (d, J = 173.8 Hz, HBpin), 23.67 ppm ($O(CH_2)_4N$-Bpin, **A***), 2.09 (t, J = 109.1 Hz, $(O(CH_2)_4N-BH_2)_2$,* **C***), -16.11 (q, J= 76.8 Hz, $O(CH_2)_4N-BH_3$,* **B***).*

Figure 39: Stacked NMR spectra - desilylation of 4-(methyl(phenyl)silyl)morpholine.

The reaction proceeds to give full conversion of the silazane 4-(methyl(phenyl)silyl)morpholine. However, two additional products are observed in the reaction mixture which have formed *via* a side reaction. These are assigned from the crude mixture as morpholine borane dimer $(O(CH_2)_4N-BH_2)_2$ and 2,4,4,5,5-pentamethyl-2-phenyl-1,3,2-dioxasilolane (PhMeSi(pin)).[156]

In this side reaction the pinacol group has shifted from boron to silicon generating a siloxane and morpholine borane (Scheme 74). Morpholine borane then dehydrocouples to form the dimer $(O(CH_2)_4N-BH_2)_2$ displaying analogous reactivity to that previously reported in the Webster group.[152] This side reaction is unusual as it involves the cleavage of two B-O bonds. Driess and co-workers have previously reported this type of reactivity in stoichiometric reactions with a nickel complex and Chen and co-workers have observed this with scandium β-diketiminates.[164, 165] The observed reactivity suggests that silylene forms *in situ*.[166, 167] It seems plausible that by altering the reaction conditions this side route could become the predominant pathway but this has yet to be tested.

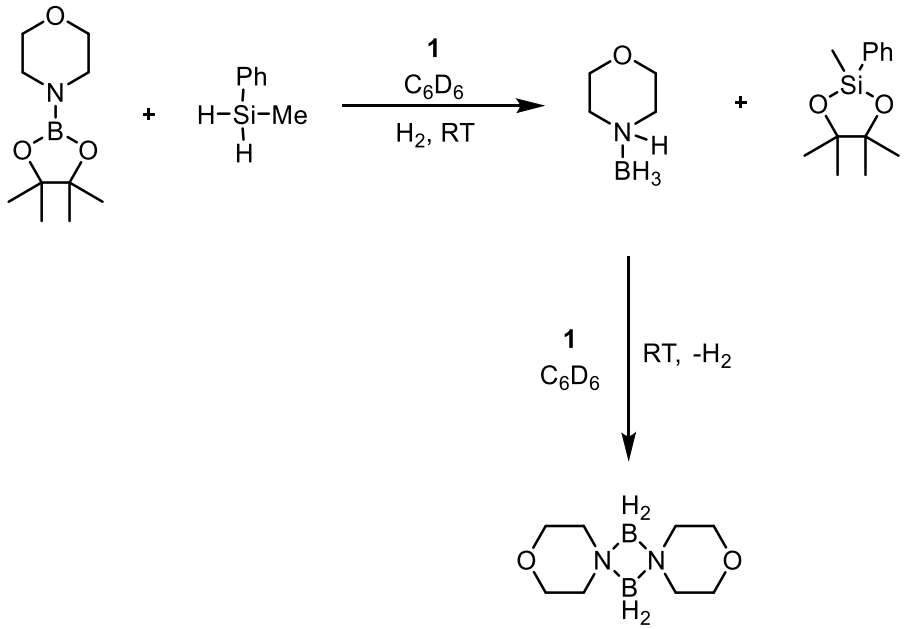

Scheme 74: Observed side reaction with B to Si pinacol-hydrogen shift and subsequent amine borane dimerization.

With desilylation reactivity established with silazanes it can be postulated that catalytic desilylation activity could be extended to siloxanes. Reactions with previously synthesised siloxanes (Chapter 4) and pinacolborane in the presence of **1** were attempted and showed a high degree of desilylation activity (Scheme 75).

5.2 – Desilylation of siloxanes

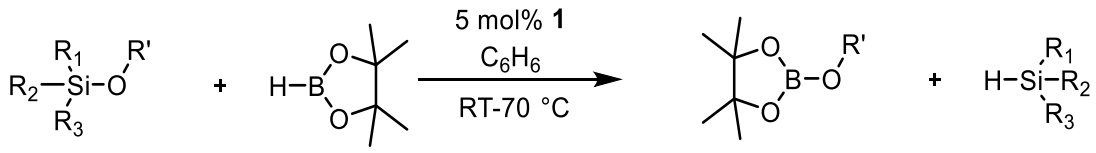

Scheme 75: Iron catalysed desilylation of siloxanes.

With desilylation reactivity established with siloxanes an investigation of the substrate scope was undertaken (Table 28).

Table 28: Substrate scope for desilylation of siloxanes.

Entry	*Substrates*	*Spec. Conversion (%)[a]* *[Isolated Yield (%)]*	*Product*	*Time (hrs)*
1	BnO−SiHPhMe HBpin	*48* *100[b][86]*		*18* *48*
2	^{t}BuO−SiHPhMe HBpin	*51* *100[b][91]*		*18* *48*
3	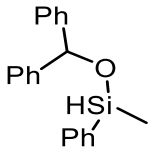 HBpin	*trace* *100[c][83]*	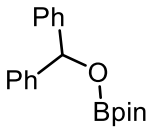	*24* *48*
4	^{t}BuO−SiH$_2$Ph HBpin	*100[b][86]*	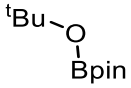	*24*
5	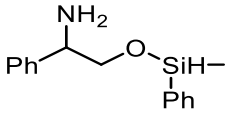 HBpin	*100*	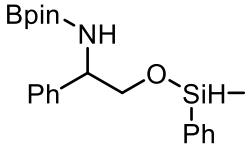	*24*
6	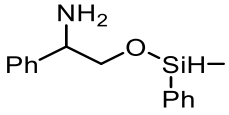 HBpin x2	*100[c][67]*	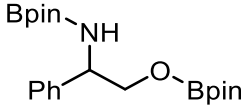	*24*

Conditions: [a] ***1****, 5 mol %, siloxane (0.5 mmol), pinacolborane (0.5 mmol), C_6H_6 (0.35 ml), RT, conversion calculated via ^{1}H from silane formed with 1,3,5-trimethoxybenzene used as an internal standard. [b] 50 °C, 24 hrs [c] 70 °C.*

Reactivity of siloxanes with pinacolborane in the presence of **1** was found to be less facile than that of the silazanes investigated. Reactions generally do not reach full conversion at room temperature even after 18-24 hours (Entries 1-3). Heating reactions to 50 °C with certain substrates (Entries 1,2 and 4) allows full conversion to be achieved. Higher temperatures are required in certain cases (Entries 3 and 7). Sterics again appear to play a role in this system with the bulky β-diketiminate ancillary ligand hindering the formation of the four-membered transition states with siloxanes leading to more cumbersome reactivity by comparison to secondary amine silazanes. Reacting a silyl protected phenylglycinol (Entry 6) with pinacolborane led to an intriguing result. Rather than desilylation, dehydrocoupling was observed. By altering the number of equivalents of pinacolborane tandem catalysis can

be achieved with concurrent desilylation occurring to give a diboryl product. No shift in pinacol was observed with siloxanes as opposed to silazanes. This is presumably due to silylene formation being unfavourable from siloxanes precursors.

Having delved into the substrate scope of desilylation chemistry catalysed by **1** and based upon the studies presented in this thesis on other catalytic systems some mechanistic considerations were devised.

5.3 - Mechanistic considerations

Given the propensity of **1** to form iron hydride catalytic intermediates in the presence of a hydride source like pinacolborane it is plausible that this precedes desilylation catalysis. In addition to work presented in this thesis this has previously been reported in hydroboration chemistry with **1** and pinacolborane.[168] As this catalysis works for siloxanes and silazanes with saturated amino groups it can be postulated that the reaction occurs *via* sigma bond metathesis. In view of this a catalytic cycle is proposed (Scheme 76).

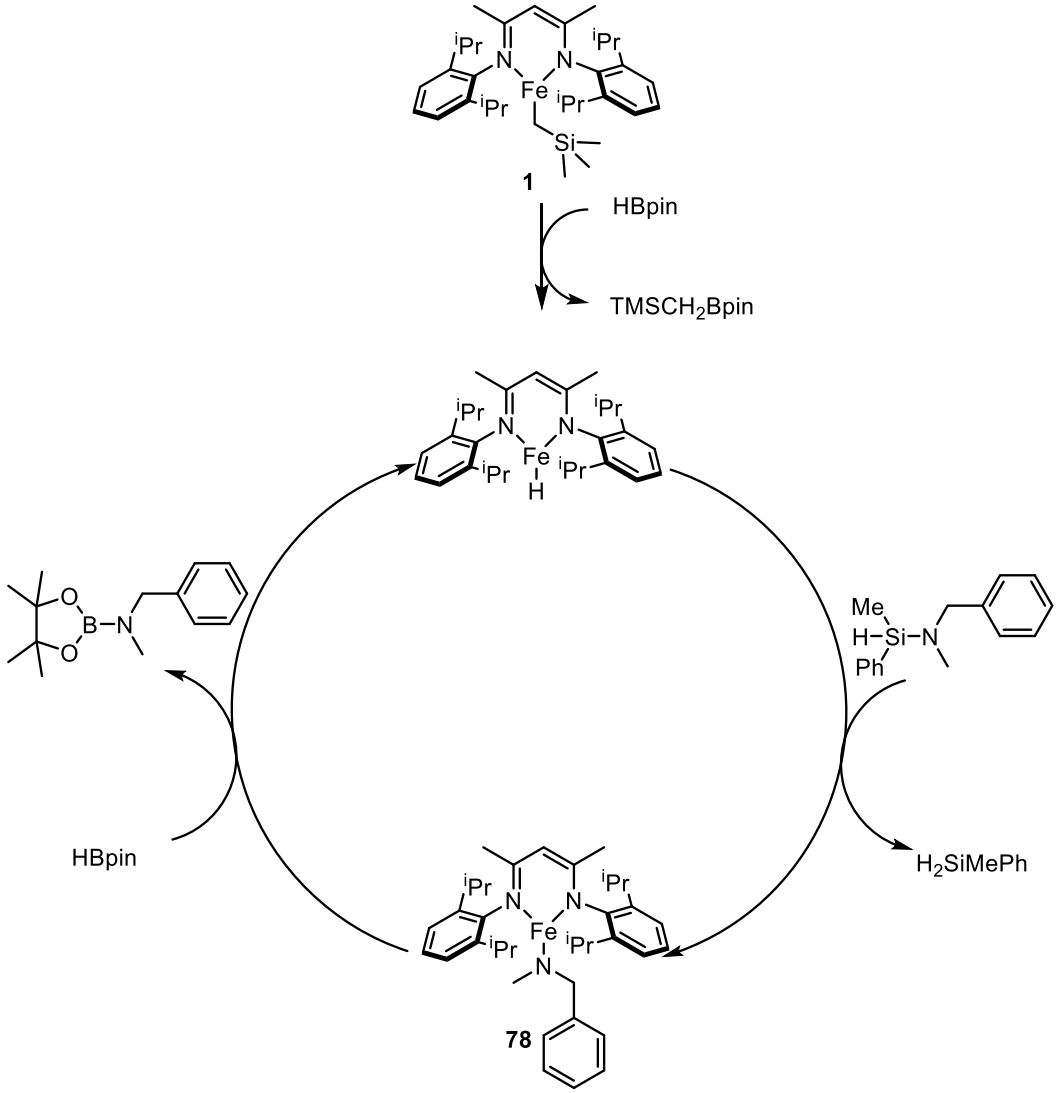

Scheme 76: Postulated catalytic cycle for desilylation of secondary silazanes.

In the desilylation cycle an iron hydride is generated from the reaction of **1** with HBpin as observed by ^{1}H and ^{11}B NMR signals at 0.15, 1.27 ppm and 34.2 ppm respectively, which are in agreement with the literature values for $TMSCH_2Bpin$.[168] Iron hydride reacts with silazane/siloxane releasing silane and generating an iron amido/alkoxide (in this example **78** (Scheme 76)). The incipient iron amido/alkoxide species then reacts with an equivalent of pinacolborane releasing the aminoborane/alkoxyborane completing the catalytic cycle. In an effort to support this **78** was synthesised and reacted stoichiometrically with pinacolborane. The results of this reaction at first appear perplexing as only trace amounts of aminoborane were detected with **78** remaining largely unreacted. The iron hydride species **79** was not detected in the reaction mixture. In rationalising these observations it is important to make reference of the previously reported work in the Webster group.[168] In hydroboration reactions catalysed by **1** an iron hydride species is expected to play a role in the catalytic cycle. However upon reacting **1** with pinacolborane, no hydride species were observed in solution. As has been mentioned previously, the monomeric hydride species is too short-lived to be detectable in solution and is largely evidenced by its dimeric counterpart **79** in systems where it acts as a catalytic resting state.[8] A lack of detection of this dimeric hydride does not rule out the possibility of the catalytic cycle proceeding via an iron hydride, indeed truly reactive intermediates can prove highly elusive to detect. It is useful to draw comparison between the hydroboration and desilylation catalytic cycles as in both a smaller than spectroscopically detectable quantity of iron hydride likely facilitates reactivity. The driving force for these desilylation reactions is the formation of products that are more enthalpically favoured. The cleavage of an N-Si bond and formation of an N-B bond and the associated decrease in enthalpy[169] make these reactions favourable (Bond dissociation energies = N-Si, ΔH_f = 355 $kJmol^{-1}$ and N-B, ΔH_f = 389 $kJmol^{-1}$).[169-172]

As discussed, siloxanes and silazanes with a tertiary amino group react in a less facile manner than silazanes with a secondary amino group. It is plausible that this secondary substituted amino group facilitates an alternative reaction pathway which results in the observed higher catalytic turnover. On this basis an alternative mechanism is postulated for silazanes with mono substituted amino groups (Scheme 77).

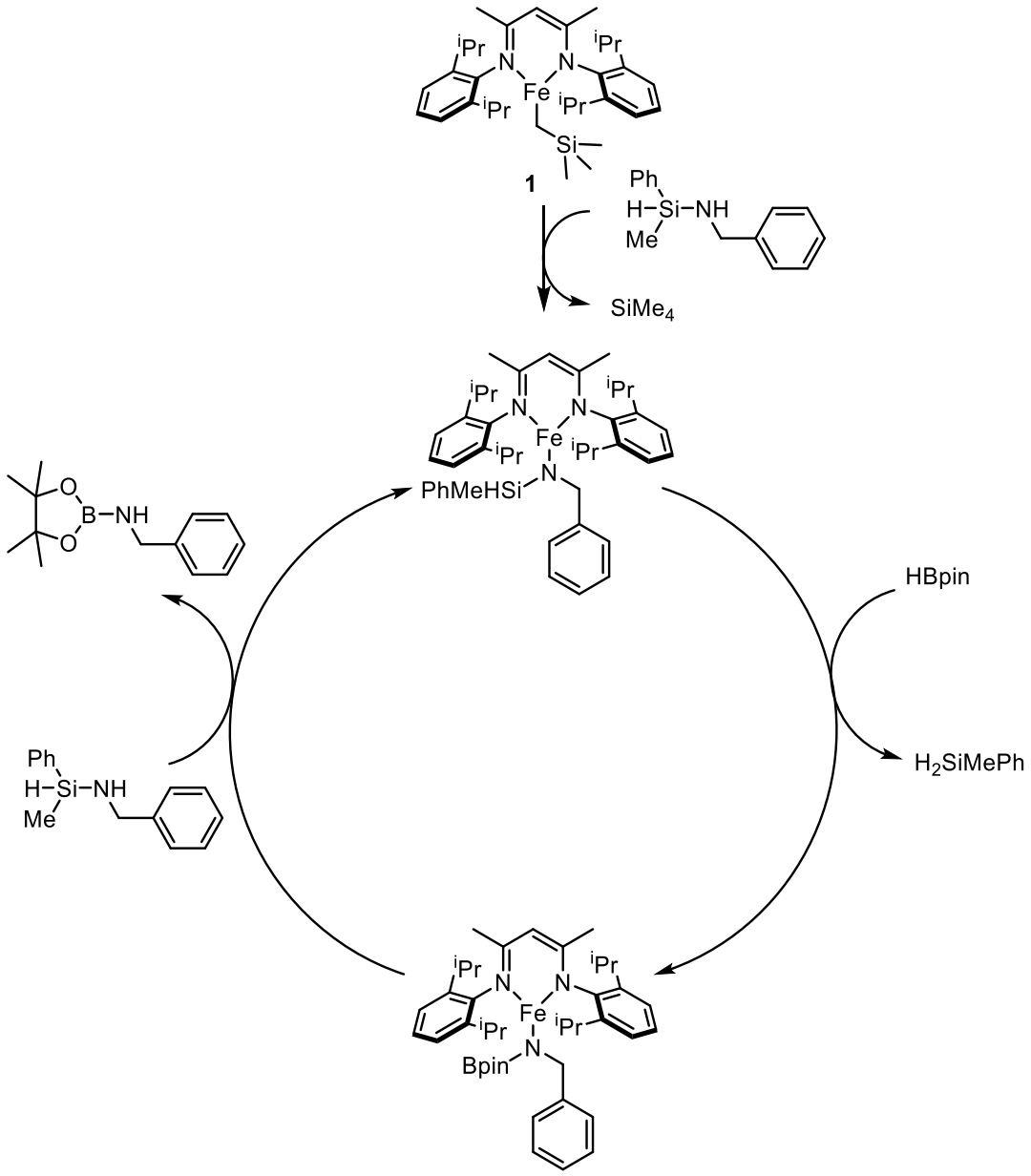

Scheme 77: Postulated catalytic cycle for desilylation of primary silazanes.

In this catalytic cycle, **1** reacts with an equivalent of silazane generating an iron amidosilyl species. An equivalent of pinacolborane then reacts with the iron amidosilyl species *via* σ-bond metathesis releasing silane and forming an iron amidoborane complex. Such species have been postulated previously and their alkaline earth analogues isolated as well as iron aminoborane complexes.[153, 159] The iron amidoborane species then reacts with an equivalent of silazane *via* protonlysis releasing aminoborane and completing the catalytic cycle. Reactions between **1** and diisopropylaniline to form the amido complex ^{Diip}LFe-NHDipp, (**6**) and subsequent reaction with pinacolborane lead to the instaneous formation of **79**. This demonstrates that the desilylation of silazanes with mono substituted amino groups and silazanes with secondary substituted amino groups proceed *via* the same mechanism.

5.4 - Future applications

The desilylation chemistry presented here was explored as a result of serendipitous findings. The monomolecular reactions that have been probed could serve as template for depolymerisation reactions (Scheme 78).[173-175] Polysilazanes and polysiloxanes are heavily relied upon in industrial applications, particularly in ceramics.[176-178] These materials are non-biodegradable and at the end of their lifetimes need to be burnt to be disposed of. This catalytic desilylation method could be used as a more sustainable alternative with lower temperatures required to breakdown materials.

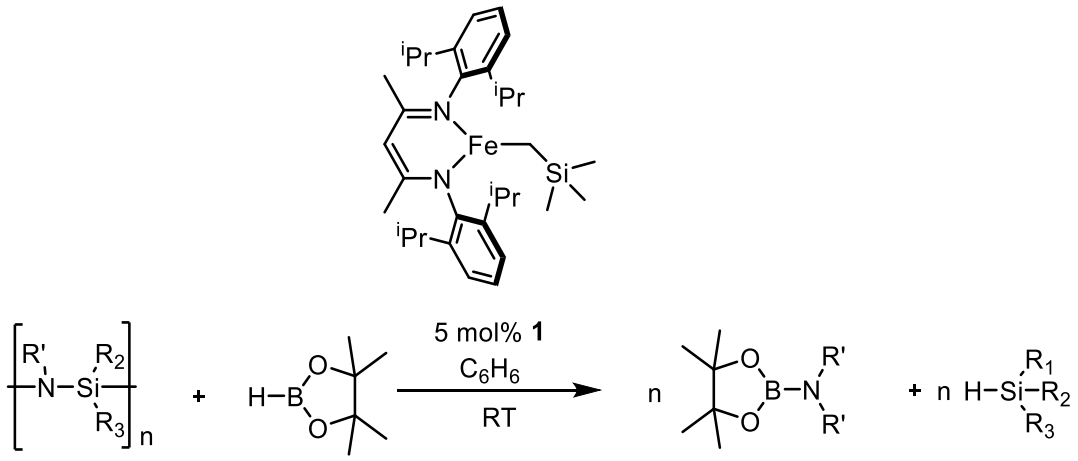

Scheme 78: Plausible route to de-polymerisation of polysilazanes.

5.5 - Conclusions from Chapter 5

The results in this chapter report that investigations into tandem dehydrocoupling reactivity with silazanes instead give serendipitous desilylation activity. The results show that catalytic reactivity occurs with a range of different silazanes and was determined to be facile with certain substrates. A side reaction is observed with a shift in pinacol from boron to silicon. Desilylation reactivity was then further extended to siloxanes. It was determined that siloxanes react more slowly than silazanes requiring higher temperatures and longer reaction times. A preliminary mechanistic investigation suggested that the mechanisms do not differ between saturated secondary- and tertiary-substituted amine or alkoxide substrates.

6 - Summary

Chapter 1 gave an introduction to iron complexes and their applications in catalysis. Specific focus was given to iron β-diketiminate complexes and their intriguing properties which make them of great interest in catalytic studies. Phosphines were highlighted as an important class of compounds in coordination chemistry with widespread use in industry and academia. Attention was then drawn to the literature precedent on hydrophosphination reactions. Focus on iron-catalysed hydrophosphination shows that the field is burgeoning but few reports go into great mechanistic detail. Dehydrocoupling reactions have been introduced as useful catalytic reactions for the synthesis of main group - main group bonds. Catalytic systems were discussed that can give rise to homocoupling reactions which is in stark contrast to heterocoupling reactivity.

Chapter 2 delved into the synthesis of three-coordinate iron(II) β-diketiminate complexes. These complexes have been used successfully as precatalysts in phosphine catalysis. Whilst initially attempts at hydrophosphination reactions proved unsuccessful these reactions led to serendipitous phosphine dehydrocoupling activity. The scope of this reactivity was investigated. Iron-catalysed dehydrocoupling was probed and reactivity was determined to be radical in nature. An iron phosphido species was proposed as a catalytic intermediate. Spectroscopic evidence was found to support this but isolation of the complex is inhibited by decomposition. TEM studies were undertaken to determine whether the active iron species are nanoparticulate. No evidence for repeating nanoparticulate structures was observed *via* TEM images, ruling out nanoparticles as the predominate species in phosphine dehydrocoupling. Switching solvents led to a change in chemistry and the observation of catalytic hydrophosphination of alkenes.

Chapter 3 saw this hydrophosphination reactivity extended to alkynes. In benzene Markovnikov addition was favoured with iron β-diketiminate complexes. Subsequently a full substrate scope was presented. Switching solvents was then determined to lead to a complete shift in selectivity with *anti*-Markovnikov addition favoured in DCM. A full substrate scope under these conditions was then discussed. The diverging mechanisms of these two hydrophosphination reactions were considered. A dimeric iron-acetylide complex was isolated and the mechanism for Markovnikov addition was determined to be radical in origin. Kinetic analyses were attempted but failed to yield any useful data. Reaction profiles of iron alkyl and iron acetylide complexes were different and it was determined that the iron acetylide dimer was not an on cycle intermediate. Deuterium labelling studies added some extra mechanistic insight and a mechanism was proposed based on the experimental findings. Background reactions established the non-innocence of DCM in oxidation to an iron(III) chloro complex. Reaction profiles confirmed that this was consistent with the precatalyst and hence *anti*-Markovnikov addition was found to be a Lewis acid-catalysed process. Hydrophosphination reactivity was further extended to phosphalkenes and phosphaalkynes in intramolecular hydrophosphination reactions. Attempts were made to synthesise a suitable precatalyst for enantioselective hydrophosphination. Complexes were synthesised successfully but proved to be poor hydrophosphination catalysts.

Chapter 4 explored heterodehydrocoupling with iron(II) β-diketiminate complexes. Initial studies focused on phosphine-silane coupling which was found to be remarkably selective over the previously discussed phosphine homocoupling. The substrate scope was scrutinised with tertiary silanes discovered to be a limitation. As with previous systems reactivity can be attributed to radical species. Kinetic analyses were attempted but did not give any insight into the reaction mechanism due to a surprising switch in reactivity whereby homocoupling becomes the dominant pathway. A mechanism is proposed based on experimental findings. Reactivity was extended to encompass amine-silane coupling. A full substrate scope was investigated. Amine-silane coupling reactions did not display radical character and crucially full kinetic analysis was conducted on this system. Determination of the reaction rate law led to a postulated mechanism. The rate-determining step is the final protonolysis reaction with an equivalent of amine. Heterodehydrocoupling of alcohols and silanes was then investigated. A full substrate scope was analysed and mechanism proposed which is analogous to the amine silane catalytic cycle.

Chapter 5 reports serendipitous results with catalytic desilylation reactivity described. This reactivity was further scrutinised with a variety of silazanes and pinacolborane. Reactions between siloxanes and pinacolborane were also observed to show desilylation activity. Two plausible mechanisms are postulated. The results presented are proposed as a model for depolymerisation of (poly)silazanes.

7 – Further Work

Chapter 2 focused on phosphine dehydrocoupling. The mechanistic investigations presented herein allow us to propose a mechanism for this system. Further work needs to be done to pin down the exact nature of this system. Kinetic studies *via* React IR and iron Mossbauer studies could shed more light on the reactivity of this system.

Chapter 3 focused on alkyne hydrophosphination. The observed activity and selectivities in benzene are proposed to be due to low reactivity between **66** and alkenes. This is proposed to be due to a better binding affinity of the *sp*-hybridised alkynes. Further work could look to extend the scope of this reactivity with other substrates containing *sp*-hybridised carbons such as allenes. The work presented herein has largely focused on iron in phosphine catalysis. Iron is a highly earth abundant metal but in terms of abundance the most earth abundant metal is aluminium. Despite its abundance very few hydrofunctionalisation catalysis studies have focused on aluminium. Hydrophosphination reactions presented in Chapter 3 with aluminium trichloride suggest that there is plenty of scope for aluminium catalysed hydrophosphination. Indeed there are plenty of aluminium β-diketiminate complexes reported in the literature which could potentially be used in hydrophosphination reactions (Figure 40).

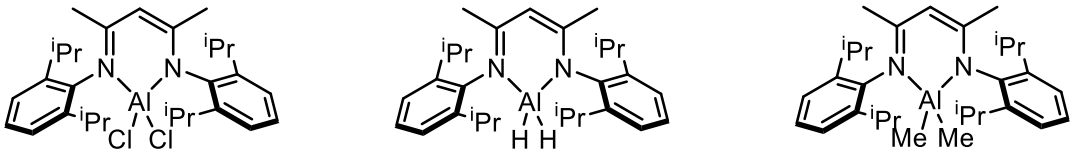

83 **84** **85**

Figure 40: Aluminium β-diketiminate complexes – potential hydrophosphination precatalysts.

Aluminium β-diketiminate complexes much like their iron counterparts have received little focus as precatalysts due to their sensitivity to air and moisture. As described herein iron β-diketiminate complexes are paramagnetic which makes characterisation and *in situ* analysis challenging. In stark contrast aluminium β-diketiminate complexes are diamagnetic which is highly advantageous in reaction monitoring studies. A few examples of aluminium catalysed hydrofunctionalisation and dehydrocoupling reactions have been reported but by and large this area of research remains scarcely explored.[133, 179-181]

Chapter 4 focused on heterodehydrocoupling reactions with silanes. Like phosphine homocoupling, further mechanistic work could be conducted on phosphine silane dehydrocoupling to provide more clarity on the mechanism. Amine silane dehydrocoupling is facile with **1**. Substrates synthesised include dimers which suggests that this reactivity could be extended to synthesise (poly)silazanes *via* dehydropolymerisation. $Fe(HMDS)_2$ could be used in place of **1** as a catalyst for these dehydropolymerisation reactions.

Chapter 5 uncovered serendipitous desilylation results. This study could be used as model for depolymerisation with iron β-diketiminate complexes. Further optimisation could be undertaken to make the pinacol shift to form a pinacol silane, the dominant reaction pathway. A full kinetics study of the desilylation of silyl morpholine could gage further mechanistic insight.

8 - Experimental Data

General considerations: Reagents were purchased from Sigma Aldrich or Alfa Aesar and used without further purification. DIBAL-H was purchased as a solution in hexane or THF and titrated prior to use.[182] Laboratory grade THF and benzene was purchased from Fisher Scientific and dried over sodium/benzophenone and distilled before use. Diphenyl phosphine, dicyclohexyl phosphine and Cyclohexyl phosphine were purchased from Sigma Aldrich and used without further purification. Phenyl phosphine was purchased from Alfa Aesar and used without further purification. NMR data was collected at 300, 400 or 500 MHz on Bruker or Agilent instruments in C_6D_6 at 298 K and referenced to residual protio solvent. Heated and anhydrous reactions were undertaken in Schlenk tubes or Teflon-sealed J-Young reaction tubes. All manipulations are carried out under an inert atmosphere using standard Schlenk and glovebox techniques, unless otherwise stated.

Compounds synthesised in Chapter 2:

Method for the synthesis of pro-ligands L1 and L2: All techniques in this procedure were carried out in air. In a two-neck 500 mL round-bottomed flask, 2,4-pentanedione (6.68 g, 0.067 mol) was mixed with 300 mL of ethanol and 2,6-diisopropylaniline (28.67 g, 0.162 mol). To the mixture was added 7.5 mL of hydrochloric acid (12 M) and the solution was refluxed with vigorous stirring for 3 days. The resulting slurry was then allowed to cool to room temperature and filtered. The filtered solid was dried under reduced pressure, and the filtrate was evaporated on a rotary evaporator. The dried mass was combined with the filtrate residue and the mixture was refluxed in 250 mL hexane at 80 °C for 1 h. The mixture was then cooled and filtered. Next the solid residue was treated with 300 mL of a saturated aqueous solution of Na_2CO_3 and 500 mL of Dichloromethane (DCM). The slurry was stirred until the solid dissolved. Stirring was then ceased giving a yellowish organic solution and a pale yellow aqueous layer. The organic layer was separated using a separatory funnel and then dried over $MgSO_4$. The solution was filtered and dried under reduced pressure to yield a yellowish powder that upon washing with 50 mL of cold methanol (-20 °C) yields the desired β-diketimine as a white powder.[183]

Method for the preparation of precatalysts 1 and 60: To a Schlenk containing a stirred solution of β-diketimine (1.75 g, 4.18 mmol) in Tetrahydrofuran (THF) (20 mL), n-butyl lithium (2.5 M in hexane, 1.67 mL, 4.18 mmol) was added at -78 °C. This was then allowed to warm to room temperature and the resulting pale yellow solution was stirred for 30 mins. Next solid $FeCl_2(THF)_{1.5}$ (982 mg, 4.28 mmol) was added to the solution. The resulting yellow solution was stirred for 45 min. Solid $LiCH_2SiMe_3$ (394 mg, 4.18 mmol) was then added and a very dark orange solution was obtained. After 30 mins the solution had turned dark red. After another 15 mins stirring the solvent was removed *in vacuo*. Any residual THF was then removed by stirring the residue with pentane (3 x 25 mL) and subsequent evaporation of all volatiles. Next, the residue was extracted with pentane via cannula filtration. The orange extract was concentrated to approximately 10 mL and cooled to -25 °C to afford **1** as yellow crystals.[7] Complex **60** (red crystals) was synthesised using the same procedure and crystallised as the THF adduct.

(^{DIPP}Nacnac)FeCH$_2$TMS (1)

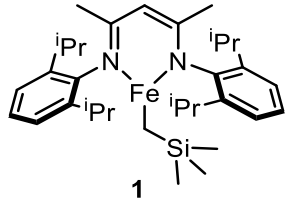

1

Re-crystallised from pentane, yellow crystals, 1.52g, 65%. ^{1}H NMR: (500 MHz, C_6D_6, 298 K) = 111.81 (s, 1H, a-CH), 72.81 (s, 6H, c-CH_3), 55.02 (s, 9H, Si(CH_3)$_3$), −8.28 (s, 4H, m-H), −14.15 (s , 12H, iPr-CH_3), −67.03 (s, 2H, p-H), −97.66 (s, 12H, iPr-CH_3), −124.63 (s, 4H, iPr-CH). IR (solid) ν 2959, 2867, 1524, 1459, 1376, 1235, 1100, 981, 843, 756 cm^{-1}. Anal. Calc. for $C_{33}H_{52}N_2FeSi$ (560.72) requires: C, 70.69; H, 9.35; N, 5.00. Found: C, 70.66; H, 9.44; N, 5.20. Melt.pt: 158-160^{o}C. μ_{eff} = 5.6. For crystallographic data, see page 180.

(^{DMP}Nacnac)FeCH$_2$TMS.THF (60)

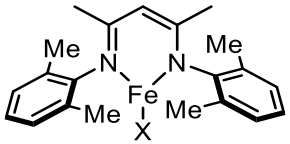

60

X = CH_2TMS.THF

Re-crystallised from pentane, red crystals, 1.09 g, 58%. ^{1}H NMR: (500 MHz, C_6D_6, 298 K) = 81.20 (s, 1H, a-CH), 60.94 (s, 6H, c-CH_3), 32.25 (s, 9H, Si(CH_3)$_3$), 3.43 (s, 4H) (THF), 2.47 (s, 4H (THF)), −1.71 (s, 4H, Ar m-H), -13.48 (s, 2H, CH_2TMS), −51.78 (s, 12H, Ar-CH_3), −65.40 (s, 2H, Ar p-H). Anal. Calc. for $C_{27}H_{44}N_2FeSiO$ requires: C, 66.91; H, 8.52; N, 5.38. Found: C, 66.68; H, 8.42; N, 5.69. Melt.pt: 76-80 ^{o}C. IR (solid) ν 2946, 1522, 1366, 1180, 1035, 850, 760 cm^{-1}. For crystallographic data, see page 181.

(^{DIPP}Nacnac)FeI (62)

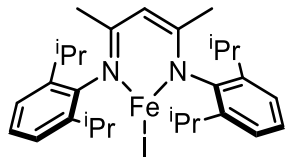

62

^{1}H NMR (400 MHz, C_6D_6, 298 K): 18.06 (4H, m-CH), 8.75 (12H, iPr-CH_3), 4.34 (12H, iPr-CH_3), -19.55 (4H,iPr-CH), -27.90 (2H, p-CH), -62.33 (6H, c-CH_3), -88.22 (1H, α-CH). IR: (solid) ν 2955, 1521, 1311, 1258, 1172, 1023, 932, 768, 623 cm^{-1}. Melt pt: 148-152 ^{o}C

(^{DIPP}Nacnac)FePPh$_2$ (66)

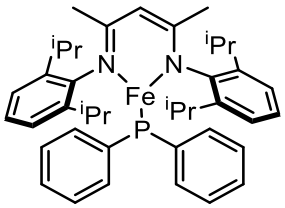

66

^{1}H NMR: (500 MHz, C_6D_6, 298 K) 76.75 (1H, α-CH), 33.19 (6H, c-CH_3), 20.41 (4H, o-CH), 3.39 (12H, iPr-CH_3), -1.28 (4H, m-CH),-17.26 (12H, iPr-CH_3), -20.34 (2H, p-CH), -23.83 (2H, p-CH), -63.25 (4H, m-CH) -80.69 (4H, iPr-CH). LC-MS (ESI): [M+2H] 660.3208, Melt pt: Decomposes at room temperature in solid state.

(^{DIPP}Nacnac)FeNPh$_2$ (68)

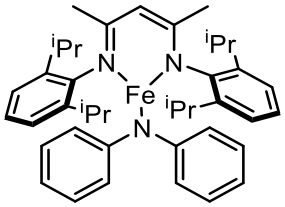

68

Recrystallised from pentane, orange crystals, Yield = 83 mg, 52 %, ^{1}H NMR (500 MHz, C_6D_6, 298 K): 94.41 (1H, α-CH), 56.94 (6H, c-CH_3), 49.34 (4H, o-CH), -6.96 (4H, m-CH), -8.49 (12H, iPr-CH_3), -32.83 (4H, m-CH), -45.99 (2H, p-CH), -60.40 (2H,p-CH), -75.47 (12H, iPr-CH_3), -122.99 (4H, iPr-CH). IR (solid) ν 2958, 1522, 1462, 1375, 1172, 1052, 932, 866, 795 cm^{-1}. Melt pt: 160-162 °C. Anal calc. for $C_{41}H_{51}FeN_3$ requires: C, 76.74; H, 8.01; N, 6.55, Found: C, 76.96; H, 8.16; N, 6.56. For crystallographic data see page 182.

Procedure for the synthesis of secondary phosphines: Secondary phosphines were synthesised in accordance with literature reports (see below).[30, 74]

Synthesis of secondary phosphine oxides: In a 250 mL Schlenk under an inert Nitrogen atmosphere a solution of the corresponding aryl halide (3.3 eq.) in 50 mL THF was prepared. This was slowly added *via* cannula to a separate Schlenk containing a suspension of magnesium (51.2 mmol, 3.3 eq.) in 30 ml THF cooled in an ice bath. The solution was stirred for 15 mins after which time the ice bath was removed and the solution was allowed to warm to room temperature. The solution was stirred for an additional four hours at room temperature, the mixture was then again cooled with an ice bath and diethyl phosphite (15.5 mmol, 1.0 eq.) was added slowly. The mixture was then stirred for 15 minutes at low temperatures and then again warmed to room temperature and stirred for a further 2 hours. Subsequently 40 ml 0.1 M HCl were added drop wise over a period of 5 minutes at 0 °C, followed by addition of 40 ml methyl tert-butyl ether (MTBE) and stirring for further 5 minutes. The upper organic phase was decanted from the formed gel. 50 ml of DCM were added to the remaining gel and the mixture agitated well for additional 5 minutes. The resultant mixture was then filtered through a frit equipped with Celite. After washing the Celite with DCM (2 x 30mL) the organic phases were combined, dried over $MgSO_4$ and the

solvent was removed *in vacuo*. The crude product was then purified either by recrystallization from EtOAc:pentane (1:1) or silica column chromatography (40 to 100% EtOAc/pentane) ,to give the product as a white solid.

Secondary phosphine oxide (R)	Yield (%)
p-C_6H_4Me	57
p-C_6H_4OMe	65
p-$C_6H_4NMe_2$	68
p-C_6H_4Cl	52
p-C_6H_4F	50
p-$C_6H_4CF_3$	43
o-C_6H_4Me	67
o-C_6H_4OMe	36

Reduction of secondary phosphine oxides

In a 250 mL Schlenk under an inert Nitrogen atmosphere a solution of phosphine oxide (1 eq) in 50 ml THF was prepared. Diisobutyl aluminium hydride (DIBAL-H) in THF (3-5 eq.) was then added slowly. The solution was then stirred for 30 mins to 16 hrs at ambient temperature or 35 °C (depending on the reactivity of the secondary phosphine oxide, with heteroatom containing substrates requiring extended stirring). Then 50 mL freshly degassed MTBE was added slowly via syringe. The solution was then cooled to 0 °C in an ice bath. Subsequently 30 mL of freshly degassed 2M NaOH (aq) was added via syringe over a period of 15 mins. Vigorous gas evolution was observed. Then 10 ml of freshly degassed saturated brine solution was added slowly. The solution was then allowed to warm to room temperature. Stirring was stopped allowing the layers to separate. The organic layer was then transferred via cannula to a second 250 ml Schlenk with freshly oven dried $MgSO_4$ (7 g). After stirring for 10 minutes the solution was filtered via cannula and the solvent removed in vacuo yielding the phosphine as a colourless oil or a white solid. If unreacted secondary phosphine oxide remained in the product, this could be removed by passage through a pipette plugged with glass paper and silica, eluting with pentane up to 40% DCM/pentane (glovebox).

Secondary phosphine (R)	Yield (%)
p-C_6H_4Me	76
p-C_6H_4OMe	66
p-$C_6H_4NMe_2$	80
p-C_6H_4Cl	81

p-C_6H_4F	46
p-$C_6H_4CF_3$	62
o-C_6H_4Me	48
o-C_6H_4OMe	24

General method for the dehydrocoupling of phosphines: To a sealed Schlenk tube 5 mol% (0.025 mmol) of precatalyst **1** or **60** was added in 0.35 mL of benzene. 0.5 mmol of phosphine was then added to the reaction vessel and the corresponding solution was stirred at 70 °C for 24 hrs (or otherwise stated). To obtain spectroscopic yield and/or isolated yield the reaction mixture was passed through a short silica plug, eluting with DCM. The solution was charged with a known quantity of 1,3,5-trimethoxybenzene, concentrated then an NMR sample prepared using C_6D_6. This isolation method was necessary to remove the paramagnetic component from the reaction mixture, allowing analysis by ^{1}H NMR.

Phosphine dehydrocoupling:

1,1,2,2-Tetraphenyldiphosphane-$P_2(C_6H_5)_4$ (Table 6, Entry 1)

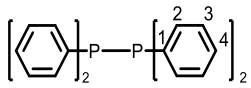

Isolation by washing with hexane; white solid, 78 mg, 85%. ^{1}H NMR: (500 MHz, C_6D_6, 298 K) = 7.57-7.52 (m, CH, 8H), 6.97-6.94 (m, CH, 12H). ^{13}C{^{1}H} NMR: (126 MHz, C_6D_6, 298 K) = 137.0 (t, ^2J = 5.2 Hz, C2), 135.2 (t, ^1J = 12.9 Hz, C1), 129.3 (s, C4), 129.0 (t, ^3J = 3.0 Hz, C3). ^{31}P{^{1}H} NMR: (203 MHz, C_6D_6, 298 K) = −14.0. Concurrent with literature reports.[70, 79]

P_2(p-Tolyl)$_4$ (Table 6, Entry 2)

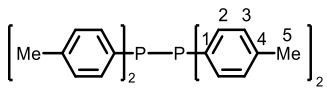

Isolation by washing with hexane; white solid, Yield: 73 mg, 68%. ^{1}H NMR: (500 MHz, C_6D_6, 298 K) = 7.65-7.61 (m, CH, 8H), 6.87-7.84 (m, CH, 8H), 1.97 (s, 12 H). ^{13}C{^{1}H} NMR: (126 MHz, C_6D_6, 298 K) = 139.2 (s, C4), 135.4 (t, ^2J = 13.0 Hz, C2), 134.0 (t, ^1J = 4.7 Hz, C1), 129.8 (t, ^3J =3.4 Hz, C3), 21.5 (s, C5), ^{31}P{^{1}H} NMR: (203 MHz, C_6D_6, 298 K) = −16.5. Concurrent with literature reports.[74]

P_2(p-C_6H_4OMe)$_4$ (Table 6, Entry 3)

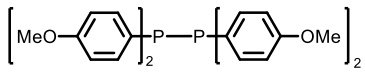

Not isolated. $^{31}P\{^{1}H\}$ NMR: (203 MHz, C_6D_6, 298 K) = −17.8. Concurrent with literature reports.[74]

$P_2(p\text{-}C_6H_4NMe_2)_4$ (Table 6, Entry 4)

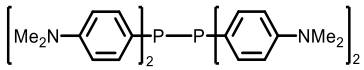

Yield: 81 mg, 60% ^{1}H NMR:(500 MHz, C_6D_6, 298 K) = δ 7.69-7.56 (m, 8H, CH-Ar), 6.67-6.50 (m, 8H, CH-Ar), 2.48 (s, 24H, NCH_3). $^{31}P\{^{1}H\}$ NMR: (203 MHz, C_6D_6, 298 K) = −18.5. Data comparable with literature reports.[74]

$P_2(p\text{-}C_6H_4Cl)_4$ (Table 6, Entry 5)

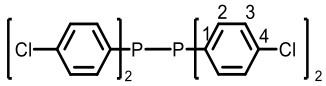

Yield: 104 mg, 82%. ^{1}H NMR: (500 MHz, C_6D_6, 298 K) = δ 7.27-7.18 (m, 8H, CH-Ar), 7.03-6.97 (m, 8H, CH-Ar). $^{13}C\{^{1}H\}$ NMR: (126 MHz, C_6D_6, 298 K) = 136.3 (s, C4), 136.1 (t, ^{2}J =13.1 Hz, C2), 134.1 (t, ^{3}J =3.4 Hz, C3), 129.4 (t, ^{1}J =5.9 Hz, C1). $^{31}P\{^{1}H\}$ NMR: (203 MHz, C_6D_6, 298 K) = −16.4. Concurrent with literature reports.[74]

$P_2(p\text{-}C_6H_4F)_4$ (Table 6, Entry 6)

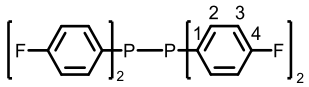

Isolation by washing with hexane. 99 mg, 90%. ^{1}H NMR: (500 MHz, C_6D_6, 298 K) = 7.25-7.16 (app. ddd, J = 8.6, 5.7, 2.7 Hz, 8H), 6.62 (app. dd, J = 8.8, 8.6 Hz, 8H). $^{13}C\{^{1}H\}$ NMR: (126 MHz, C_6D_6, 298 K) = 136.9 (td, ^{4}J = 13.8, 8.0 Hz, C4), 131.4 (dd, ^{3}J = 8.9, 5.3 Hz, C3), 116.5 (d, ^{1}J = 3.7 Hz, C1), 116.2 (t, ^{2}J =3.8 Hz, C2). $^{31}P\{^{1}H\}$ NMR: (203 MHz, C_6D_6) = −16.8. ^{19}F NMR (376 MHz, C_6D_6, 298 K) = −111.2.

$P_2(p\text{-}C_6H_4CF_3)_4$ (Table 6, Entry 7)

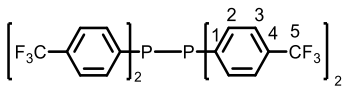

Isolation by washing with hexane. Yield: 91 mg, 57%. ^{1}H NMR: (500 MHz, C_6D_6, 298 K) = 7.32-7.22 (m, 8H), 7.12-7.10 (m, 8H). $^{13}C\{^{1}H\}$ NMR: (126 MHz, C_6D_6, 298 K) = 134.0 (q, ^{2}J = 15.0 Hz, C2), 130.9 (q, ^{4}J = 26.0 Hz, C4), 128.2 (s, C3), 125.1 (app. quintet, ^{5}J = 3.6 Hz, C5), 123.2 (t, ^{1}J = 10.0 Hz, C1). $^{31}P\{^{1}H\}$ NMR: (203 MHz, C_6D_6, 298 K) = −13.2. ^{19}F NMR (376 MHz, C_6D_6, 298 K) = −62.7.

P_2(o-Tolyl)$_4$ (Table 6, Entry 8)

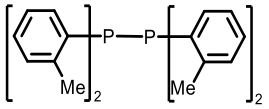

Not isolated. $^{31}P\{^1H\}$ NMR: (203 MHz, C_6D_6, 298 K) = −33.7. Crude data comparable to literature reports. [74]

P_2(o-C_6H_4OMe)$_4$ (Table 6, Entry 9)

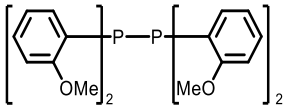

Not isolated. $^{31}P\{^1H\}$ NMR: (203 MHz, C_6D_6, 298 K) = −42.3. Crude data comparable to literature reports.[184]

$P_2(C_6H_{11})_4$ (Table 6, Entry 10)

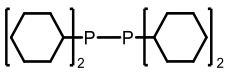

Not isolated. $^{31}P\{^1H\}$ NMR: (203 MHz, C_6D_6, 298 K) = −21.3. Crude data comparable to literature reports.[185]

General method for hydrophosphination of alkenes using $HPPh_2$: Styrene (1.04 mmol, 1.82 eq) was added to a solution of $HPPh_2$ (99 µL, 0.57 mmol, 1 eq) and **1**(16 mg, 5 mol%) in CH_2Cl_2(0.35 mL) and stirred in a sealed tube at 70 °C under N_2 for 24 h. The reaction mixture was concentrated *in vacuo*, then under an ambient atmosphere passed through a pipette plugged with silica, eluting with 4% EtOAc/pentane. The solution was concentrated then analysed by ^1H NMR spectroscopy using 1,2-DCE as a standard

Alkene hydrophosphination

Phenethyldiphenylphosphane - Table 9, Entry 1

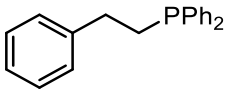

Colourless oil, 124mg (75%). ^1H NMR:(300 MHz,$CDCl_3$, 298 K) δ 7.47 –7.15 (m, 14H), 2.73 - 2.67 (m, 2H), 2.39 -2.33 (m, 2H).$^{13}C\{^1H\}$NMR:(75 MHz, $CDCl_3$, 298 K) δ 142.7(d, *J* = 12.7 Hz), 138.6(d, *J* = 19.2 Hz), 132.8(d, *J* = 13.2 Hz), 128.9, 128.6(d, *J* = 6.2 Hz), 128.2, 128.0, 126.1, 32.3(d, *J* = 3.3 Hz), 30.2(d, *J* = 7.7 Hz).$^{31}P\{^1H\}$ NMR:(121 MHz, $CDCl_3$, 298 K) δ -15.0. IR (solid) ν 3055, 2936, 1603, 1585, 1481 cm^{-1}.

(2-([1,1'-Biphenyl]-4-yl)ethyl)diphenylphosphane - Table 9, Entry 2

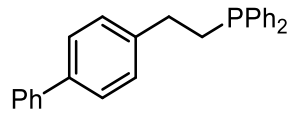

Colourless oil, 152 mg (73%). ^{1}H NMR:(300 MHz, $CDCl_3$, 298 K) δ 7.70 -7.33 (m, 19H), 2.90 -2.85 (m, 2H), 2.55 -2.50 (m, 2H).^{13}C{^{1}H} NMR:(75 MHz, $CDCl_3$, 298 K) δ 141.7 (d, *J* = 13.0 Hz), 141.1, 139.0, 138.5 (d, *J* = 12.4 Hz), 132.7 (d, *J* = 18.6 Hz), 128.7, 128.62, 128.56, 128.50 (d, *J* = 6.5 Hz), 127.2, 127.03, 126.98, 31.9 (d, *J* = 17.7 Hz), 30.2 (d, *J* = 12.4 Hz).^{31}P{^{1}H} NMR:(121 MHz, $CDCl_3$, 298 K) δ −14.9.IR (solid) ν 3050, 2944, 2903, 1586, 1481, 1433, 821, 744, 693 cm^{-1}.

(3-Bromophenethyl)diphenylphosphane - Table 9, Entry 3

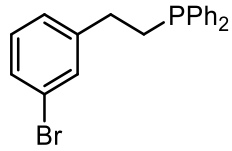

Colourless oil, 193mg (92%). ^{1}H NMR:(300 MHz, $CDCl_3$, 298 K) δ 7.55 -7.52(m, 4H), 7.42-7.36 (m, 8H), 7.18-7.15 (m, 2H), 2.80 -2.72 (m, 2H), 2.44 -2.39 (m, 2H).^{13}C{^{1}H} NMR:(75 MHz, $CDCl_3$, 298 K) δ 144.9 (d, *J* = 13.4 Hz), 138.1 (d, *J* = 12.4Hz), 132.8 (d, *J* = 18.6Hz), 131.2, 130.0, 129.2, 128.8, 128.6 (d, *J* = 6.9Hz), 126.9, 122.5, 31.9 (d, *J* = 18.3Hz), 30.0 (d, *J* = 12.8Hz).^{31}P{^{1}H} NMR:(121 MHz, $CDCl_3$, 298 K) δ −15.2.IR (solid) ν 3057, 2943, 2923, 2830, 1583, 1567,1491,1475, 1464, 1431, 885, 796, 775, 739, 695cm^{-1}.

Butyl 3-(diphenylphosphaneyl)propanoate - Table 9, Entry 4

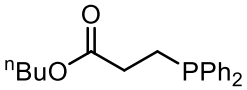

Colourless oil, 167mg (94%). ^{1}H NMR:(300 MHz, $CDCl_3$, 298 K) δ 7.49 -7.46 (m, 4H), 7.37-7.35(m, 6H), 4.08 (t, 2H, *J*= 6.7 Hz), 2.44 -2.39 (m, 4H), 1.61 (app. tt, 2H, *J* = 15.5, 6.7 Hz), 1.37 (app. tq, 2H, *J* = 15.5, 7.4 8Hz),0.95(t, 3H, *J* = 7.4 Hz).^{13}C{^{1}H} NMR:(75 MHz, $CDCl_3$, 298 K) δ 173.3 (d, *J* = 15.2 Hz), 137.8 (d, *J* = 18.6 Hz), 132.8 (d, *J* = 18.6 Hz), 128.9, 128.6 (d, *J* = 6.8Hz), 64.6, 30.9, 30.7, 23.0 (d, *J* = 11.5 Hz), 19.2, 13.8.^{31}P{^{1}H} NMR:(121 MHz, $CDCl_3$, 298 K) δ −14.9. IR (solid) ν 3054, 2958, 2872, 1731, 1586, 1481, 1465, 1433, 1348, 737, 696 cm^{-1}.

Diphenyl(2-phenylpropyl)phosphane - Table 9, Entry 5

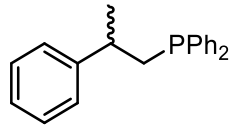

Colourless oil, 85mg (49%). ^{1}H NMR:(300 MHz, $CDCl_3$, 298 K) δ 7.49-7.45 (m, 4 H), 7.38-7.31 (m, 8H), 7.24-7.19 (m, 2H), 2.89-2.80 (m, 1 H), 2.51 (ddd, *J* = 13.7, 8.7, 1.3 Hz, 1 H), 2.38 (dd, *J* = 13.7, 8.7 Hz, 1 H), 1.47 (d, *J* = 6.9 Hz, 3H). ^{31}P{^{1}H} NMR:(121 MHz, $CDCl_3$, 298 K) δ −19.9. Comparable to literature reports.[186]

Compounds synthesised in Chapter 3:

(([DIPP]Nacnac)Fe(CCPh))$_2$ (72):

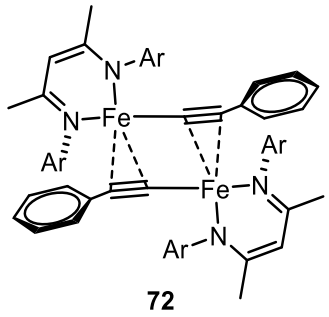

72

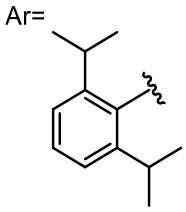

Complex **1** (112 mg, 0.2 mmol) was added to a sealed J-Young Schlenk tube with 2 mL of C_6H_6. Phenylacetylene (22 µL, 0.2mmol) was then added and the solution stirred at room temperature for 24 hrs. Volatiles were then removed *in vacuo* to yield a red solid. The resultant compound was re-dissolved in the minimal amount of a 50:50 mixture of toluene and pentane and left to crystallize at room temperature. After two days large red crystals were isolated by decantation of the eluent (62 mg, 54%). ^{1}H NMR (300 MHz, C_6D_6, 298 K): δ 34.89 (6H, c-CH_3), 28.39 (4H, o/m-Ph), 20.56 (4H, m-Ar), 14.63 (6H, c-CH_3), 12.89 (4H, m-Ar), -4.80 (2H, p-Ph), -10.94 (12H, iPr-CH_3), -12.17 (12H, iPr-CH_3), -13.28 (12H, iPr-CH_3), -23.87 (2H, p-Ar), -25.55 (4H, m-Ar), -66.58 (8H, iPr-C*H*), -70.01 (12H, iPr-CH_3), -85.23 (2H, p-Ar). IR (solid): v 2960, 1591, 1380, 1317, 1206, 1172, 934, 793, 755. Melt pt: 148-150 °C. Reasonable elemental analysis could not be found for this complex. For crystallographic data see page 183.

([DIPP]Nacnac)FeCl(py) (73):

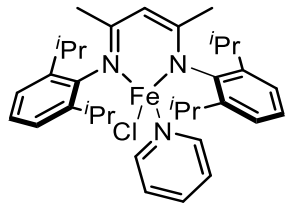

73

To a schlenk containing **1 (**112 mg, 0.2 mmol) DCM was added (2ml) the subsequent solution was heated to 70 °C and stirred for 10 minutes. Stirring was then ceased and the solvent removed *in vacuo*. Pentane was added to the resulting green solid followed by an excess of pyridine. The solution was then cooled to - 35 °C yielding green crystals.Recrystallised from pentane, green crystals, Yield = 31 mg, 26 %,^{1}H NMR (300 MHz, C_6D_6, 298 K): δ 44.36 (1H, p-py-CH), 27.90 (2H, o/m-py-CH), 22.11 (4H, m-Ar), 19.26 (2H, o/m-py-CH), -2.49 (12H, iPr-CH_3), 11.68 (12H, iPr-CH_3), -27.51 (1H, α-CH), -41.56 (2H, p-Ar), -85.70 (6H, c-CH_3) ppm. Melt pt:

165-167 °C, IR (solid): v 2868, 1596, 1435, 1381, 1194, 1166, 1019, 934, 863, 755 cm^{-1}. For crystallographic data see page 184.

Method for the catalytic hydrophosphination reactions

To a sealed Schlenk tube 5 mol% (0.025 mmol) of precatalyst **2** was added in 0.35 mL of benzene or DCM. 1 mmol of Terminal alkyne and 0.5 mmol of phosphine were then added to the reaction vessel and the corresponding solution was stirred at 50 °C for 3 hrs (or otherwise stated). Phosphine products were isolated via flash chromatography (10: 90, DCM : Hexane).

General method for catalytic alkyne hydrophosphination reactions:

Precatalyst **2** (14 mg, 0.025 mmol, 5 mol%) was added to a sealed Schlenk tube in 0.35 mL of benzene or CH_2Cl_2.Terminal alkyne (1 mmol) and $HPPh_2$ (87 µL, 0.5 mmol) were then added to the reaction vessel and the corresponding solution was stirred at 50 °C for 3 hrs (C_6H_6)or at 70 °C for 24 hrs (CH_2Cl_2). For scale up synthesis of Table 2, Entry 1 **2** (140 mg, 0.25 mmol, 5 mol %) was added to a sealed Schlenk tube in 3.5 ml of benzene. Phenyl acetylene(10mmol) and $HPPh_2$(870µl, 5 mmol) were then added to the reaction vessel and the corresponding solution was stirred at 50 °C for 24hrs. The solvent was removed *in vacuo* and purified by column chromatography in air (2% Et_2O in petroleum ether (40-60) on alumina). The product was isolated as a white solid, 1.29 g, 89%.

Method for the isolation of phosphine oxides:

Crude reaction mixtures were exposed to air and worked up on the bench. In reactions where phosphine substrates are not fully consumed the crude mixture was first eluted on silica gel (petroleum ether) to remove the unreacted phosphine, a second fraction was then taken using diethyl ether(Et_2O) as the eluent. Hydrogen peroxide (30% in H_2O) was added to the Et_2O phase and the solution stirred for 5-10 minutes. Stirring was then ceased and the solution quenched with de-ionised water. The layers were then separated and the aqueous layer was washed with diethyl ether 3(2 x 20mL) and the organic layers combined, dried over $MgSO_4$ and filtered. Volatiles were then removed *in vacuo* and products were isolated by flash chromatography on silica gel (Et_2O and petroleum ether (40-60)).

Alkyne hydrophosphination – Markovnikov addition

Diphenyl(1-phenylethenyl)phosphine - Table 11, Entry 1

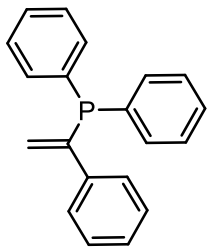

White solid,1.29 g (89%).^{1}H NMR (500 MHz, C_6D_6, 298 K): δ 7.70 (2H, d, J= 7.8 Hz, Ar-H), 7.50-7.47 (4H, m, Ar-H), 7.06-6.95 (9H, m, Ar-H), 5.91 (1H, d, *J* = 12.2, 1.5Hz, PC=CH_{trans}), 5.08 (1H, dd, *J* =5.6, 1.5 Hz, PC=CH_{cis}). $^{13}C\{^1H\}$ NMR (125 MHz, C_6D_6, 298 K): δ 149.9 (d, *J* = 21.9 Hz, P*C*=CH_2), 142.5 (d, *J* = 10.5 Hz, ArCP), 136.5 (ArC), 136.4 (m-ArCH), 135.1 (d, *J* = 20.3 Hz, o-

ArCH), 129.5(o-ArCH), 129.2(d, *J* = 6.7 Hz, p-ArCH), 129.1(p-ArCH), 127.6 (d, *J* = 10.5 Hz, m-ArCH), 124.6 (d, *J* = 4.8 Hz, PC=*C*H_2).$^{31}P\{^1H\}$ NMR (202 MHz, C_6D_6, 298 K): δ - 4.9 ppm. IR (solid) 3062, 3028, 1588, 1478, 1432, 912, 696 cm^{-1}. Melting point: 97-99 °C.

Diphenyl(1-phenylethenyl)phosphine oxide – Table 11, Entry 1

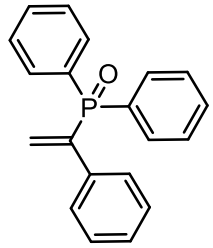

Colorless oil, 122 mg (82%).^1H NMR (300 MHz, $CDCl_3$, 298 K): δ 7.75-7.68 (4H, m, Ar-H), 7.54-7.40 (7H, m, Ar-H), 7.26-7.22 (4H, m, Ar-H), 6.25 (1H, d, *J* = 40.3, 0.9 Hz, PC=CH_{trans}), 5.75 (1H, dd, *J* = 19.8, 0.9 Hz, PC=CH_{cis}).$^{13}C\{^1H\}$ NMR (75 MHz, $CDCl_3$, 298 K): δ 144.3 (d, *J* = 91.9 Hz, P*C*=CH_2), 132.2 (ArC), 132.1 (m-ArCH), 132.0 (d, *J* = 10.4 Hz, PC=*C*H_2), 131.6(d, *J* = 103.2 Hz, ArCP), 128.6 (o-ArCH), 128.5 (d, *J* = 10.8 Hz, o-ArCH), 128.4 (m-ArCH), 128.29 (p-ArCH), 128.1 (d, *J* = 4.7 Hz, p-ArCH). $^{31}P\{^1H\}$ NMR (121 MHz, $CDCl_3$, 298 K): δ 31.2 ppm. IR (solid) 3057, 1437, 1188, 1116, 846, 723, 693 cm-1. HRMS (APCI+): m/z calcd. for $C_{20}H_{18}OP$ 305.1092[M+H]+; found 305.1095.

[1-(3-Methylphenyl)ethenyl](diphenyl)phosphine oxide- Table 11, Entry 2

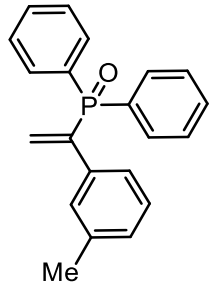

Colourless oil, 105 mg (66%). ^1H NMR (300 MHz, $CDCl_3$, 298 K): δ 7.74-7.67 (4H, m, Ar-H), 7.56-7.41 (7H, m, Ar-H), 7.15-7.04 (3H ,m, Ar-H), 6.23 (1H, d, *J* = 40.3 Hz, PC=CH_{trans}), 5.74 (1H, d, *J* = 19.8 Hz, PC=CH_{cis}) 2.17 (3H, s, CH_3). $^{13}C\{^1H\}$ NMR (75 MHz, $CDCl_3$, 298 K): δ 144.3 (d, *J* = 92.5 Hz, P*C*=CH_2), 138.0 (ArC(CH_3)), 132.0 (d, *J* = 9.6 Hz, m-ArCH), 131.9 (ArC), 131.8 (ArCH), 131.7 (d, *J* = 103.6 Hz, ArCP), 131.3 (d, *J* = 9.8 Hz, PC=*C*H_2),128.9 (ArCH), 128.8 (d, *J* = 4.6 Hz, p-ArCH), 128.4 (d, *J* = 12.0 Hz, o-ArCH), 128.2 (ArCH),125.2 (ArCH),21.4 (Me).$^{31}P\{^1H\}$ NMR(121 MHz, $CDCl_3$, 298 K): δ 31.1 ppm. IR (solid) 3054, 1437, 1116, 1181, 721, 692, 603 cm^{-1}. HRMS (EI+): m/z calcd. for $C_{21}H_{18}OP$ 317.1090 [M-H]+; found 317.1088.

[1-(4-Fluorophenyl)ethenyl](diphenyl)phosphine oxide –Table 11, Entry 3

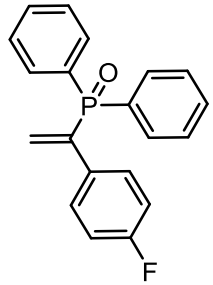

Colorless oil, 113 mg (80%).^{1}H NMR (300 MHz, $CDCl_3$, 298 K): δ 7.67-7.60(5H, m, Ar-H),7.49-7.35(7H, m, Ar-H), 6.87 (2H, dd, *J* = 8.5, 8.7 Hz, Ar-H), 6.22 (1H, d, *J* =39.6Hz, PC=CH_{trans}), 5.61 (1H, d, *J* =19.8 Hz, PC=CH_{cis}).^{13}C{^{1}H} NMR(75 MHz, $CDCl_3$, 298 K): δ 160.4 (d, *J* = 216.6 Hz, ArCF), 143.3 (d, *J* = 92.7Hz, P*C*=CH_2), 132.1 (ArC), 132.0 (d, *J* = 9.8 Hz, m-ArCH), 131.9 (p-ArCH), 131.3 (d, *J* = 118.1 Hz, ArCP), 130.6 (ArCH), 129.9 (d, *J* =8.1 Hz, PC=*C*H_2), 128.6 (d, *J* = 12.2 Hz, o-ArCH), 115.6 (d, *J* = 21.7 Hz, m-ArCH). ^{31}P{^{1}H} NMR (121 MHz, $CDCl_3$, 298 K): δ 31.5ppm. IR (solid) 3056, 1506, 1437, 1158, 1116, 725, 694 cm^{-1}. HRMS (EI+): m/z calcd. for $C_{20}H_{15}FOP$ 321.08939 [M-H]+; found 321.08939.

[1-(4-Methoxyphenyl)ethenyl](diphenyl)phosphine-Table 11, Entry 4

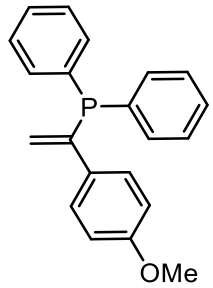

White solid, Yield = 118 mg, 74 %, ^{1}H NMR (300 MHz, C_6D_6, 298 K):δ 7.50(2H, dd, *J* = 8.5, 1.3 Hz, Ar-H), 7.35-7.07 (10H, m, Ar-H), 6.75(2H, dd, *J* = 8.5 Hz, Ar-H), 5.95 (1H, dd, *J* = 12.8 Hz, 0.8Hz, PC=C*H*$_{trans}$), 5.09 (1H, dd, *J* = 5.8Hz, 0.8Hz, PC=C*H*$_{cis}$), 3.68(3H, s, CH_3). ^{13}C{^{1}H} NMR(75 MHz, C_6D_6, 298 K): δ 159.2(ArCOMe),147.7 (d, *J* = 16.1 Hz, P*C*=CH_2),135.5(d, *J* = 9.8Hz, ArCP), 134.3 (d, *J* = 19.8Hz, o-ArCH), 128.9(p-ArCH), 128.5 (d, *J* =7.3 Hz, m-ArCH), 128.0 (d, *J* =11.2 Hz, o-ArCH),123.0 (ArC),122.9 (d, *J* = 4.9Hz, PC=*C*H_2), 113.7 (m-ArCH), 55.2(CH_3). ^{31}P{^{1}H} NMR(121 MHz, C_6D_6, 298 K): δ -4.5 ppm.IR (solid) 3056, 1602, 1509, 1437, 1116, 1176, 725, 693 cm-1. HRMS(EI+): m/z calcd. for $C_{21}H_{18}O_2P$ 333.1039 [M-H]+; found 333.1041.

[(Trimethylsilyl)ethenyl](diphenyl)phosphine- Table 11, Entry 6

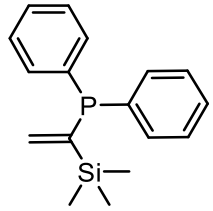

Yellow oil, 85 mg (60%). ^{1}H NMR (300 MHz, $CDCl_3$, 298 K): δ 7.30-7.23 (10H, m, Ar-H), 6.78 (1H, dd, *J* = 20.0, 18.8 Hz, PC=CH_{trans}), 6.28 (1H, dd, *J* = 20.0, 19.0 Hz, PC=CH_{cis}), 0.00 (9H, s, TMS).^{13}C{^{1}H} (75 MHz, C_6D_6, 298 K): δ 145.6 (d, *J* = 19.7 Hz, P*C*=CH_2), 135.9 (d, *J* = 19.8 Hz, ArCP), 134.8 (d, *J* = 18.8 Hz, o-ArCH), 130.0 (p-ArCH), 129.9 (d, *J* = 6.6 Hz, m-ArCH), 129.7 (d, *J* = 7.2 Hz, PC=*C*H_2), 0.0 ($Si(Me)_3$).^{31}P{^{1}H} NMR(121 MHz, C_6D_6, 298 K): δ -4.8. (phosphine oxide) IR (solid) 2865, 1437, 1190, 1119, 881, 729, 693 cm-1. HRMS (EI+): m/z calcd. for $C_{17}H_{20}OPSi$ 299.1016 [M-H]+; found 299.1016.

[(Triisopropylsilyl)ethenyl](diphenyl)phosphine – Table 11, Entry 7

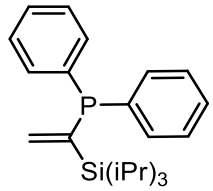

Yellow oil,^{1}H NMR (300 MHz, $CDCl_3$, 298 K): δ 7.35-7.32 (4H, Ar-H, m), 7.27-7.25(6H, Ar-H, m), 6.89(1H, CH-, dd, *J*=20.3 Hz, 17.9Hz), 6.25(1H, CH-, t, *J*= 20.2 Hz, 20.2Hz), 1.04 (3H, $SiCH(Me)_2$, m), 1.02(18H, Me, s) ^{13}C{^{1}H}(175 MHz, $CDCl_3$, 298 K): δ 146.5 (d, *J* = 19.3 Hz, ArCP), 142.9 (d, *J* = 11.8 Hz, ArC_o), 137.9(d, *J* = 10.9 Hz, ArC_p), 133.3(d, *J* = 18.7 Hz, P*C*=CH_2), 128.5(t, *J*= 14.7 Hz, 6.8 Hz, PC=*C*H_2), 18.6(iPr), 10.7(CMe_2). ^{31}P{^{1}H} NMR: (121 MHz, $CDCl_3$, 298 K): δ -3.44 ppm. Phosphine oxide IR (solid) 3058, 1437, 1183, 1118, 840, 728, 694 cm^{-1}

[Diphenylethenyl](diphenyl)phosphine – Table 11, Entry 9

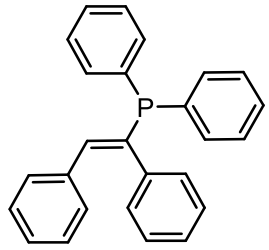

^{1}H NMR (300 MHz, $CDCl_3$, 298 K): δ 7.40 (4H, Ar-H, m), 7.25 (6H , Ar-H, m), 7.09 (5H, Ar-H, m), 7.01 (3H, Ar-H, m), 6.85 (2H, Ar-H, m), 6.42 (1H, C-H, d, *J* = 9.0Hz) ^{13}C{^{1}H}(175 MHz, $CDCl_3$, 298 K): δ 143.1 (d, *J* = 9.7Hz, ArCP), 132.4 (d, *J* = 9.4Hz, P*C*=C), 131.9 (ArC), 131.8 (ArC), 130.3 (ArC), 129.9 (d, *J* = 4.5Hz, PC=*C*), 129.0 (ArC), 128.8 (d, *J* = 1.5 Hz, ArC), 128.4, 128.2 (d, *J*= 1.6 Hz, ArC_{ip}), 127.8. ^{31}P{^{1}H} NMR: (121 MHz, $CDCl_3$, 298 K): δ 9.4 ppm

[1-(4-tert-Butylphenyl)ethenyl](diphenyl)phosphine –Table 11, Entry 13

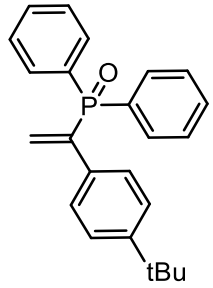

Colorless oil, 128 mg (75%). ^{1}H NMR (300 MHz, $CDCl_3$, 298 K): δ 7.69-7.61 (4H, m, Ar-H), 7.49-7.30 (8H, m, Ar-H), 7.21-7.18 (3H, m, Ar-H), 6.18 (1H, d, *J* = 40.8, 0.9Hz, PC=C*H*$_{trans}$), 5.60 (1H, d, *J* = 20.0, 0.9Hz, PC=C*H*$_{cis}$),1.19(9H, s, $C(CH_3)_3$).^{13}C{^{1}H} (175 MHz, $CDCl_3$, 298 K): δ 151.3 (ArCtBu), 143.8 (d, *J* = 92.4 Hz, P*C*=CH_2), 134.4 (d, *J* = 9.9 Hz, PC=*C*H_2), 132.1 (d, *J* = 9.7 Hz, m-ArCH), 131.9 (d, *J* = 2.8 Hz, o-ArCH), 131.8 (d, *J* = 103.3Hz, ArCP), 131.3 (ArC), 128.5 (d, *J* = 12.1 Hz, o-ArCH), 127.8 (d, *J* = 4.7Hz, p-ArCH),125.4 (o-ArCH), 34.6($C(CH_3)_3$), 31.2 ($C(CH_3)_3$).^{31}P{^{1}H} NMR(121 MHz, $CDCl_3$, 298 K): δ 31.7 ppm. IR (solid) 3058, 1437, 1117, 1071, 798, 727, 692 cm-1. HRMS (APCI+): m/z calcd. for $C_{24}H_{26}OP$ 361.1721 [M+H]+; found 361.1720.

[1-(4-Aminophenyl)ethenyl](diphenyl)phosphine oxide – Table 11, Entry 14

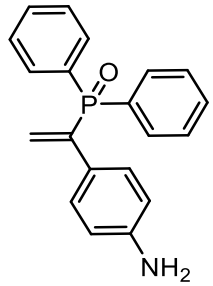

Yellow oil, 89 mg (52%). ^{1}H NMR (300 MHz, $CDCl_3$, 298 K): δ 7.72-7.68 (4H, m, Ar-H), 7.50-7.42 (6H, m, Ar-H), 7.32(2H, d, *J* = 8.3 Hz, Ar-H), 6.54 (2H, d, *J* = 8.3 Hz, Ar-H), 6.15 (1H, d, *J* = 41.4 Hz, PC=C*H*$_{trans}$), 5.55(1H, d, *J* = 20.1Hz, PC=CH_{cis}).^{13}C{^{1}H} (75 MHz, $CDCl_3$, 298 K): δ 148.1 (d, *J* = 108.5 Hz, P*C*=CH_2), 146.5(CNH_2), 132.5 (d, *J* = 9.9 Hz, PC=*C*H_2), 132.0 (d, *J* = 106.8 Hz, ArCP), 131.9 (d, J = 9.6 Hz, m-ArCH), 131.7 (ArCH), 129.5 (ArC), 129.1 (d, *J* = 5.0 Hz, p-ArCH), 128.3 (d, *J* = 12.1 Hz, o-ArCH), 114.8 (m-ArCH).^{31}P{^{1}H} NMR(121 MHz, $CDCl_3$, 298 K): δ 31.5ppm. IR (solid) 3214, 3056, 1607, 1514, 1436, 1172, 1116, 722, 693 cm-1. HRMS(EI+): m/z calcd. for $C_{20}H_{17}NOP$ 318.1042 [M-H]+; found 318.1041.

Phenyl(1-phenylethenyl)phosphine oxide- Table 11, Entry 16

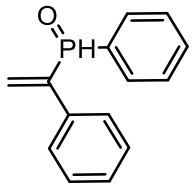

^{1}H NMR (300 MHz, $CDCl_3$, 298 K): δ 7.70-7.63 (2H, m, Ar-H), 7.43-7.42 (4H, m, Ar-H), 7.35 (1H, dd, *J* = 517.0, 16.2 Hz, PH), 7.22-7.19 (5H, m, Ar-H), 6.12 (1H, d, *J* = 46.1, 0.8 Hz, PC=CH_{trans}),5.83 (1H, dd, *J* = 19.8, 0.8Hz, PC=CH_{cis}).^{13}C{^{1}H} (75 MHz, $CDCl_3$, 298 K): 143.4 (d, *J* = 91.7Hz, P*C*=CH_2),132.8 (d, *J* = 97.1 Hz, ArCP), 132.3 (d, *J* = 9.3 Hz, o-ArCH), 132.0 (d, *J* = 7.2 Hz, PC=*C*H_2), 131.8 (ArC), 128.6 (ArCH), 128.4 (o-ArCH), 128.3 (p-ArCH), 128.2 (m-ArCH), 128.1 (d, *J* = 4.6 Hz, m-ArCH).^{31}P{^{1}H} NMR(121 MHz, $CDCl_3$, 298 K): δ 31.3ppm. IR (solid) 3058, 2980, 1438, 754, 694 cm-1. HRMS (EI+): m/z calcd.for $C_{13}H_{14}OP$ 230.0860, [M+2H]+; found 230.0863.

Method for radical clock experiments:

Using the method for catalytic hydrophosphination reactions, the reaction mixture was prepared with phenylacetylene as the alkyne and (chloromethyl)cyclopropane (20 mol %, 0.1 mmol, 18 mg) added to the reaction solution. C_6H_6: the solution was stirred at 50 °C for 3 hrs then analysed by 1H and ^{31}P{^{1}H} NMR. In C_6H_6 $HPPh_2$(-40.0 ppm, ^{31}P{^{1}H} NMR) and *anti*-Markovnikov product is observed (unoxidised species at -23.1 ppm, ^{31}P{^{1}H} NMR).CH_2Cl_2: the reaction mixture was prepared, heated to 70 °C until the reaction had initiated and product (Table 2, Entry 1) had started to form, at which point the radical clock was added. In CH_2Cl_2 only anti-Markovnikov product was observed, the reaction gives complete conversion after 24 hrs.

Alkyne hydrophosphination – *anti*-Markovnikov addition

(*Z*)-Diphenyl(styryl)phosphine oxide- Table 12, Entry 1

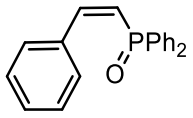

White solid, 125 mg (86%). ^{1}H NMR (300 MHz, $CDCl_3$, 298 K): δ 7.70-7.60 (6H, m, Ar-H), 7.47 (1H, d, J = 40.3, 14.1 Hz, PCH=C*H*), 7.35-7.26 (6H, m, Ar-H), 7.11-7.09 (3H, m, Ar-H), 6.28 (1H, d, *J* = 19.6, 14.1 Hz, PCH=C).^{13}C{^{1}H} (125 MHz, $CDCl_3$, 298 K): δ 149.9 (d, *J* = 1.8 Hz, *C*H=CHP), 134.8 (d, *J* = 7.6 Hz, ArC), 134.0 (d, *J* =105.4 Hz, CH=*C*HP), 131.3 (d, *J* = 3 Hz, o-ArCH), 130.9 (d, *J* = 10.0 Hz, m-ArCH), 130.2 (d, *J* = 1.4 Hz, ArCH), 129.3 (p-ArCH), 128.4(d, *J* = 11.9 Hz, o-ArCH), 128.0 (m-ArCH), 121.8 (d, *J* = 98.2 Hz, ArCP).^{31}P{^{1}H} NMR(121 MHz, $CDCl_3$, 298 K): δ 21.19 ppm. HRMS (APCI+): m/z calcd. for $C_{20}H_{18}OP$ 305.1093 [M+H]+; found 305.1095.

(*Z*)-(3-Methylstyryl)diphenylphosphine oxide-Table 12, Entry 2

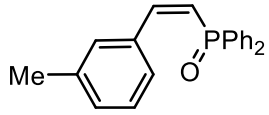

White solid, 89mg (56%). ^{1}H NMR (300 MHz, $CDCl_3$, 298 K): δ 7.68 (3H, ddd, *J* = 12.1, 7.9, 1.5 Hz, Ar-H), 7.50 (1H, dd, *J* = 40.5, 13.9 Hz, PCH=C*H*), 7.40-7.19 (8H, m, Ar-H), 6.98-6.90 (3H, m, Ar-H), 6.20 (1H, dd, *J* = 19.3, 14.1 Hz, PC*H*=C), 2.13 (3H, s, CH_3).^{13}C{^{1}H} (75 MHz, $CDCl_3$, 298 K): δ 150.3 (d, *J* = 1.4 Hz, *C*H=CHP), 137.6 (ArC), 134.7 (d, *J* = 6.8 Hz, ArCH), 133.8 (d, *J* = 105.7 Hz, CH=*C*HP), 131.4 (d, *J* = 2.8 Hz, ArCH), 130.9 (d, *J* = 9.7 Hz, m-ArCH), 130.1 (ArC), 128.4 (d, *J* = 12.1 Hz, o-ArCH), 127.9 (ArCH), 127.1 (d, *J* = 1.2 Hz, ArC), 121.5 (d, *J* = 98.8 Hz, ArCP), 21.2 (CH_3).^{31}P{^{1}H} NMR (121 MHz, $CDCl_3$, 298 K): δ 20.79 ppm. HRMS (APCI+): m/z calcd. for $C_{21}H_{20}OP$ 319.1246 [M+H]+; found 319.1252.

(*Z*)-(4-Methoxystyryl)diphenylphosphine oxide- Table 12, Entry 3

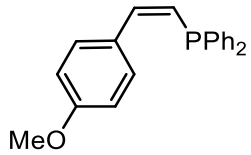

^{1}H NMR (300 MHz, $CDCl_3$, 298 K): δ 7.52-7.41 (6H, Ar-H, m), 7.36-7.27 (7H, Ar-H, m), 6.87(2H, d, *J* = 8.8Hz), 6.35 (1H, CH-, dd, *J* = 12.6Hz, 2.82Hz), 3.70(3H, OMe, s) ^{13}C{^{1}H}(175 MHz, $CDCl_3$, 298 K): δ 160.0 (Ar-OMe), 143.7 (d, *J* = 19.2Hz, *C*H=CP), 139.5 (d, *J* = 9.2Hz, ArCP), 132.8 (d, *J* = 18.8Hz, ArC_oH), 131.1 (d, *J* = 9.1Hz, ArC_mH), 129.8 (ArC), 128.6 (d, *J* = 6.6Hz, ArC_pH) 128.5 (ArCH), 126.8 (d, *J* = 14.8 Hz, CH=*C*P), 114.0 (ArCH), 55.3(CH_3) ^{31}P{^{1}H} NMR: (121 MHz, $CDCl_3$, 298 K): δ -23.80 ppm

(*Z*)-(Trimethylsilyl)diphenylphosphine oxide- Table 12, Entry 5

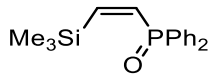

White solid, 83 mg (55%). ^{1}H NMR (300 MHz, $CDCl_3$, 298 K): δ 7.72-7.65 (4H, m, Ar-H), 7.55-7.44 (6H, m, Ar-H), 7.28 (1H, dd, *J* = 29.6, 20.3 Hz, PC*H*=C), 6.70 (1H, dd, *J* = 31.5, 20.3 Hz, PCH=C*H*), 0.16 (9H, s). ^{13}C{^{1}H} (125 MHz, $CDCl_3$, 298 K): δ 155.3 (d, *J* = 5.0 Hz, *C*H=CHP), 143.0 (ArC), 136.8 (d, *J* = 90.6 Hz, ArCP), 132.5 (d, *J* = 102.8 Hz, *C*HP), 131.8 (d, *J* = 2.8 Hz, p-ArCH), 131.4 (d, *J* = 9.7 Hz, m-ArCH), 128.6 (d, *J* = 12.0 Hz, o-ArCH), -1.89 ($Si(Me)_3$). ^{31}P{^{1}H} NMR (121 MHz, $CDCl_3$, 298 K): δ 22.6 ppm.

(*Z*)-(Triisopropylsilyl)diphenylphosphine oxide-Table 12, Entry 6

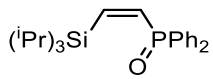

White solid, 169 mg (88%). ^{1}H NMR (500 MHz, $CDCl_3$, 298 K): δ 7.73-7.69 (4H, m, Ar-H), 7.52-7.43 (6H, m, Ar-H), 7.19 (1H, dd, *J* = 34.2, 17.6 Hz, PC*H*=C), 7.00 (1H, dd, *J* = 49.9, 17.6 Hz,

PCH=C*H*), 1.57 (3H, septet, *J* = 7.3 Hz, C*H*(CH_3)$_2$), 1.05 (18H, d, *J* = 7.3 Hz, CH(C*H*$_3$)$_2$). $^{13}C\{^1H\}$ (125 MHz, $CDCl_3$, 298 K): δ 151.7 (d, *J* = 7.6 Hz, *C*H=CHP), 140.0 (d, *J* = 102.0 Hz, ArCP), 134.3 (d, *J* = 102.0 Hz, P*C*=CH_2), 131.4 (d, *J* = 1.9 Hz, p-ArCH), 131.6 (d, *J* = 9.5 Hz, m-ArCH), 128.5 (d, *J* = 11.4 Hz, o-ArCH), 19.2 (*C*H(CH_3)$_2$), 12.7 (CH(*C*H_3)$_2$). $^{31}P\{^1H\}$ NMR (200 MHz, $CDCl_3$, 298 K): δ 18.8 ppm.

(*Z*)-(4-tertButylstyryl)diphenylphosphine oxide- Table 12, Entry 11

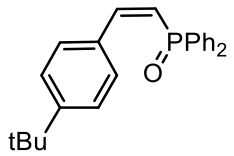

White solid, 78 mg (68%). ^1H NMR (300 MHz, $CDCl_3$, 298 K): δ 7.70-7.63 (4H, ddd, *J* = 12.0, 8.0, 1.5 Hz, Ar-H), 7.52 (2H, d, *J* = 8.5 Hz, Ar-H), 7.35-7.25 (6H, m, Ar-H), 7.11 (2H, d, *J* = 8.5 Hz, Ar-H), 6.22 (1H, d, *J* = 19.9, 14.0 Hz, PC*H*=C), 1.15 (9H, s, C(CH_3)$_3$). $^{13}C\{^1H\}$ (75 MHz, $CDCl_3$, 298 K): δ 152.6 (s, ArC), 149.9 (d, *J* = 1.3 Hz, *C*H=CHP), 134.0 (d, *J* = 105.5 Hz, CH=*C*HP), 132.0 (d, *J* = 7.2 Hz, ArC), 131.4 (d, *J* = 2.9 Hz, p-ArCH), 131.0 (d, *J* = 9.7 Hz, m-ArCH), 130.0 (d, *J* = 1.2 Hz, o-ArCH), 128.4 (d, *J* = 12.1 Hz, o-ArCH), 124.9 (m-ArCH), 120.6 (d, *J* = 99.0 Hz, Ar*C*P), 34.7 (*C*(CH_3)$_3$), 31.1 (C(*C*H_3)$_3$). $^{31}P\{^1H\}$ NMR (121 MHz, $CDCl_3$, 298 K): δ 21.28 ppm. HRMS (APCI+): m/z calcd. for $C_{24}H_{26}OP$ 361.1724 $[M+H]^+$; found 361.1721.

Method for reaction monitoring studies:

Reactions were prepared using phenyl acetylene as the substrate and the appropriate precatalyst using the general method for catalytic hydrophosphination in C_6H_6 or CH_2Cl_2. The Schlenk tube was immersed in an oil bath pre-heated to 50 °C (C_6H_6) or 70 °C (CH_2Cl_2). With the Schlenk tube under an inert atmosphere, aliquots (100 µl) were removed at known time periods, rapidly cooled to room temperature, diluted with C_6D_6 and a ^1H NMR spectrum collected immediately. The % conversion was calculated from the ratio of alkenyl peaks associated with the product in comparison to the quantity of unreacted $HPPh_2$. It should be noted that reactions need to be stirred in order to obtain complete conversion to product and therefore *in situ* NMR monitoring is not possible for this reaction.

Method for AIBN reaction:

Using the method for catalytic hydrophosphination reactions, the reaction mixture was prepared with phenylacetylene as the alkyne and AIBN (20 mol%, 0.1 mmol, 16 mg) added to the reaction solution instead of **1**.

Method for the synthesis of Ligands *SS*-L4 and *RR*-L4

To a solution of 2,4-pentandione (0.65 ml, 6.25 mmol, 1 eq) in Toluene (10 ml) R or S - Ph(Me)$CHNH_2$ (0.75 g , 6.25 mmol, 1 eq) and p-Toluene Sulfonic acid (1.425 g, 6.25 mmol) were added. A Dean-stark condenser was attached and the solution was refluxed for 3 hours. The solution was then allowed to cool to room temperature and a further equivalent of *R* or *S* - Ph(Me)$CHNH_2$ (0.75 g , 6.25 mmol) was added. The solution was then refluxed vigorously (175 °C) for 5 days (Note- vigorous heating is required to remove water from the solution ensuring the reaction goes to completion). The solution was then allowed to cool to room temperature. The resulting suspension was added to a solution of potassium hydroxide (KOH, 0.45 M, 200 ml) and subsequently stirred for 30 minutes. Stirring was then ceased and the phases were separated. The Aqueous phase was extracted with Toluene (2 x 100 ml). The organic phases were combined and dried over Anhydrous Sodium Sulphate. The solution was then filtered and the solvent removed *in vacuo* yielding a brown oil.[187]

***RR*-L4**

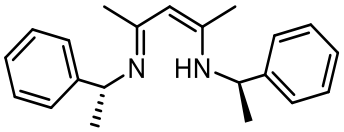

Yield = 1.1 g, 59%, yellow oil.

^{1}H NMR ($CDCl_3$, 300 MHz, 298 K): δ 11.85 (s_{br}, 1H, N*H*); 7.26 – 7.09 (m, 10H, Ar); 4.61 (q, *J* = 7 Hz, 2H, Ph-C*H*-CH_3); 4.42 (s, 1H, α-C*H*); 1.50 (s, 6H, CH_3-C=N); 1.41 (d, *J* = 7 Hz, 6H, Ph-CH-CH_3).
^{13}C {^{1}H} NMR ($CDCl_3$, 75 MHz, 298 K): δ 159.8 (2×*C*=N); 146.9 (2×C_{ip}); 128.4 (4×C_o); 126.4 (2×C_p); 126.2 (4×C_m); 95.2 (α-*C*H); 55.9 (2×Ph-*C*H-CH_3); 25.9 (2×*C*H_3-C=N); 19.6 (2×Ph-CH-*C*H_3).
IR (oil): ν 2969, 1606, 1571, 1354, 1290, 1138, 1018, 743, 698 cm^{-1}.
[α_D] = -123.5 (10^{-3} g/mL toluene).

***SS*-L4**

Yield = 890 mg, 47%, yellow oil.

[α_D] = +123.3 (10^{-3} g/mL toluene).

Method for the synthesis of Ligand *R*-L5

A solution of freshly distilled diisopropylamine (1.40 mL, 10.0 mmol) in dry THF (4 mL) was cooled at -78 °C. To this solution n-BuLi (4.27 mL, 10.0 mmol) was added dropwise over 15 min. The solution was then stirred for 30 min at -78 °C before (*R*)-2-methyl 5-phenyloxazoline (736 mg, 4.54 mmol) dissolved in THF (4 mL) was added. On addition of the oxazoline, a color change from yellow to dark red was observed. The reaction mixture was stirred for 2 h, followed by slow addition (30 min) of 2,2,2-trifluoro-N-p-tolylacetimidoyl chloride (761 mg , 4.54 mmol) dissolved in THF (4 mL). After overnight stirring (14 hrs) the reaction was quenched by addition of saturated aqueous ammonium chloride solution (5 mL) and then allowed to warm to room temperature. The organic phase was separated, and the aqueous

layer was extracted with DCM (3 × 10 mL). The combined organic layers were washed with brine (1 × 10 mL), dried with anhydrous magnesium sulphate and the solvent removed *in vacuo* to give the crude product as a brown oil. The crude product was purified by column chromatography (10% EtOAc: 90% Petroleum ether) and dried under vacuum to yield a pure yellow oil.[138]

[2-((4*R*)-Phenyl-4,5-dihydrooxazol-2-yl)-1-(trifluoro-methyl)vinyl]-*p*-tolyl-amine (*R*-L5)

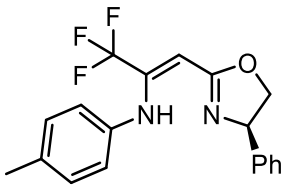

Yield = 341 mg, 33 %, yellow oil.

^{1}H NMR ($CDCl_3$, 300 MHz, 298 K): δ 10.39 (s_{br}, 1H, N*H*); 7.29 – 7.17 (m, 5H, Ar); 7.02 – 6.96 (m, 4H, Ar); 5.29 (s, 1H, α-C*H*); 5.24 (dd, *J* = 9.2, 8.1 Hz, 1H, CH_2-CH-Ph); 4.51 (dd, *J* = 10.1, 8.4 Hz, 1H, CH_2-CH-Ph); 3.95 (t, *J* = 8.3 Hz, 1H, C*H*-Ph); 2.32 (s, 3H, CH_3-Ph). ^{13}C{^{1}H} NMR ($CDCl_3$, 75 MHz, 298 K): δ 165.7 (*C*=N); 143.9 (q, *J* = 34.9 Hz, *C*-CF_3); 142.6 (C_{ip}); 136.4(C_{ip}); 135.9 (C_p); 129.4, 128.7, 127.6 , 126. 5 (2×C_o or 2×C_m); 125.9 (C_p); 120.4 (q, *J* = 250 Hz, *C*F_3); 84.5 (q, *J* = 4.6 Hz, α-*C*H); 73.4 (CH_2-*C*H-Ph); 69.5 (*C*H_2CHPh); 20.9 (*C*H_3-Ph). ^{19}F NMR ($CDCl_3$, 239 MHz, 298 K): δ - 62.79 ppm. IR (oil): ν 2966, 1644, 1558, 1295, 1131, 994, 824, 698 cm^{-1}. [α_D] = -260.0 (10^{-3} g/mL DCM). m.p. = 50-52 °C

Method for the synthesis of *SS*-75 and *RR*-75

The complexes were synthesised utilising the same protocol as **1**.[7]

***RR*-75**

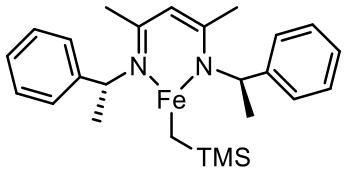

Yield = 650 mg, 44 %, dark yellow oil.

^{1}H NMR (C_6D_6, 300 MHz, 298 K, α-CH not observed[1]): δ 60.94 (s, 6H, C-CH_3); 17.72 (s, 9H, $SiMe_3$); 12.23 (s, Ph-C*H*-CH_3, 2H); - 4.54 (s, 4H, Ar_m); - 13.35 (s, 6H, Ar); - 46.16 (s, 2H, CH_2-TMS); - 54.62 (s, 6H, CH_3).
IR (oil): ν 1627, 1207, 1166, 1019, 907, 758 cm^{-1}.

***SS*-75**

Yield = 360 mg, 25 %, dark yellow oil.

Method for the synthesis of phosphino-alkenes and phosphino-alkynes

Phosphino alkenes (Table 10, Entries 1, 2, 3, and 4) and phosphino alkynes (Table 10, Entries 5 and 6) were synthesised in a two steps procedure from their corresponding phosphonates.

Standard synthesis of alkenyl phosphonates

Method A (for linear alkenyl phosphonates): An excess (1.1 eq., 29.2 mmol, 5 mL) of triethyl phosphite was added to a round bottom flask containing 5-bromo pent-1-ene (26.5 mmol and 3.14 mL), and the resulting neat solution was stirred at 150 °C overnight. Excess phosphite was then removed *in vacuo* to yield a pale yellow oil which was purified by distillation (70-90 °C, 0.1 mBar) to yield the product as a colourless oil.[41, 42]

Method B (for branched alkenyl phosphonates): An excess of n-BuLi (1.2 eq., 48mmol, 20.5 mL of a solution in toluene 2.34M) was added to a solution of diethyl alkyl phosphonate (alkyl = Me (40 mmol, 4.34 mL); Et (40 mmol, 6.49 mL)) in THF at −45 °C. The solution was stirred for 45 minutes and 5-bromo pent-1-ene (40 mmol, 4.73 ml) or 6-bromo hex-1-ene (40 mmol, 5.80 mL), the resulting neat solution was stirred at 150 °C overnight. Excess phosphite was then removed *in vacuo* to yield a yellow-tinged oil, which was purified by distillation (100-120 °C, 0.1 mBar) to yield the product as a colourless oil.

General method for the synthesis of alkynyl phosphonates

The alkynyl phosphonates (precursors to alkynyl phosphines) were synthesised from the corresponding alkynyl bromides.[188] The alkynyl bromides were synthesised by treating a solution of phenylacetylene (30 mmol, 3.29 mL) in THF (in a sealed Schlenk) with n-BuLi at −78 °C followed by dropwise addition of either 1,3-dibromo propane (1 eq, 30 mmol, 3.05 mL) or 1,4-dibromo butane (1 eq, 30 mmol, 3.58 mL). The resulting solution was then allowed to warm to room temperature and stirred overnight. Saturated brine solution was then added dropwise at 0 °C. Stirring was then ceased, the layers were separated and the organic layer washed with dichloromethane (3 x 20mL), dried over $MgSO_4$, filtered and dried *in vacuo* to yield a yellow oil. The yellow oil was purified by column chromatography (10% EtOAc: 90% Petroleum ether) and dried under vacuum to yield a pure colourless oil. The resulting bromides were then reacted with triethyl phosphite in an analogous procedure to that of the alkenyl phosphonate synthesis.[42]

General method for phosphonate reduction. Synthesis of alkenyl and alkynyl phosphines

Phosphino alkenes and phosphino alkynes were synthesised in the same manner. Lithium aluminium hydride ($LiAlH_4$, 2 eq., 9.75 mmol, 370 mg) was added to a Schlenk tube along with 30 mL of ethereal solvent (tetraglyme for volatile phosphines (Table 10, Entries 1, 2, 3, and 4) and diethyl ether for non-volatile phosphines (Table 10, Entries 5 and 6). Then under a purge of nitrogen, aluminium trichloride ($AlCl_3$, 6 eq., 29.25 mmol, 3.90 g) was added generating $AlCl_2H$ *in situ*. Note order of addition is key to generating the active reductant.[41] The phosphonate was then added dropwise and the solution was kept at 0 °C using an ice bath. The solution was allowed to warm to room temperature and stirred for period of 1-14 hours depending on the phosphonate. Volatile phosphines (Table 10, Entries 1, 2, 3, and 4) were then vacuum transferred *via* trap-to-trap distillation before quenching excess of reductant. Solutions in diethyl ether of non-volatile phosphines (Table 10, Entries 5 and 6) were quenched with degassed water and the organic layer was separated, dried over $MgSO_4$

and then the solvent was removed *in vacuo.* The yellowish oil obtained was purified by distillation to yield a pure colourless oil.[41, 42]

Synthesis of secondary phosphino-alkene-pent-4-enylphenylphosphine

Phosphino alkene pent-4-enylphenylphosphine was synthesised in a two steps procedure from the precursor phosphine, pent-4-enyl diphenylphosphine:

(a) Pent-4-enyl diphenylphosphine synthesis

Potassium diphenylphosphide ($KPPh_2$) was generated *in situ* from potassium bis(trimethylsilyl) amide (KHMDS) (10 mmol, 1.99 g) and diphenylphosphine (10 mmol, 1.74 mL) in THF. 5-Bromo-pent-1-ene (14 mmol, 1.2 mL) was then added dropwise. The resulting off-white solution was stirred for 90 minutes and the THF was then removed *in vacuo*. 15mL of pentane were added to the resulting residue followed by addition of 15 mL of degassed water. Stirring was ceased and the organic layer was separated *via* cannula, dried over $MgSO_4$ and filtered *via* cannula. Pentane was then removed *in vacuo* to give a yellow oil. This yellow oil was distilled under vacuum (130 °C, 0.1 mBar) to yield a pure colourless oil.[188]

Pent-4-enyldiphenylphosphine

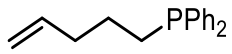

Yield = 2.27g, 83%, colourless oil.^{1}H NMR: (300 MHz, C_6D_6, 298 K): δ7.45–7.41 (m, 4H, Ph,); 7.12–7.04 (m, 6H, Ph,); 5.69–5.56(m, 1H, =C*H*); 4.99–4.90 (m, 2H, =CH_2); 2.05–1.91 (m, 4H, CH_2); 1.57–1.44(m, 2H, CH_2).^{13}C{^{1}H} NMR(C_6D_6, 75 MHz, 298 K): δ 140.2 (d, *J* = 14.0 Hz, 2×*C*ip); 138.8 (=*C*H);133.6 (d, *J* = 18.3 Hz, 4×*C*o); 129.2 (2×*C*p); 129.1 (4×*C*m); 115.8 (=*C*H_2); 35.6 (d, *J* = 13.1 Hz, *C*H_2); 23.4 (d, *J* = 12.6 Hz, *C*H_2); 14.7 (d, *J* = 17.2 Hz, *C*H_2). ^{31}P{^{1}H} NMR(C_6D_6, 121 MHz, 298 K): -15.8 ppm.

(b) Reduction with sodium amide

Liquid ammonia (excess, 40 mL approx.) was condensed at −78 °C into a Schlenk containing chunks of sodium metal (11.8 mmol, 0.70 g). The resulting blue solution was stirred at −78 °C for 1 hour. Then pent-4-enyl diphenylphosphine (5.9 mmol, 1.50 g) was added dropwise and the resulting brown solution was stirred at −50 °C for 3 hours. Solid ammonium chloride (excess, 54 mmol, 0.63 g) was then added carefully under a nitrogen flush. The resulting colourless solution was stirred and allowed to warm to room temperature with ammonia boiling off overnight. The resulting residue was washed with pentane, filtered *via* cannula and the solvent removed *in vacuo* to give a yellow oil. This yellow oil was then distilled under vacuum (90 °C, 0.12 mBar) to yield Pent-4-enylphenylphosphine as a pure colourless oil.[188]

Pent-4-enylphenylphosphine

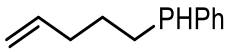

Yield = 578 mg, 51%, colourless oil.^{1}H NMR:(300 MHz, C_6D_6, 298 K) δ 7.40–7.35 (m, 2H, Ph); 7.09–7.04 (m, 3H, Ph); 5.64–5.55 (m, 1H, =*C*H); 4.97–4.90 (m, 2H, =C*H*$_2$); 4.08 (dm, *J* = 205 Hz, 1H, P*H*); 1.93–1.85(m, 2H, C*H*$_2$); 1.65 –1.52 (m, 2H, C*H*$_2$); 1.48 –1.35(m, 2*H*).^{13}C{^{1}H} NMR: (75 MHz, C_6D_6, 298 K): δ 138.6 (=C*H*); 134.3 (d, J= 15.5 Hz, *C*ip);129.0 (d, J= 5.7Hz, 2×*C*o), 128.6 (2×*C*m); 128.5(*C*p); 115.5 (=*C*H$_2$); 35.5 (d, *J* = 8.4 Hz, *C*H$_2$); 28.1 (d, J= 8.5 Hz, *C*H$_2$); 23.4 (d, *J* = 11.3 Hz, *C*H$_2$).^{31}P{^{1}H} NMR: (121 MHz, C_6D_6, 298 K): δ -51.4ppm.

General method for intramolecular hydrophosphination reactions

To a sealed J-youngs NMR tube 10 mol% (0.025 mmol) of precatalyst **1** or **60** was added in 0.35 mL of benzene. 0.25 mmol of phosphine was then added to the reaction vessel and the corresponding solution was heated at 90 °C for 16 hrs (or otherwise stated). To obtain spectroscopic yield and/or isolated yield the reaction mixture was passed through a short silica plug, eluting with DCM. The solution was charged with a known quantity of 1,3,5-trimethoxybenzene, concentrated then an NMR sample prepared using C_6D_6. This isolation method was necessary to remove the paramagnetic component from the reaction mixture, allowing analysis by ^{1}H NMR. Phospholane and phosphinane products (Table 19, Entries 1-4) were isolated by trap to trap distillation or via flash chromatography (10 % DCM : 90 % Pentane) depending on volatility.

(2S)-2-Methyl-1-phenylphospholane (Major) and (2R)-2-Methyl-1-phenylphospholane (Minor) -Table 19, Entry 7

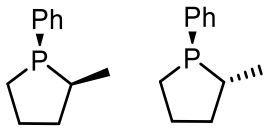

Spectroscopic yield: 100%; Isolated yield: 44% ^{1}H NMR (300 MHz, C_6D_6, 298 K, only major isomer observable): δ 7.40 –7.53 (m, 2H, Ph); 7.11 –7.04 (m, 3H, Ph); 2.19 –2.09(m, 1H); 1.81 –1.78 (m, 3H); 1.62–1.60 (m, 1H); 1.57 –1.52 (m, 1H); 1.23 (dd, 18.9 Hz, 7.4 Hz, 3H); 1.11–1.08 (m, 1H). ^{31}P{^{1}H} NMR: (121 MHz, C_6D_6): δ 1.8ppm (major, 62%), -6.2 ppm (minor, 38%). HR-MS (NSI)([M+H]): 179.0990(calcd.), 179.0987(obs.)

Compounds synthesised in Chapter 4:

(^{DIPP}Nacnac)FeNMeBn (78):

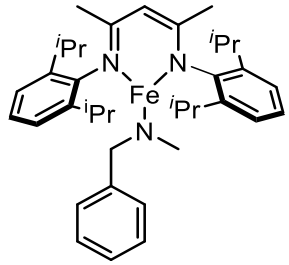

78

Complex **1** (112 mg, 0.2 mmol) was added to a sealed J-Young Schlenk tube with 2 mL of C_6H_6. N-methylbenzylamine (22 µL, 0.2mmol) was then added and the solution stirred at 60 °C for 18 hrs. Volatiles were then removed *in vacuo* to yield a brown solid, Yield = 78 mg, 52%, ^{1}H NMR (300 MHz, C_6D_6, 298 K): δ 116.9 (1H, α-CH), 88.6 (2H, (NR)- *o*-CH), 34.8 (2H, (NR)-*m*-CH), 27.2 (1H, (NR)-*p*-CH), 7.3 (6H, $(CH_3)_2$-L), -12.9 (4H, *m*-CH), -19.9 (12H, *i*Pr-CH_3), -81.0 (2H, *p*-CH), -122.0 (16H, *i*Pr-CH_3, *i*Pr-CH). UV/Vis (toluene): 375 nm (7300 $M^{-1}cm^{-1}$), 422 nm (2200 $M^{-1}cm^{-1}$), 485 nm (513 $M^{-1}cm^{-1}$) IR (solid) v 2926, 1459, 1262, 1206, 1172, 933, 849, 793, 732 cm^{-1}.[109]

(^{DIPP}Nacnac)FeOCHPh$_2$ (80)

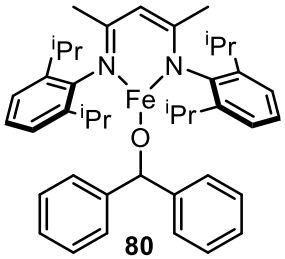

80

In a glovebox complex **1** (112 mg, 0.2 mmol) was added to a sealed J-Young Schlenk tube with 2 mL of C_6H_6. The tube was then removed from the glovebox and transferred onto a schlenk line. Diphenylmethanol (37 mg, 0.2mmol) was then added and the solution stirred at 60 °C for 18 hrs. Volatiles were then removed *in vacuo* to yield a green solid, Yield = 46 mg, 35%, ^{1}H NMR (300 MHz, C_6D_6, 298 K): δ 111.14 (1H, R-CH), 109.19 (4H, (OR)-o-CH), 51.12 (6H, $(CH_3)_2$-L), 28.85 (4H, (OR)-m-CH), 21.36 (2H, (OR)-p-CH), -16.44 (4H, L(Ar)-m-CH), -23.41 (12H, iPr-CH_3), -74.96 (2H, L(Ar)-p-CH), -120.23 (16H, iPr-CH_3, iPr-CH). UV/Vis (toluene): 489 nm (548 M^{-1}cm-1). Melt pt: 160-162 °C[109]

General method for catalytic dehydrocoupling reactions:

To a sealed Schlenk tube 5 mol% (15 mg, 0.025 mmol) of precatalyst **1** was added in 0.35 mL of benzene. 0.5 mmol silane and 0.5 mmol of phosphine/amine/alcohol were then added to the reaction vessel and the corresponding solution was stirred at RT for 24 hrs (or otherwise stated).

Phosphine silane dehydrocoupling:

Silaphosphanes synthesised are in accordance with literature reports.[80]

Diphenyl(phenylsilyl)phosphane - Table 21, Entry 1

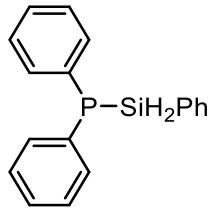

^{1}H NMR (300 MHz, C_6D_6, 298 K): δ 7.57-7.35 (9H, m, *ortho*-Si*Ph, meta*-Si*Ph, para*-Si*Ph, meta*-P*Ph*$_2$), 7.12-6.87 (6H, m, *para*-P*Ph*$_2$, *ortho*-P*Ph*$_2$), 4.88 (2H, d, *J* = 19.8Hz, H_2Si). ^{13}C{^{1}H}(75 MHz, C_6D_6, 298 K): δ 135.9 (d, *J* = 2.2Hz, *ortho*-Si*Ph*), 134.6 (d, *J* = 16.2 Hz, *ipso*-Si*Ph*), 133.9 (d, *J* = 17.4 Hz, *ipso*-P*Ph*$_2$), 130.0 (*para*-Si*Ph*), 128.6 (d, *J* = 6.6 Hz, *meta*-P*Ph*$_2$), 128.0 (d, *J* = 8.0 Hz , *ortho*-P*Ph*$_2$) 127.8 (d, *J* = 2.4 Hz, *para*-P*Ph*$_2$), 127.6 (*para*-Si*Ph*).^{31}P{^{1}H} NMR: (121 MHz, C_6D_6, 298 K): δ -71.0 ppm, ^{29}Si{^{1}H} (99 MHz,C_6D_6, 298 K): -32.0 (d, *J* = 31.8 Hz) ppm. [80]

Dicyclohexyl(phenylsilyl)phosphane - Table 21, Entry 2

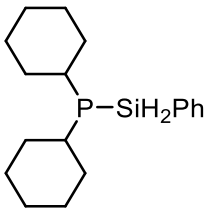

^{1}H NMR (300 MHz, C_6D_6, 298 K): δ 7.66 (2H, m, *ortho*-Si*Ph*), 7.12-7.09 (3H, m, *meta*-Si*Ph*, *para*-Si*Ph*), 4.78 (2H, d, *J* = 15.2Hz, H_2Si), 1.93-1.09 (20H, m, Cy-H).^{13}C{^{1}H}(75 MHz, C_6D_6, 298 K): δ 136.0 (d, *J* = 3.2 Hz, *ortho*-Si*Ph*), 131.7 (d, *J* = 11.5Hz, *ipso*-Si*Ph*), 129.5 (*para*-Si*Ph*), 128.0 (*meta*-Si*Ph*), 32.6 (d, *J* = 8.6 Hz, *ortho*-P*Cy*$_2$), 31.1 (d, *J* = 15.9 Hz, *ipso*-P*Cy*$_2$), 27.4 (*para*-P*Cy*$_2$), 26.3 (*meta*-P*Cy*$_2$).^{31}P{^{1}H} NMR: (121 MHz, C_6D_6, 298 K): δ -63.8 ppm ^{29}Si{^{1}H} (99 MHz, C_6D_6, 298 K): -39.2 (d, *J* = 42.7 Hz) ppm. [80]

(Diphenylsilyl)diphenylphosphane - Table 21, Entry 3

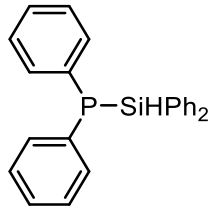

^{1}H NMR (300 MHz, C_6D_6, 298 K): δ 7.53-7.34 (6H, m, *ortho*-Si*Ph*$_2$, *para*-Si*Ph*$_2$), 7.11-6.93 (14H, m, *meta*-Si*Ph*$_2$, *meta*-P*Ph*$_2$, *para*-P*Ph*$_2$, *ortho*-P*Ph*$_2$), 5.18 (1H, d, *J* = 14.4 Hz, SiH).^{13}C{^{1}H}(75 MHz, C_6D_6, 298 K): δ 135.9 (d, *J* = 3.2 Hz, *ortho*-Si*Ph*$_2$), 134.4 (d, *J* = 17.4 Hz, *ipso*-Si*Ph*$_2$), 132.4

(d, *J* = 11.8 Hz, *ipso*-P*Ph*$_2$), 129.9 (*para*-Si*Ph*$_2$), 128.4 (d, *J* = 6.8 Hz, *ortho*-PPh$_2$), 128.2 (*meta*-P*Ph*$_2$), 128.0 (*meta*-Si*Ph*$_2$), 127.8 (*para*-P*Ph*$_2$). $^{31}P\{^1H\}$ NMR: (121 MHz, C_6D_6, 298 K): δ -66.3 ppm. $^{29}Si\{^1H\}$ (99 MHz, C_6D_6, 298 K): -13.8 (d, *J* = 29.0 Hz) ppm. [80]

Dicyclohexyl(diphenylsilyl)phosphane - Table 21, Entry 4

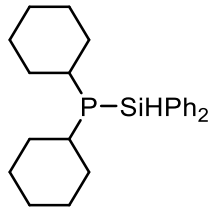

^1H NMR (300 MHz, C_6D_6, 298 K): δ 7.85-7.70 (2H, m, *para*-Si*Ph*$_2$), 7.24-7.96 (8H, m, *ortho*-Si*Ph*$_2$, *meta*-Si*Ph*$_2$), 5.02 (1H, d, *J* = 10.4 Hz, SiH), 1.91-1.49 (10H, m, Cy-H), 1.35-1.03 (10H, m, Cy-H).$^{13}C\{^1H\}$ (75 MHz, C_6D_6, 298 K): δ 135.9 (d, *J* = 3.6 Hz, *ortho*-Si*Ph*$_2$), 129.5 (d, *J* = 10.8 Hz, *ipso*-Si*Ph*$_2$), 128.2 (*para*-Si*Ph*$_2$), 128.0 (*meta*-Si*Ph*$_2$), 33.5 (d, *J* = 9.8 Hz, *ortho*-P*Cy*$_2$), 31.2 (d, *J* = 15.9 Hz, *ipso*-P*Cy*$_2$), 27.5 (*para*-P*Cy*$_2$), 26.3 (*meta*-P*Cy*$_2$).$^{31}P\{^1H\}$ NMR: (121 MHz, C_6D_6, 298 K): δ -61.1 ppm. $^{29}Si\{^1H\}$ (99 MHz, C_6D_6, 298 K): -16.8 (d, J_{SiP}= 38.6 Hz) ppm. [80]

(Methyl(phenyl)silyl)diphenylphosphane - Table 21, Entry 5

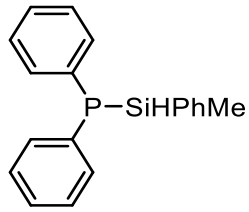

^1H NMR (300 MHz, C_6D_6, 298 K): δ 7.49-7.40 (6H, m, *ortho*-Si*Ph*Me, *para*-Si*Ph*Me), 7.04-6.94 (9H, m, *meta*-Si*Ph*Me, *meta*-P*Ph*$_2$, *para*-P*Ph*$_2$, *ortho*-P*Ph*$_2$), 5.02 (1H, dd, *J* = 20.2 Hz, 3.0 Hz, SiH), 0.29 (3H, $SiCH_3$).$^{13}C\{^1H\}$(75 MHz, C_6D_6, 298 K): δ 135.1 (d, *J* = 2.8 Hz, *ortho*-Si*Ph*Me), 134.4 (d, *J* = 17.8 Hz, *ipso*-P*Ph*$_2$), 133.7 (d, *J* = 16.9 Hz, *ipso*-Si*Ph*Me), 129.7 (*para*-Si*Ph*Me), 128.5 (dd, *J* = 15.0 Hz, 6.7 Hz, *ortho*-P*Ph*$_2$), 128.3 (*meta*-P*Ph*$_2$), 128.0 (*para*-P*Ph*$_2$), 127.7 (*meta*-Si*Ph*Me), -6.3 (SiPh*Me*).$^{31}P\{^1H\}$ NMR: (121 MHz, C_6D_6, 298 K): δ -64.7 ppm. $^{29}Si\{^1H\}$ (99 MHz, C_6D_6, 298 K): -14.7 (d, *J* = 26.4 Hz) ppm.

Dicyclohexyl(methyl(phenyl)silyl)phosphane - Table 21, Entry 6

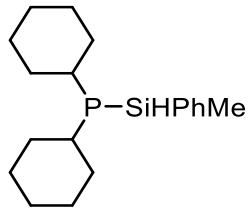

^1H NMR (300 MHz, C_6D_6, 298 K): δ 7.62 (2H, m, *ortho*-Si*Ph*Me), 7.11 (3H, m, *para*-Si*Ph*Me, *meta*-Si*Ph*Me), 4.90 (1H, d, *J* = 14.7 Hz, SiH), 1.81-1.59 (11H, m, Cy-H), 1.28-1.00 (9H, m, Cy-H), 0.49 (3H, $SiCH_3$).$^{13}C\{^1H\}$(75 MHz, C_6D_6, 298 K): δ 136.1 (d, *J* = 10.3 Hz, *ipso*-Si*Ph*Me), 135.0 (d, *J* = 5.8 Hz, *ortho*-Si*Ph*Me), 129.2 (*meta*-Si*Ph*Me), 127.6 (*para*-Si*Ph*Me), 33.0 (dd, *J*= 7.7 Hz, 7.3 Hz, *meta*-P*Cy*$_2$), 32.7 (dd, *J*= 29.6 Hz, 13.1 Hz, *ortho*-P*Cy*$_2$) 31.1 (dd, *J* = 43.0 Hz, 16.2 Hz,

ipso-P*Cy*$_2$), 27.6 (q, *J* = 7.7 Hz, 7.3 Hz, *meta*-P*Cy*$_2$), 26.4 (d, *J* = 5.7 Hz, *para*-P*Cy*$_2$), -4.4 (SiPh*Me*). $^{31}P\{^1H\}$ NMR: (121 MHz, C_6D_6, 298 K): δ -58.9 ppm.$^{29}Si\{^1H\}$ (99 MHz, C_6D_6, 298 K): -19.0 (d, *J* = 36.8 Hz) ppm.

Amine silane dehydrocoupling:

Silazanes synthesised are in accordance with literature reports.[84, 86, 89]

N-benzyl-1,1-diphenylsilanamine - Table 23, Entry 1

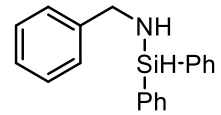

^1H NMR (500 MHz, C_6D_6, 298 K): δ 7.59 (4H, m, *ortho*-Si*Ph*$_2$), 7.12-7.06 (11H, m, *meta*-Si*Ph*$_2$, *para*-Si*Ph*$_2$, *meta*-NMeCH$_2$*Ph*, *para*-NMeCH$_2$*Ph, ortho*-NMeCH$_2$*Ph*), 5.55 (1H, s, SiH), 3.98 (1H, s, NH), 3.83 (2H, s, ArCH$_2$).$^{13}C\{^1H\}$ NMR (125 MHz, C_6D_6, 298 K): δ 143.3 (*ipso*-NHCH$_2$*Ph*), 135.0 (*ipso*-Si*Ph*$_2$), 129.9 (*ortho*-Si*Ph*$_2$), 128.2 (*meta*-NHCH$_2$*Ph*), 128.0 (*para*-Si*Ph*$_2$), 127.0 (*meta*-Si*Ph*$_2$), 126.5 (*ortho*-NHCH$_2$*Ph*), 126.4 (*para*-NHCH$_2$*Ph*), 47.0 (Ar*C*N).$^{29}Si\{^1H\}$ NMR (99 MHz, C_6D_6, 298 K): δ -17.1 ppm.

N-butyl-1,1-diphenylsilanamine - Table 23, Entry 2

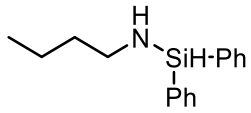

^1H NMR (500 MHz, C_6D_6, 298 K): δ 7.65 (4H, m, *ortho*-Si*Ph*$_2$), 7.17-7.11 (7H, m, *meta*-Si*Ph*$_2$, *para*-Si*Ph*$_2$), 5.56 (1H, s, SiH), 2.70 (2H, s, NHC*H*$_2$CH$_2$CH$_2$CH$_3$), 1.24 (2H, s, NHCH$_2$C*H*$_2$CH$_2$CH$_3$), 1.12 (2H, m, NHCH$_2$CH$_2$C*H*$_2$CH$_3$) 0.74 (3H, m, NHCH$_2$CH$_2$CH$_2$C*H*$_3$), 0.68 (1H, bs, NH).$^{13}C\{^1H\}$ NMR (125 MHz, C_6D_6, 298 K): δ 135.8 (*ipso*-Si*Ph*$_2$), 134.9 (*ortho*-Si*Ph*$_2$), 129.7 (*meta*-Si*Ph*$_2$), 128.2 (*para*-Si*Ph*$_2$), 42.5 (N*C*H$_2$CH$_2$CH$_2$CH$_3$), 36.4 (NCH$_2$*C*H$_2$CH$_2$CH$_3$), 19.7 (NCH$_2$CH$_2$*C*H$_2$CH$_3$), 13.7 (NCH$_2$CH$_2$CH$_2$*C*H$_3$).$^{29}Si\{^1H\}$ NMR (99 MHz, C_6D_6, 298 K): δ -17.9 ppm.

N,1,1-triphenylsilanamine - Table 23, Entry 3

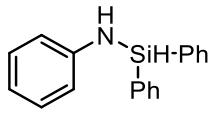

^1H NMR (500 MHz, C_6D_6, 298 K): δ 7.58 (4H, m, *ortho*-Si*Ph*$_2$), 7.12 (6H, m, *meta*-Si*Ph*$_2$, *para*-Si*Ph*$_2$), 6.95 (2H, m, *meta*-NH*Ph*) 6.61 (3H, m, *para*-NH*Ph, ortho*-NH*Ph,*), 5.75 (1H, s, SiH), 3.48 (1H, s, NH).$^{13}C\{^1H\}$ NMR (125 MHz, C_6D_6, 298 K): δ 146.6 (*ipso*-NH*Ph*), 135.0 (*ortho*-Si*Ph*$_2$), 133.3 (*ipso*-Si*Ph*$_2$), 130.3 (*meta*-NH*Ph*), 129.2 (*meta*-Si*Ph*$_2$), 128.2 (*para*-Si*Ph*$_2$), 118.8 (*para*-NH*Ph*), 116.6 (*ortho*-NH*Ph*). $^{29}Si\{^1H\}$ NMR (99 MHz, C_6D_6, 298 K): δ -23.9 ppm.

1,1-Diphenyl-N-propylsilanamine - Table 23, Entry 5

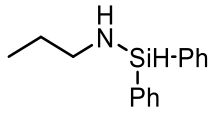

^{1}H NMR (500 MHz, C_6D_6, 298 K): δ 7.64-7.57 (4H, m, *ortho*-Si*Ph*$_2$), 7.17-7.12 (6H, m, *meta*-Si*Ph*$_2$, *para*-Si*Ph*$_2$), 5.56 (1H, s, SiH), 2.65 (2H, m, NHC*H*$_2$CH$_2$CH$_3$), 1.26 (2H, m, NHCH$_2$C*H*$_2$CH$_3$), 0.91 (1H, bs, NH), 0.69 (3H, m, NHC*H*$_2$CH$_2$C*H*$_3$).^{13}C{^{1}H} NMR (125 MHz, C_6D_6, 298 K): δ 135.8 (*ipso*-Si*Ph*$_2$), 134.9 (*ortho*-Si*Ph*$_2$), 129.8 (*meta*-Si*Ph*$_2$), 127.8 (*para*-Si*Ph*$_2$), 44.8 (N*C*H$_2$CH$_2$CH$_3$), 22.3 (NCH$_2$*C*H$_2$CH$_3$), 11.1 (NCH$_2$CH$_2$*C*H$_3$) .^{29}Si{^{1}H} NMR (99 MHz, C_6D_6, 298 K): δ -17.7 ppm.

N-benzyl-1-methyl-1-phenylsilanamine (Major) and N,N'-dibenzyl-1-methyl-1-phenylsilanediamine (Minor) - Table 23, Entry 6

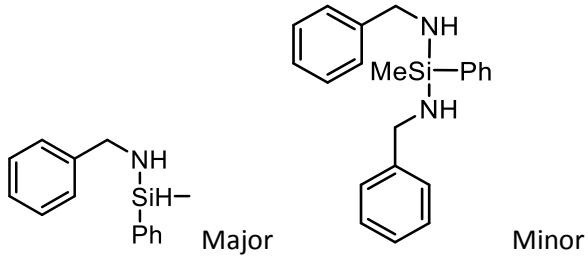

Major Minor

^{1}H NMR (500 MHz, C_6D_6, 298 K): *Major:* δ 7.62-7.56 (2H, m, *ortho*-Si*Ph*Me), 7.18-7.08 (8H, m, *meta*-Si*Ph*Me, *para*-Si*Ph*Me*, meta*-NMe*Ph, para*-NMe*Ph, ortho*-NMe*Ph*), 5.11 (1H, s, SiH), 3.87 (2H, m, ArCH$_2$), 1.12 (1H, s, NH), 0.23 (3H, s, CH$_3$). *Minor:* δ 7.68-7.51 (2H, m, *ortho*-Si*Ph*Me), 7.21-7.05 (13H, m, *meta*-Si*Ph*Me, *para*-Si*Ph*Me*, meta*-NMe*Ph, para*-NMe*Ph, ortho*-NMe*Ph*), 3.75 (4H, m, ArCH$_2$), 0.95 (2H, s, NH), 0.21 (3H, s, CH$_3$).^{13}C{^{1}H} NMR (125 MHz, C_6D_6, 298 K): *Major:* δ 144.1 (*ipso*-NHCH$_2$*Ph*), 137.3 (*ipso*-Si*Ph*), 134.1 (*ortho*-Si*Ph*), 129.6 (*para*-Si*Ph*Me), 128.2 (*meta*-NHCH$_2$*Ph*), 127.7 (*meta*-Si*Ph*Me), 127.0 (*ortho*-NHCH$_2$Ph), 126.3 (*para*-NHCH$_2$*Ph*), 45.4 (NH*C*H$_2$Ph), -3.2 (SiMe). *Minor:* δ 143.5 (*ipso*-NHCH$_2$*Ph*), 138.5 (*ipso*-Si*Ph*Me), 134.1 (*ortho*-Si*Ph*Me), 129.3 (*para*-Si*Ph*Me), 128.2 (*meta*-NHCH$_2$*Ph*), 127.8 (*meta*-Si*Ph*Me), 127.0 (*ortho*-NHCH$_2$Ph), 126.4 (*para*-NHCH$_2$*Ph*), 46.7 (Ar*C*H$_2$N), -2.8 (Si*Me*).^{29}Si{^{1}H} NMR (99 MHz, C_6D_6, 298 K): δ -12.9 ppm (Major) –15.6 ppm (Minor).

N-butyl-1-methyl-1-phenylsilanamine - Table 23, Entry 7

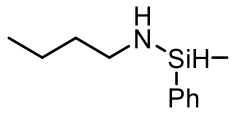

^{1}H NMR (500 MHz, C_6D_6, 298 K): δ 7.57 (2H, m, *ortho*-Si*Ph*Me), 7.18-7.12 (3H, m, *meta*-Si*Ph*Me, *para*-Si*Ph*Me), 5.07 (1H, s, SiH), 2.64 (2H, m, NHC*H*$_2$CH$_2$CH$_2$CH$_3$), 1.23-1.15 (4H, m, NHCH$_2$C*H*$_2$CH$_2$CH$_3$, NHCH$_2$CH$_2$C*H*$_2$CH$_3$), 0.78 (3H, s, NHCH$_2$CH$_2$CH$_2$C*H*$_3$), 0.34 (1H, bs, NH), 0.25 (3H, s, SiC*H*$_3$).^{13}C{^{1}H} NMR (125 MHz, C_6D_6, 298 K): δ 137.9 (*ipso*-Si*Ph*Me), 134.0 (*ortho*-Si*Ph*Me), 129.4 (*para*-Si*Ph*Me), 127.8 (*meta*-Si*Ph*Me), 42.3 (N*C*H$_2$CH$_2$CH$_2$CH$_3$), 36.5 (N*C*H$_2$CH$_2$CH$_2$CH$_3$), 19.8 (N*C*H$_2$CH$_2$CH$_2$CH$_3$), 13.8 (NCH$_2$CH$_2$CH$_2$CH$_3$), -3.0 (Si*Me*).^{29}Si{^{1}H} NMR (99 MHz, C_6D_6, 298 K): δ -14.2 ppm.

1-Methyl-N,1-diphenylsilanamine - Table 23, Entry 8

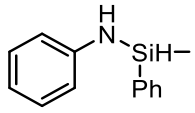

^{1}H NMR (500 MHz, C_6D_6, 298 K): δ 7.51 (2H, m, *ortho*-Si*Ph*Me), 7.14-6.99 (5H, m, *meta*-Si*Ph*Me, *para*-Si*Ph*Me, *meta*-NH*Ph*), 6.59 (3H, m, *para*-NHPh, *ortho*-NHPh), 5.20 (1H, s, SiH), 3.21 (1H, s, NH), 0.26 (3H, s, CH_3).^{13}C{^{1}H} NMR (125 MHz, C_6D_6, 298 K): δ 147.8 (*ipso*-NH*Ph*), 135.5 (*ipso*-Si*Ph*Me), 134.0 (*ortho*-Si*Ph*Me), 130.0 (*meta*-Si*Ph*Me), 129.2 (*meta*-NH*Ph*), 129.1 (*para*-Si*Ph*Me), 118.4 (*para*-NH*Ph*), 116.3 (*ortho*-NH*Ph*), -3.7 (Si*Me*). ^{29}Si{^{1}H} NMR (99 MHz, C_6D_6, 298 K): δ -19.1 ppm.

1-Methyl-1-phenyl-N-propylsilanamine (Major) and 1-Methyl-1-phenyl-N,N'-dipropylsilanediamine (Minor) - Table 23, Entry 10

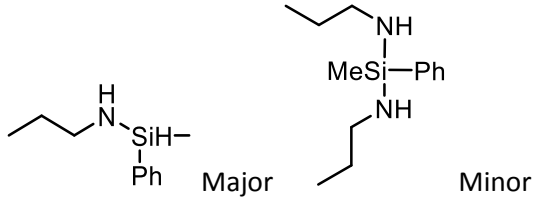

^{1}H NMR (500 MHz, C_6D_6, 298 K):*Major*: δ 7.68-7.46 (2H, m, *ortho*-Si*Ph*Me), 7.12-7.03 (3H, m, *meta*-Si*Ph*Me, *para*-Si*Ph*Me), 5.08 (1H, s, SiH), 2.60 (2H, m, NHCH_2CH$_2$CH$_3$), 1.63 (2H, m, NHCH_2CH$_2$CH$_3$), 1.12 (3H, m, NHCH_2CH$_2$CH$_3$), 0.70 (1H, bs, 1H), 0.24 (3H, s, SiCH_3). *Minor*: δ 7.68-7.46 (2H, m, *ortho*-Si*Ph*), 7.12-7.03 (3H, m, *meta*-Si*Ph*Me, *para*-Si*Ph*Me), 3.20-2.96 (4H, m, NHCH_2CH$_2$CH$_3$), 1.52 (4H, m, NHCH$_2$CH_2CH$_3$), 1.17 (6H, m, NHCH$_2$CH$_2$CH_3), 0.78 (2H, bs, NH), 0.30 (3H, s, SiCH_3).^{13}C{^{1}H} NMR (125 MHz, C_6D_6, 298 K): *Major:* δ 141.8 (*ipso*-Si*Ph*Me), 134.0 (*ortho*-Si*Ph*Me), 129.6 (*para*-Si*Ph*Me), 127.0 (*meta*-Si*Ph*Me), 28.2 (NHCH_2CH$_2$CH$_3$), 24.1 (NHCH$_2$CH_2CH$_3$), 23.1 (NHCH$_2$CH$_2$CH_3), -3.1 (Si*Me*). *Minor:* δ 140.8 (*ipso*-Si*Ph*Me), 134.8 (*ortho*-Si*Ph*Me), 129.9 (*para*-Si*Ph*Me), 127.2 (*meta*-Si*Ph*Me), 28.0 (NHCH_2CH$_2$CH$_3$), 23.4 (NHCH$_2$CH_2CH$_3$), 22.8 (NHCH$_2$CH$_2$CH_3), -3.1 (Si*Me*).^{29}Si{^{1}H} NMR (99 MHz, C_6D_6, 298 K): δ –13.3 ppm (Major) -15.6 ppm (Minor)

N-(2,2-diphenylhexyl)-1-methyl-1-phenylsilanamine - Table 23, Entry 11

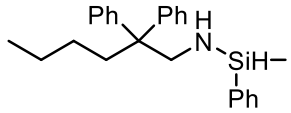

^{1}H NMR (500 MHz, C_6D_6, 298 K): δ 7.47 (2H, m, *ortho*-Si*Ph*), 7.15-7.02 (13H, m, *meta*-Si*Ph*, *para*-Si*Ph*, *ortho*-C*Ph*$_2$, *meta*-C*Ph*$_2$, *para*-C*Ph*$_2$), 4.93 (1H, s, SiH), 3.39 (2H, s, CH_2NH), 2.07 (2H, s, Ph$_2$CCH_2CH$_2$), 1.14 (2H, s, CH_2CH$_2$CH$_3$), 0.88 (2H, s, CH_2CH$_3$), 0.70 (3H, s, CH$_2$CH_3), 0.3 (1H, s, NH), 0.1 (3H, CH$_3$).^{13}C{^{1}H} NMR (125 MHz, C_6D_6, 298 K): δ 147.3 (*ipso*-C*Ph*$_2$), 147.2 (*ipso*-Si*Ph*), 137.7 (*para*-Si*Ph*), 134.0 (*ortho*-Si*Ph*), 129.6 (*meta*-Si*Ph*), 128.3 (*ortho*-C*Ph*$_2$), 127.9 (*meta*-C*Ph*$_2$), 125.8 (*para*-C*Ph*$_2$), 51.8 (NHCH_2C(Ph$_2$)CH$_2$CH$_2$CH$_2$CH$_3$), 49.6(NHCH$_2$C(Ph$_2$)CH$_2$CH$_2$CH$_2$CH$_3$), 35.9 (NHCH$_2$C(Ph$_2$)CH_2CH$_2$CH$_2$CH$_3$), 26.4 (NHCH$_2$C(Ph$_2$)CH$_2$CH_2CH$_2$CH$_3$), 23.5 (NHCH$_2$C(Ph$_2$)CH$_2$CH$_2$CH_2CH$_3$), 14.1 (NHCH$_2$C(Ph$_2$)CH$_2$CH$_2$CH$_2$CH_3), -3.1 (Si*Me*).^{29}Si{^{1}H} NMR (99 MHz, C_6D_6, 298 K): δ –12.4 ppm.

1-Methyl-1-phenyl-N-((1-propylcyclohexyl)methyl)silanamine - Table 23, Entry 12

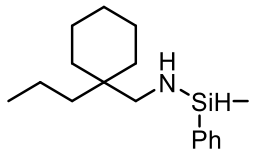

^{1}H NMR (500 MHz, C_6D_6, 298 K): δ 7.60-7.50 (2H, m, *ortho*-Si*Ph*Me), 7.20 – 7.12 (3H, m, *meta*-Si*Ph*Me, *para*-Si*Ph*Me), 5.33 (1H, s, SiH), 2.57 (1H, s, NH), 1.94 (2H, m, NHC*H*$_2$C(Cy)CH$_2$CH$_2$CH$_3$), 1.59-0.87 (14H, m, Cy-H, NHCH$_2$C(Cy)C*H*$_2$CH$_2$CH$_3$, NHCH$_2$C(Cy)CH$_2$C*H*$_2$CH$_3$), 0.3 (3H, s, CH$_3$). ^{13}C{^{1}H} NMR (125 MHz, C_6D_6, 298 K): δ 138.0 (*ipso*-Si*Ph*Me), 134.1 (*ortho*-Si*Ph*Me), 129.4 (*meta*-Si*Ph*Me), 124.2 (*para*-Si*Ph*Me), 41.4 (*C*H$_2$NH), 36.9 (*C*CH$_2$NH), 33.8 (*C*CH$_2$CH$_2$CH$_3$), 33.7 (*ortho*-*C*H$_2$), 26.7 (*para*-*C*H$_2$), 22.2 (*meta*-*C*H$_2$), 21.7 (*C*CH$_2$CH$_2$CH$_3$), 18.3 (CCH$_2$*C*H$_2$CH$_3$), 15.0 (CCH$_2$CH$_2$*C*H$_3$), -2.9 (Si*Me*). ^{29}Si{^{1}H} NMR (99 MHz, C_6D_6, 298 K): δ – 11.4 ppm.

N,N'-dibenzyl-1-phenylsilanediamine (Major) and N-benzyl-1-phenylsilanamine (Minor) - Table 23, Entry 17

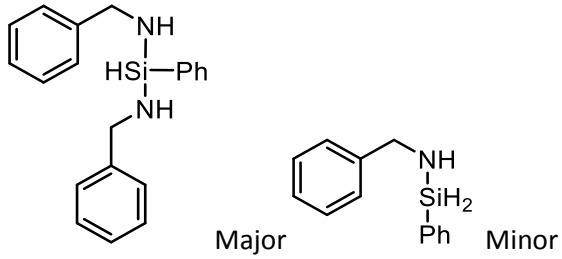

^{1}H NMR (500 MHz, C_6D_6, 298 K): *Major:* δ 7.65-7.58 (2H, m, *ortho*-Si*Ph*), 7.18-7.04 (13H, m, *meta*-Si*Ph*, *para*-Si*Ph, ortho*-NHCH$_2$*Ph*, *meta*-NHCH$_2$*Ph*, *para*-NHCH$_2$*Ph*), 5.19 (1H, s, SiH), 3.93 (4H, s, ArCH$_2$), 1.06 (2H, bs, NH). *Minor:* δ 7.58-7.46 (2H, m, *ortho*-Si*Ph*), 7.04 (8H, m, *meta*-Si*Ph*, *para*-Si*Ph, ortho*-NHCH$_2$*Ph*, *meta*-NHCH$_2$*Ph*, *para*-NHCH$_2$*Ph*), 5.46 (2H, m, SiH$_2$), 3.82 (2H, s, ArCH$_2$), 1.12 (1H, bs, NH). ^{13}C{^{1}H} NMR (125 MHz, C_6D_6, 298 K): *Major*: δ 144.2 (*ipso*-NH*Ph*), 137.2 (*ipso*-Si*Ph*), 134.3 (*ortho*-Si*Ph*), 129.3 (*para*-Si*Ph*), 128.2 (*meta*-NH*Ph*), 128.0 (*meta*-Si*Ph*), 126.9 (*ortho*-NH*Ph*), 126.3 (*para*-NH*Ph*), 45.4 (Ar*C*H$_2$NH). *Minor:* δ 143.7 (*ipso*-NH*Ph*), 136.0 (*ipso*-Si*Ph*), 134.5 (*ortho*-Si*Ph*), 129.8 (*para*-Si*Ph*), 128.1 (*meta*-Si*Ph*), 127.0 (*ortho*-NH*Ph*), 126.4 (*para*-NH*Ph*), 46.1 (Ar*C*H$_2$NH). One resonance obscured by C_6D_6 solvent. ^{29}Si{^{1}H} NMR (99 MHz, C_6D_6, 298 K): δ – 33.2 ppm (Major) – 25.5 ppm (Minor).

N,N',1-triphenylsilanediamine - Table 23, Entry 19

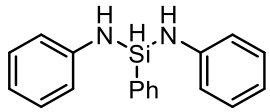

^{1}H NMR (500 MHz, C_6D_6, 298 K): δ 7.61 (2H, m, *ortho*-Si*Ph*), 7.12 (4H, m, *meta*-NH*Ph*), 7.00 (3H, m, *meta*-Si*Ph*, *para*-Si*Ph*), 6.66 (6H, m, *ortho*-NHPh, *para*-NHPh), 5.59 (1H, s, SiH), 3.47 (2H, s, NH). ^{13}C{^{1}H} NMR (125 MHz, C_6D_6, 298 K): δ 145.8 (*ipso*-NH*Ph*), 134.5 (*ortho*-Si*Ph*), 133.1 (*ipso*-Si*Ph*), 130.7 (*meta*-Si*Ph*), 129.3 (*meta*-NH*Ph*), 128.3(*para*-Si*Ph*), 119.2 (*para*-NH*Ph*), 116.8 (*ortho*-NH*Ph*). ^{29}Si{^{1}H} NMR (99 MHz, C_6D_6, 298 K): δ -35.0 ppm.

1-Phenyl-N-propylsilanamine (Major) and 1-Phenyl-N,N'-dipropylsilanediamine (Minor) - Table 23, Entry 20

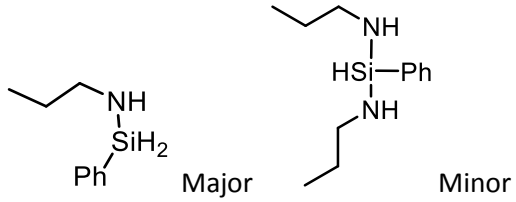

^{1}H NMR (500 MHz, C_6D_6, 298 K): *Major:* δ 7.66-7.58 (2H, m, *ortho*-Si*Ph*), 7.18-7.13 (3H, m, *meta*-Si*Ph*, *para*-Si*Ph*), 4.36 (2H, s, SiH_2), 2.74 (2H, m, $NHC\mathit{H_2}CH_2CH_3$), 1.75 (1H, bs, NH), 1.30 (2H, m, $NHCH_2C\mathit{H_2}CH_3$), 0.76 (3H, s, $NHCH_2CH_2C\mathit{H_3}$). *Minor:* δ 7.66-7.58 (2H, m, *ortho*-Si*Ph*), 7.18-7.13 (3H, m, *meta*-Si*Ph*, *para*-Si*Ph*), 5.10 (1H, m, SiH), 2.52 (4H, m, $NHC\mathit{H_2}CH_2CH_3$), 1.70 (2H, bs, NH), 1.25 (4H, m, $NHCH_2C\mathit{H_2}CH_3$), 0.70 (6H, s, $NHCH_2CH_2C\mathit{H_3}$). ^{13}C{^{1}H} NMR (125 MHz, C_6D_6, 298 K, only major product observable): *Major:* δ 134.8 (*ipso*-Si*Ph*), 134.3 (*ortho*-Si*Ph*), 129.7 (*para*-Si*Ph*), 128.2 (*meta*-Si*Ph*), 43.6 ($NC\mathit{H_2}CH_2CH_3$), 27.7 ($NCH_2\mathit{C}H_2CH_3$), 11.3 ($NCH_2CH_2\mathit{C}H_3$).^{29}Si{^{1}H} NMR (99 MHz, C_6D_6, 298 K): δ -26.3 ppm (Major) -29.1 ppm (Minor).

N-(2-methoxyphenyl)-1-methyl-1-phenylsilanamine - Table 23, Entry 26

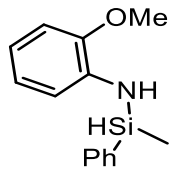

^{1}H NMR (500 MHz, C_6D_6, 298 K): δ 7.56 (2H, m, *ortho*-Si*Ph*Me), 7.13 (3H, m, *meta*-Si*Ph*Me, *para*-Si*Ph*Me), 6.86-6.52 (4H, m, NH*Ph*OMe), 5.31 (1H, s, SiH), 4.41 (1H, s, NH), 3.29 (3H, s, OCH_3), 0.3 (3H, s, CH_3).^{13}C{^{1}H} NMR (125 MHz, C_6D_6, 298 K): δ 150.2 (*ortho*-NH*Ph*OMe), 139.2 (*ipso*-Si*Ph*Me), 138.1 (*ipso*-NH*Ph*OMe), 136.3 (*para*-Si*Ph*Me), 132.2 (*ortho*-Si*Ph*Me), 128.0 (*meta*-Si*Ph*Me), 123.7 (*meta*-NH*Ph*OMe), 120.4 (*para*-NH*Ph*OMe), 117.4 (*ortho*-NH*Ph*OMe), 112.7 (*meta*-NH*Ph*OMe), 57.1 ($NHPhOC\mathit{H_3}$), -1.1 (Si*Me*).^{29}Si{^{1}H} NMR (99 MHz, C_6D_6, 298 K): δ -16.5 ppm.

1-Methyl-1-phenyl-N-(p-tolyl)silanamine - Table 23, Entry 27

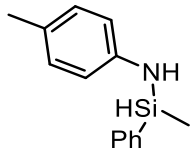

^{1}H NMR (500 MHz, C_6D_6, 298 K): δ 7.53 (2H, m, *ortho*-Si*Ph*Me), 7.15 (3H, m, *meta*-Si*Ph*Me, *para*-Si*Ph*Me), 6.81 (2H, m, *ortho*-NH*Tol*), 6.55 (2H, m, *meta*-NH*Tol*), 5.26 (1H, s, SiH), 3.20 (1H, s, NH), 2.06 (3H, s, $ArCH_3$), 0.3 (3H, s, CH_3).^{13}C{^{1}H} NMR (125 MHz, C_6D_6, 298 K): δ 144.2 (ipso-NH*Tol*), 135.6 (*ipso*-Si*Ph*Me), 133.8 (*ortho*-Si*Ph*Me), 129.9 (*meta*-Si*Ph*Me), 129.6 (*meta*-NH*Tol*), 127.5 (*para*-Si*Ph*Me), 127.0 (*para*-NH*Tol*), 116.2 (*ortho*-NH*Tol*), 20.7 ($ArC\mathit{H_3}$), -3.8 (Si*Me*).^{29}Si{^{1}H} NMR (99 MHz, C_6D_6, 298 K): δ – 19.4 ppm.

N-benzyl-N-methyl-1,1-diphenylsilanamine - Table 24, Entry 1

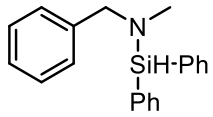

^{1}H NMR (500 MHz, C_6D_6, 298 K): δ 7.64 (4H, m, *ortho*-Si*Ph*$_2$), 7.16-7.07 (11H, m, *meta*-Si*Ph*$_2$, *para*-Si*Ph*$_2$, *ortho*-NMeCH$_2$*Ph*, *meta*-NMeCH$_2$*Ph*, *para*-NMeCH$_2$*Ph*), 5.64 (1H, s, SiH), 3.94 (2H, s, ArCH$_2$), 2.39 (3H, s, CH$_3$).^{13}C{^{1}H} NMR (125 MHz, C_6D_6, 298 K): δ 140.4 (*ipso*-NMeCH$_2$*Ph*), 135.2 (*ipso*-Si*Ph*$_2$), 135.0 (*ortho*-Si*Ph*$_2$), 129.9 (*meta*-NMeCH$_2$*Ph*), 128.3 (*ortho*-NMeCH$_2$*Ph*), 128.2 (*para*-Si*Ph*$_2$), 128.0 (meta-Si*Ph*$_2$), 126.7 (*para*-NMeCH$_2$*Ph*), 55.5 (Ar*C*N), 35.0 (N*Me*).^{29}Si{^{1}H} NMR (99 MHz, C_6D_6, 298 K): δ -10.9 ppm.

4-(Diphenylsilyl)morpholine - Table 24, Entry 3

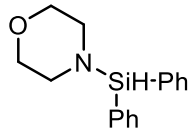

^{1}H NMR (500 MHz, C_6D_6, 298 K): δ 7.55 (4H, m, *ortho*-Si*Ph*$_2$) 7.18-7.11 (6H, m, *meta*-Si*Ph*$_2$, *para*-Si*Ph*$_2$) 5.38 (1H, s, SiH) 3.36 (4H, s, OCH$_2$) 2.78 (4H, s, NCH$_2$).^{13}C{^{1}H} NMR (125 MHz, C_6D_6, 298 K): δ 135.2 (*ortho*-Si*Ph*$_2$), 134.4 (*ipso*-Si*Ph*$_2$), 130.0 (*para*-Si*Ph*$_2$), 128.1 (*meta*-Si*Ph*$_2$), 68.3 (O*C*H$_2$), 46.7 (N*C*H$_2$).^{29}Si{^{1}H} NMR (99 MHz, C_6D_6, 298 K): δ -13.3 ppm.

N-benzyl-N,1-dimethyl-1-phenylsilanamine - Table 24, Entry 4

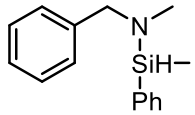

^{1}H NMR (500 MHz, C_6D_6, 298 K): δ 7.56 (2H, m, *ortho*-Si*Ph*Me), 7.22-7.10 (8H, m, *meta*-Si*Ph*Me, *para*-Si*Ph*Me*, meta*-NMe*Ph, para*-NMe*Ph, ortho*-NMe*Ph*), 5.17 (1H, s, SiH), 3.85 (2H, s, ArCH$_2$), 2.33 (3H, s, CH$_3$), 0.36 (3H, s, CH$_3$).^{13}C{^{1}H} NMR (125 MHz, C_6D_6, 298 K): δ 140.6 (*ipso*-NMe*Ph*), 137.3 (*ipso*-Si*Ph*Me), 134.4 (*ortho*-Si*Ph*Me), 133.4 (*para*-Si*Ph*Me), 129.9 (*para*-NMe*Ph*), 129.5 (*meta*-NMe*Ph*), 128.2 (*meta*-Si*Ph*Me), 126.6 (*ortho*-NMe*Ph*), 55.4 (Ar*C*H$_2$NCH$_3$), 34.9 (N*C*H$_3$), -3.6 (Si*Me*). ^{29}Si{^{1}H} NMR (99 MHz, C_6D_6, 298 K): δ -7.3 ppm.

4-(Methyl(phenyl)silyl)morpholine - Table 24, Entry 7

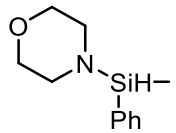

^{1}H NMR (500 MHz, C_6D_6, 298 K): δ 7.48 (2H, m, *ortho*-Si*Ph*Me), 7.20 (3H, m, *meta*-Si*Ph*Me, *para*-Si*Ph*Me), 4.89 (1H, s, SiH), 3.33 (4H, s, OCH$_2$), 2.67 (4H, s, NCH$_2$), 0.22 (3H, s, CH$_3$).^{13}C{^{1}H} NMR (125 MHz, C_6D_6, 298 K): δ 136.6 (*ipso*-Si*Ph*Me), 134.2 (*ortho*-Si*Ph*Me), 129.7 (*para*-Si*Ph*Me), 128.0 (meta-Si*Ph*Me), 68.2 (O*C*H$_2$), 46.4 (N*C*H$_2$), -4.1 (Si*Me*).^{29}Si{^{1}H} NMR (99 MHz, C_6D_6, 298 K): δ -9.6 ppm.

N,N'-dibenzyl-N,N'-dimethyl-1-phenylsilanediamine (Major) and N-benzyl-N-methyl-1-phenylsilanamine (Minor) - Table 24, Entry 9

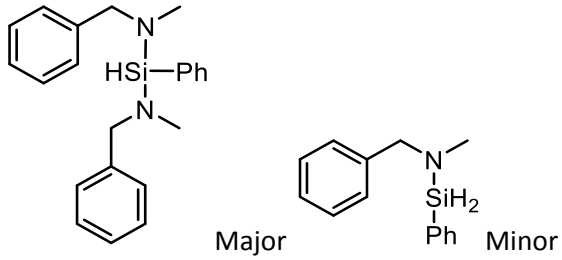

^{1}H NMR (500 MHz, C_6D_6, 298 K): *Major:* δ 7.68-7.57 (2H, m, *ortho*-Si*Ph*), 7.22-7.06 (13H, m, *meta*-Si*Ph*, *para*-Si*Ph, ortho*-NMeCH$_2$*Ph*, *meta*-NMeCH$_2$*Ph*, *para*-NMeCH$_2$*Ph*), 5.33 (1H, s, SiH), 3.97 (2H, s, ArCH$_2$), 2.42 (3H, s, CH$_3$). *Minor:* δ 7.57 (2H, m, *ortho*-Si*Ph*), 7.06 (8H, m, *meta*-Si*Ph*, *para*-Si*Ph, ortho*-NMeCH$_2$*Ph*, *meta*-NMeCH$_2$*Ph*, *para*-NMeCH$_2$*Ph*), 5.17 (2H, s, SiH$_2$), 3.83 (2H, s, ArCH$_2$), 2.31 (3H, s, CH$_3$).^{13}C{^{1}H} NMR (125 MHz, C_6D_6, 298 K): *Major:* δ 140.6 (*ipso*-NMeCH$_2$*Ph*), 135.7 (*ipso*-Si*Ph*), 134.7 (*ortho*-Si*Ph*), 134.3 (*para*-Si*Ph*), 129.8 (*meta*-Si*Ph*), 128.2 (*meta*-NMeCH$_2$*Ph*), 127.8 (*ortho*-NMeCH$_2$*Ph*), 126.6 (*para*-NMeCH$_2$*Ph*), 54.3 (Ph*C*H$_2$NMe), 34.0 (N*Me*). *Minor:* δ 140.5 (*ipso*-NMeCH$_2$*Ph*), 135.7 (*ipso*-Si*Ph*), 134.8 (*ortho*-Si*Ph*), 134.4 (*para*-Si*Ph*), 129.9 (*meta*-Si*Ph*), 128.1 (*meta*-NMeCH$_2$*Ph*), 127.8 (*ortho*-NMeCH$_2$*Ph*), 126.7 (*para*-NMeCH$_2$*Ph*), 56.1 (Ph*C*H$_2$NMe), 35.5 (N*Me*). ^{29}Si{^{1}H} NMR (99 MHz, C_6D_6, 298 K): δ -14.7 (major), -20.4 (minor) ppm.

4,4'-(Phenylsilanediyl)dimorpholine (Major) and 4-(Phenylsilyl)morpholine (Minor) - Table 24, Entry 10

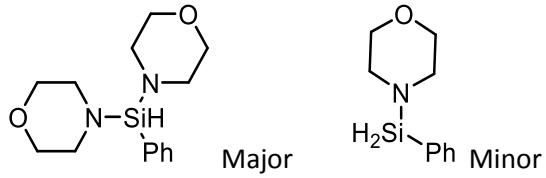

^{1}H NMR (500 MHz, C_6D_6, 298 K): *Major:* δ 7.52 (2H, m, *ortho*-Si*Ph*), 7.20-7.17 (3H, m, *meta*-Si*Ph*, *para*-Si*Ph*) 4.86 (1H, s, SiH), 3.40 (8H, s, OCH$_2$), 2.79 (8H, s, NCH$_2$). *Minor:* δ 7.35-7.34 (2H, m, *ortho*-Si*Ph*) 7.05-7.02 (3H, m, *meta*-Si*Ph*, *para*-Si*Ph*), 4.94 (2H, s, SiH$_2$), 3.34 (4H, s, OCH$_2$), 2.68 (4H, s, NCH$_2$).^{13}C{^{1}H} NMR (125 MHz, C_6D_6, 298 K): *Major:* δ 134.7 (*ipso*-Si*Ph*), 134.6 (*ortho*-Si*Ph*), 129.9 (*para*-Si*Ph*), 128.0 (*meta*-Si*Ph*), 68.2 (O*C*H$_2$), 45.7 (N*C*H$_2$). *Minor:* δ 135.7 (*ipso*-Si*Ph*), 134.8 (*ortho*-Si*Ph*), 130.9 (*para*-Si*Ph*), 128.0 (*meta*-Si*Ph*), 68.0 (O*C*H$_2$), 47.0 (N*C*H$_2$).^{29}Si{^{1}H} NMR (99 MHz, C_6D_6, 298 K): δ -20.4 ppm (Major) -23.0 ppm (Minor).

N-butyl-N,1-dimethyl-1-phenylsilanamine - Table 24, Entry 13

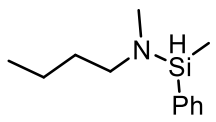

^{1}H NMR (500 MHz, C_6D_6, 298 K): δ 7.53-7.33 (2H, m, *ortho*-Si*Ph*Me), 7.18-6.95 (3H, m, *meta*-Si*Ph*Me, *para*-Si*Ph*Me) 5.05 (1H, s, SiH), 2.71 (2H, s, CH$_3$NC*H*$_2$CH$_2$CH$_2$CH$_3$), 2.41 (3H, s, C*H*$_3$NCH$_2$CH$_2$CH$_2$CH$_3$), 1.34 (2H, s, CH$_3$NCH$_2$CH$_2$C*H*$_2$CH$_3$), 1.14 (2H, s, CH$_3$NCH$_2$CH$_2$C*H*$_2$CH$_3$), 0.79 (3H, s, CH$_3$NCH$_2$CH$_2$CH$_2$C*H*$_3$), 0.3 (3H, s, SiCH$_3$). ^{13}C{^{1}H} NMR (125 MHz, C_6D_6, 298 K): δ 141.9 (*ipso*-Si*Ph*Me), 138.6 (*ortho*-Si*Ph*Me), 133.9 (*meta*-Si*Ph*Me), 122.7 (*para*-Si*Ph*Me), 55.3

($CH_3NCH_2CH_2CH_2CH_3$), 39.4 ($CH_3NCH_2CH_2CH_2CH_3$), 35.6 ($CH_3NCH_2CH_2CH_2CH_3$), 24.3 ($CH_3NCH_2CH_2CH_2CH_3$), 18.1 ($CH_3NCH_2CH_2CH_2CH_3$), 0.9 (Si*Me*). $^{29}Si\{^1H\}$ NMR (99 MHz, C_6D_6, 298 K): δ −4.26 ppm.

Alcohol silane dehydrocoupling:

Products synthesised were in accordance with literature reports.[156, 157] For spectral analysis the reaction mixtures were exposed to air then filtered through a plug of silica for the removal of iron content.

(Benzyloxy)(methyl)(phenyl)silane - Table 25, Entry 1

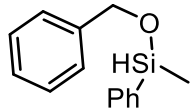

^1H NMR (500 MHz, C_6D_6, 298 K): δ 7.71 – 7.70 (2H, d, *J* = 6.5 Hz, Ar-H), 7.55-7.37 (5H, m, Ar-H), 7.29-7.25 (2H, m, Ar-H), 7.13 (1H, m, Ar-H), 4.88 (1H, s, SiH), 4.83 (2H, m, OCH_2Ph), 0.44 (3H, s, SiH*Me*). $^{13}C\{^1H\}$ NMR (125 MHz, C_6D_6, 298 K): δ 142.4 (*ipso*-OCH_2Ph), 140.4 (*ipso*-Si*Ph*Me), 134.1 (*ortho*-Si*Ph*Me), 130.2 (*para*-Si*Ph*Me), 128.3 (*meta*-OCH_2Ph), 127.9 (*meta*-Si*Ph*Me), 127.2 (*para*-OCH_2Ph), 126.6 (*meta*-OCH_2Ph), 64.8 (OCH_2Ph), -4.1 (Si*Me*). $^{29}Si\{^1H\}$ NMR (99 MHz, C_6D_6, 298 K): δ -15.8 ppm.

***tert*-Butoxy(methyl)(phenyl)silane- Table 25, Entry 3**

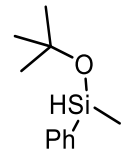

^1H NMR (500 MHz, C_6D_6, 298 K): δ 7.63 (2H, m, *ortho*-Si*Ph*Me), 7.43 (3H, m, *para*-Si*Ph*Me, *meta*-Si*Ph*Me), 5.17 (1H, s, SiH), 1.02 (9H, m, $OCH_2CH_2CH_3$), 0.37 (3H, s, Si*Me*). $^{13}C\{^1H\}$ NMR (125 MHz, C_6D_6, 298 K): δ 138.1 (*ipso*-Si*Ph*Me), 133.8(*ortho*-Si*Ph*Me), 129.6 (*para*-Si*Ph*Me), 123.1 (*meta*-Si*Ph*Me), 77.2 ($OC(CH_3)_3$), 31.2 ($OC(CH_3)_3$), 0.28 (Si*Me*). $^{29}Si\{^1H\}$ NMR (99 MHz, C_6D_6, 298 K): δ -15.5 ppm.

Methyl(phenyl)(propoxy)silane - Table 25, Entry 4

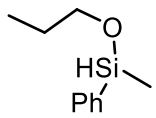

^1H NMR (500 MHz, C_6D_6, 298 K): δ 7.75 (1H, d, *J* = 7.2 Hz, *para*-Si*Ph*Me) 7.41 (2H, d, *J* = 7.4 Hz, *ortho*-Si*Ph*Me), 7.21 (2H, d, *J* = 7.2 Hz, *meta*-Si*Ph*Me), 4.44 (1H, s, SiH), 3.63 (2H, t, *J* = 6.5 Hz ,$OCH_2CH_2CH_3$), 1.52 (2H, quart, *J* = 6.9 Hz, $OCH_2CH_2CH_3$), 0.83 (3H, t, *J* = 7.4 Hz, $OCH_2CH_2CH_3$), 0.37 (3H, s, Si*Me*). $^{13}C\{^1H\}$ NMR (125 MHz, C_6D_6, 298 K): δ 134.74 (ipso-*Ph*), 134.12 (ortho-*Ph*), 129.80 (para-*Ph*), 129.40 (meta-*Ph*), 64.23 ($OCH_2CH_2CH_3$), 25.78

($OCH_2CH_2CH_3$), 10.13 ($OCH_2CH_2CH_3$), -4.36(Si*Me*). $^{29}Si\{^1H\}$ NMR (99 MHz, C_6D_6, 298 K): δ -17.84 ppm.

2-((Methyl(phenyl)silyl)oxy)-1-phenylethan-1-amine - Table 25, Entry 5

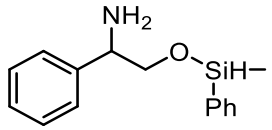

^1H NMR (500 Hz, C_6D_6, 298 K): δ 8.21 (1H, m, Ar-H), 7.91-7.73 (9H, m, Ar-H), 4.61 (1H, s, SiH), 4.37-4.25 (2H, m, OCH_2CHNH_2), 1.94 (2H, bs, NH_2), 1.78 (1H, m, OCH_2CHNH_2), 0.83 (3H, s, $SiCH_3$). $^{13}C\{^1H\}$ NMR (125 MHz, C_6D_6, 298 K): δ 142.4 (*ipso*-NH_2CH_2Ph), 133.6 (*ipso*-Si*Ph*Me), 128.3 (*ortho*-NH_2CH_2Ph), 127.8 (*ortho*-Si*Ph*Me), 127.3 (*para*-NH_2CH_2Ph), 126.8 (*para*-Si*Ph*Me), 125.1 (*meta*-Si*Ph*), 123.0 (*meta*-NH_2CH_2Ph), 28.2 (OCH_2), 24.2 (NH_2CH_2), -2.3 (Si*Me*). $^{29}Si\{^1H\}$ NMR (99 MHz, C_6D_6, 298 K): δ -17.0 ppm.

(((1R,2S,5R)-2-Isopropyl-5-methylcyclohexyl)oxy)(methyl)(phenyl)silane - Table 25, Entry 6

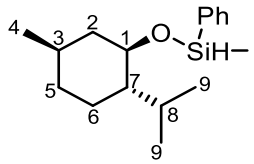

^1H NMR (500 MHz, C_6D_6, 298 K): δ 7.54-7.53 (2H, m, *ortho*-Si*Ph*Me), 7.32-7.30 (3H, m, *para*-Si*Ph*Me, *meta*-Si*Ph*Me), 4.99 (1H, s, SiH), 3.43-3.33 (1H, m, $OCH(CH_2)_2$), 2.11 (1H, m, $(CH_2)_2CHCH(CH_3)_2$), 1.86 (1H, m, $OCHCH_2^{eq}CHCH_3$), 1.51 (2H, m, $CH_3CHCH_2^{eq}CH_2$, $CH_2^{ax}CHCH(CH_3)_2$), 1.24 (1H, m, $CH_3CHCH_2CH_2$), 1.14-0.93 (4H, m, $(CH_2)_2CHCH(CH_3)_2$, $CHCH_3$), 0.80-0.76 (8H, m, $OCHCH(CH(CH_3)_2)CH_2^{ax}$,$(CH_2)_2CHCH(CH_3)_2$, $OCHCH_2^{ax}CHCH_3$,), 0.57 (1H, m, $CH_3CHCH_2^{ax}CH_2$), 0.37 (3H, s, SiMe). $^{13}C\{^1H\}$ NMR (125 MHz, C_6D_6, 298 K): δ 138.5 (*ipso*-Si*Ph*Me), 135.9 (*ortho*-Si*Ph*Me), 131.9 (*para*-Si*Ph*Me), 129.8 (*meta*-Si*Ph*Me), 76.1 (*C*-1), 51.9 (*C*-7), 46.5 (*C*-2), 36.4 (*C*-5), 33.6 (*C*-3), 27.2 (*C*-8), 24.7 (*C*-6), 24.2 (*C*-4), 23.1 (*C*-9), 17.6 (*C*-9), 0.0 (Si*Me*).$^{29}Si\{^1H\}$ NMR (99 MHz, C_6D_6, 298 K): δ -18.5 ppm. $[\alpha]_D$= -70.2334°.

(Benzhydryloxy)(methyl)(phenyl)silane - Table 25, Entry 7

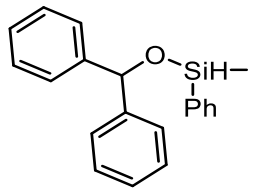

^1H NMR (500 MHz, C_6D_6, 298 K): δ 7.41-7.38 (2H, m, Ar-H), 7.23-7.05 (13H, m, Ar-H), 5.65 (1H, s, Si-H), 4.88 (1H, s, OC*H*), 0.25 (3H, s, $SiCH_3$).$^{13}C\{^1H\}$ NMR (125 MHz, C_6D_6, 298 K): δ 145.9 (*ipso*- $OCH(Ph)_2$), 137.2 (*ipso*-Si*Ph*Me), 135.7 (*ortho*-Si*Ph*Me), 131.8 (*para*-$OCH(Ph)_2$), 129.9 (*meta*-$OCH(Ph)_2$), 128.9 (*meta*-Si*Ph*Me), 128.4 (*ortho*- $OCH(Ph)_2$), 125.0 (*para*-Si*Ph*Me), 80.1 ($OCH(Ph)_2$), -0.80 (Si*Me*).$^{29}Si\{^1H\}$ NMR (99 MHz, C_6D_6, 298 K): δ -1.0 ppm.

(((3S,10S,13R)-10,13-dimethyl-17-((R)-6-Methylheptan-2-yl)-2,3,4,5,8,9,10,11,12,13,14,15,16,17-tetradecahydro-1H-cyclopenta[a]phenanthren-3-yl)oxy)(methyl)(phenyl)silane - Table 25, Entry 9

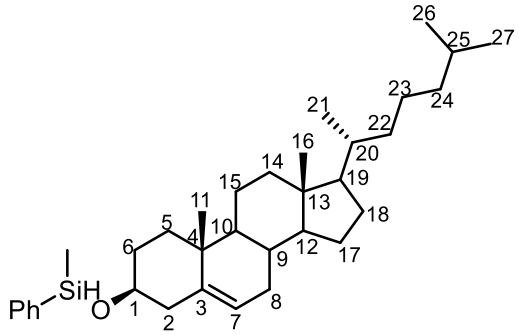

^{1}H NMR (500 MHz, C_6D_6, 298 K): δ 7.82 (2H, m, *ortho*-Si*Ph*Me), 7.37-7.09 (3H, m, *para*-Si*Ph*Me, *meta*-Si*Ph*Me), 5.35 (1H, m, C*H*-7) 4.40 (1H, s, SiH) 3.91 (1H, m, C*H*-1), 2.55 (2H, m, CH_2-2), 1.95-1.88 (2H, m, C*H*-8, C*H*-14), 1.77-1.58 (4H, m, C*H*-5, CH_2-6, C*H*-18) 1.58-1.47 (3H, m, C*H*-8, CH_2-15, C*H*-25), 1.40-1.20 (5H, m, C*H*-9, C*H*-17, C*H*-18, C*H*-19, C*H*-22), 1.25-1.11 (5H, m, C*H*-5, C*H*-14, C*H*-20, C*H*-23) 1.10-1.00 (4H, m, C*H*-17, C*H*-23, CH_2-24) 1.00-0.90 (6H, m, CH_3-11, C*H*-22, C*H*-12, C*H*-10), 0.90 (9H, m, CH_3-21, CH_3-26, CH_3-27), 0.61 (3H, s, CH_3-16) 0.42 (3H, s, Si*Me*). ^{13}C{^{1}H} NMR (125 MHz, C_6D_6, 298 K): δ 141.4 (*C*-3), 136.8 (*ipso*-Si*Ph*), 135.3 (*ortho*-Si*Ph*), 134.6 (*para*-Si*Ph*), 130.2 (*meta*-Si*Ph*), 121.9 (*C*-7), 73.1 (*C*-1), 57.2 (*C*-12), 56.6 (*C*-19), 50.6 (*C*-10), 42.9 (*C*-13), 42.7 (*C*-2), 40.3 (*C*-14), 40.0 (*C*-24), 37.7 (*C*-5), 36.9 (*C*-4), 36.8 (*C*-22), 36.3 (*C*-21), 32.6 (*C*-9), 32.4 (*C*-8), 32.3 (*C*-6), 28.8 (*C*-18), 28.4 (*C*-25), 24.8 (*C*-17), 24.4 (*C*-23), 23.2 (*C*-27), 22.9 (*C*-26), 19.6 (*C*-11), 19.1 (*C*-21), 12.2 (*C*-16), -2.5 (Si*Me*)^{29}Si{^{1}H} NMR (99 MHz, C_6D_6, 298 K): δ -1.6 ppm, -16.6 ppm. $[\alpha]_D$= -27.578°.

(3,7-Dimethylocta-1,6-dien-3-yl)oxy)(methyl)(phenyl)silane - Table 25, Entry 10

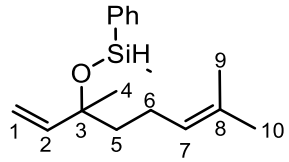

^{1}H NMR (500 MHz, C_6D_6, 298 K): δ 7.74 (2H, m, *ortho*-Si*Ph*Me), 7.28 (3H, m, *para*-Si*Ph*Me, *meta*-Si*Ph*Me), 5.90 (1H, m, OC(CH_3)CH_2CH_2C*H*), 5.47 (1H, s, Si-H), 5.26 (1H, s, CH_2CHC(CH_3)O), 5.05 (2H, m, CH_2CHC(CH_3)O, CH_2C*H*C(CH_3)$_2$), 2.20 (2H, m, OC(CH_3)CH_2CH_2CH), 1.71-1.64 (7H, m, CH_2CHC(CH_3)$_2$, OC(CH_3)C$H_2^a$$CH_2$CH), 1.37-1.26 (4H, m, OC(CH_3)C$H_2^b$$CH_2$CH, OC(C$H_3$)$CH_2CH_2$CH), 0.47 (3H, s, Si*Me*). ^{13}C{^{1}H} NMR (125 MHz, C_6D_6, 298 K): δ 144.4 (*C*-2), 133.7 (*C*-8), 129.6 (*ipso*-Si*Ph*Me), 128.3 (*ortho*-Si*Ph*Me), 127.8 (*para*-Si*Ph*Me), 124.5 (*C*-7), 123.0 (*meta*-Si*Ph*Me), 112.3 (*C*-1), 77.0 (*C*-3), 42.9 (*C*-5), 27.0 (*C*-4), 25.7 (*C*-10), 22.8 (*C*-6), 17.6 (*C*-9), 1.0 (Si*Me*). ^{29}Si{^{1}H} NMR (99 MHz, C_6D_6, 298 K): δ -16.0 ppm.

((3,7-Dimethyloct-6-en-1-yl)oxy)(methyl)(phenyl)silane - Table 25, Entry 11

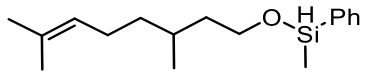

^{1}H NMR (500 MHz, C_6D_6, 298 K): δ 7.73 (1H, d, *J* = 6.8 Hz, *para*-Si*Ph*Me), 7.20-7.08 (4H, m, *ortho*-Si*Ph*Me, *meta*-Si*Ph*Me), 5.12 (1H, s, CHC(C*H*$_3$)$_2$), 4.80 (1H, s, Si-H), 3.76 (2H, m, OC*H*$_2$CH$_2$CH(Me)CH$_2$), 1.93 (2H, m, OCH$_2$CH$_2$CH(CH$_3$)C*H*$_2$), 1.59 (4H, m, OCH$_2$CH$_2$C*H*(CH$_3$)CH$_2$, CH$_2$CHC(C*H*$_3$)$_2$), 1.48 (3H, m, CH$_2$CHC(C*H*$_3$)$_2$), 1.34 (2H, m, OC*H*$_2$CH$_2$CH(CH$_3$)CH$_2$), 1.14-1.08 (2H, m, OCH$_2$C*H*$_2$CH(CH$_3$)CH$_2$), 0.82-0.80 (3H, m, OCH$_2$CH$_2$CH(C*H*$_3$)CH$_2$), 0.32 (3H, s, Si*Me*). ^{13}C{^{1}H} NMR (125 MHz, C_6D_6, 298 K): δ 134.2 (*ipso*-Si*Ph*Me), 133.1 (CH$_2$CH=*C*(*Me*)$_2$), 129.5 (*meta*-Si*Ph*Me), 128.9 (*ortho*-Si*Ph*Me), 127.2 (*para*-Si*Ph*Me), 124.0 (CH$_2$*C*H=C(*Me*)$_2$), 59.8 (O*C*H$_2$CH$_2$CH(Me)CH$_2$), 38.7 (OCH$_2$*C*H$_2$CH(Me)CH$_2$), 36.2 (OCH$_2$CH$_2$*C*H(Me)CH$_2$), 28.0 (O*C*H$_2$CH$_2$CH(Me)*C*H$_2$), 24.5 (CH$_2$CH=C(*Me*)$_2$), 18.3 (*C*H$_2$CH=C(*Me*)$_2$), 16.4 (O*C*H$_2$CH$_2$CH(*Me*)CH$_2$), -5.3 (Si*Me*).^{29}Si{^{1}H} NMR (99 MHz, C_6D_6, 298 K): δ -18.7 ppm

(E)-((3,7-Dimethylocta-2,6-dien-1-yl)oxy)(methyl)(phenyl)silane - Table 25, Entry 12

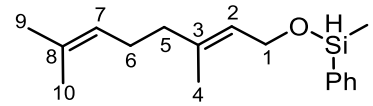

^{1}H NMR (500 MHz, C_6D_6, 298 K): δ 7.89 -7.71 (2H, m, *ortho*-Si*Ph*Me), 7.31-7.25 (3H, m, *para*-Si*Ph*Me, *meta*-Si*Ph*Me), 5.69 (1H, m, OCH$_2$C*H*C), 5.25 (1H, m, C*H*C(CH$_3$)$_2$,), 4.50 (2H, m, OC*H*$_2$CHC), 4.34 (1H, s, SiH) 2.18-2.11 (4H, m, (CH$_3$)$_2$CC*H*$_2$CH$_2$, (CH$_3$)$_2$CCH$_2$C*H*$_2$), 1.73-1.51 (9H, m, CHC(CH$_3$)$_2$, CHC(C*H*$_3$)$_2$), 0.50 (3H, s, Si*Me*).^{13}C{^{1}H} NMR (125 MHz, C_6D_6, 298 K): δ 137.7 (*C*-3), 137.0 (*ipso*-Si*Ph*Me), 134.2 (*ortho*-Si*Ph*Me), 133.9 (*para*-Si*Ph*Me), 133.4 (*meta*-Si*Ph*Me), 131.0 (*C*-8), 124.2 (*C*-2), 123.7 (*C*-7), 59.6 (*C*-1), 39.6 (*C*-5), 26.5 (*C*-6), 25.3 (*C*-9), 17.4 (*C*-10), 16.2 (*C*-4), -3.7 (Si*Me*).^{29}Si{^{1}H} NMR (99 MHz, C_6D_6, 298 K): δ -17.3 ppm.

(2,4-Di-tert-butylphenoxy)(phenyl)silane - Table 26, Entry 1

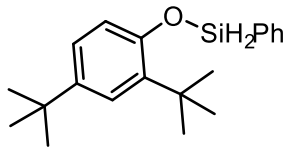

^{1}H NMR (500 MHz, C_6D_6, 298 K): δ 7.90 -7.40 (5H, m, Ar-H), 7.02-6.89 (3H, m, Ar-H), 5.78 (1H, s, SiH), 1.51 (9H, s, tBu), 1.20 (9H, s, tBu).^{13}C{^{1}H} NMR (125 MHz, C_6D_6, 298 K): δ 150.8 (*ipso*-O*C*$_6$H$_3$tBu$_2$), 144.6 (*ortho*-O*C*$_6$H$_3$tBu$_2$), 138.5 (*para*-O*C*$_6$H$_3$tBu$_2$), 133.8 (*ipso*-Si*Ph*), 131.1 (*ortho*-Si*Ph*), 126.8 (*para*-Si*Ph*), 124.0 (*meta*-O*C*$_6$H$_3$tBu$_2$), 123.9 (*meta*-O*C*$_6$H$_3$tBu$_2$), 118.9 (*meta*-Si*Ph*), 117.8 (*ortho*-O*C*$_6$H$_3$tBu$_2$), 35.0 (*C*(CH$_3$)$_3$), 34.1 (*C*(CH$_3$)$_3$), 31.2 (C(*C*H$_3$)$_3$), 29.9(C(*C*H$_3$)$_3$).^{29}Si{^{1}H} NMR (99 MHz, C_6D_6, 298 K): δ -38.5 ppm.

(Benzhydryloxy)(phenyl)silane – Table 26, Entry 2

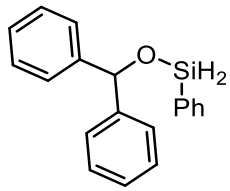

^{1}H NMR (500 MHz, C_6D_6, 298 K): δ 7.60 (1H, m, Ar-H), 7.27(4H, m, Ar-H), 7.12- 6.98 (10H, m, Ar-H), 5.91 (2H, s, H_2Si), 5.33 (1H, s, OC*H*$(Ph)_2$).^{13}C{^{1}H} NMR (125 MHz, C_6D_6, 298 K): δ 143.9 (*ipso*-OCH_2(*Ph*)$_2$), 134.3 (*ipso*-Si*Ph*), 130.6 (*ortho*-Si*Ph*), 128.2 (*para*-OCH(*Ph*)$_2$), 127.3 (*meta*-OCH(*Ph*)$_2$), 127.1 (*meta*-Si*Ph*Me), 126.7 (*ortho*-OCH_2(*Ph*)$_2$), 126.5 (*para*-Si*Ph*), 77.7 (O*C*H_2(Ph)$_2$).^{29}Si{^{1}H} NMR (99 MHz, C_6D_6, 298 K): δ -30.6 ppm.

(Benzyloxy)(phenyl)silane – Table 26, Entry 3

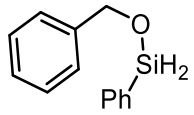

^{1}H NMR (500 MHz, C_6D_6, 298 K): δ 7.97 (1H, m, Ar-H), 7.49-7.17 (9H, m, Ar-H), 4.98 (2H, s, H_2Si), 1.30 (2H, m, OC*H*$_2$Ph). ^{13}C{^{1}H} NMR (125 MHz, C_6D_6, 298 K): δ 143.9 (*ipso*-OCH_2*Ph*), 134.3 (*ipso*-Si*Ph*), 130.7 (*ortho*-Si*Ph*), 128.3 (*para*-Si*Ph*Me), 127.3 (*meta*-OCH_2*Ph*), 127.1 (*meta*-Si*Ph*Me), 126.7 (*para*-OCH_2*Ph*), 126.5 (*meta*-OCH_2*Ph*), 77.7 (O*C*H_2Ph).^{29}Si{^{1}H} NMR (99 MHz, C_6D_6, 298 K): δ -58.9 ppm.

4,4,5,5-Tetramethyl-2-phenyl-1,3,2-dioxasilolane – Table 26, Entry 4

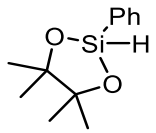

^{1}H NMR (500 MHz, C_6D_6, 298 K): δ 7.94 -7.86 (2H, m, Ar-H), 7.12 (3H, m, Ar-H), 3.28 (1H, s, SiH), 1.13 (12H, s, OC$(CH_3)_2$). ^{13}C{^{1}H} NMR (125 MHz, C_6D_6, 298 K): δ 134.4 (*ipso*-Si*Ph*), 131.0 (*ortho*-Si*Ph*), 128.6 (*para*-Si*Ph*), 123.8 (*meta*-Si*Ph*), 82.7 (O*C*$(CH_3)_2$), 22.6 (OC(*C*$H_3)_2$). ^{29}Si{^{1}H} NMR (99 MHz, C_6D_6, 298 K): δ -43.8 ppm.

Compounds synthesised in Chapter 5:

General method for catalytic desilylation:

Silazane/siloxane synthesis was achieved via dehydrocoupling (as above). After full spectroscopic conversion is achieved of silazane/siloxane, pinacolborane (HBpin, 0.5 mmol, 73 µl) is added to the J-youngs Shlenk or J-youngs NMR tube. Reactions are then monitored at room temperature over a 24 hour period (or as otherwise stated). Compounds were isolated by diluting the reaction mixture and passing through graphite to remove the iron complex.[152] Products synthesised were in accordance with literature reports and all data is comparable to literature reports.[153, 159, 179]

Silazane desilylation:

N-benzyl-N,4,4,5,5-pentamethyl-1,3,2-dioxaborolan-2-amine - Table 27, Entry 1

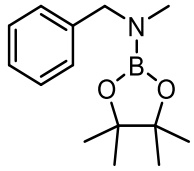

White solid, yield = 83 mg, 67%, ^{1}H NMR (500 MHz, C_6D_6, 298 K): δ 7.22-7.20 (2H, m, *meta*-MeNCH$_2$*Ph*), 7.16-7.11 (2H, m, *ortho*-MeNCH$_2$*Ph*), 7.06-7.03 (1H, m, *para*-MeNCH$_2$*Ph*), 4.09 (2H, s, ArC*H*$_2$NMe), 2.53 (3H, s, ArCH$_2$N*Me*), 1.10 (12H, s, OC(C*H*$_3$)$_2$).^{13}C{^{1}H} NMR (125 MHz, C_6D_6, 298 K): δ 140.3 (*ipso*-MeNCH$_2$*Ph*), 128.2 (*meta*-MeNCH$_2$*Ph*), 127.6 (*ortho*-MeNCH$_2$*Ph*), 126.6 (*para*-MeNCH$_2$*Ph*), 82.0 (O*C*(CH$_3$)$_2$), 52.8 (MeN*C*H$_2$Ph), 32.9 (*Me*NCH$_2$Ph), 24.4 (OC(*C*H$_3$)$_2$).^{11}B NMR (160 MHz, C_6D_6, 298 K): δ 24.6 ppm.

N-benzyl-4,4,5,5-tetramethyl-1,3,2-dioxaborolan-2-amine - Table 27, Entry 2

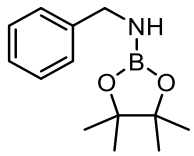

White solid, yield = 91 mg, 78%, ^{1}H NMR (500 MHz, C_6D_6, 298 K): δ 7.15-7.12 (m, 4H, Ar-H), 7.00 (m, 1H, Ar-H), 4.04 (d, *J* = 7.8 Hz, 2H, PhC*H*$_2$NH), 2.51 (s, br, 1H, NH), 1.05 (s, 12H, CH$_3$). ^{13}C{^{1}H} NMR (125 MHz, C_6D_6, 298 K): δ 143.1 (*ipso*-NHCH$_2$*Ph*), 128.1 (*ortho*-NHCH$_2$*Ph*), 126.7 (*meta*-NHCH$_2$*Ph*), 126.3 (*para*-NHCH$_2$*Ph*), 81.6 (O*C*(CH$_3$)$_2$), 45.3 (NH*C*H$_2$Ph), 24.4 (OC(*C*H$_3$)$_2$). ^{11}B NMR (160 MHz, C_6D_6, 298 K): δ 24.9 ppm.

4,4,5,5-Tetramethyl-N-phenyl-1,3,2-dioxaborolan-2-amine - Table 27, Entry 3

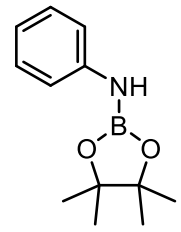

White solid, yield = 88 mg, 80%, ^{1}H NMR (500 MHz, C_6D_6, 298 K): δ 7.21-7.06 (2H, m, *meta*-NH*Ph*), 7.06-7.01 (2H, m, *ortho*-NH*Ph*), 6.75-6.66 (1H, m, *para*-NH*Ph*), 4.46 (1H, bs, NH), 1.04 (12H, s, OC(C*H*$_3$)$_2$).^{13}C{^{1}H} NMR (125 MHz, C_6D_6, 298 K): δ 143.5 (*ipso*-NH*Ph*), 128.9 (*meta*-NH*Ph*), 120.0 (*ortho*-NH*Ph*), 117.7 (*para*-NH*Ph*), 82.3 (O*C*(CH$_3$)$_2$), 24.3 (OC(*C*H$_3$)$_2$).^{11}B NMR (160 MHz, C_6D_6, 298 K): δ 24.2 ppm.

4-(4,4,5,5-Tetramethyl-1,3,2-dioxaborolan-2-yl)morpholine - Table 27, Entry 4

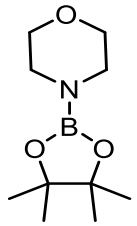

White solid, yield = 85 mg, 80%, ^{1}H NMR (500 MHz, C_6D_6, 298 K): δ 3.37 (4H, t, *J* = 4.60 Hz, OCH_2), 3.08 (4H, t, *J* = 4.77 Hz, NCH_2), 1.06 (12H, s, $OC(CH_3)_2$). $^{13}C\{^{1}H\}$ NMR (125 MHz, C_6D_6, 298 K): δ 81.8 ($OC(CH_3)_2$), 68.0 (OCH_2), 44.5 (NCH_2), 24.4 ($OC(CH_3)_2$).^{11}B NMR (160 MHz, C_6D_6, 298 K): δ 23.7 ppm.

N-butyl-4,4,5,5-tetramethyl-1,3,2-dioxaborolan-2-amine - Table 27, Entry 5

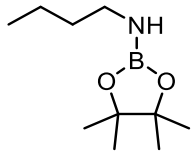

White solid, yield = 92 mg, 92%, ^{1}H NMR (500 MHz, C_6D_6, 298 K): δ 2.87 (q, *J* = 6.75 Hz, 2H, $CH_3CH_2CH_2CH_2NH$), 2.02 (s, br, 1H, NH), 1.17 (m, 4H, $CH_3CH_2CH_2CH_2NH$), 1.09 (s, 12H, CH_3), 0.78 (t, *J* = 7.2 Hz, 3H, $CH_3CH_2CH_2CH_2NH$). $^{13}C\{^{1}H\}$ NMR (125 MHz, C_6D_6, 298 K): δ 81.6 ($OC(CH_3)_2$), 40.7 ($CH_3CH_2CH_2CH_2NH$), 35.7 ($CH_3CH_2CH_2CH_2NH$), 24.4 ($OC(CH_3)_2$), 19.5 ($CH_3CH_2CH_2CH_2NH$), 13.9 ($CH_3CH_2CH_2CH_2NH$).^{11}B NMR (160 MHz, C_6D_6, 298 K): δ 24.7 ppm.

N-(2,2-diphenylpentyl)-4,4,5,5-tetramethyl-1,3,2-dioxaborolan-2-amine - Table 27, Entry 6

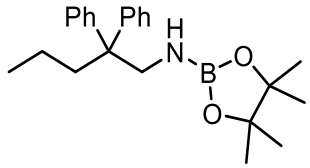

^{1}H NMR (500 MHz, C_6D_6, 298 K): δ 7.16-6.96 (10H, m, $C(Ph)_2$), 3.63 (2H, d, *J* = 6.8Hz, $CH_3CH_2CH_2C(Ph)_2CH_2NH$), 1.98-1.89 (2H, m, $CH_3CH_2CH_2C(Ph)_2CH_2NH$), 1.63-1.52 (2H, m, $CH_3CH_2CH_2C(Ph)_2CH_2NH$), 1.18-1.16 (3H, m, $CH_3CH_2CH_2C(Ph)_2CH_2NH$), 1.06 (12H, s, $OC(CH_3)_2$), 0.80 (1H, bs, NH).$^{13}C\{^{1}H\}$ NMR (125 MHz, C_6D_6, 298 K): δ 147.1 (*ipso*-$C(Ph)_2$), 128.3 (*meta*-$C(Ph)_2$), 127.8 (*ortho*-$C(Ph)_2$), 125.6 (*para*-$C(Ph)_2$), 81.5 ($OC(CH_3)_2$), 51.4 ($CH_3CH_2CH_2C(Ph)_2CH_2NH$), 48.1 ($CH_3CH_2CH_2C(Ph)_2CH_2NH$), 38.7 ($CH_3CH_2CH_2C(Ph)_2CH_2NH$), 24.4 ($OC(CH_3)_2$), 17.3 ($CH_3CH_2CH_2C(Ph)_2CH_2NH$), 14.6 ($CH_3CH_2CH_2C(Ph)_2CH_2NH$).^{11}B NMR (160 MHz, C_6D_6, 298 K): δ 24.8 ppm.

Siloxane desilylation:

2-(Benzyloxy)-4,4,5,5-tetramethyl-1,3,2-dioxaborolane - Table 28, Entry 1

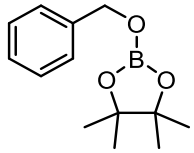

White solid, yield = 101 mg, 86%, ^{1}H NMR (500 MHz, C_6D_6, 298 K): δ 7.35-7.33 (2H, d, *J*= 6.5 Hz, *meta*-OCH_2*Ph*), 7.23-7.19 (2H, m, *ortho*-OCH_2*Ph*), 7.13-7.06 (1H, m, *para*-OCH_2*Ph*), 4.98 (2H, s, OCH_2Ph), 1.06 (12H, s, $OC(CH_3)_2$). $^{13}C\{^{1}H\}$ NMR (125 MHz, C_6D_6, 298 K): δ 139.6 (*ipso*-OCH_2*Ph*), 128.2 (*meta*-OCH_2*Ph*), 127.2 (*ortho*-OCH_2*Ph*), 126.6 (*para*-OCH_2*Ph*), 82.4 ($OC(CH_3)_2$), 66.6 (OCH_2Ph), 24.3 ($OC(CH_3)_2$). ^{11}B NMR (160 MHz, C_6D_6, 298 K): δ 22.8 ppm.

2-(*tert*-Butoxy)-4,4,5,5-tetramethyl-1,3,2-dioxaborolane - Table 28, Entries 2 and 4

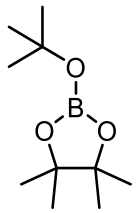

White solid, yield = 46 mg, 91%, ^{1}H NMR (500 MHz, C_6D_6, 298 K): δ 1.06 (12H, s, $OC(CH_3)_2$), 1.37 (9H, s, $OC(CH_3)_3$). $^{13}C\{^{1}H\}$ NMR (125 MHz, C_6D_6, 298 K): δ 81.3 ($OC(CH_3)_2$), 73.1 ($OC(CH_3)_3$), 29.8 ($OC(CH_3)_3$), 24.2 ($OC(CH_3)_2$).^{11}B NMR (160 MHz, C_6D_6, 298 K): δ 21.6 ppm.

2-(Benzhydryloxy)-4,4,5,5-tetramethyl-1,3,2-dioxaborolane - Table 28, Entry 3

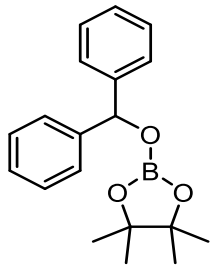

White solid, yield = 129 mg, 83%, ^{1}H NMR (500 MHz, C_6D_6, 298 K): δ 7.39 (4H, d, *J* = 7.50 Hz, *meta*-$OCH(Ph)_2$), 7.05 (4H, d, *J* = 7.60 Hz, *ortho*-$OCH(Ph)_2$) 6.99-6.95 (2H, m, *para*-$OCH(Ph)_2$), 6.25 (1H, s, $OCH(Ph)_2$), 1.06 (12H, s, $OC(CH_3)_2$).$^{13}C\{^{1}H\}$ NMR (125 MHz, C_6D_6, 298 K): δ 143.6 (*ipso*-$OCH(Ph)_2$), 128.2 (*meta*-$OCH(Ph)_2$), 127.2 (*para*-$OCH(Ph)_2$), 126.6 (*ortho*-$OCH(Ph)_2$), 82.5 ($OC(CH_3)_2$), 78.1 ($OCH(Ph)_2$), 24.2 ($OC(CH_3)_2$).^{11}B NMR (160 MHz, C_6D_6, 298 K): δ 22.8 ppm.

4,4,5,5-Tetramethyl-N-(2-((methyl(phenyl)silyl)oxy)-1-phenylethyl)-1,3,2-dioxaborolan-2-amine - Table 28, Entry 5

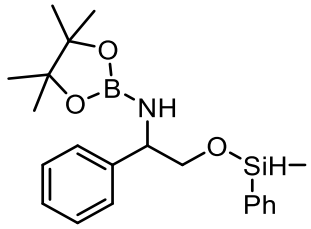

^{1}H NMR (500 MHz, C_6D_6, 298 K): δ 7.55-7.46 (2H, m, Ar-H), 7.12-6.90 (8H, m, Ar-H), 4.57 (1H, s, Si*H*Me), 3.73-3.63 (2H, m, OC*H*$_2$CHNH), 3.23 (1H, m, OCH$_2$C*H*NH), 1.06 (12H, s, OC(C*H*$_3$)$_2$), 0.20 (3H, s, SiH*Me*). ^{13}C{^{1}H} NMR (125 MHz, C_6D_6, 298 K): δ 143.6 (*ipso*-NHCH*Ph*), 142.4 (*ipso*-Si*Ph*Me), 134.2 (*ortho*-Si*Ph*Me), 133.8 (*meta*-NHCH*Ph*), 129.8 (*para*-Si*Ph*Me), 126.8 (*ortho*-NHCH*Ph*), 126.6 (*meta*-Si*Ph*Me), 123.2 (*para*-NHCH*Ph*), 81.7 (O*C*(CH$_3$)$_2$), 68.5 (O*C*H$_2$CHNH), 56.4 (OCH$_2$*C*HNH), 24.4 (OC(*C*H$_3$)$_2$) -4.8 (Si*Me*). ^{29}Si{^{1}H} NMR (99 MHz, C_6D_6, 298 K): δ -17.4 ppm. ^{11}B NMR (160 MHz, C_6D_6, 298 K): δ 25.0 ppm.

4,4,5,5-Tetramethyl-N-(1-phenyl-2-((4,4,5,5-tetramethyl-1,3,2-dioxaborolan-2-yl)oxy)ethyl)-1,3,2-dioxaborolan-2-amine - Table 28, Entry 6

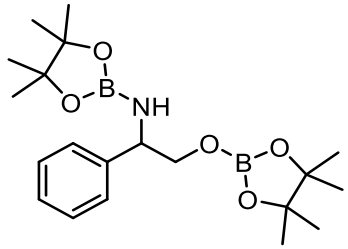

White solid, yield = 130 mg, 67%, ^{1}H NMR (500 MHz, C_6D_6, 298 K): δ 7.38-7.37 (1H, m, Ar-H), 7.13-6.98 (4H, m, Ar-H), 4.68 (1H, t, *J* = 11.3 Hz, OCH$_2$C*H*NH), 4.01 (2H, m, OC*H*$_2$CHNH), 1.62 (1H, bs, NH), 1.06 (24H, s, OC(C*H*$_3$)$_2$). ^{13}C{^{1}H} NMR (125 MHz, C_6D_6, 298 K): δ 142.9 (*ipso*-CH*Ph*), 128.2 (*meta*-CH*Ph*), 128.0 (*ortho*-CH*Ph*), 126.6 (*para*-CH*Ph*), 82.1 (O*C*(CH$_3$)$_2$), 70.1 (O*C*H$_2$CHNH), 56.2 (OCH$_2$*C*HNH), 24.3 (OC(*C*H$_3$)$_2$).^{11}B NMR (160 MHz, C_6D_6, 298 K): δ 22.6, 25.1 ppm.

Crystallographic Data:

Crystal parameters for **1**

Empirical formula	$C_{33}H_{52}FeN_2Si$
Formula weight	560.71
Temperature	150(2) K
Wavelength	1.54184 Å
Crystal system	Monoclinic
Space group	P21/n
Unit cell dimensions	a = 10.63099(17)Å alpha = 90.0°
	b = 21.3317(4)Å beta = 97.0604(16)°
	c = 14.8273(2)Å gamma = 90.0°
Volume	3337.00(9) $Å^3$
Z	4
Density (calculated)	1.116 Mg/m^3
Absorption coefficient	4.113 mm^{-1}
F(000)	1216
Crystal size	0.4090 x 0.2277 x 0.0925 mm
Theta range for data collection	4.85 to 72.04°
Index ranges	-13<=h<=11; -24<=k<=26; -18<=l<=17
Reflections collected	21792
Independent reflections	6512 [R(int) = 0.0664]
Reflections observed (>2sigma)	5417
Data Completeness	0.992
Absorption correction	Semi-empirical from equivalents
Max. and min. transmission	1.00000 and 0.60917
Refinement method	Full-matrix least-squares on F^2
Data / restraints / parameters	6512 / 0 / 347
Goodness-of-fit on F^2	1.133
Final R indices [I>2sigma(I)]	R1 = 0.0756 *wR*2 = 0.1925
R indices (all data)	R1 = 0.0881 *wR*2 = 0.1996
Largest diff. peak and hole	0.912 and -0.396 $eÅ^{-3}$

Crystal parameters for **60**

Empirical formula	$C_{29}H_{44}FeN_2OSi$
Formula weight	520.60
Temperature	150(2) K
Wavelength	0.71073 Å
Crystal system	Monoclinic
Space group	C2/c
Unit cell dimensions	a = 29.1850(4)Å alpha = 90°
	b = 11.0540(1)Å beta = 98.750(1)°
	c = 18.3670(3)Å gamma = 90°
Volume	5856.43(14) $Å^3$
Z	8
Density (calculated)	1.181 Mg/m^3
Absorption coefficient	0.578 mm^{-1}
F(000)	2240
Crystal size	0.25 x 0.25 x 0.20 mm
Theta range for data collection	3.69 to 27.46°
Index ranges	-37<=h<=37; -14<=k<=14; -23<=l<=23
Reflections collected	54697
Independent reflections	6693 [R(int) = 0.0599]
Reflections observed (>2sigma)	4995
Data Completeness	0.998
Absorption correction	Semi-empirical from equivalents
Max. and min. transmission	0.894 and 0.841
Refinement method	Full-matrix least-squares on F^2
Data / restraints / parameters	6693 / 0 / 335
Goodness-of-fit on F^2	1.013
Final R indices [I>2sigma(I)]	R~1 = 0.0376 wR~2 = 0.0853
R indices (all data)	R~1 = 0.0612 wR~2 = 0.0957
Largest diff. peak and hole	0.435 and -0.373 $e.Å^{-3}$

Crystal parameters for **68**

Empirical formula	$C_{41}H_{51}FeN_3$
Formula weight	748.78
Temperature/K	150.00(13)
Crystal system	monoclinic
Space group	$P2_1/c$
a/Å	18.4131(4)
b/Å	18.2697(4)
c/Å	10.6177(2)
α/°	90
β/°	90.850(2)
γ/°	90
Volume/Å^3	3571.42(13)
Z	4
ρcalcg/cm3	5.570
μ/mm 1	1.861
F(000)	6352.0
Crystal size/mm3	0.519 × 0.417 × 0.327
Radiation	MoKα (λ = 0.71073)
2Θ range for data collection/°	7.004 to 54.966
Index ranges	-23 ≤ h ≤ 23, -23 ≤ k ≤ 23, -13 ≤ l ≤ 13
Reflections collected	55675
Independent reflections	8162 [R_{int} = 0.0364, R_{sigma} = 0.0261]
Data/restraints/parameters	8162/0/416
Goodness-of-fit on F2	1.016
Final R indexes [I>=2σ (I)]	R_1 = 0.0355, wR_2 = 0.0796
Final R indexes [all data]	R_1 = 0.0458, wR_2 = 0.0838
Largest diff. peak/hole / e Å^{-3}	0.30/-0.30

Experimental

Single crystals of $C_{41}H_{51}FeN_3$ **68** were isolated. A suitable crystal was selected and placed on a New Xcalibur, EosS2 diffractometer. The crystal was kept at 150.00(13) K during data collection. Using Olex2[189], the structure was solved with the olex2.solve[190] structure solution program using Charge Flipping and refined with the ShelXL[191] refinement package using Least Squares minimisation.

Crystal structure determination of 68

Crystal Data for $C_{41}H_{51}FeN_3$ (*M* =748.78 g/mol): monoclinic, space group $P2_1/c$ (no. 14), *a* = 18.4131(4) Å, *b* = 18.2697(4) Å, *c* = 10.6177(2) Å, *β* = 90.850(2)°, *V* = 3571.42(13) Å^3, *Z* = 4, *T* = 150.00(13) K, μ(MoKα) = 1.861 mm^{-1}, *Dcalc* = 5.570 g/cm^3, 55675 reflections measured (7.004° ≤ 2Θ ≤ 54.966°), 8162 unique (R_{int} = 0.0364, R_{sigma} = 0.0261) which were used in all calculations. The final R_1 was 0.0355 (I > 2σ(I)) and wR_2 was 0.0838 (all data).

Crystal parameters for 71

Empirical formula	$C_{74}H_{92}Fe_2N_4$
Formula weight	1149.21
Temperature/K	150.01(10)
Crystal system	monoclinic
Space group	$P2_1/n$
a/Å	13.9894(4)
b/Å	13.2581(4)
c/Å	17.8087(5)
α/°	90
β/°	97.573(3)
γ/°	90
Volume/Å^3	3274.22(16)
Z	2
ρ_{calc}g/cm^3	1.166
μ/mm^{-1}	3.873
F(000)	1232.0
Crystal size/mm^3	0.209 × 0.128 × 0.031
Radiation	CuKα (λ = 1.54184)
2Θ range for data collection/°	7.57 to 146.142
Index ranges	-16 ≤ h ≤ 11, -15 ≤ k ≤ 16, -21 ≤ l ≤ 21
Reflections collected	21950
Independent reflections	6454 [R_{int} = 0.0487, R_{sigma} = 0.0492]
Data/restraints/parameters	6454/0/371
Goodness-of-fit on F^2	1.024
Final R indexes [I>=2σ (I)]	R_1 = 0.0427, wR_2 = 0.0941
Final R indexes [all data]	R_1 = 0.0571, wR_2 = 0.1003
Largest diff. peak/hole / e Å^{-3}	0.29/-0.26

Notes:
Asymmetric unit comprises ½ of a dimer molecule. The remainder is generated *via* an inversion centre intrinsic to the space group.

Experimental

Single crystals of $C_{74}H_{92}Fe_2N_4$ **71** were isolated. A suitable crystal was selected and placed on a **SuperNova, Dual, Cu at zero, EosS2** diffractometer. The crystal was kept at 150.01(10) K during data collection. Using Olex2 [189] the structure was solved with the olex2.solve[190] structure solution program using Charge Flipping and refined with the ShelXL[191] refinement package using Least Squares minimisation.

Crystal structure determination of 71

Crystal Data for $C_{74}H_{92}Fe_2N_4$ (*M* =1149.21 g/mol): monoclinic, space group $P2_1/n$ (no. 14), *a* = 13.9894(4) Å, *b* = 13.2581(4) Å, *c* = 17.8087(5) Å, *β* = 97.573(3)°, *V* = 3274.22(16) Å^3, *Z* = 2, *T* = 150.01(10) K, μ(CuKα) = 3.873 mm^{-1}, *Dcalc* = 1.166 g/cm^3, 21950 reflections

measured (7.57° ≤ 2Θ ≤ 146.142°), 6454 unique (R_{int} = 0.0487, R_{sigma} = 0.0492) which were used in all calculations. The final R_1 was 0.0427 (I > 2σ(I)) and wR_2 was 0.1003 (all data).

Crystal parameters for 72

Empirical formula	$C_{34}H_{46}ClFeN_3$
Formula weight	588.04
Temperature/K	150.00(10)
Crystal system	triclinic
Space group	P-1
a/Å	9.2405(3)
b/Å	12.3816(4)
c/Å	14.7386(5)
α/°	78.733(3)
β/°	78.834(3)
γ/°	83.726(2)
Volume/Å^3	1617.98(9)
Z	2
ρ_{calc}g/cm^3	1.207
μ/mm^{-1}	4.678
F(000)	628.0
Crystal size/mm^3	0.206 × 0.14 × 0.06
Radiation	CuKα (λ = 1.54184)
2Θ range for data collection/°	7.3 to 146.294
Index ranges	-11 ≤ h ≤ 11, -14 ≤ k ≤ 15, -18 ≤ l ≤ 18
Reflections collected	17807
Independent reflections	6429 [R_{int} = 0.0314, R_{sigma} = 0.0365]
Data/restraints/parameters	6429/0/362
Goodness-of-fit on F^2	1.021
Final R indexes [I>=2σ (I)]	R_1 = 0.0354, wR_2 = 0.0944
Final R indexes [all data]	R_1 = 0.0390, wR_2 = 0.0972
Largest diff. peak/hole / e Å^{-3}	0.49/-0.40

Experimental

Single crystals of $C_{34}H_{46}ClFeN_3$ **72** were isolated. A suitable crystal was selected and placed on a **SuperNova, Dual, Cu at zero, EosS2** diffractometer. The crystal was kept at 150.00(10) K during data collection. Using Olex2[189] the structure was solved with the olex2.solve [190] structure solution program using Charge Flipping and refined with the ShelXL [191] refinement package using Least Squares minimisation.

Bibliography:

1. I. Wauters, W. Debrouwer and C. V. Stevens *Beilstein J. Org. Chem.*, 2014, **10**, 1064-1096.
2. M. D. Greenhalgh, A. S. Jones and S. P. Thomas, *ChemCatChem*, 2015, **7**, 190-222.
3. L. Bourget-Merle, M. F. Lappert and J. R. Severn, *Chem. Rev.*, 2002, **102**, 3031-3066.
4. C. Chen, S. M. Bellows and P. L. Holland, *Dalton. Trans.*, 2015, **44**, 16654-16670.
5. R. L. Webster, *Dalton. Trans.*, 2017, **46**, 4483-4498.
6. P. L. Holland, *Acc. Chem. Res.*, 2008, **41**, 905-914.
7. T. J. J. Sciarone, A. Meetsma and B. Hessen, *Inorg. Chim. Acta.*, 2006, **127**, 1815-1825.
8. J. Vela, J. M. Smith, Y. Yu, N. A. Ketterer, C. J. Flaschenriem, R. J. Lachicotte and P. L. Holland, *J. Am. Chem. Soc.*, 2005, **127**, 7857-7870.
9. Y. Yu, J. M. Smith, C. J. Flaschenriem and P. L. Holland, *Inorg. Chem.*, 2006, **45**, 5742-5751.
10. N. A. Eckert, J. M. Smith, R. J. Lachicotte and P. L. Holland, *Inorg. Chem.*, 2004, **43**, 3306-3321.
11. K. Ding, F. Zannant, J. C. Morris, W. W. Brennessel and P. L. Holland, *J. Organomet. Chem.*, 2009, **694**, 4204-4208.
12. V. C. Gibson, E. L. Marshall, D. Navarro-Llobet, A. J. P. White and J. Williams, *J. Chem. Soc., Dalton Trans.*, 2002, **102**, 4321-4322.
13. M. S. Zhou, S. P. Huang, L. H. Weng, W. H. Sun and D. S. Liu, *J. Organomet. Chem.*, 2003, **665**, 237-245.
14. R. E. Cowley, N. A. Eckert, J. Elhaik and P. L. Holland, *Chem. Commun.*, 2009, 1760-1762.
15. E. Bernoud, P. Oulie, R. Guillot, M. Mellah and J. Hannedouche, *Angew. Chem. Int. Ed. Engl.*, 2014, **53**, 4930-4934.
16. M. S. Hill, D. J. Liptrot and C. Weetman, *Chem. Soc. Rev.*, 2016, **45**, 972-988.
17. D. J. Mindiola, *Acc. Chem. Res.*, 2006, **39**, 813-821.
18. T. K. Salvador, C. H. Arnett, S. Kundu, N. G. Sapiezynski, J. A. Bertke, M. Raghibi Boroujeni and T. H. Warren, *J. Am. Chem. Soc.*, 2016, **138**, 16580-16583.
19. M. R. Crimmin, I. J. Casely and M. S. Hill, *J. Am. Chem. Soc.*, 2005, **127**, 2042-2043.
20. M. R. Crimmin, M. Arrowsmith, A. G. Barrett, I. J. Casely, M. S. Hill and P. A. Procopiou, *J. Am. Chem. Soc.*, 2009, **131**, 9670-9685.
21. M. R. Crimmin, A. G. M. Barrett, M. S. Hill, P. B. Hitchcock and P. A. Procopiou, *Organometallics*, 2007, **26**, 2953-2956.
22. M. R. Crimmin, A. G. M. Barrett, M. S. Hill, P. B. Hitchcock and P. A. Procopiou, *Organometallics*, 2008, **27**, 497-499.
23. G. Zhao, F. Basuli, U. J. Kilgore, H. Fan, H. Aneetha, J. C. Huffman, G. Wu and D. J. Mindiola, *J. Am. Chem. Soc.*, 2006, **128**, 13575-13585.
24. J. A. Osborn, F. H. Jardine, J. F. Young and G. Wilkinson, *J. Chem. Soc. A: Inorg. Phys. Theor.*, 1966, 1711-1732.
25. R. H. Crabtree, H. Felkin and G. E. Morris, *J. Organomet. Chem.*, 1977, **141**, 205-215.
26. C. Kölmel, C. Oehsenfeld and R. Ahlrichs, *Theor. Chim. Act.*, 1991, **82**, 271-284.
27. R. Noyori and S. Hashiguchi, *Acc. Chem. Res.*, 1997, **30**, 97-102.
28. J. P. Genet, *Acc. Chem. Res.*, 2003, **36**, 908-918.
29. C. A. Tolman, *Chem. Rev.*, 1977, **77**, 313-348.
30. C. A. Busacca, J. C. Lorenz, N. Grinberg, N. Haddad, M. Hrapchak, B. Latli, H. Lee, P. Sabila, A. Saha, M. Sarvestani, S. Shen, R. Varsolona, X. Wei and C. H. Senanayake, *Org. Lett.*, 2005, **7**, 4277-4280.
31. P. G. Pringle and M. B. Smith, *J. Chem. Soc., Chem. Commun.*, 1990, **23**, 1701-1702.

32. D. K. Wicht, I. V. Kourkine, B. M. Lew, J. M. Nthenge and D. S. Glueck, *J. Am. Chem. Soc*, 1997, **119**, 5039-5040.
33. D. K. Wicht, I. V. Kourkine, I. Kovacik, D. S. Glueck, T. E. Concolino, G. P. A. Yap, C. D. Incarvito and A. L. Rheingold, *Organometallics*, 1999, **18**, 5381-5394.
34. J. R. Moncarz, N. F. Laritcheva and D. S. Glueck, *J. Am. Chem. Soc.*, 2002, **124**, 13356-13357.
35. I. Kovacik, D. K. Wicht, N. S. Grewal, D. S. Glueck, C. D. Incarvito, I. A. Guzei and A. L. Rheingold, *Organometallics*, 2000, **19**, 950-953.
36. A. Carlone, G. Bartoli, M. Bosco, L. Sambri and P. Melchiorre, *Angew. Chem. Int. Ed. Engl.*, 2007, **46**, 4504-4506.
37. A. D. Sadow, I. Haller, L. Fadini and A. Togni, *J. Am. Chem. Soc.*, 2004, **126**, 14704-14705.
38. P. Muthupandi and G. Sekar, *Org. Biomol. Chem.,* 2012, **10**, 5347-5352.
39. Y. Li and T. J. Marks, *J. Am. Chem. Soc*, 1996, **118**, 707-708.
40. Y. Li and T. J. Marks, *J. Am. Chem. Soc.*, 1996, **118**, 9295-9306.
41. M. R. Douglass and T. J. Marks, *J. Am. Chem. Soc.*, 2000, **122**, 1824-1825.
42. M. R. Douglass, C. L. Stern and T. J. Marks, *J. Am. Chem. Soc.*, 2001, **123**, 10221-10238.
43. G. A. Molander, E. D. Dowdy and S. K. Pack, *J. Org. Chem.*, 2001, **66**, 4344-4347.
44. S. Hong, A. M. Kawaoka and T. J. Marks, *J. Am. Chem. Soc.*, 2003, **125**, 15878-15892.
45. J. S. Ryu, T. J. Marks and F. E. McDonald, *J. Org. Chem.*, 2004, **69**, 1038-1052.
46. M. R. Douglass, M. Ogasawara, S. Hong, M. V. Metz and T. J. Marks, *Organometallics,* 2002, **21**, 283-292.
47. M. A. Kazankova, M. O. Shulyupin, A. A. Borisenko and I. P. Beletskaya, *Russ. J. Organ. Chem.*, 2002, **38**, 1479-1484.
48. H. Ohmiya, H. Yorimitsu and K. Oshima, *Angew. Chem. Int. Ed. Engl.*, 2005, **44**, 2368-2370.
49. A. Kondoh, H. Yorimitsu and K. Oshima, *J. Am. Chem. Soc.*, 2007, **129**, 4099-4104.
50. M. O. Shulyupin, M. A. Kazankova and I. P. Beletskaya, *Org. Lett.*, 2002, **4**, 761-763.
51. M. A. Kazankova, I. V. Efimova, A. N. Kochetkov, A. A. Afanas'ev and I. P. Beletskaya, *Russ. J. Organ. Chem.*, 2002, **38**, 1465-1474.
52. K. Takaki, G. Koshoji, K. Komeyama, M. Takeda, T. Shishido, A. Kitani and K. Takehira, *J. Org. Chem.*, 2003, **68**, 6554-6565.
53. J. Sugiura, T. Kakizawa, H. Hashimoto, H. Tobita and H. Ogino, *Organometallics*, 2005, **24**, 1099-1104.
54. A. Di Giuseppe, R. De Luca, R. Castarlenas, J. J. Perez-Torrente, M. Crucianelli and L. A. Oro, *Chem. Commun.*, 2016, **52**, 5554-5557.
55. L. Routaboul, F. Toulgoat, J. Gatignol, J. F. Lohier, B. Norah, O. Delacroix, C. Alayrac, M. Taillefer and A. C. Gaumont, *Chem. Eur. J.*, 2013, **19**, 8760-8764.
56. K. J. Gallagher and R. L. Webster, *Chem. Commun.*, 2014, **50**, 12109-12111.
57. K. J. Gallagher, M. Espinal-Viguri and R. L. Webster, *Adv. Synth. Catal.*, 2016, **358**, 2460-2468.
58. J. K. Pagano, C. A. Bange, S. E. Farmiloe and R. Waterman, *Organometallics*, 2017, **36**, 3891-3895.
59. M. Kamitani, M. Itazaki, C. Tamiya and H. Nakazawa, *J. Am. Chem. Soc.*, 2012, **134**, 11932-11935.
60. M. Itazaki, S. Katsube, M. Kamitani and H. Nakazawa, *Chem. Commun.*, 2016, **52**, 3163-3166.
61. B. J. Ackley, J. K. Pagano and R. Waterman, *Chem. Commun.*, 2018, in press.

62. H. R. Sharpe, A. M. Geer, W. Lewis, A. J. Blake and D. L. Kays, *Angew. Chem. Int. Ed. Engl.*, 2017, **56**, 4845-4848.
63. F. Alonso, Y. Moglie, M. J. González-Soria, G. Radivoy and M. Yus, *Green. Chem.*, 2012, **14**, 2699-2702.
64. Y. Moglie, M. J. González-Soria, I. Martín-García, G. Radivoy and F. Alonso, *Green. Chem.*, 2016, **18**, 4896-4907.
65. E. M. Leitao, T. Jurca and I. Manners, *Nat. Chem.*, 2013, **5**, 817-829.
66. R. Waterman, *Chem. Soc. Rev.*, 2013, **42**, 5629-5641.
67. R. L. Melen, *Chem. Soc. Rev.*, 2016, **45**, 775-788.
68. E. W. Corcoran and L. G. Sneddon, *J. Am. Chem. Soc.*, 1984, **106**, 7793-7800.
69. E. W. Corcoran and L. G. Sneddon, *J. Am. Chem. Soc.*, 1985, **107**, 7446-7450.
70. V. P. W. Bôhm and M. Brookhart, *Angew. Chem. Int. Ed. Engl.*, 2001, **40**, 4694-4696.
71. J. D. Masuda, A. J. Hoskin, T. W. Graham, C. Beddie, M. C. Fermin, N. Etkin and D. W. Stephan, *Chem. Eur. J.*, 2006, **12**, 8696-8707.
72. L. Greb, S. Tamke and J. Paradies, *Chem. Commun.*, 2014, **50**, 2318-2320.
73. M. W. Lui, N. R. Paisley, R. McDonald, M. J. Ferguson and E. Rivard, *Chem. Eur. J.*, 2016, **22**, 2134-2145.
74. S. Molitor, J. Becker and V. H. Gessner, *J. Am. Chem. Soc.*, 2014, **136**, 15517-15520.
75. A. L. Schwan, M. R. Roche, J. F. Gallagher and G. Ferguson, *Can. J. Chem.*, 1994, **72**, 312-324.
76. R. Dobrovetsky, K. Takeuchi and D. W. Stephan, *Chem. Commun.*, 2015, **51**, 2396-2398.
77. S. J. Geier and D. W. Stephan, *Chem. Commun.*, 2008, 99-101.
78. A. M. Geer, A. L. Serrano, B. de Bruin, M. A. Ciriano and C. Tejel, *Angew. Chem. Int. Ed. Engl.*, 2015, **54**, 472-475.
79. L. B. Han and T. D. Tilley, *J. Am. Chem. Soc.*, 2006, **128**, 13698-13699.
80. R. Shu, L. Hao, J. F. Harrod, H. G. Woo and E. Samuel, *J. Am. Chem. Soc.*, 1998, **120**, 12988-12989.
81. A. J. Roering, S. N. Macmillan, J. M. Tanski and R. Waterman, *Inorg. Chem.*, 2007, **46**, 6855-6857.
82. J. X. Wang, A. K. Dash, J. C. Berthet, M. Ephritikhine and M. S. Eisen, *J. Organomet. Chem.*, 2000, **610**, 49-57.
83. W. Xie, H. Hu and C. Cui, *Angew. Chem. Int. Ed. Engl.*, 2012, **51**, 11141-11144.
84. A. E. Nako, W. Chen, A. J. P. White and M. R. Crimmin, *Organometallics*, 2015, **34**, 4369-4375.
85. O. Glemser, K. Beltz and P. Naumann, *Z. Anorg. Allg. Chem.,* 1956, **291**, 51-66.
86. H. Q. Liu and J. F. Harrod, *Can. J. Chem.*, 1990, **68**, 1100-1105.
87. H. Q. Liu and J. F. Harrod, *Can. J. Chem.*, 1992, **70**, 107-110.
88. H. Q. Liu and J. F. Harrod, *Organometallics*, 1992, **11**, 822-827.
89. J. F. Dunne, S. R. Neal, J. Engelkemier, A. Ellern and A. D. Sadow, *J. Am. Chem. Soc.*, 2011, **133**, 16782-16785.
90. M. S. Hill, D. J. Liptrot, D. J. Macdougall, M. F. Mahon and T. P. Robinson, *Chem. Sci.*, 2013, 4212-4222.
91. C. Bellini, J. F. Carpentier, S. Tobisch and Y. Sarazin, *Angew. Chem. Int. Ed. Engl.*, 2015, **54**, 7679-7683.
92. M. Perez, C. B. Caputo, R. Dobrovetsky and D. W. Stephan, *Proc. Natl. Acad. Sci. U. S. A.*, 2014, **111**, 10917-10921.
93. N. T. Coles and R. L. Webster, *Isr. J. Chem.*, 2017, **57**, 1070-1081.
94. E. Balaraman, A. Nandakumar, G. Jaiswalab and M. K. Sahoo, *Catal. Sci. Technol.*, 2017, **7**, 3177-3195.

95. M. Stender, R. J. Wright, B. E. Eichler, J. Prust, M. M. Olmstead, H. B. Roesky and P. P. Power, *J. Chem. Soc., Dalton Trans.*, 2001, 3465-3469.
96. J. Feldman, S. J. Mclain, A. Parthasarathy, W. J. Marshall, J. C. Calabrese and S. D. Arthur, *Organometallics*, 1997, 1514-1516.
97. D. J. Mindiola, P. L. Holland and T. H. Warren, *Inorg. Synth.*, 2010, **35**, 1-55.
98. A. Postigo, S. Barata, A. Ogawa and M. Sonada, *Tetraphenyldiphosphine*, Encyclopedia of Reagent for Organic Synthesis, 2008, John Wiley Sons Ltd. : New York.
99. M. Berthod, A. Favre-Re´guillon, J. Mohamad, G. Mignani, G. Docherty and M. Lemaire, *Synlett.*, 2007, **10**, 1545 - 1548.
100. R. Waterman, *Organometallics*, 2007, **26**, 2492-2494.
101. V. Naseri, R. J. Less, R. E. Mulvey, M. McPartlin and D. S. Wright, *Chem. Commun.*, 2010, **46**, 5000-5002.
102. C. Ha, J. H. Horner, M. Newcomb, T. R. Varick, B. R. Arnold and J. Lusztyk, *J. Org. Chem.*, 1993, **58**, 1194 - 1198.
103. M. Newcomb, T. R. Varick, C. Ha, M. B. Manek and X. Yue, *J. Am. Chem. Soc.*, 1992, **114**, 8158-8163.
104. V. P. Morgalyuk, P. V. Petrovskii, K. A. Lysenko and E. E. Nifant'ev, *Zh. Obshch. Khim.,* 2010, **80**, 105-110.
105. J. M. Smith, A. R. Sadique, T. R. Cundari, K. R. Rodgers, G. Lukat-Rodgers, R. J. Lachicotte, C. J. Flaschenriem, J. Vela and P. L. Holland, *J. Am. Chem. Soc.*, 2006, **128**, 756-769.
106. E. C. Y. Tam, D. C. Apperley, J. D. Smith, M. P. Coles and J. R. Fulton, *Inorg. Chem.*, 2017, **56**, 14831-14841.
107. A. M. Kawaoka and T. J. Marks, *J. Am. Chem. Soc.*, 2005, **127**, 6311-6324.
108. J.-N. Li, L. Liu, F. Fu and Q.-X. Guo, *Tetrahedron*, 2006, **62**, 4453-4462.
109. J. Vela, S. Vaddadi, T. R. Cundari, J. M. Smith, E. A. Gregory, R. J. Lachicotte, C. J. Flaschenriem and P. L. Holland, *Organometallics*, 2004, **23**, 5226-5239.
110. R. Grubba, K. Kaniewska, Ł. Ponikiewski, B. Cristóvão, W. Ferenc, A. Dragulescu-Andrasi, J. Krzystek, S. A. Stoian and J. Pikies, *Inorg. Chem.*, 2017, **56**, 11030-11042.
111. G. Scalmani and M. J. Frisch, *J. Chem. Phys.*, 2010, **132**, 114110-114115.
112. D. M. York and M. Karplus, *J. Phys. Chem. A*, **103**, 11060-11079.
113. C. Adamo and V. Barone, *J. Chem. Phys.*, 1999, **110**, 6158-6170.
114. M. P. Waller, H. Braun, N. Hojdis and M. Bühl *J. Chem. Theory. Comput.*, 2007, **3**, 2234-2242.
115. D. W. Randall, S. D. George, P. L. Holland, B. Hedman, K. O. Hodgson, W. B. Tolman and E. I. Solomon, *J. Am. Chem. Soc.*, 2000, **122**, 11632-11648.
116. D. Andrae, U. Häußermann, M. Dolg, H. Stoll and H. Preuß, *Theor. Chim. Acta.*, 1990, **77**, 123-141.
117. Y. Zhao and D. Truhlar, *Theor. Chem. Acc.*, 2008, **120**, 215-241.
118. A. G. Avent, A. V. Khvostov, P. B. Hitchcock and M. F. Lappert, *Chem. Commun.*, 2002, 1410-1411.
119. O. Eisenstein, P. B. Hitchcock, A. V. Khvostov, M. F. Lappert, L. Maron, L. Perrin and A. V. Protchenko, *J. Am. Chem. Soc.*, 2003, **125**, 10790-10791.
120. M. Arrowsmith, M. S. Hill, G. Kociok-Köhn, D. J. MacDougall, M. F. Mahon and I. Mallov, *Inorg. Chem.*, 2012, **51**, 13408-13418.
121. C. A. Jaska and I. Manners, *J. Am. Chem. Soc.*, 2004, **126**, 1334-1335.
122. R. Colton and D. Dakternieks, *Inorg. Chim. Acta.*, 1993, **208**, 173-177.
123. N. A. Bell, M. Goldstein, T. Jones and I. W. Nowell, *Acta. Cryst. B*, 1980, **36**, 708-710.
124. J. R. Vance, A. Schafer, A. P. Robertson, K. Lee, J. Turner, G. R. Whittell and I. Manners, *J. Am. Chem. Soc.*, 2014, **136**, 3048-3064.

125. J. F. Sonnenberg and R. H. Morris, *Catal. Sci. Tech.*, 2014, **4**, 3426-3438.
126. W. Luo, P. G. Campbell, L. N. Zakharov and S.-Y. Liu, *J. Am. Chem. Soc.*, 2011, **133**, 19326-19329.
127. S. Kawaguchi, S. Nagata, A. Nomoto, M. Sonoda and A. Ogawa, *J. Org. Chem.*, 2008, **73**, 7928–7933.
128. S. Nagata, S. Kawaguchi, M. Matsumoto, I. Kamiya, A. Nomoto, M. Sonoda and A. Ogawa, *Tet. Lett.*, 2007, **48**, 6637–6640.
129. *Washington, DC Pat.,* 1962.
130. D. G. Blackmond, *Angew. Chem. Int. Ed. Engl.*, 2005, **44**, 4302-4320.
131. D. G. Blackmond, *J. Am. Chem. Soc.*, 2015, **137**, 10852-10866.
132. A. Panda, M. Stender, R. J. Wright, M. M. Olmstead, P. Klavins and P. P. Power, *Inorg. Chem.*, 2002, **41**, 3909-3916.
133. V. Rodriguez-Ruiz, R. Carlino, S. Bezzenine-Lafollee, R. Gil, D. Prim, E. Schulz and J. Hannedouche, *Dalton Trans.*, 2015, **44**, 12029-12059.
134. Y. Sunada, S. Ishida, F. Hirakawa, Y. Shiota, K. Yoshizawa, S. Kanegawa, O. Sato, H. Nagashima and T. Iwamoto, *Chem. Sci.*, 2016, **7**, 191-198.
135. P. O. Oguadinma and F. Schaper, *Organometallics*, 2009, 4089–4097
136. I. El-Zoghbi, A. Ased, P. O. Oguadinma, E. Tchiriou and F. Schaper, *Can. J. Chem.*, 2010, **88**, 1040-1045.
137. C. Camp and J. Arnold, *Dalton Trans.*, 2016, **45**, 14462-14498.
138. S. K. Bertilsson, L. Tedenborg, D. A. Alonso and P. G. Andersson, *Organometallics*, 1999, **18**, 1281-1286.
139. P. Müller and C. Fruit, *Chem. Rev.*, 2003, 2905–2920.
140. H. J. Becher, D. Fenske and E. Langer, *Chem. Ber.*, 1973, **106**, 177-187.
141. S. E. Tunney and J. K. Stille, *J. Org. Chem.*, 1987, **52**, 748-753.
142. Y. Okugawa, K. Hirano and M. Miura, *Angew. Chem. Int. Ed. Engl.*, 2016, **55**, 13558-13561.
143. G. Bai, P. Wei and D. W. Stephan, *Dalton Trans.*, 2006, 1141-1146.
144. H. C. Johnson, E. M. Leitao, G. R. Whittell, I. Manners, G. C. Lloyd-Jones and A. S. Weller, *J. Am. Chem. Soc.*, 2014, **136**, 9078-9093.
145. G. M. Adams, A. L. Colebatch, J. T. Skornia, A. I. McKay, H. C. Johnson, G. C. Lloyd Jones, S. A. Macgregor, N. A. Beattie and A. S. Weller, *J. Am. Chem. Soc.*, 2018, **140**, 1481-1495.
146. D. J. Liptrot, M. S. Hill and M. F. Mahon, *Angew. Chem. Int. Ed. Engl.*, 2014, **53**, 6224-6227.
147. H. Fischer, *Chem. Rev.*, 2001, **101**, 3581-3610.
148. A. Studer, *Chem. Eur. J.*, 2001, **7**, 1159-1164.
149. A. K. King, A. Buchard, M. F. Mahon and R. L. Webster, *Chem. Eur. J.*, 2015, **21**, 15960-15963.
150. K. B. Dillon, F. Mathey and J. F. Nixon, *Phosphorus: The Carbon Copy: From Organophosphorus to Phospha-organic Chemistry*, John Wiley Sons, Ltd.: New York, , 1998.
151. J. C. Slater, *J. Chem. Phys.*, 1964, **41**, 3199-3205.
152. N. T. Coles, M. F. Mahon and R. L. Webster, *Organometallics*, 2017, **36**, 2262-2268.
153. E. A. Romero, J. L. Peltier, R. Jazzar and G. Bertrand, *Chem. Commun.*, 2016, **52**, 10563-10565.
154. J. M. Smith, R. J. Lachicotte and P. L. Holland, *Organometallics*, 2002, **21**, 4808-4814.
155. T. R. Dugan, E. Bill, K. C. MacLeod, W. W. Brennessel and P. L. Holland, *Inorg. Chem.*, 2014, **53**, 2370-2380.

156. D. Mukherjee, R. R. Thompson, A. Ellern and A. D. Sadow, *ACS. Catal.*, 2011, **1**, 698-702.
157. A. A. Toutov, K. N. Betz, M. C. Haibach, A. M. Romine and R. H. Grubbs, *Org. Lett.*, 2016, **18**, 5776-5779.
158. X. Liang Luo and R. H. Crabtree, *J. Am. Chem. Soc.*, 1989, **111**, 2527-2535.
159. D. J. Liptrot, M. Arrowsmith, A. L. Colebatch, T. J. Hadlington, M. S. Hill, G. Kociok-Kohn and M. F. Mahon, *Angew. Chem. Int. Ed. Engl.*, 2015, **54**, 15280-15283.
160. B. Wrackmeyer, B. Schwarze and W. Milius, *J. Organomet. Chem.*, 1995, **489**, 201-205.
161. B. Wrackmeyer, G. Kehr and S. Z. Ali, *Z. Naturforsch. B*, 1998, **53**, 393-395.
162. T. Wideman, E. Cortez, E. E. Remsen, G. A. Zank, P. J. Carroll and L. G. Sneddon, *Chem. Mater.*, 1997, **9**, 2218-2230.
163. A. P. Robertson, E. M. Leitao and I. Manners, *J. Am. Chem. Soc.*, 2011, **133**, 19322-19325.
164. T. J. Hadlington, T. Szilvasi and M. Driess, *Angew. Chem. Int. Ed. Engl.*, 2017, **56**, 7470-7474.
165. W. Wang, Y. Lv, X. Gou, X. Leng and Y. Chen, *Chin. J. Chem.*, 2014, **32**, 752-756.
166. A. G. Moiseev and W. J. Leigh, *J. Am. Chem. Soc.*, 2006, **128**, 14442-14443.
167. K. A. Erickson, M. P. Cibuzar, N. T. Mucha and R. Waterman, *Dalton Trans.*, 2018, **47**, 2138-2142.
168. M. Espinal-Viguri, C. R. Woof and R. L. Webster, *Chem. Eur. J.*, 2016, **22**, 11605-11608.
169. S. W. Benson, *J. Chem. Educ.*, 1965, **42**, 502.
170. T. L. Cottrell, *The Strengths of Chemical Bonds*, Butterworth, 2nd edn., 1958.
171. B. D. Darwent, *National Standard Reference Data Series*, Washington, National Bureau of Standards, 1970.
172. J. A. Kerr, *Chem. Rev.*, 1966, **66**, 465-500.
173. M. Newborough, D. Highgate and P. Vaughan, *Appl. Therm. Eng.*, 2002, **22**, 1875-1883.
174. A. Aguado, L. Martínez, L. Becerra, M. Arieta-araunabeña, S. Arnaiz, A. Asueta and I. Robertson, *J. Mater. Cycles Waste Manag.*, 2014, **16**, 201-210.
175. C. Xu, R. A. Arancon, J. Labidi and R. Luque, *Chem. Soc. Rev.*, 2014, **43**, 7485-7500.
176. Z. Ren and S. Yan, *Prog. Mater. Sci.*, 2016, **83**, 383-416.
177. M. Owen, *Surf. Coating Int. B-Coat. Trans.*, 2004, **87**, 71-76.
178. T. Konegger, L. F. Williams and R. K. Bordia, *J. Am. Ceram. Soc.*, 2015, **98**, 3047-3053.
179. Z. Yang, M. Zhong, X. Ma, K. Nijesh, S. De, P. Parameswaran and H. W. Roesky, *J. Am. Chem. Soc.*, 2016, **138**, 2548-2551.
180. V. K. Jakhar, M. K. Barman and S. Nembenna, *Org. Lett.*, 2016, **18**, 4710-4713.
181. A. Bismuto, S. P. Thomas and M. J. Cowley, *Angew. Chem. Int. Ed. Engl.*, 2016, **55**, 15356-15359.
182. T. R. Hoye, A. W. Aspass, B. M. Elkov and T. D. Ryba, *Org. Lett.*, 2005, **7**, 2205-2208.
183. P. H. M. Budzelaar, A. B. van Oort and A. G. Orpen, *Eur. J. Inorg. Chem.,* 1998, 1486-1494.
184. H. C. Aspinall and M. R. Tillotson, *Inorg. Chem.*, 1996, **35**, 5-8.
185. D. L. Dodds, M. F. Haddow, A. G. Orpen, P. G. Pringle and G. Woodward, *Organometallics*, 2006, **25**, 5937-5945.
186. H. Hu and C. Cui, *Organometallics*, 2012, **31**, 1208-1211.
187. Y. Yu, A. R. Sadique, J. M. Smith, T. R. Dugan, R. E. Cowley, W. W. Brennessel, C. J. Flaschenriem, E. Bill, T. R. Cundari and P. L. Holland, *J. Am. Chem. Soc.*, 2008, **130**, 6624-6638.

188. K. M. Gericke, D. I. Chai and M. Lautens, *Tetrahedron*, 2008, **64**, 6002-6014.
189. O. V. Dolomanov, L. J. Bourhis, R. J. Gildea, J. A. K. Howard and H. Puschmann, *J. Appl. Cryst.*, 2009, **42**, 339-341.
190. L. J. Bourhis, O. V. Dolomanov, R. J. Gildea, J. A. K. Howard and H. Puschmann, *Acta. Cryst. A.*, 2015, **71**, 59-75.
191. G. M. Sheldrick, *Acta. Cryst. C.*, 2015, **71**, 3-8.